Coupling data measured in operating theatre with patient-specific biomechanical model of heart and vessels to augment haemodynamic monitoring of patients undergoing general anaesthesia

Arthur Le Gall

INSTITUT POLYTECHNIQUE DE PARIS

NNT : 2021IPPAX056

Thèse de doctorat

Exploitation conjointe d'un modèle biomécanique patient-spécifique de coeur et vaisseaux et de données mesurées au bloc opératoire pour augmenter le monitorage hémodynamique des patients sous anesthésie générale

Thèse de doctorat de l'Institut Polytechnique de Paris
préparée à l'École Polytechnique

École doctorale n°626 École doctorale de l'Institut Polytechnique de Paris (EDIPP)
Spécialité de doctorat : Mécanique des fluides et des solides, acoustique

Thèse présentée et soutenue à Palaiseau, le 12 Octobre 2021, par

ARTHUR LE GALL

Composition du Jury :

Pr. Karim Asehnoune PUPH, CHU Nantes, Université de Nantes (Laboratoire EA3826 Thérapeutiques cliniques et expérimentales des infections)	Président
Prof. Gernot Plank Professor, Medical University of Graz (Team Plank, Presicion medicine)	Rapporteur
Dr. Nicolas Nesseler Docteur, CHU Rennes, Université de Rennes 1 (UMR 991 Foie, métabolisme et cancer)	Rapporteur
Prof. Mette Olufsen Professor, North Carolina State University (Mathematical biology research group)	Examinateur
Pr. Catherine Paugam-Burtz PUPH, APHP, Université de Paris, UMR-S 1149 CRI Centre de recherche sur l'inflammation	Examinateur
Dr. Dominique Chapelle Directeur de recherche, Inria (équipe MΞDISIM)	Directeur
Dr. Radomír Chabiniok Assistant professor, UT Southwestern medical center dallas, TX (Team TOFMOD)	Co-directeur
Pr. Étienne Gayat PUPH, APHP, Université de Paris (UMR-S 942 MASCOT Marqueurs cardiovasculaires en situations de stress)	Co-directeur, invité
Pr. Alexandre Mebazaa PUPH, APHP, Université de Paris, (UMR-S 942 MASCOT Marqueurs cardiovasculaires en situations se stress)	Invité

À ma femme, Sanata, amoureusement, sans qui rien n'est possible.
À mes enfants, Gabin, Perle et Énora, tendrement.
À ma mère, mon père et mes grands parents chacun fier là d'où ils sont.
À ma fratrie, Marie, Martin et Basile.

Remerciements

Je tiens à remercier chaleureusement mes directeurs de thèse, les docteurs Radomír Chabiniok, professeur-assistant à UT Southwestern Medical Center à Dallas, et Dominique Chapelle, directeur de recherche à Inria-Saclay ainsi que le professeur Étienne Gayat, médecin à l'hôpital Lariboisière et professeur des universités à l'université de Paris. Votre encadrement multidisciplinaire et bienveillant a permis de progressivement m'amener à manipuler des notions de modélisation biomécanique depuis la théorie de la mécanique des milieux continus, jusqu'à l'application en condition clinique dans le domaine de l'anesthésie-réanimation. Merci Radek pour ton compagnonnage tout au long de cette introspection. Tu as été un réel tuteur me permettant de m'approprier progressivement la complexité des éléments de modélisation représentant la physiologie cardiovasculaire. Ta vision sur les applications et potentialités des résultats de modélisation a fortement influé sur l'orientation clinique de cette thèse, merci également pour cela. Dominique, merci d'avoir su faire preuve de patience et de confiance tout au long de cette thèse. Il n'était pas évident *a priori* que je puisse faire preuve de suffisamment de plasticité cérébrale pour m'éloigner autant de mes disciplines originelles. Tes conseils, toujours avisés, et l'étude minutieuse de tes fameuses notes de discussions ont largement contribués à l'aboutissement de ce travail. Étienne, notre collaboration fut plus longue encore que ces 5 années de thèse. Au cours de ces gardes passées ensembles lorsque j'étais interne, ta virtuosité dans les lignes de codes m'a littéralement interrogé, puis inspiré. Tu m'a donc appris qu'à l'impossible nul n'est tenu, et qu'en associant travail et curiosité, aucun objectif n'était inaccessible. Je te remercie également d'avoir toujours été de bon conseil et aidant dans l'orientation de mes choix professionnels. Avoir partagé ces quelques années à travailler sous votre direction fut un réel plaisir en raison également des grandes qualités humaines qui vous caractérisent.
Je souhaite remercier aussi Gernot Plank, professeur à l'université de Graz, et Nicolas Nesseler, médecin en anesthésie-réanimation cardiovasculaire au CHU de Rennes, qui ont accepté de rapporter sur mon manuscrit. Je remercie Gernot Plank pour ses commentaires constructifs et ses questions qui permettront de préciser les applications des découvertes de ma thèse, en particulier concernant l'estimation de la relation pression-volume en télédiastole du ventricule gauche. Nicolas, merci d'avoir su prendre le temps et l'énergie pour lire ma thèse. Connaître mon travail scientifique nous permettra sûrement d'envisager des sujets de recherche fondamentale, translationnelle et clinique en commun, je suis déjà enthousiaste.
Je veux également remercier chaleureusement tous les membres du jury: Catherine Paugam, professeur d'anesthésie-réanimation à l'université de Paris et directrice générale adjointe de l'Assistance Publique-Hôpitaux de Paris; Mette Olufsen, professeur à l'université de New York State North Carolina; Karim Asehnoune, professeur d'anesthésie-réanimation à l'université de Nantes et; Alexandre Mebazaa, professeur d'anesthésie-réanimation à l'université de Paris. Merci de vous être intéressé à mon travail, et d'avoir su orienter la discussion sur des perspectives potentielles.

Je tiens à remercier particulièrement Fabrice Vallée, anesthésiste-réanimateur, mon mentor médical et scientifique. Nous avons démarré ensemble une aventure qui me dépasse largement, et qui est l'histoire d'une collaboration de recherche translationnelle durable entre le département d'anesthésie-réanimation de l'Hôpital Lariboisière, et plus particulièrement "le temple", entité officieuse de l'unité Inserm Mascot, et les équipes MΞDISIM et Parietal d'Inria Saclay, entre-autres. Je fus le deuxième étudiant en Master de Fabrice, le premier à effectuer une thèse en étroite collaboration avec "le temple", et maintenant je ne compte plus les thésards et étudiants en master qui sont issus des fruits de cette collaboration. Je suis fier d'avoir contribué à poser une des pierres fondatrices de cette organisation de recherche dont les thématiques me sont chères.
Je souhaite remercier particulièrement également Federica Caforio et François Kimmig, avec qui j'ai partagé quelques années de ma thèse. J'ai beaucoup appris scientifiquement à leur contact, mais aussi humainement. J'ai été impressionné par le respect, la curiosité, la bienveillance et l'altruisme dont vous faite preuve envers et contre tout. Je pense sans me tromper que ma thèse serait loin de ressembler à ce qu'elle est si je ne vous avais pas rencontré et je vous remercie pour cela. François, je ne te remercierai jamais assez du temps consacré à m'expliquer les équations dérivées partielles. Merci de m'avoir aidé à décoder les notes de Dominique. Je suis fier d'avoir su apprendre autant grâce à toi. Merci d'avoir été un moteur pour ma santé physique, de m'avoir appris à nager, de m'avoir permis de parler à ma machine, de tous tes tips and tricks pour survivre à l'administration à l'École Polytechnique. La liste est encore longue mais merci pour tout, et je suis content que nos collaborations soient amenées à se poursuivre. Federica il y a tellement à faire pour te remercier à la juste valeur de ta contribution. Tu inspires la joie de vivre, la motivation, la positivité. Ne serait-ce que pour cela, un grand merci. Merci aussi pour tes enseignements sur les analyses de sensibilité, pour les initiations aux langues étrangères, également pour ton aide sur le décodage des notes de Dominique... Merci encore à tous les deux.
Je veux remercier aussi toutes les personnes dont la contributions sont moins directes dans mon travail de thèse, mais tout aussi importantes pour l'équilibre d'un doctorant. Je pense à cette formidable équipe MΞDISIM et chacun de ses membres. Chacune des discussions tenues avec vous étaient emprunte d'un mélange d'intelligence, de légèreté et de bonne humeur. C'est un vrai bonheur d'évoluer dans cet environnement. Donc un grand merci à Philippe Moireau, responsable d'équipe, modèle de rigueur et d'intelligence dans le travail, et en même temps d'une conversation des plus agréables et inspirantes. Partenaire de practice, j'attends toujours notre parcours avec impatience. Gautier Bureau, je ne pouvais évoquer nos swing avec Philippe sans avoir une pensée pour toi qui a partagé nos séances. Merci d'avoir toujours été d'une aide précieuse au jour le jour. Alexandre, j'ai vraiment apprécié travailler avec toi sur mon visualizer, avec Denis Chemla et Fabrice Vallée ou en séance d'écriture à la maison. Ton enthousiasme était inspirant. Merci pour ça. Merci Frédérique Clément, ta répartie[1] et tes idées[2] sont inspirantes. Merci Nicole, c'était une joie de te rencontrer et de travailler avec toi au quotidien. Tu faisais un peu partie de ma famille car tu as eu la joie de connaître et de t'occuper de tous les petits êtres de ma maison existants à l'époque, y compris le chat. Merci Martin, ton humour au quotidien et ta bonne humeur sans faille embellissent l'open space. Cécile, toi aussi tu as eu la charge de t'occuper d'Olympe. Partager l'open space à tes côtés était une joie. Nos discussions sur la physiologie pulmonaire étaient des plus agréables. Florent, ton Vendredi Sim sur la colorisation des présentations a été pour moi une révélation. Je ne suis pas sûr que j'arrive à mettre en oeuvre tous les bons principes de la communication avec support diapositives

[1] *c.f.* ta punchline du discours d'évaluation des équipes Inria.
[2] Je me suis rendu compte bien tard que tu étais "la" Clément du modèle "Bestel-Clément-Sorine".

mais au moins j'essaie. Jean-Marc, je te remercie pour toutes nos discussions. Tu m'as enseigné ce que accessible voulait dire, et il est très appréciable de pouvoir discuter au quotidien avec un professeur d'une façon aussi naturelle. Merci aussi pour les bons plans tourisme de la région de Briançon. Merci Jérôme Diaz pour tes leçons d'optimisation de code en python (et aussi pour les discussions SOAD). Merci Sébastien Gilles pour tes leçons sur les éléments finis, tout est limpide désormais. Merci Sébastien Imperiale pour ta gentillesse, ton humour et nos discussions de physiologie et de modélisation vasculaire. Merci à tous les doctorants de MΞDISIM que j'ai pu rencontrer, Jessica Manganotti, Ustim Khristenko, Frédérique Robin, Marija Gusseva, Guillaume Baillif, Ezgi Berberoğlu, Chloé Giraudet, Cécile Della Valle, Hajer Methenni, Mathieu Barré, Jona Joachim, Bruno Burtschell, Aurora Armiento, pour votre bonne humeur. Merci également à Bahar Carabetta et Héléna Kutniak pour votre aide et votre suivi depuis mon année de Master jusqu'à la fin de ma thèse.
Merci à Patrick Le Tallec, responsable du laboratoire de mécanique des solides de l'École Polytechnique pour son soutien dans ce projet. Merci Alexandra Joly pour ton aide précieuse quant aux questions administratives de l'École.
Je remercie aussi tous mes collègues en réanimation qui m'ont aménagé du temps pour que je puisse terminer la rédaction: Benjamin Chousterman, Romain Barthélémy, Magalie Collet, Benjamin Huot, Benjamin Soyer, Benjamin Deniau Manuel Kindermans, Matthieu Ledorze, Matthias Rossignol, Samuel Gaugain. Ne changez pas vous êtes au top. Merci aussi aux autres collègues du bloc opératoires que je ne saurais citer sans oublier quelqu'un. Les connaissances physiologiques nécessaires à la bonne conduite de ma thèse m'ont été enseignées par vous, et je vous en remercie. Je remercie aussi tous les paramedics que j'ai pu rencontré et avec qui j'ai eu la joie de côtoyer pendant ces 5 années.
J'ai aussi une pensée pour les personnes contribuants aux projets professionnels parallèles à la thèse et qui étaient tout aussi stimulants. Je pense notamment à mes amis du groupe Jeunes de la SFAR: Adrien Bouglé, Franck Verdonk, Clément Gakuba, Vincent Bruckert, Virginie Tarazona, Lamia Kerdjana, Pierre-Julien Cungi, Charlotte Kellway, Clément Dubost, Paul Abraham, Aurélien Bataille, Jean-Philippe Salaün, Philippe Guerci, Nicolas Mongardon, Lucie Baylacq, Gaëlle Bouroche, Thibault Triglia, Antoine Giraudon, Arthur James, Clément Monnet, Éléonore Bouchereau, Caroline Userovici, Idris Amrouche. Merci à messieurs les présidents Xavier Capdevilla et Francis Bonnet, et également à Raphaël Martin et Jean-Emmanuel Cumplido. Merci à Jean-Yves Lefrant pour sa confiance dans mes missions éditoriales.
Toute cette aventure n'aurait pas été possible sans mes compères de toujours, mes amis: Ludovic Levieil, Valentin Moreau, Laurent Ricard, Pauline Collet, Aurélie Noël, Lionel Chapelle, Mickaël Derman, Mickaël Saudrais, Julie Costil, Clémentine Pelletier, Arnaud Béguin, sans oublier Thibault Chény, Romain Glatre, mes deux témoins, Anaïg Marchand, Anabelle Picard, Mathieu Pencolé, Charlotte Pencolé, Camille Journel, Camille Briand, Benjamin Lecoq, Pierre-Yves Hors, Philippe Le Bayon, François Gaborit, Célia Pilon, Aude Giraud, Julie Frémond, Charles Berthelot, Adrien Poujade, Pierre Leconte, Ikram El Boukili et j'en oublie surement une longue liste. Merci également à Jean Bardon et Aurélien Mazeraud pour toutes ces discussions de travail et amicales.
Je n'oublie pas mes frères, ma soeur, ma mère, mon père et mes grands-parents pour leur soutien.
Enfin je remercie ma femme Sanata pour m'avoir supporté, aidé, épaulé pendant ces cinq années qui ont vu naître mes trois merveilleux enfants Gabin, Perle et Énora.

Contents

Introduction (English)

Context of the thesis

Anaesthesiology and intensive care is a complex specialty allowing surgical procedures while warrantying the physical and mental integrity of the patient who will benefit from the surgery, or who is suffering from critical illness. The role of the anaesthetists begins before the surgical intervention in order to anticipate the potential difficulties associated with 1/ the prior medical history of the patient; 2/ the potential interaction between the daily medical treatments of the patient and the anaesthetic or surgical procedure; and 3/ the surgical procedure itself. During the pre-operative period, the anaesthetist has to identify the risks (*e.g.* by organising a coronarography to evaluate ischemic cardiovascular disease), to optimise the pre-operative conditions of the patients (*e.g.* by stopping anticoagulant drug) in order to decrease the identified risks and to plan the anaesthetic procedure and the post-operative management. On the other hand, the intensivists are involved in any pathology associated with life-threatening condition, such as polytraumatism, septic shock, aneurysmal subarachnoid haemorrhage etc...

For these reasons anaesthetsists and intensivists are involved in cardiovascular management. Indeed a survey conducted in France during 1 year studied the causes of intra-operative death. This survey estimated that 2/3 of the total deaths were for cardiovascular reasons [16]. Furthermore intra-operative hypotension has been proven to be associated with increased post-operative morbi-mortality [21; 22; 3; 4]. Also, shock state – an acute cardiovascular insufficiency, which lead to organ dysfunction – is also a frequent cause to enter the intensive care units (ICUs). Epidemiological studies evaluated the incidence of shock state from 6 to 24% [1; 2].

Haemodynamic management is a complex task that the anaesthetists or the intensivists have to be trained for. For these reasons, international guidelines recommend the use of haemodynamic monitoring to diagnose complex cardiovascular conditions, or to evaluate the efficacy or the response of the treatments that have been chosen [18; 11; 19]. An ideal haemodynamic monitoring should be accurate, reactive, safe, non-invasive, reproducible, easy to use, and should answer a predefined medical question. To date no haemodynamic monitoring technique unites all these characteristics, and a choice has to be made by the physician regarding the haemodyamic issue he has to deal with. Especially, the most advanced haemodynamic diagnostic procedure (the left ventricular (LV) catheterisation) is never used in clinical monitoring practices, as it requires an invasive procedure performed by cardiologists in the cathlab. LV catheterisation allows to draw pressure-volume loops and to obtain crucial information regarding the myocardial consumption and heart-arteries interaction.

Modelling is a discipline that proposes mathematical descriptions of observed phenomena. In medical sciences, statistics is probably the modelling approach that is the most used. It allows to gather evidence with respect to medical practices when used in clinical studies. Personalisation of medicine using machine learning with statistical approaches is spreading into the medical community [12; 17; 23]. Biomechanical modelling is another approach. It is often based on continuum mechanics theory describing the structure and the motion of living materials. Biomechanical modelling can help to reveal patient-specific physiological quantities that are not available by clinical measurements alone (or too invasive for patients). When appropriately calibrated to patients' data (by tuning the model parameters to fit the available data recorded on patients), the results of the simulations performed using models may be interpreted as the patients' physiology, which corresponds to the concept of digital twins [7; 20; 9; 8]. For example, if the appropriate model is used, the quantification of the myocardial contractility may be accessible. To be clinically efficient and helpful for clinicians, cardiovascular modelling should

be understandable for medical communities, easy to calibrate, fast to compute with standard computing resources, and adapted to a clinical question. Therefore, the choice of the model and its components is an important issue. We believe that the biomechanical modelling approach is a suitable method to approximate patients' cardiovascular physiology. This approach is based on the physical description of microscale phenomena (such as description of the actin-myosin cross bridges creation/destruction) that are integrated over a macroscale simulated organ. The motion of the beating heart (the kinematics) is linked to the physical quantities associated with the deformation (the dynamics) using constitutive laws. These kinds of models are usually difficult to calibrate as they need rich patients' data that are often not available in routine clinical settings. We developed a reduced formulation [5] of a complete biomechanical heart and vessels model [10] which allows to decrease the computational costs and to simplify the calibration procedure. This model reduction allows to adapt biomechanical cardiovascular modelling to the clinical environment, especially for anaesthesia and critical care settings.

The potential of patient-specific biomechanical cardiovascular modelling is not limited to revealing physiological quantities. Advanced physiology may be anticipated by the attending anaesthetists or intensivists while measuring cardiovascular data on patients, or while testing patients' response to therapeutical drugs. However, simulation of therapeutic drugs effects prior to patients administration is a functionality that may be implemented in a biomechanical model. It may avoid harms in patients by preventing the treating physicians to administer inappropriate drugs. Also, one of the advantages the biomechanical modelling approach may confer is related to parameter or state estimation strategies, through which the model can interpret the changes in measured data in terms of changes in physiological quantities.

This PhD thesis is a proof-of-concept of using a complete biomechanical approach, with data measured in patients, in order to augment the cardiovascular monitoring with advanced physiological quantities.

Outlines of the thesis

Our purpose in this PhD thesis is to propose and evaluate a framework, based on biomechanical modelling, to augment monitoring of anaesthetised patients with advanced patient-specific cardiovascular physiological knowledge. To achieve this objective, we had to rigorously overcome several issues related to clinical, biomechanical, and numerical endpoints.

The core of the PhD thesis is organised in four parts, all of which treating a specific issue.

Part I: Physiological background, clinical issues and modelling overview

Since the PhD thesis was performed at the interface between two distinct but interrelated environments (*i.e.* clinical and bioengineering), the purpose of this Part is to bridge these two disciplines. By providing physiological, clinical, and biomechanical overviews of the cardiovascular concepts that are developed in the PhD thesis, Part I allows the reader to link the clinical issues arising from cardiovascular management and the bioengineering methods that may help to solve the clinical problems.

Therefore, this part puts the PhD thesis in the context of haemodynamic management at patients' bed while on general anaesthesia or in critical care wards.

Part II: Estimation of patient-specific left ventricular end-diastolic pressure-volume relationships using a biomechanical heart model

In this Part, we will present and evaluate a method to estimate the parameters of the passive law of the biomechanical model from only limited data measurements. The passive law of our biomechanical model describes the end-diastolic pressure-volume relationship of the left ventricle, which may be impaired during heart failure.

Our passive law is derived from the continuum mechanics theory, in which the stress-strain relationship of a piece of myocardium is described by an hyperelastic potential. Assuming a simplified spherical geometry of the model, with fibres uniformely distributed in the orthoradial plane, Caruel et al. [5] were able to formulate a constitutive law in which the internal pressure of the left ventricle is a function of the fibre extension (e_{fib}), the wall thickness-to-radius ratio at reference configuration (ϵ) of the left ventricle and of the parameters (C_i) of the hyperelastic potential (W_e). We rigorously studied the behaviour of our passive law when deviating from a calibrated reference configuration, and verified that it satisfies the characteristics of end-diastolic pressure-volume relationships in humans described by Klotz et al. [13].

This allowed to reduce the parametric space to 3 parameters – namely C_i, V_{ref} the volume of the left ventricle at reference configuration, and ϵ – which can be estimated from a single measurement of pressure and volume within the left ventricle. We evaluated the performance of our passive law estimation method against the existing phenomenological method described by Klotz et al. [13].

Our approach unites the rigorously derived constitutive law from continuum mechanics theory with practical clinical measurement issues, with a potential for non-invasive clinical applications.

Part III: End-systolic pressure-volume relationship: From time-varying elastance concept to biomechanically-derived time-varying elastance modelling

The time-varying elastance concept was described extensively during the 80's, and is based on a local linearisation of the non-linear end-systolic pressure-volume relationship. From a physiological standpoint, even though this concept is derived from a linear approximation of non-linear phenomena, within physiological ranges, it allows to access information regarding the contractile state of the myocardium, the interaction between the left ventricle and the arteries, and the myocardial energetics expenditure. However, estimating the slope E_{es} and intercept V_0 of this linear approximation is not trivial, and the existing methods suffer from inaccuracy or excessive inter and intra-subjects variability. Furthermore, accurate estimation of V_0 is crucial for estimation of the time-varying elastance function E(t), which can be used as a surrogate of cardiac mechanics for cardiac modelling purposes.

In this part, we will propose and study the performance of a framework based on our biomechanical modelling approach to estimate the components of the time-varying elastance concept E_{es}, V_0 and E(t). We will also describe a time-varying elastance model in which the cardiac mechanics of our biomechanical model will be replaced by the E(t) function, all other components being kept as in the biomechanical model. We will evaluate the adequacy between the time-varying elastance and the biomechanical models when varying external conditions.

Part IV: Application & perspectives: Cardiovascular modelling for haemodynamic monitoring

In this part, we will evaluate the feasibility of using a heart and vessels modelling framework, based on the biomechanical concepts presented in the previous chapters, to char-

acterise the haemodynamic profile of patients while on general anaesthesia for neuroradiological procedures. By calibrating our biomechanical model on echocardiographic data and aortic pressure and cardiac output monitoring signals, we will assess the contractility, the cardiac work and efficiency, and the ventricular-arterial coupling, based on the patient-specific simulated pressure-volume loop. We will further analyse the differences observed between the subgroups of normotensive patients and hypotensive patients, and further evaluate the haemodynamic effect of noradrenaline administration given to restore blood pressure in hypotensive patients, in terms of pressure-volume loop analysis.

By augmenting cardiovascular monitoring of anaesthetised patients with a biomechanical model of heart and vessels, our approach paves the way for further translational works, with the objective to help treating physicians in their clinical decision-making.

Personal contributions

Patents

- Chabiniok, R., Chapelle, D., Le Gall, A., Moireau, P., and Vallée, F. (1758006, France, 2017). Dispositif cardiaque

Peer-reviewed publications

- Le Gall, A., Vallée, F., Pushparajah, K., Hussain, T., Mebazaa, A., Chapelle, D., Gayat, E., and Chabiniok, R. (2020). Monitoring of cardiovascular physiology augmented by a patient-specific biomechanical model during general anesthesia. A proof of concept study. *PLOS ONE*, 15(5):e0232830
- Le Gall, A., Vallée, F., Chapelle, D., and Chabiniok, R. (2019). Minimally-Invasive Estimation of Patient-Specific End-Systolic Elastance Using a Biomechanical Heart Model. In Coudière, Y., Ozenne, V., Vigmond, E., and Zemzemi, N., editors, *Functional Imaging and Modeling of the Heart*, volume 11504, pages 266–275. Springer International Publishing, Cham

Oral presentations

- A. Le Gall, "Minimally-Invasive Estimation of Patient-Specific End-Systolic Elastance Using a Biomechanical Heart Model", *Functional Imaging and Modeling of the Heart* June 2019.
- A. Le Gall, "Monitorage hémodynamique augmenté par un modèle biomécanique de cœur et vaisseaux patient-spécifique", *Société Française d'Anesthésie-Réanimation-Médecine péri-opératoire, le congrès*, 2019

Bibliography

[1] Antonelli, M., Levy, M., Andrews, P. J. D., Chastre, J., Hudson, L. D., Manthous, C., Meduri, G. U., Moreno, R. P., Putensen, C., Stewart, T., and Torres, A. (2007). Hemodynamic monitoring in shock and implications for management: International Consensus Conference, Paris, France, 27–28 April 2006. *Intensive Care Medicine*, 33(4):575–590.

[2] Berg, D. D., Bohula, E. A., van Diepen, S., Katz, J. N., Alviar, C. L., Baird-Zars, V. M., Barnett, C. F., Barsness, G. W., Burke, J. A., Cremer, P. C., Cruz, J., Daniels, L. B., DeFilippis, A. P., Haleem, A., Hollenberg, S. M., Horowitz, J. M., Keller, N., Kontos, M. C., Lawler, P. R., Menon, V., Metkus, T. S., Ng, J., Orgel, R., Overgaard, C. B., Park, J.-G., Phreaner, N., Roswell, R. O., Schulman, S. P., Jeffrey Snell, R., Solomon, M. A., Ternus, B., Tymchak, W., Vikram, F., and Morrow, D. A. (2019). Epidemiology of Shock in Contemporary Cardiac Intensive Care Units: Data From the Critical Care Cardiology Trials Network Registry. *Circulation: Cardiovascular Quality and Outcomes*, 12(3).

[3] Bijker, J. B., Persoon, S., Peelen, L. M., Moons, K. G. M., Kalkman, C. J., Kappelle, L. J., and van Klei, W. A. (2012). Intraoperative hypotension and perioperative ischemic stroke after general surgery: a nested case-control study. *Anesthesiology*, 116(3):658–664.

[4] Bijker, J. B., van Klei, W. A., Vergouwe, Y., Eleveld, D. J., van Wolfswinkel, L., Moons, K. G. M., and Kalkman, C. J. (2009). Intraoperative Hypotension and 1-Year Mortality after Noncardiac Surgery:. *Anesthesiology*, 111(6):1217–1226.

[5] Caruel, M., Chabiniok, R., Moireau, P., Lecarpentier, Y., and Chapelle, D. (2014). Dimensional reductions of a cardiac model for effective validation and calibration. *Biomechanics and Modeling in Mechanobiology*, 13(4):897–914.

[6] Chabiniok, R., Chapelle, D., Le Gall, A., Moireau, P., and Vallée, F. (1758006, France, 2017). Dispositif cardiaque.

[7] Chabiniok, R., Moireau, P., Lesault, P.-F., Rahmouni, A., Deux, J.-F., and Chapelle, D. (2012). Estimation of tissue contractility from cardiac cine-MRI using a biomechanical heart model. *Biomechanics and modeling in mechanobiology*, 11(5):609–630.

[8] Chabiniok, R., Wang, V. Y., Hadjicharalambous, M., Asner, L., Lee, J., Sermesant, M., Kuhl, E., Young, A. A., Moireau, P., Nash, M. P., Chapelle, D., and Nordsletten, D. A. (2016). Multiphysics and multiscale modelling, data–model fusion and integration of organ physiology in the clinic: ventricular cardiac mechanics. *Interface Focus*, 6(2):20150083.

[9] Chapelle, D., Felder, A., Chabiniok, R., Guellich, A., Deux, J.-F., and Damy, T. (2015). Patient-Specific Biomechanical Modeling of Cardiac Amyloidosis – A Case Study. In van Assen, H., Bovendeerd, P., and Delhaas, T., editors, *Functional Imaging and Modeling of the Heart*, volume 9126, pages 295–303. Springer International Publishing, Cham. Series Title: Lecture Notes in Computer Science.

[10] Chapelle, D., Le Tallec, P., Moireau, P., and Sorine, M. (2012). Energy-preserving muscle tissue model: formulation and compatible discretizations. *International Journal for Multiscale Computational Engineering*, 10(2).

[11] Fleisher, L. A., Beckman, J. A., Brown, K. A., Calkins, H., Chaikof, E. L., Fleischmann, K. E., Freeman, W. K., Froehlich, J. B., Kasper, E. K., Kersten, J. R., Riegel, B., and Robb, J. F. (2007). ACC/AHA 2007 Guidelines on Perioperative Cardiovascular Evaluation and Care for Noncardiac Surgery: Executive Summary: A Report of the American College of Cardiology/American Heart Association Task Force on Practice Guidelines (Writing Committee to Revise the 2002 Guidelines on Perioperative Cardiovascular Evaluation for Noncardiac Surgery). *Circulation*, 116(17):1971–1996.

[12] Hatib, F. and Sibert, K. (2018). Machine-learning Algorithm to Predict Hypotension Based on High-fidelity Arterial Pressure Waveform Analysis. *PERIOPERATIVE MEDICINE*, page 12.

[13] Klotz, S., Hay, I., Dickstein, M. L., Yi, G.-H., Wang, J., Maurer, M. S., Kass, D. A., and Burkhoff, D. (2006). Single-beat estimation of end-diastolic pressure-volume relationship: a novel method with potential for noninvasive application. *AJP: Heart and Circulatory Physiology*, 291(1):H403–H412.

[14] Le Gall, A., Vallée, F., Chapelle, D., and Chabiniok, R. (2019). Minimally-Invasive Estimation of Patient-Specific End-Systolic Elastance Using a Biomechanical Heart Model. In Coudière, Y., Ozenne, V., Vigmond, E., and Zemzemi, N., editors, *Functional Imaging and Modeling of the Heart*, volume 11504, pages 266–275. Springer International Publishing, Cham.

[15] Le Gall, A., Vallée, F., Pushparajah, K., Hussain, T., Mebazaa, A., Chapelle, D., Gayat, E., and Chabiniok, R. (2020). Monitoring of cardiovascular physiology augmented by a patient-specific biomechanical model during general anesthesia. A proof of concept study. *PLOS ONE*, 15(5):e0232830.

[16] Lienhart, A., Auroy, Y., Péquignot, F., Benhamou, D., Warszawski, J., Bovet, M., and Jougla, E. (2006). Survey of anesthesia-related mortality in France. *Anesthesiology*, 105(6):1087–1097.

[17] Pirracchio, R., Petersen, M. L., Carone, M., Rigon, M. R., Chevret, S., and van der Laan, M. J. (2015). Mortality prediction in intensive care units with the Super ICU Learner Algorithm (SICULA): a population-based study. *The Lancet Respiratory Medicine*, 3(1):42–52.

[18] Powell-Tuck, J., Allison, S. P., Carlson, G. L., Lewington, A. J., and Pearse, R. M. (2011). British Consensus Guidelines on Intravenous Fluid Therapy for Adult Surgical Patients. British Guidelines on IV fluids.

[19] Rhodes, A., Evans, L. E., Alhazzani, W., Levy, M. M., Antonelli, M., Ferrer, R., Kumar, A., Sevransky, J. E., Sprung, C. L., Nunnally, M. E., Rochwerg, B., Rubenfeld, G. D., Angus, D. C., Annane, D., Beale, R. J., Bellinghan, G. J., Bernard, G. R., Chiche, J.-D., Coopersmith, C., De Backer, D. P., French, C. J., Fujishima, S., Gerlach, H., Hidalgo, J. L., Hollenberg, S. M., Jones, A. E., Karnad, D. R., Kleinpell, R. M., Koh, Y., Lisboa, T. C., Machado, F. R., Marini, J. J., Marshall, J. C., Mazuski, J. E., McIntyre, L. A., McLean, A. S., Mehta, S., Moreno, R. P., Myburgh, J., Navalesi, P., Nishida, O., Osborn, T. M., Perner, A., Plunkett, C. M., Ranieri, M., Schorr, C. A., Seckel, M. A., Seymour, C. W., Shieh, L., Shukri, K. A., Simpson, S. Q., Singer, M., Thompson, B. T., Townsend, S. R., Van der Poll, T., Vincent, J.-L., Wiersinga, W. J., Zimmerman, J. L., and Dellinger, R. P. (2017). Surviving Sepsis Campaign: International Guidelines for Management of Sepsis and Septic Shock: 2016. *Intensive Care Medicine*, 43(3):304–377.

[20] Sermesant, M., Chabiniok, R., Chinchapatnam, P., Mansi, T., Billet, F., Moireau, P., Peyrat, J., Wong, K., Relan, J., Rhode, K., Ginks, M., Lambiase, P., Delingette, H., Sorine, M., Rinaldi, C., Chapelle, D., Razavi, R., and Ayache, N. (2012). Patient-specific electromechanical models of the heart for the prediction of pacing acute effects in CRT: A preliminary clinical validation. *Medical Image Analysis*, 16(1):201–215.

[21] Sessler, D. I., Sigl, J. C., Kelley, S. D., Chamoun, N. G., Manberg, P. J., Saager, L., Kurz, A., and Greenwald, S. (2012). Hospital Stay and Mortality Are Increased in Patients Having a "Triple Low" of Low Blood Pressure, Low Bispectral Index, and Low Minimum Alveolar Concentration of Volatile Anesthesia:. *Anesthesiology*, 116(6):1195–1203.

[22] Sun, L. Y., Wijeysundera, D. N., Tait, G. A., and Beattie, W. S. (2015). Association of intraoperative hypotension with acute kidney injury after elective noncardiac surgery. *The Journal of the American Society of Anesthesiologists*, 123(3):515–523.

[23] Yoon, J. H., Jeanselme, V., Dubrawski, A., Hravnak, M., Pinsky, M. R., and Clermont, G. (2020). Prediction of hypotension events with physiologic vital sign signatures in the intensive care unit. *Critical Care*, 24(1):661.

Introduction (Français)

Contexte de la thèse

L'anesthésie-réanimation est une spécialité complexe dont le but est de rendre possible le traitement chirurgical en garantissant l'intégrité physique et mentale des patients qui doivent bénéficier d'une intervention invasive, ou souffrant d'une maladie relevant d'une prise en charge en unité de soins critiques. Le rôle des anesthésistes-réanimateurs débute bien avant l'opération, afin d'anticiper les potentielles difficultés associées 1/ aux antécédents médicaux du patients ; 2/ aux interactions entre les traitements réguliers du patient et la chirurgie et ; 3/ la procédure chirurgicale en elle même. Pendant la période pré-opératoire, l'anesthésiste-réanimateur doit engager tous les moyens diagnostiques (par exemple en organisant une coronarographie afin d'évaluer le risque ischémique d'une éventuelle maladie coronarienne) et thérapeutiques (par exemple en organisant l'interruption d'un éventuel traitement anticoagulant pris par le patient de façon régulière) pour décroître les risques liés à cette interaction patient-chirurgie. La procédure anesthésique et la prise en charge post-opératoire sont aussi planifiées durant cette évaluation pré-opératoire. De l'autre côté, en secteur de soins critique, l'anesthésiste-réanimateur est impliqué dans toutes les pathologies qui sont associées de façon directe ou indirecte avec la survie du patient, telles que les états de choc, le polytraumatisme, la rupture d'anévrysme intracrânien etc...

Pour toutes ces raisons, les anesthésistes-réanimateurs sont impliqués dans la prise en charge cardiovasculaire des patients dont ils ont la charge. Une enquête conduite en France au début des années 2000 à étudié la mortalité per-opératoire des patients. Dans 2/3 des cas, le décès per-opératoire était survenu pour des raisons cardiovasculaire [16]. De plus, les hypotensions per-opératoires ont été associées à une augmentation de la morbi-mortalité post-opératoire [21 ; 22 ; 3 ; 4]. Les états de choc, qui sont une défaillance cardio-circulatoire aiguë suffisamment sévère pour pérenniser une dysfonction d'organe est aussi un motif fréquent d'admission en unité de soins critiques. Des études épidémiologiques évaluent l'incidence des états de choc de 6 à 24% des admissions en réanimation [1 ; 2]

La gestion hémodynamique des patients est une tâche difficile, et les anesthésistes-réanimateurs doivent y être entraînés. Pour cela, des recommandations internationales préconisent l'utilisation d'un monitorage hémodynamique afin de diagnostiquer des situations hémodynamiques complexes, ou d'évaluer l'efficacité des thérapeutiques mises en œuvre [18 ; 11 ; 19]. Un monitorage idéal devrait être précis, réactif, sûr, non-invasif, reproductible, fiable, facile d'utilisation, et doit répondre à une question clinique prédéfinie. À ce jour, aucun monitorage ne réunit toutes ces caractéristiques, et le choix doit être fait par le médecin traitant selon les enjeux hémodynamiques particuliers associés à l'interaction patient-chirurgie identifié en pré-opératoire. En réalité, le monitorage hémodynamique le plus complet, le cathétérisme ventriculaire gauche, n'est jamais utilisé en pratique clinique courante en anesthésie-réanimation, car le cathétérisme cardiaque gauche nécessite une procédure invasive de mesure intra-ventriculaire de la pression et du volume réalisée uniquement par les cardiologues en salle de cathétérisme. Le cathétérisme gauche permet de dessiner des boucles pression-volume (PV) elles-mêmes permettant de donner des informations sur la consommation énergétique du myocarde, ou sur l'interaction entre le cœur et les vaisseaux.

La modélisation est une discipline permettant de décrire des phénomènes observables en termes mathématiques. En sciences médicales, la statistique est probablement l'approche la plus utilisée. Cet outil permet d'apporter des preuves aux pratiques médicales, quand la statistique est utilisée dans le contexte de la recherche clinique. La médecine personnalisée utilisant des méthodes d'apprentissage statistique diffuse actuellement dans la communauté médicale pour améliorer les soins aux patients [12 ; 17 ; 23]. La modélisation

biomécanique est une autre approche, fondée sur la mécanique des milieux continus, décrivant la structure et le mouvement de matériaux vivants. La modélisation biomécanique peut aider à récupérer des informations physiologiques qui sont souvent inaccessibles à la mesure, soit car la mesure est inexistante ou irréalisable, soit car la procédure de mesure est trop invasive. Quand le modèle est calibré sur les données du patient en ajustant les paramètres du modèle sur les données patient disponibles, les résultats des simulations peuvent représenter la physiologie réelle du patient (concept du jumeau numerique) [7 ; 20 ; 9 ; 8]. Par exemple, si un modèle approprié est utilisé, la quantification de la contractilité peut être accessible pour l'anesthésiste-réanimateur traitant. Afin d'être cliniquement efficient et utile pour les cliniciens, la modélisation cardiovasculaire doit idéalement être compréhensible pour les communautés médicales, facile à calibrer, les résultats doivent être accessibles rapidement, avec des ressources informatiques raisonnables, et doit pouvoir répondre à une (au moins) question clinique. Ainsi, le choix du modèle est un enjeu important de la modélisation cardiovasculaire. Nous pensons que la modélisation biomécanique est l'approche la plus adaptée pour représenter la physiologie cardiovasculaire des patients. Cette approche est fondée sur la description physique de phénomènes microscopiques (comme la formation/destruction des ponts d'actine-myosine), eux mêmes intégrés sur une échelle macroscopique correspondant à l'organe simulé. Le mouvement du cœur battant (la cinématique) est liée aux grandeurs physiques associés à la déformation (la dynamique) par des lois de comportements. Ce type de modèle est en général difficile à calibrer car cela nécessite des données patients détaillées et riches qui ne sont, le plus souvent, pas accessibles en pratique clinique courante. Nous avons développé une formulation réduite [5] d'un modèle biomécanique complet de cœur et vaisseaux [10], qui permet de diminuer les coûts de calculs et de simplifier la procédure de calibration. Ce modèle réduit permet d'introduire la modélisation cardiovasculaire biomécanique auprès de l'environnement clinique, spécialement pour l'anesthésie et réanimation.

Le potentiel de la modélisation biomécanique cardiovasculaire n'est pas uniquement de révéler des grandeur physiologiques inaccessibles à la mesure. D'ailleurs, ces informations peuvent être anticipées par les médecins anesthésistes-réanimateurs traitants quand ils mesurent des données cardiovasculaires chez les patients, ou quand ils pratiquent des épreuves thérapeutiques. En effet, la simulation des effets des thérapeutiques candidates au traitement des patients est une fonctionnalité qui pourrait être implémentée dans le cadre de l'utilisation de modèles biomécaniques de coeur et vaisseaux. Cela pourrait ainsi alerter le médecin sur les effets potentiellement délétères ou bénéfiques d'un médicament qu'il souhaitait administrer. Un autre avantage que la modélisation cardiovasculaire biomécanique pourrait conférer est liée aux méthodes d'estimation d'états ou de paramètres, pour lesquelles le model interprète les changements dans les données mesurées, dont il se nourrit en continu, en termes de changements de grandeurs physiologiques.

Cette thèse est une preuve de concept de l'utilisation d'une approche basée sur un modèle biomécanique complet de coeur et vaisseaux, qui, couplée aux mesures physiologiques continues enregistrées durant une anesthésie générale, a le potentiel d'être adaptée en pratique clinique, dans le but d'augmenter le monitorage cardiovasculaire avec des simulations de physiologies avancées (comme des boucles pression-volume), qui sont usuellement inaccessible à la mesure.

Plan de la thèse

Le but de ce travail de thèse est de proposer et d'évaluer une méthode, basée sur la modélisation biomécanique, pour augmenter le monitorage cardiovasculaire des patients sous anesthésie générale, avec une connaissance physiologique cardiovasculaire avancée.

Pour atteindre cet objectif, nous avons dû surmonter certaines problématiques cliniques, biomécaniques et numériques.

Le cœur de cette thèse est organisée en 4 parties, toutes développant un aspect spécifique.

Partie I : Contexte physiologique, enjeux cliniques et approche de modélisation biomécanique

Puisque cette thèse a été effectuée à l'interface entre deux environnements distincts mais interconnectés (*c.à.d* clinique et bioingénierie), l'objectif de la présente partie est de mettre en relation ces deux disciplines. En apportant le contexte physiologique, et les enjeux biomécaniques du système cardiovasculaire développés dans la présente thèse, la Partie I amène le lecteur à faire le lien entre les problématiques cliniques issues de la gestion cardiovasculaire des patients, et les méthodes de modélisation biomécaniques permettant d'aider à résoudre certaines de ces problématiques.

Ainsi, cette partie replace la thèse en perspective de la gestion hémodynamique appliquée au lit des patients sous anesthésie générale ou admis en secteur de soins critiques

Partie II : Estimation patient-spécifique de la relation pression-volume ventriculaire en télédiastole au moyen d'un modèle biomécanique de cœur et vaisseaux

Dans cette Partie, nous présenterons et évaluerons une méthode d'estimation des paramètres de la loi de comportement passive du coeur utilisée dans notre modèle biomécanique de coeur et vaisseaux, à partir d'une quantité/richesse limitée de données patients mesurées. La loi passive de notre modèle décrit la relation pression-volume en télédiastole du ventricule gauche, qui peut être altérée au cours de l'insuffisance cardiaque avec fraction d'éjection préservée (ICpFEVG), par exemple.

Notre loi passive est issue de la mécanique des milieux continus, dans laquelle les relation force-déplacements d'un petit échantillon de tissu myocardique est décrite par un potentiel hyperélastique. En supposant une géométrie simplifiée sphérique du modèle, avec des fibres myocardiques distribuées uniformément dans le plan orthoradial, Caruel et al. [5] ont réussi à formuler une loi de comportement dans laquelle la pression interne ventricule gauche était une fonction non-linéaire dépendant du niveau d'extension des fibres (e_{fib}), du ratio entre l'épaisseur du myocarde et le diamètre interne du ventricule en configuration de référence (ϵ), et des paramètres (C_i) du potentiel hyperélastique (W_e). De façon rigoureuse, nous avons étudié le comportement de cette loi passive quand des déviations à partir d'une calibration originale ont été appliquées, et nous avons vérifié que les caractéristiques physiologiques de la relation pression-volume ventriculaire en télédiastole décrites chez les humains [13] étaient respectées .

Cette étude rigoureuse, nous a permis de réduire l'espace paramétrique de la loi passive au nombre de 3 – C_i, V_{ref} le volume du ventricule gauche en configuration de référence et ϵ– eux même pouvant être estimés à partir d'un seul point de mesure de la pression et du volume ventriculaire. Nous évaluerons la performance de notre méthode contre une autre méthode existante, décrite par Klotz et al. [13].

Notre approche permet de réunir la méthode rigoureuse biomécanique de description de la loi de comportement en diastole du ventricule gauche, avec les contraintes cliniques de disponibilité des mesures pour calibrer cette loi passive, avec un potentiel pour une utilisation non-invasive.

Partie III : Relation pression-volume en télésystole : Du concept d'élastance variable au modèle d'élastance variable dérivé du modèle biomécanique

Le concept d'élastance variable dans le temps a été étudié en détail dans les années 80, et est basé sur une linéarisation locale de la relation non-linéaire entre la pression et le volume intra-ventriculaire en fin de systole, ou télésystole. D'un point de vue physiologique, même si le concept repose sur l'approximation linéaire d'un phénomène non-linéaire, dans une fourchette de valeur observable en physiologie, il permet d'accéder à des informations concernant l'état contractile du myocarde, l'interaction entre le ventricule gauche et le système artériel et la dépense énergétique du myocarde. Cependant, l'estimation de la pente E_{es} et de l'intersection V_0 de cette approximation linéaire n'est pas triviale, et les méthodes existantes souffrent d'une imprécision ou d'une variabilité intra- et/ou inter-individuelle importante. En modélisation, une estimation précise de V_0 est importante pour l'estimation de la fonction d'élastance variable E(t), qui pourra être alors utilisée en lieu et place des modèles de mécanique cardiaque.

Dans cette partie, nous proposerons et étudierons les performances d'une méthode, basée sur notre approche biomécanique, permettant d'estimer les composants E_{es} et V_0 du concept d'élastance variable ainsi que sa fonction E(t). Nous décrirons également un modèle d'élastance variable dans lequel la mécanique cardiaque de notre modèle biomécanique sera remplacée par la fonction E(t), tous les autres composants du modèle biomécanique étant maintenus par ailleurs. Nous évaluerons l'adéquation entre les modèles biomécanique et d'élastance variable lors d'experimentations *in silico*, dans lesquels nous ferons varier les conditions externes à la mécanique cardiaque.

Part IV : Application & perspectives : Modélisation cardiovasculaire pour le monitorage hémodynamique des patients sous anesthésie générale

Dans cette partie, nous évaluerons la faisabilité de l'utilisation d'un modèle biomécanique de cœur et vaisseaux, basé sur les concepts biomécaniques présentés dans les chapitres précédents, afin de caractériser le profil hémodynamique des patients sous anesthésie générale pour des procédures de neuroradiologie interventionnelle. En calibrant notre modèle biomécanique sur les données échocardiographiques et les données continues de pression artérielle et de débit cardiaque mesurées chez nos patients, nous évaluerons la contractilité, le travail myocardique et l'efficience cardiaque, ainsi que le couplage ventriculo-aortique, à partir de simulations patient-spécifiques de boucles pression-volume ventriculaire. Nous analyserons également les différences observées entre le sous-groupe de patients ayant présenté ou n'ayant pas présenté une hypotension artérielle. Nous analyserons également ces boucles pressions-volumes simulées lors des modifications induites par l'administration de Noradrénaline utilisée pour restaurer la pression artérielle.

En augmentant le monitorage cardiovasculaire des patients sous anesthésie générale au moyen d'un modèle biomécanique de coeur et vaisseaux, notre approche permet d'envisager de présenter une aide à la décision clinique. Des travaux translationnels futurs devront confirmer nos résultats.

Contributions personnelles

Brevets

- Chabiniok, R., Chapelle, D., Le Gall, A., Moireau, P., and Vallée, F. (1758006, France, 2017). Dispositif cardiaque

Publications

- Le Gall, A., Vallée, F., Pushparajah, K., Hussain, T., Mebazaa, A., Chapelle, D., Gayat, E., and Chabiniok, R. (2020). Monitoring of cardiovascular physiology augmented by a patient-specific biomechanical model during general anesthesia. A proof of concept study. *PLOS ONE*, 15(5) :e0232830

- Le Gall, A., Vallée, F., Chapelle, D., and Chabiniok, R. (2019). Minimally-Invasive Estimation of Patient-Specific End-Systolic Elastance Using a Biomechanical Heart Model. In Coudière, Y., Ozenne, V., Vigmond, E., and Zemzemi, N., editors, *Functional Imaging and Modeling of the Heart*, volume 11504, pages 266–275. Springer International Publishing, Cham

Présentations orales

- A. Le Gall, "Minimally-Invasive Estimation of Patient-Specific End-Systolic Elastance Using a Biomechanical Heart Model", *Functional Imaging and Modeling of the Heart* June 2019.

- A. Le Gall, "Monitorage hémodynamique augmenté par un modèle biomécanique de cœur et vaisseaux patient-spécifique", *Société Française d'Anesthésie-Réanimation-Médecine péri-opératoire, le congrès*, 2019

Bibliographie

[1] Antonelli, M., Levy, M., Andrews, P. J. D., Chastre, J., Hudson, L. D., Manthous, C., Meduri, G. U., Moreno, R. P., Putensen, C., Stewart, T., and Torres, A. (2007). Hemodynamic monitoring in shock and implications for management : International Consensus Conference, Paris, France, 27–28 April 2006. *Intensive Care Medicine*, 33(4) :575–590.

[2] Berg, D. D., Bohula, E. A., van Diepen, S., Katz, J. N., Alviar, C. L., Baird-Zars, V. M., Barnett, C. F., Barsness, G. W., Burke, J. A., Cremer, P. C., Cruz, J., Daniels, L. B., DeFilippis, A. P., Haleem, A., Hollenberg, S. M., Horowitz, J. M., Keller, N., Kontos, M. C., Lawler, P. R., Menon, V., Metkus, T. S., Ng, J., Orgel, R., Overgaard, C. B., Park, J.-G., Phreaner, N., Roswell, R. O., Schulman, S. P., Jeffrey Snell, R., Solomon, M. A., Ternus, B., Tymchak, W., Vikram, F., and Morrow, D. A. (2019). Epidemiology of Shock in Contemporary Cardiac Intensive Care Units : Data From the Critical Care Cardiology Trials Network Registry. *Circulation : Cardiovascular Quality and Outcomes*, 12(3).

[3] Bijker, J. B., Persoon, S., Peelen, L. M., Moons, K. G. M., Kalkman, C. J., Kappelle, L. J., and van Klei, W. A. (2012). Intraoperative hypotension and perioperative ischemic stroke after general surgery : a nested case-control study. *Anesthesiology*, 116(3) :658–664.

[4] Bijker, J. B., van Klei, W. A., Vergouwe, Y., Eleveld, D. J., van Wolfswinkel, L., Moons, K. G. M., and Kalkman, C. J. (2009). Intraoperative Hypotension and 1-Year Mortality after Noncardiac Surgery :. *Anesthesiology*, 111(6) :1217–1226.

[5] Caruel, M., Chabiniok, R., Moireau, P., Lecarpentier, Y., and Chapelle, D. (2014). Dimensional reductions of a cardiac model for effective validation and calibration. *Biomechanics and Modeling in Mechanobiology*, 13(4) :897–914.

[6] Chabiniok, R., Chapelle, D., Le Gall, A., Moireau, P., and Vallée, F. (1758006, France, 2017). Dispositif cardiaque.

[7] Chabiniok, R., Moireau, P., Lesault, P.-F., Rahmouni, A., Deux, J.-F., and Chapelle, D. (2012). Estimation of tissue contractility from cardiac cine-MRI using a biomechanical heart model. *Biomechanics and modeling in mechanobiology*, 11(5) :609–630.

[8] Chabiniok, R., Wang, V. Y., Hadjicharalambous, M., Asner, L., Lee, J., Sermesant, M., Kuhl, E., Young, A. A., Moireau, P., Nash, M. P., Chapelle, D., and Nordsletten, D. A. (2016). Multiphysics and multiscale modelling, data–model fusion and integration of organ physiology in the clinic : ventricular cardiac mechanics. *Interface Focus*, 6(2) :20150083.

[9] Chapelle, D., Felder, A., Chabiniok, R., Guellich, A., Deux, J.-F., and Damy, T. (2015). Patient-Specific Biomechanical Modeling of Cardiac Amyloidosis – A Case Study. In van Assen, H., Bovendeerd, P., and Delhaas, T., editors, *Functional Imaging and Modeling of the Heart*, volume 9126, pages 295–303. Springer International Publishing, Cham. Series Title : Lecture Notes in Computer Science.

[10] Chapelle, D., Le Tallec, P., Moireau, P., and Sorine, M. (2012). Energy-preserving muscle tissue model : formulation and compatible discretizations. *International Journal for Multiscale Computational Engineering*, 10(2).

[11] Fleisher, L. A., Beckman, J. A., Brown, K. A., Calkins, H., Chaikof, E. L., Fleischmann, K. E., Freeman, W. K., Froehlich, J. B., Kasper, E. K., Kersten, J. R., Riegel, B., and Robb, J. F. (2007). ACC/AHA 2007 Guidelines on Perioperative Cardiovascular Evaluation and Care for Noncardiac Surgery : Executive Summary : A Report of the American College of Cardiology/American Heart Association Task Force on Practice Guidelines (Writing Committee to Revise the 2002 Guidelines on Perioperative Cardiovascular Evaluation for Noncardiac Surgery). *Circulation*, 116(17) :1971–1996.

[12] Hatib, F. and Sibert, K. (2018). Machine-learning Algorithm to Predict Hypotension Based on High-fidelity Arterial Pressure Waveform Analysis. *PERIOPERATIVE MEDICINE*, page 12.

[13] Klotz, S., Hay, I., Dickstein, M. L., Yi, G.-H., Wang, J., Maurer, M. S., Kass, D. A., and Burkhoff, D. (2006). Single-beat estimation of end-diastolic pressure-volume relationship : a novel method with potential for noninvasive application. *AJP : Heart and Circulatory Physiology*, 291(1) :H403–H412.

[14] Le Gall, A., Vallée, F., Chapelle, D., and Chabiniok, R. (2019). Minimally-Invasive Estimation of Patient-Specific End-Systolic Elastance Using a Biomechanical Heart Model. In Coudière, Y., Ozenne, V., Vigmond, E., and Zemzemi, N., editors, *Functional Imaging and Modeling of the Heart*, volume 11504, pages 266–275. Springer International Publishing, Cham.

[15] Le Gall, A., Vallée, F., Pushparajah, K., Hussain, T., Mebazaa, A., Chapelle, D., Gayat, E., and Chabiniok, R. (2020). Monitoring of cardiovascular physiology augmented by a patient-specific biomechanical model during general anesthesia. A proof of concept study. *PLOS ONE*, 15(5) :e0232830.

[16] Lienhart, A., Auroy, Y., Péquignot, F., Benhamou, D., Warszawski, J., Bovet, M., and Jougla, E. (2006). Survey of anesthesia-related mortality in France. *Anesthesiology*, 105(6) :1087–1097.

[17] Pirracchio, R., Petersen, M. L., Carone, M., Rigon, M. R., Chevret, S., and van der Laan, M. J. (2015). Mortality prediction in intensive care units with the Super ICU Learner Algorithm (SICULA) : a population-based study. *The Lancet Respiratory Medicine*, 3(1) :42–52.

[18] Powell-Tuck, J., Allison, S. P., Carlson, G. L., Lewington, A. J., and Pearse, R. M. (2011). British Consensus Guidelines on Intravenous Fluid Therapy for Adult Surgical Patients. British Guidelines on IV fluids.

[19] Rhodes, A., Evans, L. E., Alhazzani, W., Levy, M. M., Antonelli, M., Ferrer, R., Kumar, A., Sevransky, J. E., Sprung, C. L., Nunnally, M. E., Rochwerg, B., Rubenfeld, G. D., Angus, D. C., Annane, D., Beale, R. J., Bellinghan, G. J., Bernard, G. R., Chiche, J.-D., Coopersmith, C., De Backer, D. P., French, C. J., Fujishima, S., Gerlach, H., Hidalgo, J. L., Hollenberg, S. M., Jones, A. E., Karnad, D. R., Kleinpell, R. M., Koh, Y., Lisboa, T. C., Machado, F. R., Marini, J. J., Marshall, J. C., Mazuski, J. E., McIntyre, L. A., McLean, A. S., Mehta, S., Moreno, R. P., Myburgh, J., Navalesi, P., Nishida, O., Osborn, T. M., Perner, A., Plunkett, C. M., Ranieri, M., Schorr, C. A., Seckel, M. A., Seymour, C. W., Shieh, L., Shukri, K. A., Simpson, S. Q., Singer, M., Thompson, B. T., Townsend, S. R., Van der Poll, T., Vincent, J.-L., Wiersinga, W. J., Zimmerman, J. L., and Dellinger, R. P. (2017). Surviving Sepsis Campaign : International Guidelines for Management of Sepsis and Septic Shock : 2016. *Intensive Care Medicine*, 43(3) :304–377.

[20] Sermesant, M., Chabiniok, R., Chinchapatnam, P., Mansi, T., Billet, F., Moireau, P., Peyrat, J., Wong, K., Relan, J., Rhode, K., Ginks, M., Lambiase, P., Delingette, H., Sorine, M., Rinaldi, C., Chapelle, D., Razavi, R., and Ayache, N. (2012). Patient-specific electromechanical models of the heart for the prediction of pacing acute effects in CRT : A preliminary clinical validation. *Medical Image Analysis*, 16(1) :201–215.

[21] Sessler, D. I., Sigl, J. C., Kelley, S. D., Chamoun, N. G., Manberg, P. J., Saager, L., Kurz, A., and Greenwald, S. (2012). Hospital Stay and Mortality Are Increased in Patients Having a “Triple Low” of Low Blood Pressure, Low Bispectral Index, and Low Minimum Alveolar Concentration of Volatile Anesthesia :. *Anesthesiology*, 116(6) :1195–1203.

[22] Sun, L. Y., Wijeysundera, D. N., Tait, G. A., and Beattie, W. S. (2015). Association of intraoperative hypotension with acute kidney injury after elective noncardiac surgery. *The Journal of the American Society of Anesthesiologists*, 123(3) :515–523.

[23] Yoon, J. H., Jeanselme, V., Dubrawski, A., Hravnak, M., Pinsky, M. R., and Clermont, G. (2020). Prediction of hypotension events with physiologic vital sign signatures in the intensive care unit. *Critical Care*, 24(1) :661.

Part I

Physiological knowledge, clinical issues, and modelling overview

CHAPTER 1

Physiological knowledge, clinical issues, and modelling overview

In the present Chapter, we will review the theoretical concepts of the cardiac physiology, the principles of cardiovascular biomechanical modelling, the clinical issues for the anaesthetists and the intensivists and the issues related to haemodynamic monitoring. We present herein the rationale for the need of an improvement of haemodynamic monitoring, and propose to use a biomechanical model of heart and vessels to solve for this endpoint. The biomechanical model used in this PhD thesis is also presented in this Chapter, along with the data measurement protocol. The operational calibration procedure by which we turn the biomechanical framework into patient-specific regime is also presented in the present Chapter.

Since this thesis stands at the interface between medicine, physiology, physics, biomechanics and modelling, the purpose of this chapter is to provide to the reader the minimal background necessary for the understanding of the whole manuscript. In this chapter, from a clinical perspective, an overview of cardiovascular physiology is provided, from molecular mechanism of cardiac contraction to a complex interpretation of pressure-volume relationship. The specific issues of cardiovascular medicine for the anaesthetists and for the intensivists are also treated. From the description of haemodynamic failure the anaesthetists and the intensivists have to face, we will bring the reader to discover the available diagnostic and monitoring methods, along with their respective limitations, which allow to emphasise the helpful information for clinical decision-making.

We will discuss how mathematical modelling may help to fill the gap between imprecise or harmful diagnostic or monitoring methods and potentially helpful information which could help to improve patient's management. In a more specific sense, through simple example, we will present how mathematical modelling may help to optimise the benefit risk balance of the diagnostic strategy, by limiting the invasiveness of the explorations or by improving the accuracy of the measurement. We will give a global overview of cardiovascular modelling before digging deeper in the biomechanical heart and vessel model used in the thesis.

1.1 Cardiovascular Physiology

The aim of this Section is to provide a global overview of the cardiovascular physiology, necessary for the understanding of our modelling approach. Details for cardiac physiology can be found in various publications [42; 24; 92].

The cardiovascular physiology is typically described by the concepts of preload, afterload and cardiac physiology. The preload designates all the phenomena that bring the heart to a pre-contraction state. It includes the venous return, the cardiac rhythm, the heart lung interaction, the right - left ventricles interdependency, and the diastolic function of the heart. The afterload designates all the phenomena which are opposed to the heart during ejection of blood. It is mainly composed by vascular mechanisms, and intrathoracic conditions. The cardiac physiology is described by its molecular to organ level physiology, from cross bridges formation to ejection of blood through valves. The cardiovascular physiology is synchronised through electrical activity, paced by specific myocardial cells, and is regulated by the neuro-humoral sympathetic pathway.

1.1.1 Electrical activation of the myocardium

The cardiac cells are polarised with positive charge outside the cellular membrane and negative charge inside the cell. The electrical depolarisation field necessary for induction of cardiac contraction is mediated through specific cardiac cells which exert excitatory and conductive properties. The pacemaker cells of the sinus node located in the right atrium demonstrated a self-excitatory behaviour. A slow sodium and calcium intakes occur passively, decreasing slowly the resting potential from around -55 millivolts to a threshold (around -40 millivolts) that triggers the opening of the rapid sodium channels (see Figure 1.1). A transient inversion of pacemaker cell polarity occurs and spreads along the fast conductive tissue (*i.e.* the anterior, middle, and posterior internodal pathways composed by Purkinje-like cells – See Figure 1.2) of the atrium (at a speed velocity up to 1 $m.s^{-1}$).

The conduction is slowed down in the atrio-ventricular node (AV-node), located on the fibrous tissue between the atrio-ventricular valves (mitral and tricuspid – Figure 1.2).

The cells of the A-V node demonstrated greater resistance to the ion transfer than the other conductive cells in the heart, because of a reduced number of gap junctions. Special Purkinje fibres lead from the A-V node through the A-V bundle into the ventricles. They transmit action potentials at a velocity of 1.5 to 4.0 $m.s^{-1}$. This conductive pathways allow synchrony of the cardiac contraction. The action potential which spreads along the conductive tissue is also transmitted to cardiac muscle cells but at a speed velocity around 0.3 to 0.5 $m.s^{-1}$.

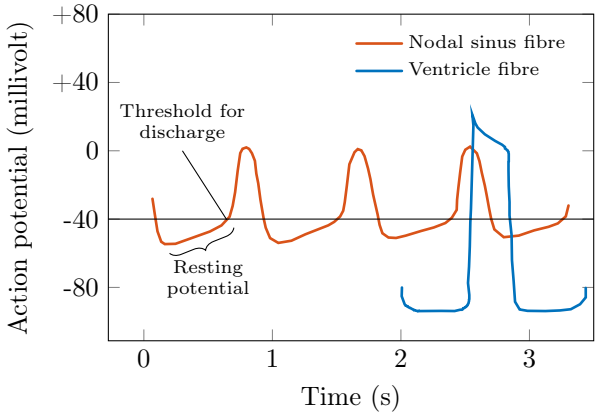

Figure 1.1 – Rhythmical discharge of a sinus nodal fiber. Also, the sinus nodal action potential is compared with that of a ventricular muscle fiber. *Reproduced from Hall [42]*

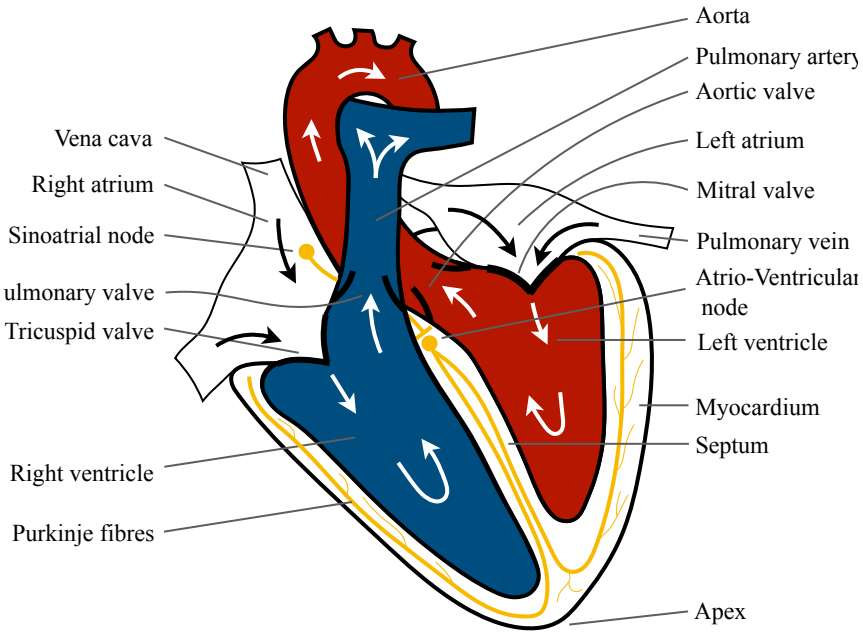

Figure 1.2 – Sinus node and the Purkinje system of the heart, showing also the A-V node, and ventricular bundle branches. *Reproduced from Kimmig et al. [55] with permission*

1.1.2 Excitation-contraction coupling

The mechanisms involved in the excitation-contraction coupling of the cardiac muscle shares similarity with the skeletal muscle, and is closely related to calcium homeostasis.

The cardiac muscle is organised as a syncytium. The unitary cells, are separated by intercalated disks (see Figure 1.3). Cells are arranged as filaments, and contained myofibrils of actin and myosin, in a contractile unit called the sarcomere. The cellular membrane is organised in fold, which penetrates deeply inside the muscle, called the transverse tubule or T tubule. Another important component of the excitation-contraction coupling is represented by the sarcoplasmic reticulum.

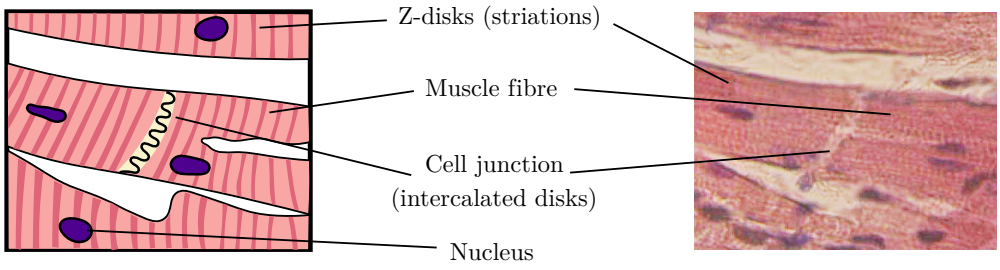

Figure 1.3 – Cardiac fibers organization. **Left:** Schematic. **Right:** Microscope image. The cells are linked together by the junctions called intercalated disks. They form an array of branching fibers. The striation appearing on the image originate from the sarcomeres. The right panel is a modification of the work of Dr. S. Girod, Anton Becker, licensed under CC BY 2.5. *Reproduced from Kimmig et al. [55] thesis with permission.*

The T tubule is composed by voltage dependent calcium channels. The polarity inversion is sensed by these receptors which change their conformation to allow a calcium inflow from the extracellular to the intracellular space. The increase in intracellular concentration activates the ryanodine receptors located on the membrane of the sarcoplasmic reticulum, which allow a passive flow of calcium from sarcoplasmic reticulum to intracellular space. Furthermore, the intercalated disks are composed by gap junctions that allow passive exchange of ions from cell to cell. These mechanisms participate to the step by step increase in intracellular calcium concentration.

The intracellular calcium concentration triggers the molecular mechanisms of the cardiac contraction. The contractile unit is called sarcomere and is composed by actin filaments, attached on one side by the Z band, and free on the other side, and by myosin filament. Another actin filament attached to another Z band close the sarcomere. The myosin filament is intercalated between the actin filaments. The troponine C is the receptor of the calcium, located on the actin filament. It is linked to a protein called tropomyosin. At rest, the tropomyosin masks the myosin head fixation site, located on the actin filament. When activated by the troponin C, the tropomyosin changes its conformation and frees the fixation site. On the myosin side, the head of the myosin can attach and contract (see Figure 1.5). This process is energy-consuming as it necessitates hydrolysis of ATP for the detachment of the myosin head from the actin fixation sites. The actin filaments slide along the myosin filaments in a contractile motion.

All the calcium channels stay opened during a few milliseconds, and the intracellular calcium concentration is restored by the re-uptakes of the calcium by the T tubule and the sarcoplasmic reticulum, using ATPase calcium pumps. The action of troponin C on the tropomyosin is released, hiding the myosin head fixation sites. This stage corresponds to the relaxation of the myocardium and is also energy-consuming.

1.1.3 Mechanics of the systole

The molecular phenomenon described above underlie the mechanics of the systole. But the heart is a pump which have finally to sucks then eject blood from the venous to the

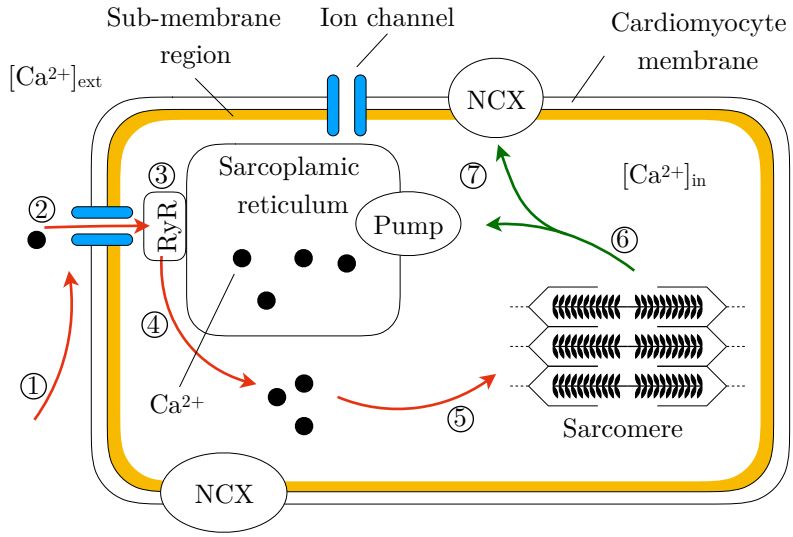

Figure 1.4 – Schematic of a cardiomyocyte. The sequence of events occurring during activation (red arrows) and relaxation (green arrows) is also presented: (1) the action potential travels on the membrane, (2) calcium ion channels are activated and let calcium ions in, (3) this calcium flux triggers the sarcoplasmic reticulum, (4) calcium is released in the cytosol, (5) calcium ions are captured by the sarcomere, (6) calcium ions are taken from the sarcomere, (7) calcium ions are uptaken by the sarcoplasmic reticulum or removed from the cells by the exchangers. *Reproduced from Kimmig et al. [55] thesis with permission.*

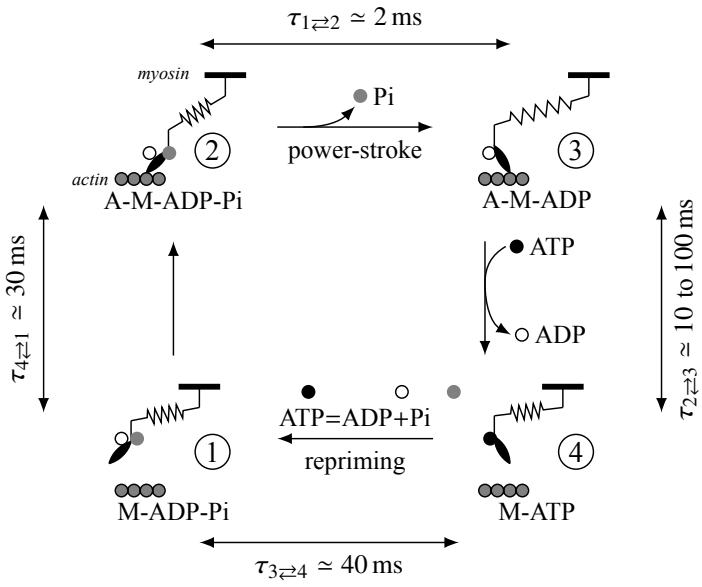

Figure 1.5 – Representation of the Lymn–Taylor cycle, where each mechanical state (1 - 4) is associated with a chemical state (M- ADP-Pi, A-M-ADP-Pi, A-M-ADP and M-ATP). During one cycle, the myosin motor executes one power-stroke and splits one ATP molecule Representation of the Lymn–Taylor cycle, where each mechanical state (1 - 4) is associated with a chemical state (M- ADP-Pi, A-M-ADP-Pi, A-M-ADP and M-ATP). During one cycle, the myosin motor executes one power-stroke and splits one ATP molecule. *Reproduced from Caruel and Truskinovsky [18].*

arterial system. The heart is a 4 cavity chambers composed by the 2 atrium and the 2 ventricle, respectively the right and left atria and ventricles (Figure 1.2). The atria are separated from the ventricles by valves (tricuspid and mitral, respectively for the right and the left heart). The ventricles are separated from the pulmonary artery and the aorta by the pulmonary and the aortic valves.

The blood first enters the right atrium following a pressure gradient, flows into the right ventricle during the relaxation of the right ventricle then the contraction of the right atrium. During the systole, the right ventricle ejects the blood into the pulmonary circulation. In parallel, the left atrium fills. When the pressure inside the left atrium is superior to the left ventricle, the mitral valve opens and the blood flows into the left ventricle. Again the contraction of the left atrium complete the filling of the LV. Finally, the contraction of the LV ejects the blood from the LV to the aorta.

The relaxation and the contraction of the LV and the right ventricle (RV) occurs simultaneously, synchronised by the quasi instantaneous spread of the electrical field by the Purkinje fibre (see Section 1.1.1). Also, the filling and the contraction of the atrium are synchronised. It begins during the ventricular systole, and the atrium systole occurs during the late diastole of the LV.

If the relaxation-contraction sequence of the 4 cavity-chambers are synchronised the mechanical nature and role of each chamber is different, and determined by anatomical architecture. The LV is a thick muscular structure, composed by cardiomyocytes oriented circularly. The objective is to optimise a squeezing motion, and to develop sufficient force to overcome the aortic pressure, necessary for blood ejection in the aorta. On the contrary, the right ventricle is a thin structure which have to overcome pulmonary pressure ($\approx$ one-fourth the aortic pressure). The RV wraps the LV, separated by the interventricular septum, which develop most of the ejecting force of the RV. The free wall of the RV is composed by cardiomyocyte oriented in the long axis of the RV. The effect of the free wall is more prominent during the diastole, as it allows efficient pressure decrease, with a suction effect.

1.1.4 Determinants of the systole

The quality of the circulating blood within the heart is affected by various determinants.

First, as discussed in Chapter 1.1.5, the filling of the heart is affected by the passive properties of the heart. The relationship between the volume and the pressure at end-diastole is underlain by continuum mechanics theory and behave as a non-hookean material. The passive law is determined by the constitutive stiffness of the myocardium (related to the collagen and elastin fibres stiffness and the cardiomyocytes stiffness) and also by the thickness of the myocardium (see Equation (2.20)). Furthermore, the passive law is also affected by external surrounding pericardial or thoracic pressure that may be applied on the heart. The preload is defined at the organ level as the end-diastolic pressure of the ventricle. It is associated with a end-diastolic volume through the passive law of the myocardium. It is a temporary state which depends on external conditions (see Figure 1.6). Indeed, the preload is greatly affected by the amount of circulating blood available for entering the ventricle, or by the ability of the heart to empty into the arterial system. Among the factors that may affect the filling of the LV, we can cite the venous return, the heart-lung interaction, the intrathoracic pressure, the pericardial pressure, the relaxation of the LV, the stiffness of the LV, and the residual Pressure-Volume inside the LV at the end of the systole.

The preload and the corresponding volume of the LV has significant effect on cardiac physiology as it is responsible from the Frank-Starling effect [34]. It describes the relation-

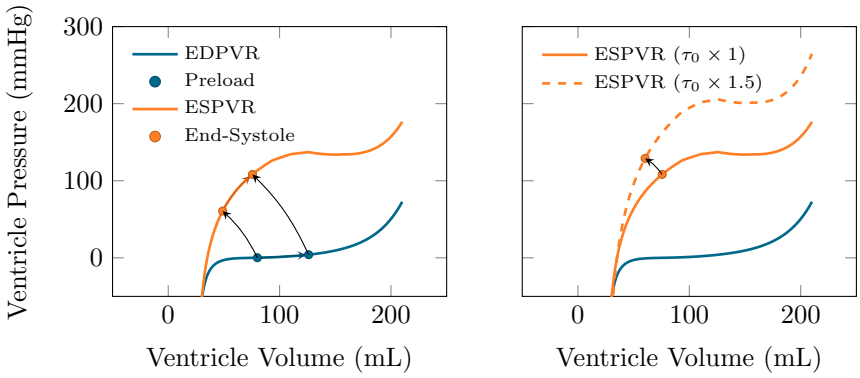

Figure 1.6 – Determinants of the systole. **Left:** Frank-Starling effect. The end-systolic pressure-volume relationship (ESPVR) represents the maximal pressure-volume point the ventricle can reach after an electrical stimulation, for a given end-diastolic filling condition – called preload. The preload is linked to the filling by the passive law, and described the end-diastolic pressure-volume relationship (EDPVR). When the preload increases (blue arrow), the stretch of the myocardial fibres increases. According to the so-called Frank-Starling effect, it modifies the strength of contraction along the ESPVR (orange arrow). **Right:** Effect of the contractility. The orange curve represent the Frank-Starling effect for a given intracellular calcium concentration. The contractility (τ_0) represents the ability of the heart to increase the calcium available for muscular contraction. Consequently, it increases, for a given preload and afterload, the strength of contraction. It corresponds to a homothetic transformation of the ESPVR.

ship between the maximal force developed by a cardiac muscle, with respect to its initial length. The force-length relationship is not linear. Integrated over the cardiac muscle and at the organ level, the relationship is called the end-systolic pressure volume relationship (ESPVR) (see Figure 1.6). The mechanisms that underlain the Frank-Starling effect are not fully understood. One hypothesis involves the optimal actin-myosin cross bridges formation related to the sarcomere length which maximise the number of myosin heads attachment. A differential sensitivity to intracellular calcium concentration with respect to fibre length has also been advanced [5; 45]. Another mechanism involves the titin fibres inside the sarcomere. The elastic recoil would help the actine-myosin sliding motion [2; 43].

The contractility is a experimental concept, which represents, at the tissue level, the maximal force the myocardial fibre can develop, independently of the loading conditions. It has unit of pressure. The contractility is affected by all the mechanism that modulated the intracellular calcium and potassium concentration.When integrated to a organ level, it represents the maximal force the ventricle can produce. It is independent of the preload and the afterload of the heart (See Figure 1.6) but can be modulated by autonomous nervous system or by circulating molecule which can raise either the intracellular calcium concentration (*e.g.* the inhibitors of the Phosphodiesterase III, which increase the intracellular AMPc concentration necessary for the opening of the calcium channels of the sarcoplasmic reticulum) or the either the muscular sensitivity to the intracellular calcium (*e.g.* the Levosimendan which enhance the effect of the Calcium on the troponine C). The heart rate can also modulate the contractility [71]. Indeed, when the cardiac rhythm increases, the re-uptake calcium capacity of the ATPase pumps are overcome [4], increasing in turn the contractility – the Bowditch effect [76].

The synchronicity of the ventricular contraction is also a mechanism which influences the output. As explain in Section 1.1.3, the electrical field is transmitted to the ventricular muscle by the specific conductive tissue – the Purkinje fibres. Even though the activation

is fast, the sequence of ventricular contraction is important. The interventricular septum is the first to be activated, and consequently the first to contract. The Purkinje fibers lead from the septum to the apex then to the free wall of the LV. The ventricular contraction follows this path. It pushes the blood from the mitral valve to the apex, then it turns up to the aortic valve (see Figure 1.2).

The afterload represents the force the ventricle has to overcome to eject blood into the aorta. It is related to vascular determinants, such as the aortic compliance, the arteriolar resistances, and the aortic wave reflexions [74]. It is also modulated by geometry of the heart. Indeed, the Laplace law explain that the wall tension is inversely proportional to the wall thickness.

$$T = \frac{P \cdot r}{2h} \tag{1.1}$$

Where T is the wall tension, P is the ventricular pressure, r is the radius of the LV, and h its wall thickness. We can see from Equation (1.1), that if ventricle pressure increases, the LV may decrease the tension by increasing the wall thickness, or by decreasing the radius. Hypertrophy of the myocardium is therefore an adaptative mechanism to chronically increased blood pressure.

1.1.5 Physiology of the diastolic function

Diastolic function of the heart designates all the physiological phenomena observed between the end of the myocardial contraction and the beginning of the consecutive cardiac cycle, the so-called diastolic period. At rest, this period equals approximately two thirds of the cardiac cycle, during which occurs the left ventricle relaxation, and the passive filling of the LV .

The relaxation is a process which consists of the isovolumic relaxation period and of the early filling of the LV. The inversion of the transmitral pressure gradient represents the switch between the two phases. It leads to the opening of the mitral valve, and the consecutive filling of the LV. At a molecular level, it corresponds to the detachment of actin-myosin cross-bridges [84] (see Section 1.1.2). The decrease in intracellular calcium concentration is caused by the activation of calcium ATPase which allow re-uptakes of calcium from sarcoplasm into sarcoplasmic reticulum and T tubles. These active transports are energy-consuming (Figure 1.4). The isovolumic relaxation is followed by a phase that is called the early filling of the ventricle, from opening of the mitral valve to atrial contraction. The pressure gradient between the left atrium and ventricle is positive and drives the early filling of the heart. The passive filling (from the LV viewpoint) is represented by the atrial contraction (which is an active process), itself responsible for a substantial part of the filling (around 20%). The filling of the LV is therefore determined by a dynamic or active component – the active LV relaxation – and by a static or passive component. The latter is related to structural components of the myocardium (cytoskeleton of the myocardial cells, connective tissue) or architectural organisation of the left ventricle [65].

The filling of the LV is therefore sensitive to phenomena that alter both the relaxation and the passive filling. On one hand, the relaxation of the LV is altered when the synchrony of the electrical activation of the LV is lost, or when delivery of oxygen is impaired (*e.g.* bundle branch block, myocardial ischaemia). On the other hand, the LV compliance is altered during myocardial remodelling (*e.g* fibrosis, storage disease or myocardial hypertrophy). The pathologies that impair the relaxation and/or the passive filling are responsible for diastolic dysfunction that can evolve into diastolic heart failure. As stated above, systolic dysfunction is necessarily associated with diastolic dysfunction, caused by the relaxation impairment. However, an isolated diastolic dysfunction exists and is mainly caused by the alteration of the passive properties of the LV. It is responsible for an entity

called “heart failure with preserved left ventricular ejection fraction (HFpLVEF)”. Typically, the impairment of the LV diastolic function is responsible for an increase of filling pressure that can ultimately lead to hydrostatic pulmonary oedema. Therefore, an acute increase of the filling pressure could decompensate a latent diastolic heart failure. For example, arrhythmias are frequently associated with an impairment of the LV diastolic function. Under normal circumstances, the proportional filling fraction attributable to the atrial contraction is around 20%. When the atrial contraction is lost (*e.g.* during atrial fibrillation), the total filling fraction of the LV occurs during the LV relaxation. Therefore, the loss of atrial contraction in case of alterations of the passive properties of the myocardium may precipitate a decompensation of HFpLVEF and lead to a sudden and life-threatening rise of LVEDP. Finally, we remark that all the pathologies that can acutely alter the diastolic function, such as acute atrial fibrillation, coronary heart disease, sepsis, malignant hypertension, constrictive pericarditis, may cause diastolic heart failure and may become a reason to enter the intensive care unit. Also, rapid changes in haemodynamic conditions could also be responsible for an acute decompensation of diastolic heart failure. During general anaesthesia, the tachycardia is frequent (*e.g.* stress, nociception, bleeding, hypovolemia) and responsible for shortening of the diastolic period, that can alter the LV filling. Fluid overload can also trigger an acute decompensation, especially if systolic function is altered [32]. Finally, a highly increased LV afterload (*e.g.* systemic arterial hypertension) may alter the LV relaxation and increase the end-diastolic volume and pressure. All these conditions frequently occur in peri-operative settings, becoming a high-risk period for patients with an impaired LV diastolic function.

1.1.6 Cardiac output and its determinants

The role of the cardiovascular system is to bring oxygen and nutrients to organs. It schematically involves a vector (the blood), a tank (the vessels) and a pump (the heart). The oxygen and nutrients are dissolved into the blood, which is brought from pulmonary (oxygen) or portal (nutrients) circulations (the providers) to the organs (the customers). The energy is brought by the heart, and the vessels can be seen as the pipelines. The cardio-circulatory system warranty the supply chain by maintaining the cardiac output (which contains the oxygen and nutrients) while distributing the blood to the organs. Each organ regulates its supply by controlling the amount of blood it requires for exerting their functions. The heart passively follows the metabolic demand if only: 1/ sufficient enough amount of blood is able to enter the heart and; 2/ the energetic expenditure does not override the heart capabilities.

It is important to notice that human heart is composed by two atria and two ventricles, respectively the right and the left atrium/ventricle, connected in series through the pulmonary circulation. Therefore the two aforementioned principles apply both to the right and the left heart, and both the right and the left hearts are affected by the pulmonary circulation physiology.

1.1.6.1 Functional anatomy of the vessels

Presented as pipes, vessels are seen as passive components of the cardiovascular system. However, it is not true, as their functions are not limited only to contain blood but also to regulate the cardiovascular final products (cardiac output and arterial/venous pressure). Therefore, vessels are actively participating to cardiovascular physiology. We can differentiate the vessels by their anatomical properties. All the vessels share common characteristics. They are composed by a inner, thin endothelial layer called the *intima*, by a medium musculo-elastic layer called the *media*, and by a solid fibrous layer called the

adventitia. If the *intima* and the adventitia are well preserved throughout the different vessels, the composition of the media determines the type of vessels.

The arteries are vessels whose functions are 1/ to bring the blood from the heart to organs; 2/ to damper the pulsatile energy caused by the cardiac physiology and; 3/ to regulate organ blood flows and. We can differentiate between large elastic arteries (typically the aorta or the carotid artery) for which the *media* is rich of elastin fibres who preferentially participate to the damping of the oscillatory phenomena of the cardiovascular circulation, and the small muscular arteries also called the arteriole (typically the renal afferent glomerular artery) for which the *media* is rich of vascular smooth muscles, who preferentially regulate the blood flow entering the organ, by controlling the size of the *lumen*. The endothelium of the arteriole can sense a physicochemical modification of the blood, and react accordingly. For example, a decrease in partial pressure of dissolved oxygen (hypoxia) results in nitric oxide synthesis through the activation of the endothelial Nitric Oxide Synthase (eNOS). The nitric oxide is captured by the vascular smooth muscle cells, and triggers a relaxation through the increase in the concentration of cyclic guanosine monophosphate (cGMP) [35]. It leads to a vasodilation of the capillary bed. However a longer term effect can lead to vasoconstriction through calcium sensitisation, mediated by Rho kinase, themselves activated by the guanylyl cyclase that have been activated by the NO in an GMPc independent pathway [22] (see Figure 1.7): "the hypoxic augmentation". For example in the lung, this mechanism participates to the so-called hypoxic pulmonary vasoconstriction [22]. It leads to redistribution of pulmonary blood flow towards more oxygenated *alveoli*, optimising therefore the oxygenation capability of the lung. It illustrates the regulatory function of the endothelial cells of the pulmonary vessels.

The capillaries, which are the thinner vessels, are composed by one layer of endothelial cells and few vascular smooth muscle cells. They are considered as a whole organ such their functions are important. Indeed, the capillaries regulate the arteriolar function through secretion of vasoactive molecules by the endothelial cells, and are the interface between blood and the organs. They can exchange gas, nutrients, cells, proteins, enzyme, and are therefore the gate for endocrine (from organ to organ), and paracrine (from cell to cell) communications. The capillaries can be continuous, fenestrated or sinusoidal, depending on their function. The continuous capillaries realise a sealed membrane, such as in the brain, the so-called blood brain barrier. The fenestrated and sinusoidal capillaries are porous structures which allow exchanges between the blood and the tissue. The selectivity to the molecules that are allowed to be exchanged is tightly regulated by the endothelial cells themselves, and is specific to each organ. Furthermore, a thin layer of proteoglycans (hydrophilic viscous proteins), called the glycocalyx lines the endothelial surface. The glycocalyx plays a role in the differential permeability of the endothelium, as it modifies the surrounding environment of the endothelial cells, depending on its physical and proteic composition, which is specific of each tissue [113; 6; 3].

The veins are capacitive vessels. It contains more than half the total blood volume of the body [42]. The *media* of the veins is composed by a thin muscular layer, that allows the veins to contract. The total volume contained in the veins can be separated into the constrained and the non constrained volumes wether it participates or not to the circulating blood. Indeed, the venous system can be seen as a passive blood reservoir which can can fill from or pour into the circulation. Therefore, the venous system exert also a regulatory function, as it can modulate the blood flow which returns to the heart.

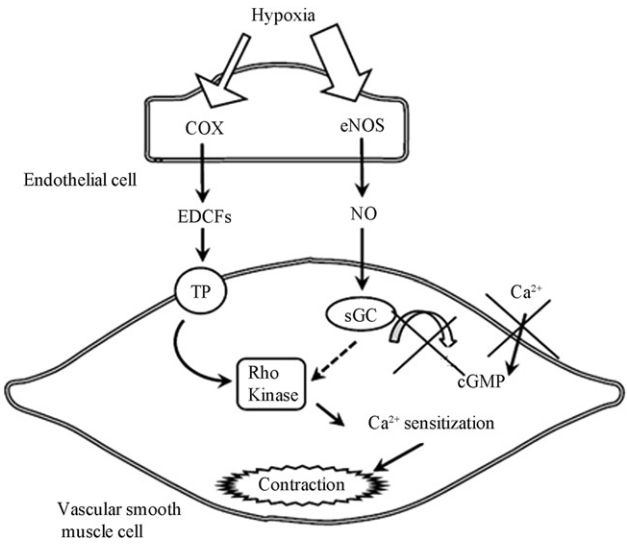

Figure 1.7 – A summary of the two endothelium-dependent pathways activated in hypoxic augmentation, which involves cyclooxygenase (COX) and endothelium nitric oxide synthase (eNOS), with the latter being the dominating one. On the one hand, endothelium-derived contracting factors (EDCFs) are released and activate thromboxane-prostanoid receptors (TP), which partly contribute to the hypoxic augmentation. On the other hand, nitric oxide (NO) activates soluble guanylyl cyclase (sGC) through a cGMP-independent mechanism, which involves activation of Rho kinase and calcium (Ca2þ) sensitization, but is independent of calcium influx from the extracellular environment. *Reproduced from Chan and Vanhoutte [22]*

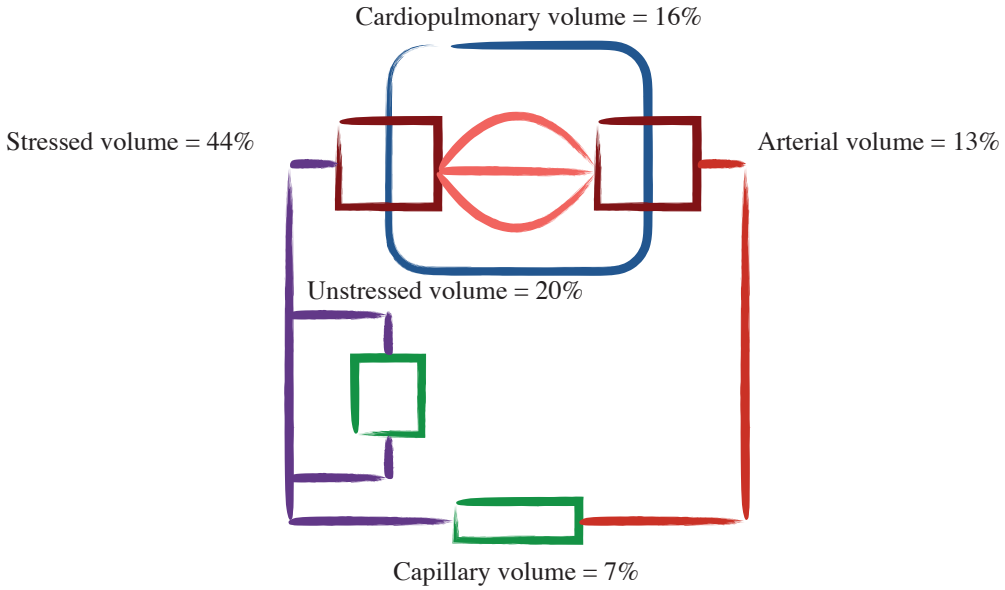

Figure 1.8 – Schematic representation of the repartition of the total blood volume in the cardiocirculatory system. The venous volume is divided into stressed and unstressed volumes, whether the respective venous volumes participate to the circulating blood. *Reproduced from Hall [42].*

1.1.6.2 Regulation of the circulating blood

From mitochondria to peripheral vascular resistance

Oxygen and nutrients are used by the cells to produce energy (the fuel) and proteins (end product of the cells). Mitochondria is an organelle specialised in aerobic energy production. It is tightly linked with the glucose metabolism. First, one molecule of glucose is transformed into 2 molecules of pyruvate by a mechanism called the "glycolysis" which generate 2 adenosine triphosphate (ATP, the support of energy) from 2 adenosine diphosphate (ADP), and one molecule of pyruvate. The pyruvate is associated with co-enzyme A to form the acetyl co-enzyme A (acetylCoA) which can pass through the inner mitochondrial membrane and enter the "Krebs cycle". The AcetylCoA is used with oxaloacetic acid by the citrate synthase, to form the first product of the Krebs cycle, the citric acid. During successive chemical reactions, the Krebs cycle generates 2 molecules of ATP, produces 16 molecules of hydrogen (H+), 4 molecules of carbon dioxide (CO2), degrades 2 molecules of AcetylCoA and regenerates 2 molecules of oxaloacetic acid [42]. The H+ are carried by the co-enzyme NAD- and FAD- which are reduced into NADH and FADH.

Another actor of the energetic production is located in the mitochondrial inner membrane and is called the "mitochondrial respiratory chain". It is composed by by five super enzymatic complexes which can use the energy given by the degradation of the co-enzymes NADH and FADH to successively (from complex I to complex IV) take out the 16 hydrogen atoms. It creates an electrochemical gradient between the inner membrane. During the process, electrons are exchanged. Finally, the fifth complex is composed by an ATP synthetase enzyme, which uses the electrochemical gradient, along with oxygen molecules and the exchanged electron, to produce ATP and H2O. This is called the "mitochondrial respiration". This process produces tremendous quantity of ATP as on glucose entering the glycolysis generates 2 ATP during glycoysis, 2 ATP during Krebs cycle and 30 ATP during mitochondrial respiration.

The glucose metabolism and the ATP generation is regulated by multiple feedback control mechanisms. For example, the availability of ADP limits the glycolysis rate and the mitochondrial respiration. Indeed, the ATP is used by the cell as energetical source for chemical reactions, including protein production. ADP is consequently regenerated and can be used to create another ATP molecules. Therefore, the total amount of energetical reactions in the cell will determine the total amount of energy to produce from glucose and oxygen. If ADP is lacking, the glucose metabolism is deviated toward "glycogenogenesis" which takes place in the liver.

If oxygen is lacking or in case of mitochondrial respiration uncoupling (*e.g.* sepsis or intoxication to cyanate, during which the mitochondria is failing to maintain the electrochemical gradient necessary for ATP production), the mitochondria cannot use the AcetylCoA. The pyruvate accumulates and is metabolised by the lactate deshydrogenase into lactic acid. This is called the "anaerobic gycolysis". From one glucose molecule, it generates 2 ATP and 2 molecules of lactic acid. The lactic acid produced can be used as a quick source of pyruvate if oxygen is available. The lactic acid can be transport by blood into other organs where it can be used in aerobic glycolysis (*e.g.* in the heart where extraction of oxygen is maximal).

But how metabolism regulates blood flow? The Poiseuille law describes the physical principle which drives circulation in a tube

$$\mathrm{P} = \frac{8\mu \mathrm{LQ}}{\pi \mathrm{R}^4} \tag{1.2}$$

with P the pressure gradient across the pipe, μ the viscosity of the fluid, L the length

of the pipe, R the radius of the pipe and Q the flow in the pipe. If we denote by r the resistance to the blood flow,

$$r = \frac{8\mu L}{\pi R^4} \tag{1.3}$$

and rewrite Equation (1.2) accordingly,

$$Q = \frac{P}{r} \tag{1.4}$$

we can immediately see what would be the effect of local regulation of the size of the vessel on the resistance r and in turn on the local blood flow Q. Therefore, when considering the endothelial reaction to hypoxia, which initially causes activation of eNOS (see Section 1.1.6.1), the NO mediated vasodilation would decrease resistance and increase blood flow. Furthermore, another consequence of hypoxia is a local production of lactic acid. This can occur during exercise for example where large quantities of lactic acid is released in muscle circulation. As the pKa of lactic acid is lower than the blood pH, it causes local acidemia, which in turn activates the eNOS, inducing a NO mediated vasodilation [53].

If we consider all the local blood flows of the body integrate it over the entire circulation, the cardiac output (Q_c) output will be composed by the sum of all the local blood flows, themselves regulated by metabolic demand.

$$Q_c = \sum^{i} \frac{P_i}{r_i} \tag{1.5}$$

If we denote by PVR the peripheral vascular resistance, the sum of all the local resistance (r_i) of the body, it yields

$$\frac{1}{PVR} = \sum^{i} \frac{1}{r_i} \tag{1.6}$$

The Poiseuille law hold true during continuous flow. However, the arterial pressure can be described by the mean arterial pressure (MAP). This approximation allows to write Q_c as:

$$Q_c = \frac{MAP - RAP}{PVR} \tag{1.7}$$

with MAP the mean arterial pressure, PVR the peripheral vascular resistance, and RAP the right atrial pressure.

Since the peripheral vascular resistance is a component which is regulated at the level of the organ, the heart plays a role in regulating the circulating blood volume by adapting the force required to eject blood on the left side (*i.e.* aortic pressure), and by adapting the force required to sucks the blood into the right heart (*i.e.* right atrial pressure). Therefore, in Equation (1.7), the Q_c is regulated by metabolism, the pressure gradient and PVR are dependent variables which adapt to warranty the organ perfusions.

The venous return

Equation (1.2) hold true concerning the venous circulation. If we consider the venous system as a capacitive reservoir which pour into the right heart, we can write

$$RV = \frac{MSFP - RAP}{R_{vs}} \tag{1.8}$$

with $RV = Q_c$, the venous return, MSFP the mean systemic filling pressure, R_{vs} the resistance of the venous system, and RAP the right atrial pressure. MSFP can be written

as a function of venous volume (V_{vs}) and capacitance (C_{vs}): MSFP $= \frac{V_{vs}}{C_{vs}}$, and corresponds to the pressure which would be measured in the venous system if RV $= 0$.

We can see that from Equation (1.8), that the cardiac output depends on the blood volume in the venous system, on the capacitance of the venous system, on the pressure in the right atrium, and on the venous flow resistance. The blood volume can be separated between stressed and unstressed volume. It is closely related to the venous system capacitance as the unstressed volume is the amount of blood necessary to fill the veins. This is the volume associated with 0 pressure in the venous system. Any extra amount of blood in the system would make the pressure to rise, and is called the stressed volume [62]. For a fixed blood volume, the modification of venous system capacitance would modify the repartition between the stressed and the unstressed volumes, and accordingly the MSFP [42].

Another determinant of the venous return is hidden in Equation (1.8). Indeed, intrathoracic pressure is important to consider as it modifies both the repartition between blood volume in the lung and in the venous system and right atrial pressure. The lung acts like a sponge and can retain or release blood volume into the systemic circulation depending on the intrathoracic pressure. For example, during spontaneous breathing, the negative pleural pressure attracts the systemic blood into the thorax. On the contrary, during mechanical ventilation, positive intrathoracic pressure squeezes the lung and expel the blood into the systemic circulation. For a given venous capacitance and resistance, the net effect on the venous return is however difficult to predict and will depend on one hand on the ability of the spontaneous breathing to decrease more the RAP than the MSFP, and on the other hand, concerning the mechanical ventilation, to increase more the MSFP than the RAP [63].

Frank-Starling mechanism

The left heart also plays an important role in the regulation of cardiac output. Indeed it has been shown that the cardiac output curve with respect to the filling of the LV is curvilinear [34; 42]. This is called the Frank-Starling mechanism and this curve can be plotted with the venous return curve. The two curves cross on the functioning point of the circulatory system. Any mechanism that will alter this cardiac function curve will lead the system to find a new equilibrium. For example, a heart failure is associated with higher right atrial pressure (congestion) and low cardiac output. The cardiac function curve is regulated by the chemical environment of the myocardium (calcium, oxygen, glucose ...). The mechanisms which interact with the myocardium homeostasis will affect the contractility, such as the sympathetic nervous system, the catecholaminergic pathway, the glucose metabolism etc...

Heart-lung interaction

Finally, the interaction between the right, the left hearts and the lung is also important to consider. The pulmonary circulation affects differently the right and the left hearts physiology. The intrathoracic pressure, as discussed earlier, plays also an important role in the heart-lung interaction.

1.2 Clinical issues

In the following section, we will describe the clinical situation in which haemodynamic is impaired, and for which haemodynamic monitoring may be useful. The main features of the following clinical situation is generally a low cardiac output associated with low

systemic arterial pressure. If this haemodynamic feature is observed, the situation is usually severe. In certain cases, we may find hypotension with high cardiac output or low cardiac output with hypertension, all these situation being life-threatening also. The haemodynamic monitoring alone may be therefore misled.

1.2.1 Heart failure

Heart failure is a clinical syndrome, defined by functional (*e.g.* breathlessness, ankle swelling and fatigue) that may be accompanied by physical (*e.g.* elevated jugular venous pressure, pulmonary crackles and peripheral oedema) symptoms, that are caused by functional and/or structural cardiac abnormality, resulting in a reduced cardiac output and/or elevated intracardiac pressure at rest or during stress, as stated by the international societies of cardiology [87; 115]. It affects approximately 1 to 2% of the adult population in developed countries. When considering patients older than 70 years old, the prevalence increases up to 10% [87]. Heart failure represents the first reason for hospitalisation for the elderly population (1 million admission a year in the US) [9]. Projections evaluated the total cost of Heart failure by 2030 to 68 billions $, representing a 127% increase from the 2013 report of the American Heart Association [51].

The 12-month all-cause mortality rates for heart failure patients after admission to hospital is estimated to 17% [64] but can reach 36% for acutely decompensated presentations [57; 90; 75; 98]. Furthermore, the natural evolution of heart failure involves successive episodes of decompensation leading to recurrent hospital admissions, all of which decreasing the overall survival from 2.5 years after the first episode to 0.5 years after the fourth [28]. In 2010, Maggioni Maggioni et al. [64] analysed the clinical presentation of more than 1,700 in-hospitalised heart failure patients all around the European union. More than three fourth of them were hospitalised with (and not necessarily for) acute decompensation on chronic heart failure or cardiogenic shock. Pulmonary oedema was observed in more than 13% and right ventricular failure in up to 5% of the studied population (Figure 1.9). A report published the same year studying 4,133 patients [79] estimated that despite hospital admission was for other reasons than heart failure in 50% of in-hospitalised patients, the causes of death in this population were mainly cardiovascular ($\approx$ 87% of 1,080 deaths). These evaluations demonstrated the extreme fragility of heart failure patients. An extra cardiac injury may lead to a decompensation of the heart failure in 50%, severe enough to be responsible for death in 25% of the cases.

It is classical to differentiate heart failure whether systolic dysfunction is observed or not. Indeed, among overall heart failure patients, systolic dysfunction is considered as one of the most significant predictor of HF mortality (Odd-Ratio (OR) = 1.23 [$CI_{95\%}$ - 1.13 to 1.46]) [1]. It is described by an impaired LV Ejection Fraction (LVEF < 0.4 – LVEF being defined by the stroke volume (SV = EDV - ESV) divided by the end-diastolic volume (EDV), ESV being the end systolic volume). However, heart failure with preserved left ventricle ejection fraction (HFpLEF – LVEF > 0.5) is also frequently observed [117] (<15% of chronic heart failure in patients younger than 50 years, 33% for patients between 50 and 70 years and 70% for patients 70 years and above). Recent studies reported that 16-30% of patients with diastolic heart failure had to be readmitted within 6 months after hospital discharge and the mortality rate is estimated to 12.1 (CI_{95} 11.7 to 12.6)% per year after the diagnosis of HFpLVEF [67]. The outcomes of the patients in-hospitalised for HFpLVEF is greatly affected and similar to those with impaired systolic function. Aetiologies for acute LV failure are numerous (see Table 1.1). For example, aortic regurgitation leads to a chronic overfilling of the LV because. It causes the LV to dilate, and then finally to impair the systolic and the diastolic function of the LV. Occlusion of coronary artery

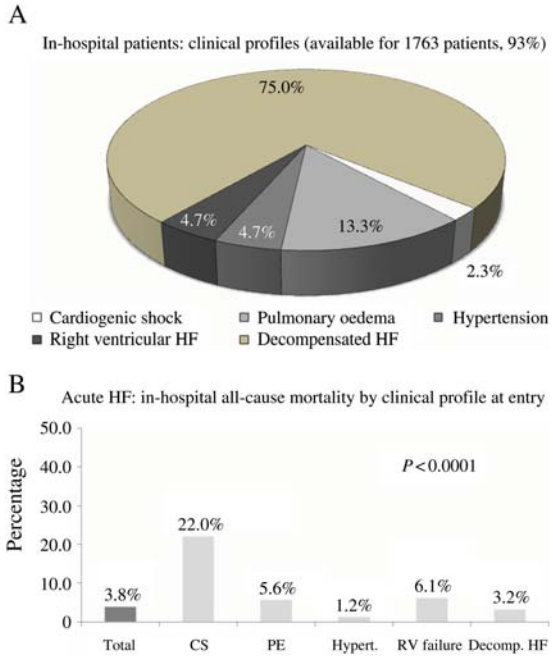

Figure 1.9 – **(A)** Stratification of in-hospital patients according to the profiles of the ESC (European Society of Cardiology) guidelines. **(B)** Total all-cause mortality stratified by the ESC clinical profiles. CS, cardiogenic shock; PE, pulmonary oedema; RV, right ventricular; HF, heart failure. *Reproduced from [64]*

causes failure of the LV and alter the systolic and the diastolic function of the LV.

Right ventricular failure is also life-threatening. The right ventricle is a capacitive chamber with a thin muscular wall, and it is not prepared to sudden increase in pulmonary arterial pressures. In case of acute increase in pulmonary arterial pressures, the RV dilates, because it can not ejects the blood in systole. It causes a decrease in cardiac output and a decrease in venous return by congestive mechanism. The right atrial pressure increases, and the blood stays in the venous and hepatic vascular system. It is source of hypoxic liver failure, acute kidney injury, or oedema. Among the cause for acute right ventricular failure, we can cite pulmonary embolism which causes a sudden increase in pulmonary arterial pressures, and occlusion of the right coronary artery, which causes a systolic dysfunction of the RV.

1.2.2 Shock states

Shock state is an acute and life-threatening circulatory insufficiency, resulting in an imbalance between delivery and consumption of oxygen. It is a frequent cause to enter the intensive care units (ICUs). Indeed, epidemiological studies evaluated the incidence of shock state from 6 to 24% [7] for all causes shock. In specific cardiovascular intensive care units, the incidence can rise up to 22% [10].

This extreme life-threatening situation is classically characterised by a low cardiac output state associated with low blood pressure. During shock state, persistence of the acute circulatory dysfunction may worsen the clinical picture and may precipitate multi-organ dysfunction, characterised by a successive failure of the organs of the patient (*e.g.* kidneys, liver).

To reverse promptly the shock state, the intensivist have to identify the limiting mechanism, responsible for the symptoms. Shock states are classically described as cardiogenic,

Table 1.1 – Aetiologies of heart failure

Heart failure	**Aetiology**
Left ventricular failure	
Systolic	Valvular diseases
	Ischemic cardiomyopathy
	Dilated cardiomyopathy
Diastolic	Ischemic cardiomyopathy
	Cardiac hypertrophy
	Chronic arterial hypertension
	Systolic heart failure
Right ventricular failure	
	Pulmonary embolism
	Ischemic cardiomyopathy
	pulmonary arterial hypertension
	Left ventricular failure

distributive, hemorragic or hypovolemic. Cardiogenic shocks are caused by an acute or decompensated heart failure whatever the origin of the heart failure. Indeed either left or right heart failure can cause cardiogenic shoc. Also cardiogenic shoc can be observed as a consequence of systolic or diastolic failure. Hypovolemic shock is observed in acute dehydration syndromes such as decompensated diabetes mellitus or peritonitis (intra-abdominal infection). The mechanism responsible for the shock is a loss of blood volume. The patient are described hemoconcentrated with high levels of haemoglobin or protein. The urine output is low and often associated with elevated serum creatinin, surrogate of acute kidney injury. Hemorrhagic shock is probably the most easy-to-diagnose shock state as the context is often informative. Hemorrhagic shocks associate low cardiac output and low blood pressure with hemorragic syndrome characterised by bleeding event (*e.g.* surgery, trauma), anaemia. Finally, the distributive shock is seen in acute inflammatory states – typically during sepsis. The infectious disease leads to acute mitochondrial and endothelial dysfunction, which in turn, cause a tremendous decrease in systemic vascular resistance. In distributive shocks, the cardiac output is maintained or increased, and the multi-organ dysfunction is mainly caused by the mitochondrial dysfunction caused by the inflammation storm. Another typical example for distributive shock with elevated cardiac output is the anaphylaxis, which is caused by an exaggerated allergic reaction.

The supportive therapy during shocks states are mainly triggered by the quick recognition of the mechanism involved. Indeed, hemorragic shock can be compensated by red blood cell transfusion. Hypovolemic shock will be reversed by fluid infusion. Distributive shock are best treated by noradrenaline or adrenaline, and cardiogenic shocks would benefit for intropic drugs. If diagnostic may be easy in some typical situations, the mechanism are often intricated and interrelated with prior pathologies of the patient. Furthermore, to consider a complete resolution of the shock, the aetiology of the haemodynamic failure have to be identified and treated accordingly. For example, red blood cell transfusion would be useless if the bleeding is not researched and treated. Distributive shock during sepsis would not be reversed if infection source is not controlled.

Also, shock state which is an acute cardio-circulatory insufficiency severe enough to lead to organ dysfunction .

1.2.3 Haemodynamic optimisation

The peri-operative period is a known risk condition for patients. Incidence of major cardiac complications after non cardiac surgery is evaluated from 2 to 3.5% [86] and it rises up to 20% in cardiac surgery [66]. Also, a survey conducted in France in 1999, observed that two third of the death occurring during surgical intervention where for cardiovascular reasons [60]. Recently, it has been observed that optimising the haemodynamic during surgery may increase post-operative outcomes. Therefore, international guidelines of anaesthesiology and intensive care societies recommend the IV fluid management titrated on cardiac output optimisation evaluated using continuous cardiac output and arterial pressure monitoring in selected patients [88; 109; 33]. Also, recently, an association between the deepness and the duration of intra-operative hypotension and post-operative morbi-mortality has been shown [97; 106; 12]. Consequently, efforts are made to detect and correct promptly IOH episodes. However, the treatment of IOH, composed by IV fluids and/or vasopressor, may be source of harm. For example, fluid overload is observed in more than 50% [32]. Also, vasopressors may cause cardiac output to decrease [108], and my impair regional perfusion [78]. Therefore, personalising haemodynamic monitoring may help the clinical-decision making on the choice and the dose of the IOH treatment.

1.3 Studying the cardiovascular physiology

The role of the intensivist and the anaesthetist is to maintain cardiovascular function while patients suffering from shock states or while patients are at risk to decompensated a previously altered cardiovascular function. Managing such complex and life-threatening conditions is not easy and it requires a solid knowledge of pathophysiology, a great observation sense and a bit of intuition. However, rational and logical way of thinking based on observation (semiology) to deduced hypotheses which have to be verified – the so-called "hypothetico-deductive" way of thinking – is probably the most efficient strategy to treat patients suffering for cardiovascular dysfunction. However, during shock states or during general anaesthesia, clinical examination may be poor and the practitioners have to gather information differently. Monitoring the cardiovascular function involves to measure physical quantities in patient to obtain information about the integrity of the cardiovascular function. It help to diagnose, to check the evolution of the pathology, or to evaluate the effect of the treatment.

1.3.1 Arterial pressure monitoring

First described by Stephen Hales in the 18^{th} century, in an experience where he observed oscillation of a column of blood contained in a tube inserted in the carotid artery of a horse, the arterial pressure monitoring is probably the most common information physicians measure on patients.

Arterial pressure measurement allows intensivist or anaesthetist to evaluate quickly and easily the integrity of the cardiovascular system. An alteration of the level of the arterial blood pressure (whatever low or high) is interpreted as a warning. Indeed, arterial hypotension is associated with poor prognosis during general anaesthesia [97; 106; 12]. Sustained arterial hypotension is also a reason to enter the intensive care unit as its presence worsen the prognosis [56; 112; 99]. On the contrary, malignant arterial hypertension is associated with stroke, pulmonary oedema, bleeding, acute myocardial infarction etc...

Furthermore, analysis of the arterial pressure characteristics may help to identify the mechanisms involved in the disease [58]. The level of the diastolic pressure may give a

Figure 1.10 – Picture of Stephen Hales while observing the oscillatory motion of the column of blood in a glass tube [41].

qualitative information with respect to PVR [58]. For example, a low diastolic pressure can be interpreted either as an excessive vasodilation, or as an aortic valve regurgitation. The difference between systolic and diastolic pressure, called the pulse pressure (PP), can also be interpreted. In case of normal diastolic pressure, a low pulse pressure could be interpreted as a decrease in systolic function or as a low preload of the LV, resulting in a low stroke volume. Also, the relationship between the SV and the PP has been interpreted as a surrogate of arterial elastance, a marker of vascular integrity, and is called the total arterial compliance [25].

$$C_{tot} = \frac{SV}{PP} \tag{1.9}$$

Therefore, for a given vascular condition (which can be seen during general anaesthesia, during steady state condition), a variation of pulse pressure could be seen as a surrogate of a variation of stroke volume.

If these information may represent a first assessment of pathophysiological alteration, the picture is not complete, as interpretation of arterial pressure value may only give indirect information regarding the stroke volume, the cardiac output, the peripheral vascular resistance, or the total arterial compliance. The reason why such alterations appeared are still unknown.

Therefore to get deeper into details, the analyse of the arterial pressure waveform can be used. Indeed, as explained in Section 1.1.6.2, the respiration affects the heart physiology in a cyclic manner [82]. When intrathoracic pressure increases, resistance to pulmonary circulation increases and in turn may increase the afterload of the right ventricle and subsequently the RAP. On the left side, it pushes the stored blood out of the lung toward the left atrium, increasing then the preload of the left ventricle. If the LV operates on the ascending part of the Starling curve, the effect would be an increase in stroke volume. Secondly, the decrease in cardiac output caused by the increase in RAP lowers the filling of the LV and subsequently the SV. When intrathoracic pressure decreases, the opposite effects are observed. We can therefore observe a cyclic variation of the SV, which can be directly transmitted to the arterial pulse pressure, if the arterial compliance is kept constant throughout respiratory cycles. Therefore, the cyclic variations are best observed when the LV operates on the ascending part of the Starling curve. This principle called the "respiratory variation of the pulse pressure" paves the way of tremendous literature regarding the probability to increase cardiac output in response to fluid challenge [82; 68].

1.3.2 Cardiac output monitoring

Cardiac output monitoring is a cornerstone in routine haemodynamic decision-making [83]. As described in Section 1.2.2 and 1.2.3, optimising haemodynamic, based on fluid responsiveness status evaluated using cardiac output monitoring, reduced morbi-mortality of in-hospitalised patients after major surgery, or during early phase of sepsis [85]. Therefore, international intensive care societies recommend the use of cardiac output monitoring in case of shock, in order to 1/ identify the type of shock; 2/ select the therapeutic intervention and; 3/ to evaluate the patient's response to therapy [19; 89].

One major concern regarding cardiac output monitoring is the difficulty to establish the targeted cardiac output value to reach. The haemodynamic optimisation strategies emphasise on the fluid responsiveness behaviour of the heart. If the patient exert evidences for inadequate value of cardiac output, in the absence of heart failure, the physician should assess the fluid responsiveness status by performing a passive leg raising manoeuvre, by evaluating the respiratory variation of the pulse pressure (PP) or of the stroke volume (SV), or by realising a mini-fluid challenge. The responsiveness to such tests should lead

the physician to administer or not a complete fluid challenge. This strategy have to be repeated until the cardiac output does not increase sufficiently enough, or in case of evidence of poor tolerance of the fluid challenge (*e.g.* pulmonary oedema, or raise in central venous pressure). With such algorithms, the risk for fluid overload is important [32].

Therefore, if arterial pressure and cardiac output monitoring are necessary for managing cardiovascular failure, it is important to combine the interpretation of the information given by monitors with other helpful information.

1.3.3 Right heart catheterisation

Right heart catheterisation can give three levels of information which can be used during management of cardiovascular failure.

First, pulmonary arterial pressures can be obtained. The catheterisation of the right atrium gives the right atrial pressure, which is meant to be the lowest as possible to allow an efficient venous return. Measuring the right atrial pressure is difficult because the order of magnitude of the true value (classically 0-5 mmHg) can be the order of magnitude of the error of measurement. Zeroing the pressure properly at the level of the heart, avoiding air bubbles in the pressure measurement lines, and verifying that the system is dampen correctly is a prerequisite for interpretation of right atrial pressure value [83; 37]. The right atrial pressure can give information whether the system is congestive if the RAP is elevated. Other pressures which can be interpreted are the pulmonary arterial pressure. In case of elevated pulmonary arterial pressures, the pulmonary wedged capillary pressure can be used to differentiate between cardiogenic or pulmonary reason for pulmonary hypertension.

Second level of information rely on thermodilution technique. Indeed, the Stewart-Hamilton principle describes the relationship between the flow of a solution, the known quantity of a dye (n_{dye}) administered in the circulating solution, and the concentration (C_{dye}) of the dye measured downstream

$$Q = \frac{n_{dye}}{\int^t C_{dye} dt} \tag{1.10}$$

The same principle could apply with heat. If we consider the administration of a cold solution in the right atrium, the heat measured on the pulmonary artery integrated over time give the cardiac output according to the modification of Equation (1.10).

$$Q = \frac{V \cdot T}{\int^t T(t) dt} \tag{1.11}$$

To date thermodilution is considered as the gold-standard in patients to measure the cardiac output.

The third level of information is given by the measurement of the venous haemoglobin saturation of the blood in the pulmonary artery (the mixed venous blood saturation $\overline{S_vO_2}$). This quantity may represent a surrogate of adequacy between delivery and consumption of oxygen.

$$VO_2 = D_aO_2 - D_vO_2 \tag{1.12}$$

with VO_2 the oxygen consumption, D_aO_2 and D_vO_2 respectively the arterial delivery and the venous delivery of oxygen. Oxygen delivery and consumption are a flow of oxygen quantity and are expressed in mL of O2 by $mL.min^{-1}$ of blood. Oxygen delivery is therefore a function of cardiac output and blood content of oxygen (respectively C_aO_2 and C_vO_2 for arterial and venous content)

$$VO_2 = Q_c \cdot (C_aO_2 - C_vO_2)\,. \tag{1.13}$$

The content of oxygen in blood is expressed in mL of O2 by mL of blood and is a function of haemoglobin level, saturation of haemoglobin of oxygen, the oxyphoric power (P_{ox}) of haemoglobin (in normal condition of acid-base equilibrium, with normal temperature $P_{ox} = 1.34$), and on the amount of dissolved oxygen in the blood (Partial pressure times the dissolution coefficient of oxygen in the blood (K_dO_2))

$$CO_2 = Hb \cdot SO_2 \cdot P_{ox} + PO_2 \cdot K_dO_2, \tag{1.14}$$

with CO_2 the content of oxygen carried by blood, SO_2 the oxygen saturation of haemoglobin in the blood, PO_2 the partial pressure of oxygen dissolved in blood.

Therefore, combining Equation (1.13) with Equation (1.14), and neglecting the dissolved fraction of oxygen in the blood, it yields:

$$\overline{S_vO_2} = S_aO_2 \cdot \left(1 - \frac{VO_2}{D_aO_2}\right) \tag{1.15}$$

When S_aO_2 is close to 1, the S_vO_2 becomes a surrogate of the oxygen extraction ratio of the body, which represents a marker of adequacy between delivery and consumption of oxygen. Indeed the extraction ratio $E_rO_2 = \frac{VO_2}{D_aO_2}$ represents the amount of oxygen that has been consumed by the body. The normal value should be below 30%.

Therefore, the pulmonary artery catheter (PAC) can be helpful in particular complex situation. Indeed, it gives a confident assessment of the cardiac output, it helps to assess if the cardiac output is adequate to the metabolic demand, and it can help to diagnose or evaluate treatment efficacy or worsening of cardio-circulatory state, by giving assessment of left and right cardiac functions or by measuring the pulmonary arterial pressure. However, the pulmonary arterial catheter may be source of harm. Even though the use of PAC for management of severely ill patients seemed beneficial during beginning of the eighties, observational studies have raised questions regarding the association between the PAC and the mortality. The observational propensity study made by Connors et al. further demonstrated that PAC was, independently to the illness severity, associated with increased risk of death [27]. Therefore the use of PAC has been progressively abandoned. Nowadays, only cardiac surgery, hepatic surgery and few intensive care units still use PAC for management of haemodynamic management in selected patients.

However, the cardiac output monitoring by other device is still recommended. It is also possible and recommended to obtain information of the extraction of oxygen by using the venous saturation of oxygen measured in the right atrium by central venous catheter [31].

1.3.4 Echocardiography

Echocardiography has become a key tool for intensivist in the management of haemodynamic alteration. Indeed, it helps to answer several questions when considering shock state identification: Is the origin of shock cardiogenic? Is the origin of shock hypovolemic? Is the cardiac output high or low? Indeed, the cardiac output can be estimated by measuring the diameter of the left ventricular outflow tract (LVOT, parsternal long axis view), and by measuring the velocity time integral of the pulsed Doppler beam recorded on the LVOT (apical view, 5-cavity chambers)

$$Q_c\ (\text{L.min}^{-1}) = \pi \left(\frac{\text{LVOT}^2\ (\text{cm}^2)}{4}\right) \cdot \text{VTI}\ (\text{cm}) \cdot \text{HR}\ (\text{beat.min}^{-1}) \tag{1.16}$$

A low Q_c associated with an impaired systolic function orients the physician to a cardiogenic origin of the shock. The systolic function of the LV can be appreciated by

estimating an ejection fraction of the LV (LVEF – normal value > 0.5)

$$\text{LVEF} = \frac{\text{EDV} - \text{ESV}}{\text{EDV}}, \tag{1.17}$$

with EDV the end diastolic volume and ESV the end systolic volume, measured on the apical view 4-cavity chambers. The contour of the epicardium of the ventricle is traced, and the surface of the ventricle is measured. A revolution of the surface is applied in order to estimate the end-diastolic and end-systolic volumes from the surfaces. The LVEF can also be estimated from measurement of the diameters of the LV, recorded on the motion-time mode, during the parasternal long axis view. Another indicator of the systolic function of the LV can be obtained on the apical view 4-cavity chambers, tissular Doppler mode, by measuring the systolic speed velocity (S-wave) of the lateral or septal mitral annulus (8 to 12 cm.s^{-1}) [17].

The right ventricular (RV) systolic function can also be assessed by echocardiography. The tissular Doppler mode can be applied on the free wall of the RV, applied on the apical view 4-cavity chambers, and the S-wave of the tricuspid annulus can be measured. A value below 12 cm.s^{-1} is associated with impaired RV systolic function. The motion-time mode can be used to measure the course of the free wall of the RV. A value below 12 mm is associated with systolic dysfunction of the RV. Usually, a decompensated right heart failure leads to a tremendous dilation of the RV which on the LV during diastole, preventing the latter to fill.

In case of preserved systolic function with low cardiac output, the following question relies on estimating both the preload of the heart. If the echocardiography can help to obtain indicators of the filling of the LV, the information obtained are not specific of hypovolemic and have to be interpreted with the context. First we can evaluate if the motion of the heart looks hyperkinetic or not. The characteristics of the VTI is helpful. Typically, the ejection time is lower than 300 ms, with VTI lower than 15 cm. The filling pressure of the LV is not elevated (best appreciated on the apical 4-cavity chambers view, by measuring the speed velocity of the transmitral flow, see Chapter 2, and by applying the simplified Bernouilli equation (1.18)). The RV is not dilated, and the diameter of the inferior vena cava is lower than 2 cm (measured on the sub-costal view). Also, typically, no pulmonary hypertension is observed (estimated by measuring the peak velocity of the tricuspid regurgitation on the apical 4-cavity chambers view).

$$\text{P} = 4\text{v}^2 \tag{1.18}$$

with v the maximal velocity of the continuous Doppler beam, and P the pressure gradient across the valve.

Echocardiography is also powerful to describe the morphology of the heart and identify morphological alterations which could impair or worsen haemodynamic state. A valvular disease can be assessed (*i.e.* aortic tricuspid or mitral stenosis or regurgitation), and the severity can be graded. Regional motion alterations orients the physician to ischemic events, whereas global hypokinetic heart might orient to myocarditis, stress cardiomyopathy or acute on chronic heart failure.

Therefore, echocardiography gives a morphological and functional assessment of the heart. It is very useful as a diagnostic tool, and it is totally non-invasive. However, the interpretation of echocardiography assessment can be affected by the image-quality recording. It requires high level expertise to get the images required for answering the beforementioned questions. Another limitation is the discontinuous character of the echocardiography. It can't be used as a monitoring tool and is considered for diagnostic or confirmation of a prior hypothesis

1.3.5 Pressure-Volume Loops and interpretation

The study of the heart can be completed by left-side catheterisation. Indeed, measuring pressure in the left ventricle may be helpful, and when it is coupled with left ventricular volume measurement, the left ventricle catheterisation can be used in a pressure-volume loop assessment. Once the cardiac contraction begins, the transmitral pressure gradient inverts and the mitral valve closes (see Figure 1.11). The LV pressure increases until it equals the aortic pressure. This phase is called the isovolumetric contraction time (IVCT). Thereafter, the aortic valve opens and the ejection phase begins. The blood is ejected through the aortic valve to the aorta. The LV volume decreases so does the rise in LV pressure. The ventricular pressure finally decrease as the systole ends, until the end-systolic pressure volume relationship point. The pressure gradient between the aorta and the ventricle inverts and the aortic valve closes. Then the LV relaxes until the mitral valve opens. This phase is called the isovolumetric relaxation.

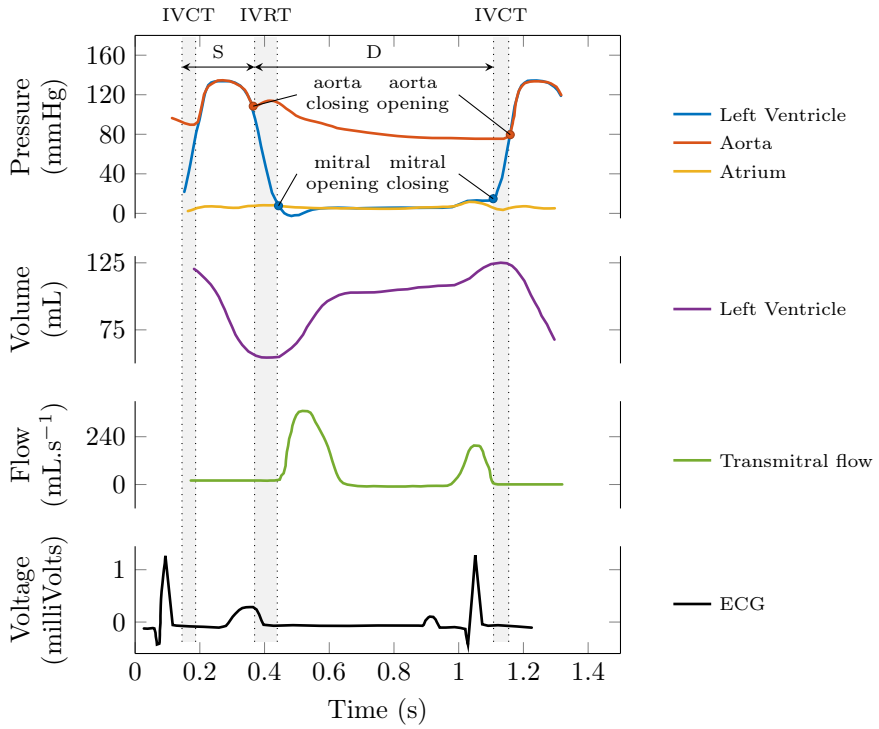

Figure 1.11 – Physiological quantities measured throughout a cardiac cycle. **From top to bottom:** The pressures measured within left atrium and ventricle, and aorta; The volume measured within the left ventricle; The blood flow through the mitral valves, between the left atrium and the left ventricle; The electrocardiographic signal. *IVCT: Isovolumic contraction time; IVRT: Isovolumic relaxation time; S: Systole; D: Diastole*

This sequence can be graphically reported in the pressure-volume diagram introduced in Section 1.1.4 as the so-called "pressure-volume loop" (PV loop). This representation is useful as it contains information about cardiac mechanics, efficiency, energetics, along with vascular information [49; 16; 92]. For example, it may help clinician to quantify heart failure severity or to evaluate the cardiac remodelling caused by a valvular disease or by chronic hypertension. The physiological quantities which can be accessed through pressure volume diagram are numerous.

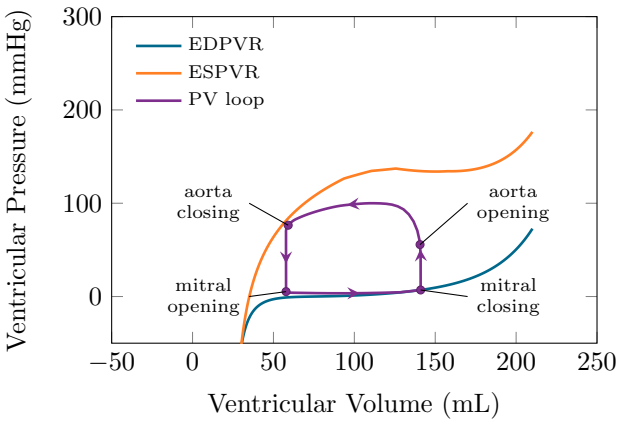

Figure 1.12 – Pressure-volume relationships in end-diastole (EDPVR), end-systole (ESPVR) and throughout a cardiac cycle (PV loop).

1.3.5.1 Valvular diseases assessment

The PV loop characteristics can be used to asses the severity of a valvular disease. Indeed, valvulopathies modifiy the functional and structural properties of the LV. Echocardiography is useful for the direct quantification of valvular stenosis or regurgitation. It can evaluate also the morphological consequences of a valvular disease (*e.g.* myocardial dilation or hypertrophy). It may also give information regarding the systolic function (*e.g.* the LV ejection fraction, or S wave of the mitral annulus) or the diastolic function (*e.g.* the E and A wave of the transmitral flow). However the functional consequences of cardiac disease is best explored by the LV catheterisation.

The characteristics of the PV loop gives important information regarding the heart pathophysiology. First is the PV assessement in end-diastole. It gives information regarding the compliance of the LV. During aortic regurgitation, the blood flows from the left atrium and from the aorta during mid-diastole. It leads to chronic overload of the left ventricle. The ventricle dilates, and, in order to decrease the wall tension (Laplace law – See Section 1.1.4), it becomes hypertrophic. This lead to a chronic increase of the filling pressure of the LV, to an impairment of the relaxation and of the compliance of the LV. It increases also the SV as the LV operates always on the top and flat part of the cardiac output/preload curve.

Aortic stenosis is associated with myocardial hypertrophy. The heart suffers from diastolic dysfunction with altered myocardial relaxation and compliance. The heart operates on a steep part of the EDPVR, for a low EDV. The systolic function is enhanced, with increased systolic pressure. The SV is low with high ESP.

Mitral regurgitation is associated with a tremendous decrease of LV afterload. Indeed during ejection, the blood either flows through the aorta or through the regurgitant mitral valve. The left auricle (LA) is chronically overloaded with increased LA pressure. In turn the LV is also chronically overloaded. The systolic function is preserved for long time. In the end the mitral regurgitation creates a high flow cardiac insufficiency, and the LV dilates at the end-stage of mitral regurgitation evolution.

Mitral stenosis is associated with chronic overload of the LA, but the LV cannot be filled adequately. The LV looks normal from PV viewpoint.

1.3.5.2 Shock state diagnostic

The PV loop characteristic may help to identify the mechanism of shock state. Concerning the cardiogenic shock, the abnormalities observed on PV loop is associated with the aetiology of the cardiac failure. In case of right ventricular failure or acute pulmonary hypertension, the limitation comes before the LV and therefore the LV looks normal, and the heart failure is therefore best evaluated by using pulmonary artery catheter. In case of left heart failure, the PV loop helps to identify LV dilation, overload, hypertrophy or impaired systolic function. The association of the abnormalities may help to identify the aetiology.

Concerning hypovolemic shock, PV loop is associated with low SV and low ESP. The EDV is low. The aetiology is confirmed by fluid loading assessment. Modification associated with preload correction is therefore observed on the PV loop (*i.e.*, Enlargement of the loop (SV and PP), shift to the right on the EDPVR). The haemorragic shock looks globally the same.

Concerning distributive shock, the PV loop is associated with increased SV and decreased PP. The LV EDV may be normal, low or elevated depending on the volume status of the patient. An impaired systolic function can be observed. But the characteristic is a tremendous decrease of the arterial elastance.

1.3.5.3 Cardiac bioenergetics

The pressure-volume area under the PV loop has the unit of a work. The intraventricular pressure, integrated over the volume can be expressed in Joules ($\mathrm{Pa} * \mathrm{m}^3 = \frac{\mathrm{N}}{\mathrm{m}^2} \cdot \mathrm{m}^3 = \mathrm{N} \cdot \mathrm{m} = \mathrm{J}$). It is called the stroke work or the external work ($\mathrm{E_w}$). In pre-clinical studies, Suga and al. have linked the stroke work to oxygen consumption of the myocardiumduring ejection [102] . However, they also stressed out the fact that isovolumetric relaxation and contraction may not participate to the calculation of the cardiac work by using only the area under the PV loop. Therefore, they introduced the concept of mechanical potential energy which is represented by the area under the ESPVR before the end-systole (see Figure 10.1 left). It is also called the internal work ($\mathrm{I_w}$). The potential energy could represent the chemical energy related to cellular basal metabolism [103]. Therefore, the total work developed by the heart during a heartbeat could be represented by the mechanical stroke work plus the potential energy – the PV area (PVA) [100]. The PVA can be related to myocardial oxygen consumption [77], and therefore the cardiac efficiency CE can be approximated by the ratio between the stroke work and the PVA $\left(\mathrm{CE} = \frac{\mathrm{E_w}}{\mathrm{E_w}+\mathrm{I_w}}\right)$.

1.3.5.4 Ventricular arterial coupling

In 1969, Suga Suga [101] proposed a model in which the ESPVR is linearised. Indeed, they observed that, under physiological ranges, the ESPVR can be locally approximated by a linear function, characterised by its slope ($\mathrm{E_{es}}$) and its intercept ($\mathrm{V_0}$) (see Figure 10.1). This linearisation implies that small deviations of the preload and/or afterload have no impact on the $\mathrm{E_{es}}$. However, it is affected by modifications of the ESPVR (*e.g.* the contractility or the starling effect). Indeed, in further works, it has been demonstrated that $\mathrm{E_{es}}$ was significantly increased by inotropic drugs experimentally [104], or clinically [13]. In the latter study, it was altered during heart failure in humans [13]. Even though $\mathrm{E_{es}}$ can represent a surrogate for systolic performance, some issues have been advanced. Indeed, it has been observed that the calculated $\mathrm{V_0}$ can be negative, which is not a physical feature. If the working systolic condition measured is close to the plateau of the Starling curve, linearisation of the ESPVR intercepts in negative $\mathrm{V_0}$. It has been demonstrated than for

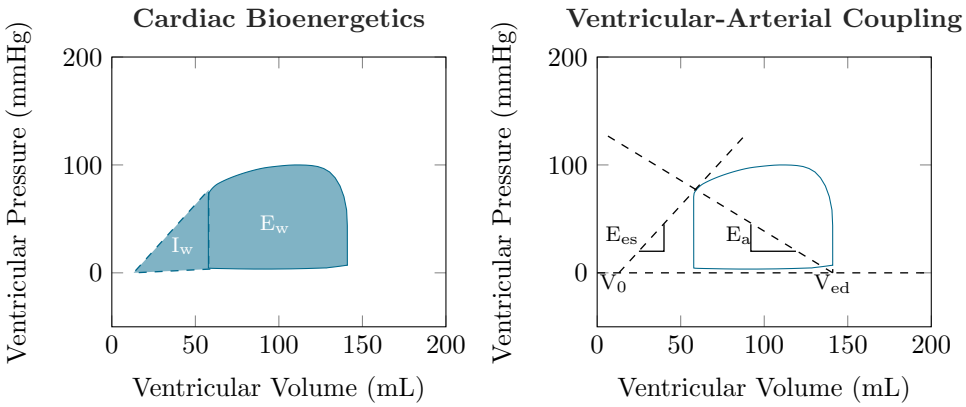

Figure 1.13 – Example of PV loop and its interpretation. **Left:** Cardiac bioenergetics. I_w*: Internal work associated with the potential energy or the energetic expenditure necessary to reach optimal conditions for ejection;* E_w*: external work associated with the energetic expenditure of the ejection;* CE*: cardiac efficiency defined as the ratio* $CE = \frac{E_w}{E_w + I_w}$. **Right:** Ventricular-arterial coupling. E_{es}*: ventricular elastance (slope of the end-systolic pressure-volume relationship, ESPVR, at end-systolic pressure-volume point);* E_a*: arterial elastance with* $E_a = \frac{P_{es}}{SV}$ *with* P_{es} *being the end-systolic pressure and* $SV = V_{ed} - V_{es}$ *the stroke volume (substraction of end-diastolic* V_{ed} *and end-systolic volumes* V_{es}*). Reproduced from Le Gall et al. [59]*

great changes of loading conditions, the locally approximated E_{es} significantly deviates from the ESPVR [52; 16].

However, the approximation was useful under clinical setting for the definition of a concept called the "Ventricular arterial coupling" (V_{va}). It exists an optimal interaction between the heart and the aorta which maximises LV power [100] with minimal oxygen consumption. The LV and the aorta are considered as two independent elastic chambers with their own systolic elastance – respectively, E_{es} for LV and for the aorta $E_a = ESP/SV$, ESP being the end systolic pressure, and SV the stroke volume. The V_{va} is therefore defined by the ratio E_a/E_{es}. It has been found, that the optimality condition (evaluated with respect to CE introduced in Section 1.3.5.3) in humans was encountered when V_{va} is close to 1 [100; 30] (see Figure 1.14). On the contrary, many pathological conditions were associated with V_{va} decoupling (*e.g* Acute heart failure, sepsis or hypertension [40]).

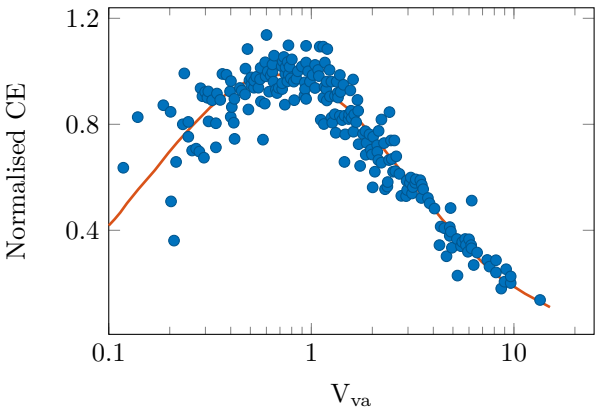

Figure 1.14 – Optimal ventricular-arterial coupling (V_{va}). Pooled data from 26 experimental runs in 8 explanted dogs' hearts. CE: Cardiac efficiency measured as the LV stroke work divided by the myocardial oxygen consumption. The results are normalised by the average maximal CE. The red line represent a normal law fitted on the data to find the V_{va} which maximises CE. In this experiment $V_{va}^{optim} = 0.638$ (CI_{95} 0.6 to 0.68) *Reproduced from De Tombe et al. [30]*

The LV catheterisation allows to obtain crucial information regarding the physiology of the system as it contains information about the energetic contained in the system, along with the interaction between heart and vessel. It helps to characterise LV dysfunction associated with cardiac pathologies or shock state. However, as it requires at least intra-ventricular catheter, which can be inserted only in the cathlab. For this reason, the PV loop analysis is only used for very specific indications or for educational purposes and has not spread into the ICU or the OR.

1.3.6 Time-Varying Elastance

Another significant implication of the ESPVR linearisation relies on the derived concept of time-varying elastance [104]. If it is possible to estimate V_0 by linearisation of ESPVR, the V_0 is supposed to be conserved during a cardiac cycle. Therefore, it is possible to describe the elastance of the LV as a function of time:

$$E(t) = \frac{P(t)}{V(t) - V_0} \tag{1.19}$$

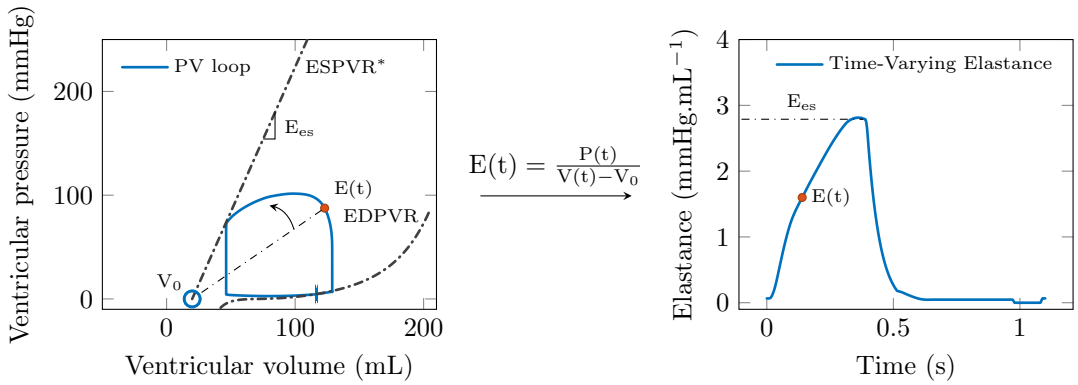

Figure 1.15 – Pressure-volume (PV) loop and time-varying elastance concept. **Right:** The time-varying elastance curve is derived from the PV loop (**Left**). The local linearisation of the ESPVR around the end-systolic PV point is characterised by its slope (E_{es}) and its intercept (V_0). The time course of the slope characterised by the red E(t) point corresponds to the time-varying elastance curve.

The time-varying elastance curve demonstrates interesting properties. Indeed, Suga Suga et al. [104] demonstrated the load-independence of this curve. They also described its conservation across subjects when the curve was normalised by the time to reach the end-systolic elastance (t_{max}) and by the E_{es} (see Figure 1.16). This property is important since it paved the way to development of single-beat and non-invasive E_{es} estimation methods [95; 26; 38].

Also, another interesting development could be the use of the time-varying curve for modelling purpose (see Chapter 8).

1.4 Issues for the anaesthetist and the intensivist

To study the haemodynamic during acute cardiovascular insufficiency at bedside in critical care unit or during surgery in operating theatre is a key aspect of the therapeutic management. Indeed, it allows to identify dysfunction, to monitor evolutive cardiovascular states

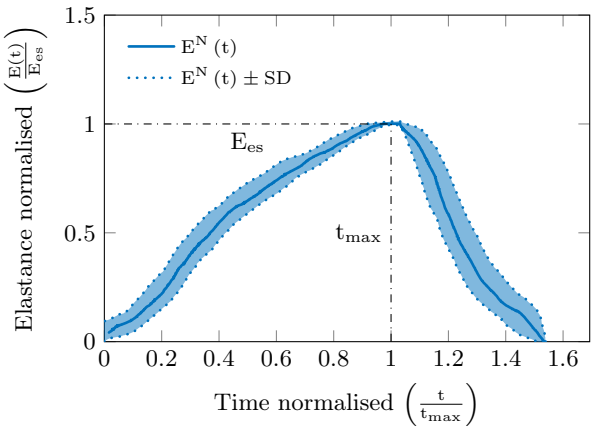

Figure 1.16 – Normalised time-varying elastance curve. The normalisation is performed in time with respect to the time to reach the end-systole (t_{max}), and in amplitude, with respect to end-systolic elastance (E_{es}). This curve represente the average $\left(E^N(t)\right)$ and the standard deviation (SD) of normalisation performed in dogs. *Reproduced from Suga et al. [104].*

or to titrate treatment. As discussed before, haemodynamic study can be performed minimally by using heart rate and blood pressure, but it can be enhanced to obtain advanced information regarding cardiovascular physiology (right or left heart catheterisation).

Ideally, monitoring should answer an *a priori* question the physician have to answer. It is not suitable to apply to every patient the most advanced haemodynamic monitoring. The choice has to take into account not only the quality or the quantity of information the monitoring can bring, but also the harm it could create. Indeed, harm can appear because of the monitor chosen. For example, pulmonary arterial catheter may be associated with rhythm disturbance, and its use in critical care units has been associated with worst outcomes for patients [27; 29]. Therefore, the practices have shifted toward less invasivity concerning haemodynamic monitoring devices, and pulmonary arterial catheter has been progressively abandoned as a routine tool. On the contrary, echocardiography has become a central tool for haemodynamic assessment. However, it necessitates high-skilled operator and it is not suitable for continuous monitoring.

The perfect monitoring device should be continuous, precise, simple, should answer to a specific question, should be non-invasive, predictive, reactive and accurate. To date no haemodynamic monitoring device is perfect. Continuous arterial pressure and cardiac output monitoring devices are the most commonly used in the OR and on the ICU. There used are recommended by international societies [33; 31]. Assessment of Q_c adequacy with respect to metabolic demand (S_vO_2), approximated by using right atrium catheter, even if it is recommended [31], is less often used. Finally, despite the tremendous amount of information it could bring, heart catheterisation are almost never used in anaesthesiology or intensive care settings. The PV loop as a monitoring device has never been evaluated, neither its potential for clinical decision making.

1.5 Modelling heart and vessels

Modelling approaches can help to fill the gap between advanced haemodynamic physiology and clinical settings. Theoretical, physical or physiological concepts can be described mathematically. The phenomenon represented is therefore described by its parameters, variables and outputs. The output is the solution of the equation. The variable is the dimension on which the output wants to be calculated, and the parameters are the other

terms of the equations that are given. Depending on what we want to look for, a parameter can become a variable. As an example, the model of consumption of oxygen is presented:

$$\begin{cases} VO_2 = Q_c \cdot (C_aO_2 - C_vO_2) \\ C_{(a/v)}O_2 = S_{(a/v)}O_2 \cdot P_{ox} \cdot [Hb] + K_d \cdot P_{(a/v)}O_2 \end{cases} \tag{1.20}$$

VO_2 is the oxygen consumption, $C_{(a/v)}O_2$ is the arterial/venous content of oxygen, Hb the haemoglobin concentration in the blood, P_{ox} the oxyphoric power of haemoglobin (the maximum amount of oxygen the haemoglobin can carry), Q_c the cardiac output, $S_{(a/v)}O_2$ the haemoglobin saturation of oxygen, K_d the dissolution coefficient of oxygen and $P_{(a/v)}O_2$ the partial pressure of oxygen.

This equation is based on knowledge. The arterial content of oxygen C_aO_2 depends on the oxygen carried by the haemoglobin and by the oxygen dissolved in the blood.

In normal atmospheric condition, the partial pressure of oxygen is low and consequently, the dissolved fraction of oxygen in the blood can be neglected, relatively to the amount of oxygen carried by the haemoglobin. Equation (1.20) can be rearranged into:

$$S_vO_2 \approx S_aO_2 \left(1 - \frac{VO_2}{[Hb] \cdot P_{ox} \cdot Q_c \cdot S_aO_2}\right) \tag{1.21}$$

In this equation, some parameters are physical constant (*e.g.* k_d and P_{ox}). Also, most of the other terms of the equations, VO_2, P_aO_2, S_aO_2, S_vO_2, [Hb] and Q_c, can easily be measured in patients. If we want to represent the S_vO_2 as a function of Q_c, then S_vO_2 is the output (Figure 1.17), Q_c is the variable and the other terms are the parameters.

But how to use efficiently such a model? A first step is to turn it into patient-specific regime. Equation (1.21) is written as a general formulation. By measuring the parameters value, this model become specific to the current patient. Most of the terms can be obtained in clinical routine practice except the VO_2, which has to be calculated or approximated. This procedure by which we choose the parameters value according to measurement is called "calibration". For example, if the [Hb] and S_aO_2 are known and constant over a given timeframe, and if during this timeframe a dataset of S_vO_2 and Q_c can be obtained (Figure 1.17), then the VO_2 can be defined as the value which fits the best the dataset.

It is nowadays possible to predict the Q_c if the S_vO_2 changes. Furthermore, this prediction remains valid if there is a change in [Hb], or S_aO_2. Indeed as these indicators are easily measurable, it is necessary to adapt the values in the model to find the new S_vO_2 – Q_c relationship. This is exemplified in Figure 1.17 right panel, where the effect of a transfusion of red blood cells is directly converted into an increase in [Hb] which modifies the relationship between S_vO_2 cardiac index. Therefore, if the cardiac output is continuously measured, the S_vO_2 is instantaneously predicted.

Another advantage of using a patient-specific model is to manage the measurement error. Indeed, we see in the left panel of Figure 1.17 that measurement error exists. The importance in the clinical decision-making depends on the level of accuracy and precision of the device that performs the measurement [20]. To use a patient-specific model may help to manage this uncertainty by giving a unique solution, which can be somehow closer to the true value of the indicator we want to get.

However, by essence a model is approximative. The confidence in the information given has to be carefully evaluated relatively to the model used. For example, Equation (1.21) is an approximation of the model (1.20), since the dissolved fraction of oxygen content is neglected. In atmospheric oxygen concentration, this approximation is reasonable as the dissolved fraction of oxygen in the blood is low relatively to the oxygen carried by the haemoglobin (0.3 ml of O_2.mL of blood^{-1} as compared to 16 mL of O_2.mL of blood^{-1},

respectively). In case of increased inspired fraction of oxygen (*e.g.* during mechanical ventilation at 100% O_2 inspired fraction) the dissolved fraction may influence the S_vO_2 value (2 mL of O_2.mL of blood^{-1} as compared to 16 mL of O_2.mL of blood^{-1}, respectively for dissolved fraction of oxygen and oxygen carried by haemoglobin).

This example gives an overview of the predictive potential of a patient-specific model. When adequately calibrated, a patient-specific model can be even more powerful since estimation methods can be applied such as data assimilation methods.

In the next section we will review example of vascular and cardiac models which can be used.

1.5.1 Vascular models

Depending on the questions we want to address, there exists many models graded by their level of complexity. The hierarchy between the vascular models can be defined as high level or low dimensional models [116] (see Figure 1.18).

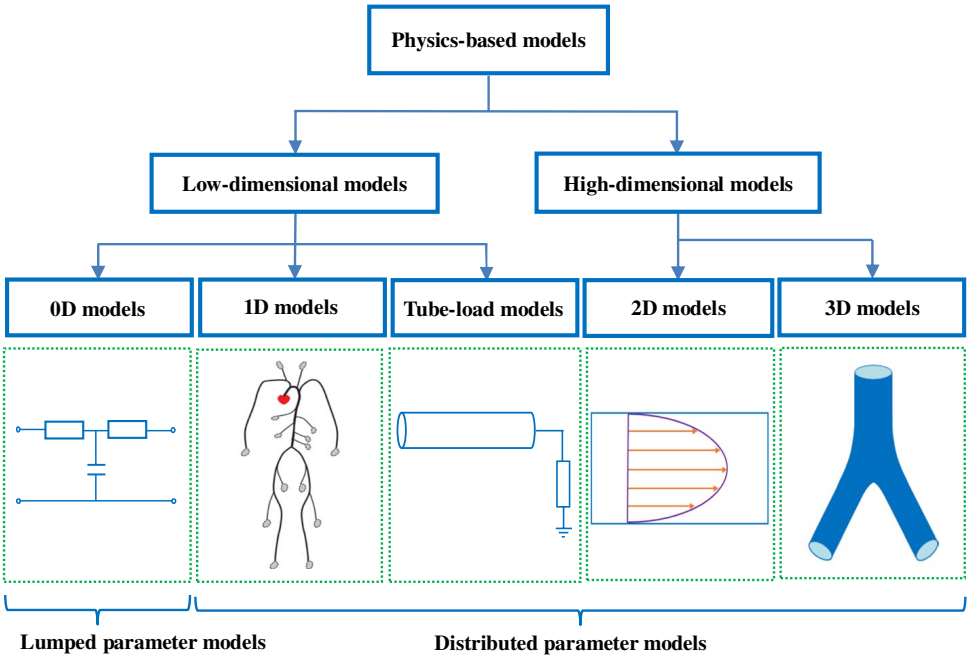

Figure 1.18 – Hierarchy between vascular models. *Reproduced from Zhou Zhou et al. [116]*

The high dimensional models (*i.e.* the 2D and 3D models) are physical based models which aim to represent in details complex haemodynamic phenomena occurring locally. The 2D models can simulate the radial flow field in an axisymmetric tube [14; 39]. The 3D model can represent also fluid-structure interaction between the vascular wall and blood [61]. The level of information obtained is very detailed (*e.g.* wall shear stress, strain/stress relationship of the wall in all the space dimensions) but the computational costs are important. For calibration purposes (*i.e.* to turn the model into patient-specific regime), complex geometrical information, which are best obtained by magnetic resonance imaging (MRI), have to be obtained. Indeed, a mesh of the vasculature and a recording of the motion of the vascular wall and/or blood flow is necessary for 3D models. For these reasons, these kinds of models cannot be readily implemented in routine anaesthesia or intensive care clinical practices.

By contrast low-dimensional models may better fit to our issues. Again, the level of

complexity of the model chosen is determined by the question the clinician wants to address. For example, a 0D model (*i.e.* a lumped-parameter model) – the most famous being the Windkessel model – would be enough if the clinical observation we want to characterise relies on global vascular indices, such as arterial compliance or vascular resistance. If the regional distribution of the blood has to be tackled, then a 1D model (which is spatially distributed) have to be considered. If a clinician wants to know which fraction of the cardiac output should flow into the kidneys, probably the 1D model would fit better than a Windkessel model. Finally, the tube-load models are temporally and spatially distributed models. They represent the large arteries by a transmission tube and the small arteries by a lumped-parameter model, connected in series. Their purpose is to take advantage of both the 0D and 1D models if the question is to focus on the physiological phenomena occurring proximally in the large artery (*e.g.* central arterial pressure), in a computational costless fashion than the 1D models do.

1.5.1.1 0D models: The arterial Windkessel

The Windkessel model represents the arterial system as an analogy with an electrical circuit. It is not designed to represent precisely the vascular phenomena occurring in any location of the vascular system. The Windkessel model, by essence, is not spatially distributed. However, it is time distributed and it has been used to estimate arterial pressure [110; 44; 111]. It is composed of association of elements connected altogether (*i.e.* Resistance R, Compliance C, Impedance Z and Inductance L). The simplest Windkessel model is composed of an input, usually the arterial flow, a resistive and capacitive component which describe the properties of the vascular system, and an output, the arterial pressure. This setting realises a mono-compartment two-elements Windkessel. By adding an impedance, then an inductance to the model, it becomes a mono-compartment three- and four- elements Windkessel model, respectively. The mono-compartment model summarises global properties of the cardiovascular system. An example of a three-elements Windkessel [110] is written as follows:

$$\frac{\mathrm{dP\,(t)}}{\mathrm{dt}} + \frac{1}{\mathrm{RC}}\mathrm{P\,(t)} = \mathrm{Z_c}\frac{\mathrm{dQ\,(t)}}{\mathrm{dt}} + \frac{\mathrm{R} + \mathrm{Z_c}}{\mathrm{RC}}\mathrm{Q\,(t)} + \frac{1}{\mathrm{RC}}\mathrm{P_{out}} \tag{1.22}$$

with P(t) the arterial pressure, Q(t) the arterial flow, R the resistance of the system, C the capacitance of the system, $\mathrm{Z_c}$ the characteristic impedance of the system, and $\mathrm{P_{out}}$ the pressure at the output of the system (*e.g.* the venous pressure).

Two mono-compartment Windkessel can be branched in series. It becomes a multi-compartment Windkessel model, which distributes in space the properties of the vascular system. It is possible to define properties for large and small arteries respectively, and to simulate a pressure for proximal and peripheral arteries.

The application of Windkessel models has been extensively described [114]. For example, Windkessel models have been used for continuous cardiac output estimation [81]. Since during diastole the aortic flow can be assumed to be equal to 0, it has been demonstrated that aortic pressure waveform during diastole follows an exponential decay [15]. Also, during diastole, a 2-elements Windkessel model simplifies [114] and becomes:

$$\mathrm{P\,(t_{diastole})} = \mathrm{P_{dicrotic}} \cdot \mathrm{e}^{-\frac{\mathrm{t_{diastole}}}{\tau}} \tag{1.23}$$

$\tau = \mathrm{R} \cdot \mathrm{C}$, being the diastolic time constant and $\mathrm{P_{dicrotic}}$ the arterial pressure at the closing of aortic valve. By fitting a Windkessel model to the diastolic period of the aortic pressure waveform, it is possible to continuously estimate τ. The continuous estimation of the

diastolic time-constant can be used as follows. By analogy with Ohm's law, the relationship between mean arterial pressure and cardiac output is written as follows:

$$\mathrm{Q_c} \approx \frac{\mathrm{MAP}}{\mathrm{R}} \tag{1.24}$$

Combining Equation (1.23) and Equation (1.24), it yields

$$\mathrm{Q_c} \approx \frac{\mathrm{MAP}}{\mathrm{C} \cdot \tau} \tag{1.25}$$

Non invasive cardiac output estimation devices use these principles with large databases to estimate C by using demographic information such as age, gender, height and weight [70], to obtain an absolute estimation of the cardiac output.

1.5.1.2 Overview of 1D models

In the 1D model, the blood is assumed to be an incompressible Newton fluid and the vessel is an axisymmetric cylindrical tube. The 1D model is governed by two equations [93], a continuity equation (Equation (1.26)) and a momentum equation (Equation (1.27)) both together describe the motion of the blood flow and the vessel wall. The formulas are as follows:

$$\frac{\partial \mathrm{q}}{\partial \mathrm{x}} + \frac{\partial \mathrm{A}}{\partial \mathrm{t}} = 0 \tag{1.26}$$

$$\frac{\partial \mathrm{q}}{\partial \mathrm{t}} + \frac{4}{3}\frac{\partial \frac{\mathrm{q}^2}{\mathrm{A}}}{\partial \mathrm{x}} = -\frac{\mathrm{A}}{\rho}\frac{\partial \mathrm{p}}{\partial \mathrm{x}} - \frac{8\mu}{\rho \mathrm{r}^2}\mathrm{q} \tag{1.27}$$

where x is the distance along the vessel, t is time, q is the blood flow rate, p is the blood pressure, A is the cross-sectional area, r is the vessel radius, ρ is the blood density and μ is the viscosity.

These models require an inflow boundary condition, which can be 1) obtained by measurements (*i.e.* MRI or echocardiography); 2) the output of a cardiac model coupled with the 1D model, or 3) the output of a simple periodic function.

The branching arteries are also boundary conditions. Usually, the branching arteries are considered as energy-preserving systems. The sum of flows in two branching arteries is exactly equal to the flow of the parent artery, and according to the continuity law, the pressure is equal in every branch of the bifurcation. However, in such models, turbulences are neglected. In some cases, such as in the aortic arch, the speed velocity and the branching angles contribute to dissipation of energy by creating vortices.

The outflow boundary condition can be simply defined by a prescribed resistive load. To further represent distal to proximal interaction, models of distal networks can be used. The 1D model can also be coupled with a tree-element Windkessel representing the distal circulation by capacitive and resistive parameters, or with a structured-three model, which takes into account wave propagation in the distal network [80].

The main objective of 1D models is to simulate the pressure and flow at any point in the arterial network, as it reproduces wave propagation in the system. Authors used the properties of 1D model to estimate central aortic pressure [8; 54], which has been associated with cardiovascular outcome [74].

1.5.1.3 Tube-load models

Tube-load models combine the simplicity of the Windkessel models and the accuracy of the 1D models. Indeed, they represent the arterial system by a transmission tube (the large

elastic arteries) and by a load (the peripheral resistive arteries). It can simulate complex interaction between arterial pressure and arterial flow at any point of the arterial system. It describes best the phenomena which occur in the large arteries. The peripheral arteries are represented by models which can be either a purely resistive load, a Windkessel model, or a generic pole-zero models as a terminal impedance [105].

By combining 1D and 0D model principles, tube-load models can describe wave propagation and reflection phenomena in the large arteries with only few parameters. It has been used for central pressure estimation [36] and transfer functions identification [105] between peripheral and central arteries.

1.5.2 Heart models

We can subdivide the heart models into lumped-parameters and biomechanical models. Biomechanical models follows physical principles and represent somehow physiology by multiscale levels. They can describe and simulate, from the cellular level up to the surrounding tissue level and motion, the cardiac physiology. Lumped-parameters or phenomenological models represent the active and/or passive properties of the heart with a function (*e.g.* the time-varying elastance) [94] or with analogy with electrical circuits [34].

Biomechanical models can be categorised with respect to the level of the geometrical dimension used. We can cite the complete 3D models which are geometrically defined in the 3 space dimensions by using a numerical mesh generated using high fidelity cardiac imaging. The detailed motion of myocardium can be described by these types of model and the fluid structure-interaction can also be considered. One-dimensional models can describe the heart as a cylinder. By using cylindrical symmetry, it simplifies calculation and calibration, while allowing to obtain detailed description of phenomenon that occur in the myocardium wall. We can cite also the spherical heart models – 0D models – which can only simulate general output without spatial distribution.

If all these models are different in their geometry and in their capabilities, they share physical principles that are independent of the geometry. For example, a passive law describing the stress/strain relationship of myocardial fibre during diastole can be applied in a model whatever the dimension. However, the geometry will impact output as parameters for the physical laws can be locally different in a 3D model for example, and homogeneous in a 0D model.

Again, the choice of model should be performed with respect to the clinical question the physician wants to address. In the following section, we will discuss only the biomechanical model that is used in the rest of the manuscript.

1.5.2.1 General architecture of heart model

A complete heart model is a complex entity which represents cardiovascular functions. As described in Section 1.1 the heart is a combination of systems which act altogether to produce the outputs, the blood circulation. The blood has to pour into the heart, the cardiac cavities needs to be filled enough, an electrical activation needs to spread along the myocardial tissue, a coupling between electrical field and mechanics has to be functional, the cardiac contraction has to be efficient, the valvular functions orient the blood in one unique direction and finally the vascular system absorbs the pulsatile energy to drive the blood flow to cells. Every component of the cardiac physiology may be somehow represented mathematically. Many approaches may be chosen to represent any specific component of the cardiac model.

In the following section, we will present the main components of the biomechanical model that is used in this manuscript. As stated earlier, the model used derives from

3D biomechanical concepts. The kinematics of a solid while deforming is linked to dynamics (*i.e.* physical quantities associated with the deformation) through constitutive laws. The fundamental laws of dynamics are based on the Newton's laws of motion: mass conservation, energy conservation, and momentum conservation.

Applied to the heart, while beating, the 3D geometry is subject to deformation and motion, and is constrained by the surrounding tissue. This kinematic behaviour is described by the derivatives of the deformation in space and time dimension, called the gradient of deformation, and further characterised by the tensors of deformation (*i.e.* Right Cauchy Green deformation tensor $\underline{\underline{C}}$ and Green-Lagrange strain tensor $\underline{\underline{e}}$). The constitutive laws describe the relationship between the deformation and the mechanical stresses (or internal forces). For example, when the heart is beating the deformation of the cavities is associated with stress applied to the myocardium, motion applied to the blood, and change in pressure within the heart cavities.

The general modelling approach in the following chapters aims at describing the kinematics, constitutive laws and dynamics of a beating heart, following the laws of continuum mechanics presented herein.

1.5.2.2 The geometry and model reduction

The beating heart is considered as a solid in large deformation and can be described according to the continuum mechanics laws. Therefore, the deformations occur in the 3 space dimensions, and the deformation field varies dynamically in time. The variations have to be described locally and integrated over the whole organ. Many modelling challenges have to be tackled to represent – in a biomechanical sense – a beating heart in 3D.

First of all, a constitutive law is consistent over the type of phenomena it aims to describe. The description at the microscopic scale of the relationship between the strain and the stress of a constricting intact myocardial cell holds true whatever the region of the considered heart. Differences may occur within population of cells, and within characteristic of the myocardial cell. A muscular cell would not behave as a pacemaker cell or as an infarcted cell. Also, most of the differences affecting uniform tissue (*i.e.* affecting cells of uniform type) are caused by the organisation of the cells into tissue, at a macroscopic scale. A 3D heart model aims at describing the phenomena occurring over the whole organ from the detailed description of local phenomena.

Many biomechanical heart models are available with different levels of complexity [21]. They allow detailed description of cardiac physiology, and when calibrated using patients' data, may help clinician in decision making. For example, by using patient-specific 3D biomechanical heart models, Sermesant Sermesant et al. [96] predicted not only patients who will benefit from cardiac resynchronisation therapy, but also the optimal location for probe placement, in order to maximise cardiac efficiency, in a patient with end-stage heart failure. The process by which the 3D models are turned into patient-specific regime is however complex as it has to consider the spatial distribution of deformation and dynamic, in all the heart complexity. This requires at least high fidelity cardiac imaging, mesh definition, 3D discretisation, description of boundary conditions, all of which being complex tasks at scientific and computing levels.

For these reasons, Caruel Caruel and Truskinovsky [18] have proposed a model, derived from a full biomechanical 3D heart model [23], in which the geometry of the heart was reduced using a spherical symmetry assumption. This symmetry allows to consider a unique local biomechanical description, which is integrated over a spherical geometry. The spatial distribution of local variations of the same phenomenon is therefore simplified to a unique averaged description. This allows to simplify the calibration – the procedure

by which the model is turned into patient-specific regime, and reduces the computational costs, allowing heart modelling to be used in a time frame compatible with anaesthesia and intensive care issues.

The spherical model is described by its radius R_{ref} and thickness d_{ref} in the stress free reference configuration Ω_{ref}. The kinematics is best described by the deformation, from Ω_{ref} of a piece of myocardium in 3 space dimensions described in an orthonormal basis, given by the radial unit vector $\underline{i}_r$, and orthoradial unit vectors $\underline{i}_{\phi 1}$ and $\underline{i}_{\phi 2}$. The displacement in radial direction is denoted by $y = R - Rref$. It can be demonstrated, assuming a radial displacement variation Δy, that the deformation variation in each orthoradial direction is described by

$$\left(d_y \underline{\underline{e}} \cdot y\right)_{\phi\phi} = (1 + y/R_{ref})\,(\Delta y/R_{ref})\,. \tag{1.28}$$

If we denote by $e_{fib} = y/R_{ref}$, then the kinematics associated with a varying radius R and wall thickness d (including a wall thickening model) is only dependent on the reference configuration $\Omega_{ref}\,(R_{ref}, d_{ref})$and e_{fib}.

$$\begin{cases} R = R_{ref} \cdot (1 + e_{fib}) \\ d = d_{ref} \cdot (1 + e_{fib})^{-2} \end{cases} \tag{1.29}$$

1.5.2.3 The active part (Bestel-Clément-Sorine)

The active part of our biomechanical model is derived and studied in detailed by Bestel [11] from the Huxley'57 model [48], which is based on the interaction between myosin and actin, the contractile proteins of the functional unit of the muscular cell – the sarcomere:

$$\begin{cases} \frac{\partial n(s,t)}{\partial t} + \dot{e}_c \frac{\partial n(s,t)}{\partial s} = (1 - n\,(s,t))\,f\,(s,t) - n\,(s,t)\,g\,(s,t), \\ n\,(s,0) = 0 \;\forall s, \end{cases} \tag{1.30}$$

with $n\,(s,t)$ the proportion of created actin-myosin cross-bridges at a given extension s and time t, and $\dot{e}_c$ the active strain of the sarcomere. The functions f and g are respectively the representation of the attachment and detachment rates of the actin-myosin cross-bridges.

$$\begin{cases} f\,(s,t) = k_{ATP} \mathbf{1}_{s \in [0,1]} \mathbf{1}_{Ca^{2+} \geq C} \\ g\,(s, \dot{e}_c, t) = \alpha |\dot{e}_c| + k_{SR} \mathbf{1}_{Ca^{2+} < C} + k_{ATP} \mathbf{1}_{Ca^{2+} \geq C} \mathbf{1}_{s \notin [0,1]}. \end{cases} \tag{1.31}$$

As described in Section 1.1.2, a myosin head may attach to the actin binding site at a rate that depends on the distance between the myosin head and the actin binding site, and if the actin binding site is not masked by the troponin-tropomyosin complex. The mechanism through which the troponin-tropomyosin conformation change to unhide the actin binding sites is a calcium dependent process.

Equation (1.31) represents the microscale components of the muscular contraction, k_{ATP} being the rate of the myosin head ATPase activity, k_{SR} the rate of the calcium re-uptake by the sarcoplasmic reticulum. C is a threshold beyond or below which the calcium concentration (Ca^{2+}) triggers muscular contraction or relaxation, respectively. α is a constant which is related to the the destruction of the actin-myosin cross-bridges when the rate of contraction is high.

Let us now introduce the unique control variable u:

$$u\,(t) = |u\,(t)\,|_+ - |u\,(t)\,|_- \text{ with } \begin{cases} |u\,(t)\,|_+ = k_{ATP} \mathbf{1}_{Ca^{2+} \geq C} \\ |u\,(t)\,|_- = k_{SR} \mathbf{1}_{Ca^{2+} < C} \end{cases} \tag{1.32}$$

This control variable u(t) is a function of the ions concentration only, and derives directly from the electrical activation model, after adequately identifying k_{ATP} and k_{SR}.

The constitutive equations of the active part of the biomechanical model presented herein are composed by two differential equations, and derived from the integration over all possible values of s. They represent a modified version of Equations (1.31) and (1.32), which includes Starling effect ($n_0(e_c)$).

After appropriate scaling, it yields:

$$\begin{cases} \dot{k}_c = -(|u| + \alpha|\dot{e}_c|)\, k_c + n_0(e_c) \cdot k_0 |u|_+ \\ \dot{\tau}_c = -(|u| + \alpha|\dot{e}_c|)\, \tau_c + \dot{e}_c k_c + n_0(e_c) \cdot \tau_0 |u|_+, \end{cases} \tag{1.33}$$

with k_c the active tissue stiffness, τ_c the active stress that can be developed in the tissue, and e_c the strain of the sarcomere, k_0 and τ_0 the value of k_c and τ_c respectively, when maximal contraction reaches the equilibrium (*i.e.* no displacement). The asymptotic active stress τ_c and stiffness k_c, generated by the sarcomere, are directly related to myocardial contractility, while taking into account the effect of actin-myosin overlap using a Frank-Starling law function $n_0(e_c)$ with value between 0 and 1 (the maximum value for the optimal extension and optimal overlap of actin and myosin chains) (see Figure 1.19), for details see [23].

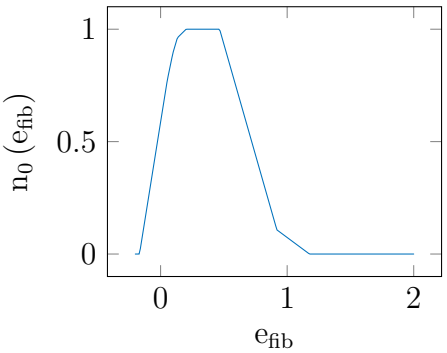

Figure 1.19 – The prescribed Starling phenomenon. $n_0(e_c)$ represents the proportion of attached myosin heads to their actin binding sites with respect to the sarcomere length (e_c).

1.5.2.4 Electrical activation

The electrical activation is a model input, governed by the function u(t) (Equation (1.32)). It represents the concentration of calcium available for cardiac contraction. The coupling with the cardiac mechanics is performed through Equation (1.33). Complete electrical activation models are available, with different levels of complexity, from full biochemical [107] to simplified membrane models [73] accounting for transmembrane potential.

Another approach would be to prescribe u(t). Indeed, under monitoring conditions when patients on GA, the electrocardiogram is continuously acquired, and the contraction/relaxation timings are therefore available. In the rest of the thesis, we used a complete prescription of u(t) (Figure 1.20).

1.5.2.5 Passive part

The complete description of the passive part of the biomechanical model used in this work is described in detailed in Part II, Chapter 2 and 3. In brief, the heart behaves as a non-hookean, hyperelastic material. The hyperelastic potential stored in the myocardium

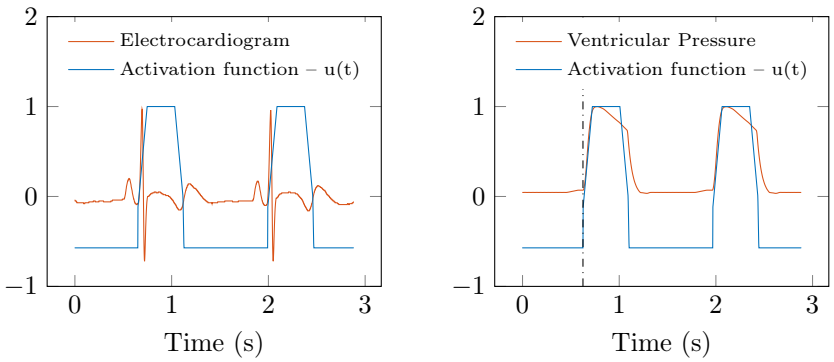

Figure 1.20 – Normalised electrical activation function u(t). **Left:** u(t) plotted with the electrocardiogram (ECG) signal recorded in a patient. The u(t) patterns are prescribed using PQ, QRS, QT timings of the ECG. The amplitude of the u(t) function is defined for all patient by [-20 ; +35]. **Right:** u(t) plotted with a simulated ventricular pressure. Dash dotted line correspond to the start of the electrical activation corresponding of the beginning of the cardiac contraction.

has been described extensively [69; 47; 46; 21]. We used a model derived from Holzapfel and Ogden [46], modified in Chapelle et al. [23]; Caruel and Truskinovsky [18]:

$$W_e = C_0 \cdot e^{C_1(J_1-3)^2} + C_2 \cdot e^{C_3(J_4-1)^2}, \tag{1.34}$$

with $J_1 = I_1 \cdot I_3^{-\frac{1}{3}}$ and $J_4 = I_4 \cdot I_3^{-\frac{1}{3}}$, being the reduced invariants of the Cauchy-Green strain tensor, $I_3 = \det\left(\underline{\underline{C}}\right)$ and (C_0, C_1, C_2, C_3) the parameters of the hyperelastic potential.

1.5.2.6 The rheological model

The myocardium model can be seen as a Maxwell-Hill model, composed by an active component described by the Bestel-Clément-Sorine model , and a passive component described by the passive law presented in Section 1.5.2.5 and detailed in Part II (see Figure 1.21).

The active branch of the model is composed by the Bestel-Clément-Sorine actin-myosin model presented in Section 1.5.2.3, characterised on the one hand by τ_c and k_c (Equation (1.33)), and on the other hand by a viscous element μ_c, which yields $\sigma_c = \tau_c + \mu_c \dot{e}_c$, the final active stress, and by a spring element E_s accounting for filaments elastic behaviour.

According to parallel and series laws for a Maxwell-Hill type model states we write

$$\begin{cases} \sigma_c = \tau_c + \mu_c \dot{e}_c = E_s e_s, \\ e_{fib} = e_s + e_c, \end{cases} \tag{1.35}$$

Therefore, the stress integrated over spherical volume (Σ_{sphere}) can be written as

$$\begin{cases} \Sigma_{sphere} = \left(\Sigma^{active}\right)_{\phi_1,\phi_2} + \left(\Sigma^{passive}\right)_{\phi_1,\phi_2} \\ \Sigma_{sphere} = \frac{\sigma_c}{1+e_{fib}} + 4\left(1 - C^{-3}\right)\frac{\partial W_e}{\partial J_1} + 2\frac{\partial W_e}{\partial J_4} + \eta \dot{C}\left(1 + 2C^{-6}\right) \end{cases} \tag{1.36}$$

$\left(\Sigma^{active}\right)_{\phi_1,\phi_2}$ and $\left(\Sigma^{passive}\right)_{\phi_1,\phi_2}$ being the stress of the active and the passive branch, respectively, oriented in the orthoradial directions (ϕ_1, ϕ_2) of the rheological model, η the viscous component of the passive branch, and assuming that $\epsilon = \frac{d_{ref}}{R_{ref}}$, the equilibrium with the internal pressure in the sphere yields:

$$\left(1 + e_{fib} - \frac{\epsilon}{2}\left(1 + e_{fib}\right)^{-2}\right)^2 \left(1 + \epsilon\left(1 + e_{fib}\right)^{-3}\right) P_{0_D} = \rho d_{ref} R_{ref} \ddot{e}_{fib} + \epsilon\left(1 + e_{fib}\right)\Sigma_{sphere} \tag{1.37}$$

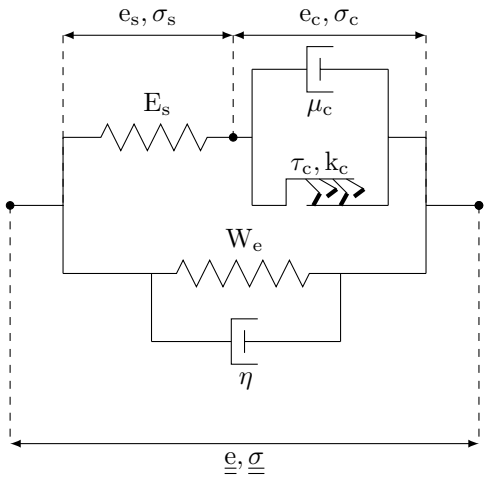

Figure 1.21 – Rheological model of Maxwell-Hill type in 1D conformation. W_e the hyperelastic potential associated with the passive tissue stiffness, η the viscous component of the passive branch; E_s and σ_s the filament stiffness and stress; τ_c, k_c the parameters of the microscopic sarcomere model, respectively the active stress and stiffness associated with a contracted conformation of myocardium at a strain e_c; σ_c accounts for the global stress of the active branch by integrating μ_c the viscous component of the active branch. $\underline{\underline{e}}$ and $\underline{\underline{\sigma}}$ are the strain and stress tensors associated with this model in three-dimensions space.

ρ being the volumic mass of water.

1.5.2.7 Valve law

The valves of the heart are modelled according to the following constitutive equations (See Figure 9.1):

$$\begin{cases} C_v \dot{P}_{0_D} = Q_v + Q_{at} - Q_{ao} \\ P_{at} - P_{0_D} = L_{at}\dot{Q}_{at} + \left(K_{at}^{\text{for/back}}\right)^{-1} Q_{at} \\ P_{0_D} - P_{ao} = L_{ar}\dot{Q}_{ao} + \left(K_{ao}^{\text{for/back}}\right)^{-1} Q_{ao} \end{cases} \tag{1.38}$$

with $Q_v = -\dot{V}$, the derivative in time of the ventricular volume, C_v the ventricular capacitance, Q_{at} and Q_{ao} respectively the atrial valve inflow and the aortic valve outflow, P_{at} and P_{ao} respectively the pressure at the entrance of the valve law and the output pressure of the model (*i.e.* the aortic pressure), L_{at} and L_{ar} respectively the inductance of the atrial and arterial valve, K_{at} and K_{ao} respectively the conductance of the atrial and arterial valve, and P_{0_D} the ventricular pressure.

1.5.2.8 Coupling heart with vessels

We used a bi-compartment Windkessel composed by two two-element Windkessel models branched in series as presented in Section 1.5.1.1, representing proximal (*e.g.* large proximal elastic vessels such as Aorta) and distal (*e.g.* small capillaries) circulations:

$$\begin{cases} C_p \dot{P}_{ao} + (P_{ao} - P_d)/R_p &= Q_{ao} \\ C_d \dot{P}_d + (P_d - P_{ao})/R_p &= (P_{ve} - P_d)/R_d, \end{cases} \tag{1.39}$$

with P_{ao}, P_d, P_{ve} representing aortic, distal arterial and venous pressures, respectively. R_p and R_d represent the proximal and distal resistances, C_p and C_d the proximal and distal

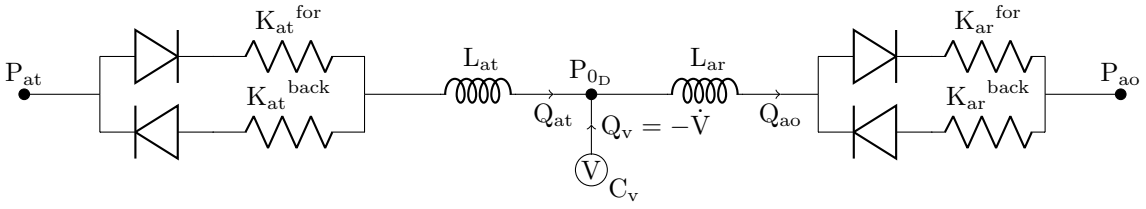

Figure 1.22 – Schematic representation of the valve law. $Q_v = -\dot{V}$, the derivative in time of the ventricular volume V, C_v the ventricular capacitance, Q_{at} and Q_{ao} respectively the atrial valve inflow and the arterial valve outflow, P_{at} and P_{ao} respectively the pressure at the beginning of the valve low and the output pressure of the model, L_{at} and L_{ar} respectively the inductance of the atrial and arterial valve, K_{at} and K_{ao} respectively the conductance of the atrial and arterial valve, and P_{0_D} the ventricular pressure.

capacitances of the model. Q_{ao} is the outflow of the ventricle.

1.5.2.9 Patient-specific biomechanical model: Patients' data and calibration procedure

The procedure by which the biomechanical model is turned into patient-specific regime is called "calibration". By using data recorded in a patient, we adjusted the values of the model parameters in order to make the model specific. In the whole thesis, we used the data extracted from a prospective database recorded between January 2015 and December 2017 in the anaesthesiology and intensive care department of Lariboisière hospital.

Patients description

Patients scheduled for intracranial endovascular procedures were selected for inclusion. Only the patients for whom continuous arterial pressure and Q_c monitoring was indicated for clinical purposes, were included. This study was approved by the appropriate Institutional Review Board – ethical committee of the Société de Réanimation de Langue Française (CE-SRLF 14-34) – which waived the need for written informed consent. Consequently, oral informed consent was obtained from all subjects after providing a protocol information letter. Every subject had the possibility to withdraw from the study at any time.

During the neuroradiological procedure, general anaesthesia (GA) was induced and maintained by using total intravenous anaesthesia (TIVA) using propofol (75-150 mg/kg/min) and remifentanil (0.2-0.5 μg/kg/min). Oro-tracheal intubation was facilitated using 0.5 mg/kg atracurium and followed, if needed, by continuous atracurium infusion (0.5 mg/kg/h). After intubation, ventilation was established to reach an end-tidal CO_2 concentration of 35 - 38 cmH_2O using a tidal volume of 6-8 ml/kg of body weight.

After GA induction, the monitoring devices were installed. Transoesophageal Doppler probe (TOD) was inserted into the oesophagus and connected to the CombiQ monitor (Deltex medical, Chichester, UK). A transthoracic echocardiography (TTE) was performed in the beginning of the interventional procedure. A radiopaque wire was advanced from the femoral artery through the aorta up to cerebral arteries. Invasive arterial pressure was recorded by connecting a fluid-filled mechanotransducer (TruWave, Edwards Lifescience, Irvine, CA, USA), as previously described [50]. For research purposes, data were recorded when the pressure catheter was in the ascending aorta.

Our standard procedure for management of intraoperative arterial hypotension (IOH), defined as the fall of mean arterial blood pressure by 20% as compared to the awake value, includes: 1) titration of saline isochloride by 250 ml step to optimise Q_c; and 2) in case of persistent IOH despite the fluid expansion, titration of diluted noradrenaline (NOR) (5μg/ml) by 5 μg steps to restore the blood pressure. This management was not modified for this research project. We separated a posteriori the population to hypotensive and normotensive groups according to whether they received NOR.

A dataset of 45 patients was available, among which 16 received NOR to restore blood pressure. A 61 patients' dataset was finally used for modelling purposes. In the following *in silico* experiments, we selected datasets among the database. We will provide the characteristics of the selection within the dedicated chapters.

Calibration procedure

The patient-specific calibration procedure was performed following sequential and systematic model parameters adjustments:

1. Adjustment of the parameters of Windkessel circulation model after imposing the flow in ascending aorta, with the objective that the simulated aortic pressure matched the measurement. As the monitoring data contain only velocity in the descending aorta, this waveform was scaled by using stroke volume (SV) obtained by transthoracic echocardiography (TTE) in the beginning of the procedure, in order to obtain a surrogate of ascending aortic flow.

2. Adjustment of the left ventricular (LV) geometry (LV volume and myocardial mass) according to the TTE measurements taken at end-diastole. The assumed LV volume at zero pressure level (the so-called reference configuration), was set according to the procedure described and analysed in details in Part II.

3. Adjustment of the passive tissue stiffness of myocardium aiming at obtaining the EDV as in TTE while applying the ventricular end-diastolic pressure (EDP). Not having an access to the ventricular or atrial pressure (P_{at}), we used a semi-quantitative method to classify LV filling pressure as high or normal [72], and we arbitrarily prescribed P_{at} value of 15 or 7 mmHg, respectively. In our simplified model, we assume the atrial pressure as the end-diastolic pressure of the LV. From this single pressure-volume point at end-diastole, we were able to estimate the tissue stiffness parameter of the myocardium (See Part II for detailed procedure).

4. Adjusment of venous pressure P_{vs}. In our model, the link between P_{vs} and P_{at} is simply set as $P_{at} = P_{vs} + 2.5$mmHg, as in Ruijsink et al. [91].

5. Adjustment of timing of the electrical activation model described in Section 1.5.2.4 by using the measured ECG (Figure 1.20).

6. Adjustment of the myocardial contractility in the model to reach the stroke volume (SV) as in the data.

The model calibration was performed for all patients at baseline. After NOR administration, we re-adjusted only the parameters that are expected to be involved by NOR (i.e. Windkessel model, timing of heart activation and myocardial contractility). Also, the TTE information was not available after NOR administration as we did not have access to the chest of the patients after the beginning of the radiological procedure.

Table 1.2 – List of parameters used for calibration (in bold the parameters which were re-calibrated after noradrenaline administration according to the new physiology state).

Sphere radius at reference configuration
Sphere thickness at reference configuration
Atrial pressure
Heartbeat duration
Time of ventricular activation
Duration of electrical activation
Myocardial stiffness factor
Proximal Windkessel resistance
Distal Windkessel resistance
Distal Windkessel capacitance
Myocardial contractility

1.6 Aim of the thesis

Our purpose in this PhD thesis is to propose and evaluate a practical framework, based on biomechanical modelling, to augment monitoring of anaesthetised patients with advanced patient-specific cardiovascular physiological knowledge. To achieve this objective, we had to rigorously overcome several issues related to clinical, biomechanical, and numerical endpoints.

Our first challenge was to turn the biomechanical model into patient-specific regime using a limited access to invasive data measurement. Indeed, the confidence in the calibration procedure is a prerequisite for the physiological and/or pathophysiological analysis of the patient-specific simulation results. The patients' advanced cardiovascular haemodynamics can be approximated only if the heart and vessel model behaves as the patients' heart. By proposing original mathematical and numerical methods, we defined a framework, using a limited set of invasive data measurements, to calibrate the circulation model, the passive and active parts, the activation, and the geometry of the biomechanical heart. We aimed to evaluate these methods by performing comparative analysis with already existing methods.

Our second challenge is linked to the *real-time* requirement imposed by the cardiovascular issues anaesthetists and intensivists have to solve. To this concern, we proposed in this thesis a time-varying model in which the active and passive part of the biomechanical model described in Section 1.5.2 are replaced by a time-varying elastance function E(t) obtained using a patient-specific version of the complete biomechanical model. We aimed to evaluate this biomechanically derived time-varying elastance model in comparison with the results obtained with the complete biomechanical (0_D) model.

We finally performed a proof of concept study, in which we tested the feasibility of using our framework to analyse the cardiovascular physiology of patients during neurosurgical interventions.

Bibliography

[1] Abraham, W. T., Fonarow, G. C., Albert, N. M., Stough, W. G., Gheorghiade, M., Greenberg, B. H., O'Connor, C. M., Sun, J. L., Yancy, C. W., and Young, J. B. (2008).

Predictors of In-Hospital Mortality in Patients Hospitalized for Heart Failure. *Journal of the American College of Cardiology*, 52(5):10.

[2] Ait-Mou, Y., Hsu, K., Farman, G. P., Kumar, M., Greaser, M. L., Irving, T. C., and de Tombe, P. P. (2016). Titin strain contributes to the Frank–Starling law of the heart by structural rearrangements of both thin- and thick-filament proteins. *Proceedings of the National Academy of Sciences*, 113(8):2306–2311.

[3] Aitoufella, H., Maury, E., Guidet, B., and Offenstadt, G. (2008). L'endothélium : un nouvel organe. *Réanimation*, 17(2):126–136.

[4] Allen, D. G. and Kurihara, S. (1980). Calcium transients in mammalian ventricular muscle. *European Heart Journal*, 1(suppl 1):5–15.

[5] Allen, D. G. and Kurihara, S. (1982). The effects of muscle length on intracellular calcium transients in mammalian cardiac muscle. *The Journal of Physiology*, 327(1):79–94.

[6] Alphonsus, C. S. and Rodseth, R. N. (2014). The endothelial glycocalyx: a review of the vascular barrier. *Anaesthesia*, 69(7):777–784.

[7] Antonelli, M., Levy, M., Andrews, P. J. D., Chastre, J., Hudson, L. D., Manthous, C., Meduri, G. U., Moreno, R. P., Putensen, C., Stewart, T., and Torres, A. (2007). Hemodynamic monitoring in shock and implications for management: International Consensus Conference, Paris, France, 27–28 April 2006. *Intensive Care Medicine*, 33(4):575–590.

[8] Bárdossy, G. and Halász, G. (2013). A "backward" calculation method for the estimation of central aortic pressure wave in a 1D arterial model network. *Computers & Fluids*, 73:134–144.

[9] Benjamin, E. J., Muntner, P., Alonso, A., Bittencourt, M. S., Callaway, C. W., and Carson, A. P. (2019). Heart Disease and Stroke Statistics—2019 Update: A Report From the American Heart Association. *Circulation*, 10:473.

[10] Berg, D. D., Bohula, E. A., van Diepen, S., Katz, J. N., Alviar, C. L., Baird-Zars, V. M., Barnett, C. F., Barsness, G. W., Burke, J. A., Cremer, P. C., Cruz, J., Daniels, L. B., DeFilippis, A. P., Haleem, A., Hollenberg, S. M., Horowitz, J. M., Keller, N., Kontos, M. C., Lawler, P. R., Menon, V., Metkus, T. S., Ng, J., Orgel, R., Overgaard, C. B., Park, J.-G., Phreaner, N., Roswell, R. O., Schulman, S. P., Jeffrey Snell, R., Solomon, M. A., Ternus, B., Tymchak, W., Vikram, F., and Morrow, D. A. (2019). Epidemiology of Shock in Contemporary Cardiac Intensive Care Units: Data From the Critical Care Cardiology Trials Network Registry. *Circulation: Cardiovascular Quality and Outcomes*, 12(3).

[11] Bestel, J. (2000). *Modèle différentiel de la contraction musculaire contrôlée. Application au système cardio-vasculaire*. PhD thesis, Université Paris IX, Paris.

[12] Bijker, J. B., Persoon, S., Peelen, L. M., Moons, K. G. M., Kalkman, C. J., Kappelle, L. J., and van Klei, W. A. (2012). Intraoperative hypotension and perioperative ischemic stroke after general surgery: a nested case-control study. *Anesthesiology*, 116(3):658–664.

[13] Bombardini, T., Costantino, M. F., Sicari, R., Ciampi, Q., Pratali, L., and Picano, E. (2013). End-Systolic Elastance and Ventricular-Arterial Coupling Reserve Predict Cardiac Events in Patients with Negative Stress Echocardiography. *BioMed Research International*, 2013:1–14.

[14] Boujena, S., Kafi, O., and El Khatib, N. (2014). A 2D Mathematical Model of Blood Flow and its Interactions in an Atherosclerotic Artery. *Mathematical Modelling of Natural Phenomena*, 9(6):46–68.

[15] Bourgeois, M. J., Gilbert, B. K., Von Bernuth, G., and Wood, E. H. (1976). Continuous determination of beat to beat stroke volume from aortic pressure pulses in the dog. *Circulation Research*, 39(1):15–24.

[16] Burkhoff, D. (2005). Assessment of systolic and diastolic ventricular properties via pressure-volume analysis: a guide for clinical, translational, and basic researchers. *AJP: Heart and Circulatory Physiology*, 289(2):H501–H512.

[17] Caballero, L., Kou, S., Dulgheru, R., Gonjilashvili, N., Athanassopoulos, G. D., Barone, D., Baroni, M., Cardim, N., Gomez de Diego, J. J., Oliva, M. J., Hagendorff, A., Hristova, K., Lopez, T., Magne, J., Martinez, C., de la Morena, G., Popescu, B. A., Penicka, M., Ozyigit, T., Rodrigo Carbonero, J. D., Salustri, A., Van De Veire, N., Von Bardeleben, R. S., Vinereanu, D., Voigt, J.-U., Zamorano, J. L., Bernard, A., Donal, E., Lang, R. M., Badano, L. P., and Lancellotti, P. (2015). Echocardiographic reference ranges for normal cardiac Doppler data: results from the NORRE Study. *European Heart Journal - Cardiovascular Imaging*, page jev083.

[18] Caruel, M. and Truskinovsky, L. (2018). Physics of muscle contraction. *Reports on Progress in Physics*, page 50.

[19] Cecconi, M., De Backer, D., Antonelli, M., Beale, R., Bakker, J., Hofer, C., Jaeschke, R., Mebazaa, A., Pinsky, M. R., Teboul, J. L., Vincent, J. L., and Rhodes, A. (2014). Consensus on circulatory shock and hemodynamic monitoring. Task force of the European Society of Intensive Care Medicine. *Intensive Care Medicine*, 40(12):1795–1815.

[20] Cecconi, M., Rhodes, A., Poloniecki, J., Della Rocca, G., and Grounds, R. M. (2009). Bench-to-bedside review: the importance of the precision of the reference technique in method comparison studies–with specific reference to the measurement of cardiac output. *Critical Care*, 13(1):201.

[21] Chabiniok, R., Wang, V. Y., Hadjicharalambous, M., Asner, L., Lee, J., Sermesant, M., Kuhl, E., Young, A. A., Moireau, P., Nash, M. P., Chapelle, D., and Nordsletten, D. A. (2016). Multiphysics and multiscale modelling, data–model fusion and integration of organ physiology in the clinic: ventricular cardiac mechanics. *Interface Focus*, 6(2):20150083.

[22] Chan, C. K. and Vanhoutte, P. M. (2013). Hypoxia, vascular smooth muscles and endothelium. *Acta Pharmaceutica Sinica B*, 3(1):1–7.

[23] Chapelle, D., Le Tallec, P., Moireau, P., and Sorine, M. (2012). Energy-preserving muscle tissue model: formulation and compatible discretizations. *International Journal for Multiscale Computational Engineering*, 10(2).

[24] Chassot, P.-G. (2015). *Précis d'anesthésie-réanimation en chirurgie cardiaque*. Université de Lausanne.

[25] Chemla, D., Hébert, J.-L., Coirault, C., Zamani, K., Suard, I., Colin, P., and Lecarpentier, Y. (1998). Total arterial compliance estimated by stroke volume-to-aortic pulse pressure ratio in humans. *American Journal of Physiology-Heart and Circulatory Physiology*, 274(2):H500–H505.

[26] Chen, C.-H., Fetics, B., Nevo, E., Rochitte, C. E., Chiou, K.-R., Ding, P.-A., Kawaguchi, M., and Kass, D. A. (2001). Noninvasive single-beat determination of LV end-systolic elastance in humans. *JACC*, 38(7):2028–2034.

[27] Connors, A. F., Speroff, T., Dawson, N. V., Thomas, C., Harrell, F. E., Wagner, D., Desbiens, N., Goldman, L., Wu, A. W., Califf, R. M., and others (1996). The effectiveness of right heart catheterization in the initial care of critically III patients. *Jama*, 276(11):889–897.

[28] Cowie, M. R., Anker, S. D., and Cleland, J. G. F. (2014). *Improving care for patients with acute heart failure: before, during and after hospitalization*. Oxford PharmaGenesis Ltd, Oxford. OCLC: 898752651.

[29] Dalen, J. E. and Bone, R. C. (1996). Is It Time to Pull the Pulmonary Artery Catheter? *JAMA*, 276:916–918.

[30] De Tombe, P. P., Jones, S., Burkhoff, D., Hunter, W. C., and Kass, D. A. (1993). Ventricular stroke work and efficiency both remain nearly optimal despite altered vascular loading. *American Journal of Physiology-Heart and Circulatory Physiology*, 264(6):H1817–H1824.

[31] Dellinger, R. P., Levy, M. M., Rhodes, A., Annane, D., Gerlach, H., Opal, S. M., Sevransky, J. E., Sprung, C. L., Douglas, I. S., Jaeschke, R., Osborn, T. M., Nunnally, M. E., Townsend, S. R., Reinhart, K., Kleinpell, R. M., Angus, D. C., Deutschman, C. S., Machado, F. R., Rubenfeld, G. D., Webb, S. A., Beale, R. J., Vincent, J.-L., and Moreno, R. (2013). Surviving Sepsis Campaign: International Guidelines for Management of Severe Sepsis and Septic Shock. *Critical Care Medicine*, 41(2):580–637.

[32] Feldheiser, A., Pavlova, V., Bonomo, T., Jones, A., Fotopoulou, C., Sehouli, J., Wernecke, K.-D., and Spies, C. (2013). Balanced crystalloid compared with balanced colloid solution using a goal-directed haemodynamic algorithm. *British Journal of Anaesthesia*, 110(2):231–240.

[33] Fleisher, L. A., Beckman, J. A., Brown, K. A., Calkins, H., Chaikof, E. L., Fleischmann, K. E., Freeman, W. K., Froehlich, J. B., Kasper, E. K., Kersten, J. R., Riegel, B., and Robb, J. F. (2007). ACC/AHA 2007 Guidelines on Perioperative Cardiovascular Evaluation and Care for Noncardiac Surgery: Executive Summary: A Report of the American College of Cardiology/American Heart Association Task Force on Practice Guidelines (Writing Committee to Revise the 2002 Guidelines on Perioperative Cardiovascular Evaluation for Noncardiac Surgery). *Circulation*, 116(17):1971–1996.

[34] Frank, O. (1959). On the dynamics of cardiac muscle. *American Heart Journal*, 58(2):282–317.

[35] Furchgott, R. F. and Zawadzki, J. V. (1980). The obligatory role of endothelial cells in the relaxation of arterial smooth muscle by acetylcholine. *Nature*, 288(5789):373–376.

[36] Gao, M., Rose, W. C., Fetics, B., Kass, D. A., Chen, C.-H., and Mukkamala, R. (2016). A Simple Adaptive Transfer Function for Deriving the Central Blood Pressure Waveform from a Radial Blood Pressure Waveform. *Scientific Reports*, 6(1):33230.

[37] Gardner, R. M. (1981). Direct blood pressure measurement–dynamic response requirements. *Anesthesiology*, 54(3):227–236.

[38] Gayat, E., Mor-Avi, V., Weinert, L., Yodwut, C., and Lang, R. M. (2011). Noninvasive quantification of LV elastance and ventricular-arterial coupling using 3D echo and arterial tonometry. *AJP: Heart and Circulatory Physiology*, 301(5):H1916–H1923.

[39] Ghigo, A. R., Fullana, J.-M., and Lagrée, P.-Y. (2017). A 2D nonlinear multiring model for blood flow in large elastic arteries. *Journal of Computational Physics*, 350:136–165.

[40] Guarracino, F., Baldassarri, R., and Pinsky, M. R. (2013). Ventriculo-arterial decoupling in acutely altered hemodynamic states. *Critical Care*, page 7.

[41] Hales, S. (1733). *Statistical Essays*, volume 2. London, W.Innys.

[42] Hall, J. E. (2011). *Guyton and Hall textbook of medical physiology.* Saunders/Elsevier, Philadelphia, Pa, 12th ed edition.

[43] Helmes, M., Lim, C. C., Liao, R., Bharti, A., Cui, L., and Sawyer, D. B. (2003). Titin Determines the Frank-Starling Relation in Early Diastole. *Journal of General Physiology*, 121(2):97–110.

[44] Her, K., Kim, J. Y., Lim, K. M., and Choi, S. W. (2018). Windkessel model of hemodynamic state supported by a pulsatile ventricular assist device in premature ventricle contraction. *BioMedical Engineering OnLine*, 17(1):18.

[45] Hibberd, M. G. and Jewell, B. R. (1982). Calcium- and length-dependent force production in rat ventricular muscle. *The Journal of Physiology*, 329(1):527–540.

[46] Holzapfel, G. A. and Ogden, R. W. (2009). Constitutive modelling of passive myocardium: a structurally based framework for material characterization. *Phil. Trans. R. Soc. A: Mathematical, Physical and Engineering Sciences*, 367(1902):3445–3475.

[47] Humphrey, J. D., Strumpf, R. K., and Yin, F. C. P. (1990). Determination of a Constitutive Relation for Passive Myocardium: II.—Parameter Estimation. *Journal of Biomechanical Engineering*, 112(3):340.

[48] Huxley, A. F. (1957). Muscle structure and theories of contraction. *Progress in Biophysics and Biophysical Chemistry*, 7:255–318.

[49] Jacob, R. and Kissling, G. (1989). Ventricular pressure-volume relations as the primary basis for evaluation of cardiac mechanics Return to Frank's diagram. *Basic Research in Cardiology*, 84(3):227–246.

[50] Joachim, J., Vallée, F., Le Gall, A., Matéo, J., Lenck, S., Millasseau, S., Houdart, E., Mebazaa, A., and Gayat, É. (2017). Velocity–pressure loops for continuous assessment of ventricular afterload: influence of pressure measurement site. *Journal of Clinical Monitoring and Computing*.

[51] Karmali, K. N., Goff, D. C., Ning, H., and Lloyd-Jones, D. M. (2014). A Systematic Examination of the 2013 ACC/AHA Pooled Cohort Risk Assessment Tool for Atherosclerotic Cardiovascular Disease. *Journal of the American College of Cardiology*, 64(10):959–968.

[52] Kass, D. A., Beyar, R., Lankford, E., Heard, M., Maughan, W. L., and Sagawa, K. (1989). Influence of contractile state on curvilinearity of in situ end-systolic pressure-volume relations. *Circulation*, 79(1):167–178.

[53] Khacho, M., Tarabay, M., Patten, D., Khacho, P., MacLaurin, J. G., Guadagno, J., Bergeron, R., Cregan, S. P., Harper, M.-E., Park, D. S., and Slack, R. S. (2014). Acidosis overrides oxygen deprivation to maintain mitochondrial function and cell survival. *Nature Communications*, 5(1):3550.

[54] Khalifé, M., Decoene, A., Caetano, F., de Rochefort, L., Durand, E., and Rodríguez, D. (2014). Estimating absolute aortic pressure using MRI and a one-dimensional model. *Journal of Biomechanics*, 47(13):3390–3399.

[55] Kimmig, F., Chapelle, D., and Caruel, M. (2019). *Multi-scale modeling of muscle contraction From stochastic dynamics of molecular motors to continuum mechanics*. PhD thesis, Paris-Saclay, Saclay.

[56] Knaus, W. A. (1991). The APACHE III prognostic system. Risk prediction of hospital mortality for critically ill hospitalized adults. *CHEST Journal*, 100(6):1619.

[57] Kociol, R. D. (2010). Generalizability and longitudinal outcomes of a national heart failure clinical registry: Comparison of Acute Decompensated Heart Failure National Registry (ADHERE) and non-ADHERE Medicare beneficiaries. *American Heart Journal*, 160(5):8.

[58] Lamia, B., Chemla, D., Richard, C., and Teboul, J. (2005). Clinical review: interpretation of arterial pressure wave in shock states. *CRITICAL CARE-LONDON-*, 9(6):601.

[59] Le Gall, A., Vallée, F., Pushparajah, K., Hussain, T., Mebazaa, A., Chapelle, D., Gayat, E., and Chabiniok, R. (2020). Monitoring of cardiovascular physiology augmented by a patient-specific biomechanical model during general anesthesia. A proof of concept study. *PLOS ONE*, 15(5):e0232830.

[60] Lienhart, A., Auroy, Y., Péquignot, F., Benhamou, D., Warszawski, J., Bovet, M., and Jougla, E. (2006). Survey of anesthesia-related mortality in France. *Anesthesiology*, 105(6):1087–1097.

[61] Lopez-Perez, A., Sebastian, R., and Ferrero, J. M. (2015). Three-dimensional cardiac computational modelling: methods, features and applications. *BioMedical Engineering OnLine*, 14(1):35.

[62] Magder, S. (2016). Volume and its relationship to cardiac output and venous return. *Critical Care*, 20(1).

[63] Magder, S. and Guerard, B. (2012). Heart–lung interactions and pulmonary buffering: Lessons from a computational modeling study. *Respiratory Physiology & Neurobiology*, 182(2-3):60–70.

[64] Maggioni, A. P., Dahlström, U., Filippatos, G., Chioncel, O., Leiro, M. C., Drozdz, J., Fruhwald, F., Gullestad, L., Logeart, D., Metra, M., Parissis, J., Persson, H., Ponikowski, P., Rauchhaus, M., Voors, A., Nielsen, O. W., Zannad, F., Tavazzi, L., and on behalf of the Heart Failure Association of the ESC (HFA) (2010). EUR *Observational* Research Programme: The Heart Failure Pilot Survey (ESC-HF Pilot). *European Journal of Heart Failure*, 12(10):1076–1084.

[65] Maurer, M. S., Spevack, D., Burkhoff, D., and Kronzon, I. (2004). Diastolic dysfunction. *Journal of the American College of Cardiology*, 44(8):1543–1549.

[66] Mebazaa, A., Pitsis, A. A., Rudiger, A., Toller, W., Longrois, D., Ricksten, S.-E., Bobek, I., Hert, S. D., Wieselthaler, G., Schirmer, U., Poldermans, D., Ranucci, M., Karpati, P. C., Wouters, P., Seeberger, M., Schmid, E. R., Weder, W., and Follath, F. (2010). Clinical review: Practical recommendations on the management of perioperative heart failure in cardiac surgery. *Critical Care*, page 14.

[67] Meta-analysis Global Group in Chronic Heart Failure (MAGGIC) (2012). The survival of patients with heart failure with preserved or reduced left ventricular ejection fraction: an individual patient data meta-analysis. *European Heart Journal*, 33(14):1750–1757.

[68] Michard, F. and Teboul, J.-L. (2000). Using heart–lung interactions to assess fluid responsiveness during mechanical ventilation. *Critical Care*, 4(5):8.

[69] Mirsky, I., Janz, R. F., Kubert, B. R., Korecky, B., and Taichman, G. C. (1976). Passive elastic wall stiffness of the left ventricle: A comparison between linear theory and large deformation theory. *Bulletin of Mathematical Biology*, 38(3):239–251.

[70] Mukkamala, R., Reisner, A., Hojman, H., Mark, R., and Cohen, R. (2006). Continuous Cardiac Output Monitoring by Peripheral Blood Pressure Waveform Analysis. *IEEE Transactions on Biomedical Engineering*, 53(3):459–467.

[71] Mulieri, L. A., Hasenfuss, G., Leavitt, B., Allen, P. D., and Alpert, N. R. (1992). Altered myocardial force-frequency relation in human heart failure. *Circulation*, 85(5):1743–1750.

[72] Nagueh, S. F., Appleton, C. P., Gillebert, T. C., Marino, P. N., Oh, J. K., Smiseth, O. A., Waggoner, A. D., Flachskampf, F. A., Pellikka, P. A., and Evangelisa, A. (2008). Recommendations for the Evaluation of Left Ventricular Diastolic Function by Echocardiography. *European Journal of Echocardiography*, 10(2):165–193.

[73] Nagumo, J., Arimoto, S., and Yoshizawa, S. (1962). An Active Pulse Transmission Line Simulating Nerve Axon. *Proceedings of the IRE*, 50(10):2061–2070.

[74] Nichols, W. W. and McDonald, D. A. (2011). *McDonald's blood flow in arteries: theoretic, experimental, and clinical principles*. Hodder Arnold, London, 6th ed edition.

[75] Nieminen, M. S., Brutsaert, D., Dickstein, K., Drexler, H., Follath, F., Harjola, V.-P., Hochadel, M., Komajda, M., Lassus, J., Lopez-Sendon, J. L., Ponikowski, P., and Tavazzi, L. (2006). EuroHeart Failure Survey II (EHFS II): a survey on hospitalized acute heart failure patients: description of population. *European Heart Journal*, 27:12.

[76] Noble, M. I. M. (1988). An introduction to modern work on the Bowditch phenomenon. *Cardiovascular Research*, 22(8):586–586.

[77] Nozawa, T., Cheng, C. P., Noda, T., and Little, W. C. (1994). Relation between left ventricular oxygen consumption and pressure-volume area in conscious dogs. *Circulation*, 89(2):810–817.

[78] Nygren, A., Thorén, A., and Ricksten, S.-E. (2006). Vasopressors and intestinal mucosal perfusion after cardiac surgery: Norepinephrine vs. phenylephrine. *Critical Care Medicine*, 34(3):722–729.

[79] O'Connor, C. M., Miller, A. B., Blair, J. E. A., Konstam, M. A., and Rn, P. W. (2010). Causes of death and rehospitalization in patients hospitalized with worsening heart failure and reduced left ventricular ejection fraction: Results from efficacy of vasopressin antagonism in heart failure outcome study with tolvaptan (EVEREST) program. *American Heart Journal*, 159(5):10.

[80] Olufsen, M. S. (1999). Structured tree outflow condition for blood flow in larger systemic arteries. *American Journal of Physiology-Heart and Circulatory Physiology*, 276(1):H257–H268.

[81] Parlikar, T., Heldt, T., Ranade, G., and Verghese, G. (2007). Model-based estimation of cardiac output and total peripheral resistance. In *2007 Computers in Cardiology*, pages 379–382, Durham, NC, USA. IEEE.

[82] Perel, A., Pizov, R., and Cotev, S. (2014). Respiratory variations in the arterial pressure during mechanical ventilation reflect volume status and fluid responsiveness. *Intensive Care Medicine*, 40(6):798–807.

[83] Pinsky, M. R. and Payen, D. (2005). Functional hemodynamic monitoring. *Critical Care*, 9(6):566.

[84] Pirracchio, R., Cholley, B., De Hert, S., Solal, A. C., and Mebazaa, A. (2007). Diastolic heart failure in anaesthesia and critical care. *British Journal of Anaesthesia*, 98(6):707–721.

[85] Poeze, M., Greve, J. W., Ramsay, G., and others (2005). Meta-analysis of hemodynamic optimization: relationship to methodological quality. *Crit Care*, 9(6):R771–9.

[86] Poldermans, D., Bax, J. J., Boersma, E., De Hert, S. G., Eeckhout, E., Fowkes, G., Gorenek, B., Hennerici, M. G., Iung, B., Kelm, M., Kjeldsen, K. P., Kristensen, S. D., Lopez-Sendon, J., Pelosi, P., Philippe, F., Pierard, L., Ponikowski, P., Schmid, J.-P., Sellevold, O. F. M., and Sicari, R. (2010). Guidelines for pre-operative cardiac risk assessment and perioperative cardiac management in non-cardiac surgery. *European Journal of Anaesthesiology*, 27:46.

[87] Ponikowski, P., Voors, A. A., Anker, S. D., Bueno, H., Cleland, J. G. F., Coats, A. J. S., Falk, V., González-Juanatey, J. R., Harjola, V.-P., Jankowska, E. A., Jessup, M., Linde, C., Nihoyannopoulos, P., Parissis, J. T., Pieske, B., Riley, J. P., Rosano, G. M. C., Ruilope, L. M., Ruschitzka, F., Rutten, F. H., and van der Meer, P. (2016). 2016 ESC Guidelines for the diagnosis and treatment of acute and chronic heart failure: The Task Force for the diagnosis and treatment of acute and chronic heart failure of the European Society of Cardiology (ESC)Developed with the special contribution of the Heart Failure Association (HFA) of the ESC. *European Heart Journal*, 37(27):2129–2200.

[88] Powell-Tuck, J., Allison, S. P., Carlson, G. L., Lewington, A. J., and Pearse, R. M. (2011). British Consensus Guidelines on Intravenous Fluid Therapy for Adult Surgical Patients. British Guidelines on IV fluids.

[89] Rhodes, A., Evans, L. E., Alhazzani, W., Levy, M. M., Antonelli, M., Ferrer, R., Kumar, A., Sevransky, J. E., Sprung, C. L., Nunnally, M. E., Rochwerg, B., Rubenfeld, G. D., Angus, D. C., Annane, D., Beale, R. J., Bellinghan, G. J., Bernard, G. R., Chiche, J.-D., Coopersmith, C., De Backer, D. P., French, C. J., Fujishima, S., Gerlach, H., Hidalgo, J. L., Hollenberg, S. M., Jones, A. E., Karnad, D. R., Kleinpell, R. M.,

Koh, Y., Lisboa, T. C., Machado, F. R., Marini, J. J., Marshall, J. C., Mazuski, J. E., McIntyre, L. A., McLean, A. S., Mehta, S., Moreno, R. P., Myburgh, J., Navalesi, P., Nishida, O., Osborn, T. M., Perner, A., Plunkett, C. M., Ranieri, M., Schorr, C. A., Seckel, M. A., Seymour, C. W., Shieh, L., Shukri, K. A., Simpson, S. Q., Singer, M., Thompson, B. T., Townsend, S. R., Van der Poll, T., Vincent, J.-L., Wiersinga, W. J., Zimmerman, J. L., and Dellinger, R. P. (2017). Surviving Sepsis Campaign: International Guidelines for Management of Sepsis and Septic Shock: 2016. *Intensive Care Medicine*, 43(3):304–377.

[90] Rudiger, A., Harjola, V.-P., Nieminen, M., and Follath, F. (2005). Acute heart failure: Clinical presentation, oneyear mortality and prognostic factors. *The European Journal of Heart Failure*, page 9.

[91] Ruijsink, B., Moireau, P., Pushparajah, K., Wong, J., Hussain, T., Razavi, R., Chapelle, D., and Chabiniok, R. (2020). Dobutamine stress testing in patients with Fontan circulation augmented by biomechanical modelling. *PLOS ONE*, Under review.

[92] Sagawa, K., Maughan, L., Suga, H., and Sunagawa, K. (1988). Cardiac contraction and the pressure volume relationship. In *Cardiac contraction and the pressure volume relationship*. Oxford University Press.

[93] Saito, M., Ikenaga, Y., Matsukawa, M., Watanabe, Y., Asada, T., and Lagrée, P.-Y. (2011). One-Dimensional Model for Propagation of a Pressure Wave in a Model of the Human Arterial Network: Comparison of Theoretical and Experimental Results. *Journal of Biomechanical Engineering*, 133(12):121005.

[94] Seemann, F., Arvidsson, P., Nordlund, D., Kopic, S., Carlsson, M., Arheden, H., and Heiberg, E. (2019). Noninvasive Quantification of Pressure-Volume Loops From Brachial Pressure and Cardiovascular Magnetic Resonance. *Circulation: Cardiovascular Imaging*, 12(1).

[95] Senzaki, H., Chen, C.-H., and Kass, D. A. (1996). Single-Beat Estimation of End-Systolic Pressure-Volume Relation in Humans: A New Method With the Potential for Noninvasive Application. *Circulation*, 94(10):2497–2506.

[96] Sermesant, M., Chabiniok, R., Chinchapatnam, P., Mansi, T., Billet, F., Moireau, P., Peyrat, J., Wong, K., Relan, J., Rhode, K., Ginks, M., Lambiase, P., Delingette, H., Sorine, M., Rinaldi, C., Chapelle, D., Razavi, R., and Ayache, N. (2012). Patient-specific electromechanical models of the heart for the prediction of pacing acute effects in CRT: A preliminary clinical validation. *Medical Image Analysis*, 16(1):201–215.

[97] Sessler, D. I., Sigl, J. C., Kelley, S. D., Chamoun, N. G., Manberg, P. J., Saager, L., Kurz, A., and Greenwald, S. (2012). Hospital Stay and Mortality Are Increased in Patients Having a "Triple Low" of Low Blood Pressure, Low Bispectral Index, and Low Minimum Alveolar Concentration of Volatile Anesthesia:. *Anesthesiology*, 116(6):1195–1203.

[98] Siirila-Waris, K., Lassus, J., Melin, J., Peuhkurinen, K., Nieminen, M. S., and Harjola, V.-P. (2006). Characteristics, outcomes, and predictors of 1-year mortality in patients hospitalized for acute heart failure. *European Heart Journal*, 160:7.

[99] Singer, M., Deutschman, C. S., Seymour, C. W., Shankar-Hari, M., Annane, D., Bauer, M., Bellomo, R., Bernard, G. R., Chiche, J.-D., Coopersmith, C. M., Hotchkiss, R. S., Levy, M. M., Marshall, J. C., Martin, G. S., Opal, S. M., Rubenfeld, G. D.,

van der Poll, T., Vincent, J.-L., and Angus, D. C. (2016). The Third International Consensus Definitions for Sepsis and Septic Shock (Sepsis-3). *JAMA*, 315(8):801.

[100] Starling, M. R. (1993). Left ventricular-arterial coupling relations in the normal human heart. *American Heart Journal*, 125(6):1659–1666.

[101] Suga, H. (1969). Time course of left ventricular pressure-volume relationship under various enddiastolic volume. *Japanese Heart Journal*, 10(6):509–515.

[102] Suga, H. (1979). Total mechanical energy of a ventricle model and cardiac oxygen consumption. *American Journal of Physiology-Heart and Circulatory Physiology*, 236(3):H498–H505.

[103] Suga, H., Hisano, R., Goto, Y., Yamada, O., and Igarashi, Y. (1983). Effect of positive inotropic agents on the relation between oxygen consumption and systolic pressure volume area in canine left ventricle. *Circulation Research*, 53(3):306–318.

[104] Suga, H., Sagawa, K., and Shoukas, A. A. (1973). Load Independence of the Instantaneous Pressure-Volume Ratio of the Canine Left Ventricle and Effects of Epinephrine and Heart Rate on the Ratio. *Circulation Research*, 32(3):314–322.

[105] Sugimachi, M., Shishido, T., Miyatake, K., and Sunagawa, K. (2001). A New Model-Based Method of Reconstructing Central Aortic Pressure from Peripheral Arterial Pressure. *The Japanese Journal of Physiology*, 51(2):217–222.

[106] Sun, L. Y., Wijeysundera, D. N., Tait, G. A., and Beattie, W. S. (2015). Association of intraoperative hypotension with acute kidney injury after elective noncardiac surgery. *The Journal of the American Society of Anesthesiologists*, 123(3):515–523.

[107] Ten Tusscher, K. H. W. J. and Panfilov, A. V. (2003). Reentry in heterogeneous cardiac tissue described by the Luo-Rudy ventricular action potential model. *American Journal of Physiology-Heart and Circulatory Physiology*, 284(2):H542–H548.

[108] Vallée, F., Passouant, O., Le Gall, A., Joachim, J., Mateo, J., Mebazaa, A., and Gayat, E. (2017). Norepinephrine reduces arterial compliance less than phenylephrine when treating general anesthesia-induced arterial hypotension. *Acta Anaesthesiologica Scandinavica*, 61(6):590–600.

[109] Vallet, B., Blanloeil, Y., Cholley, B., Orliaguet, G., Pierre, S., and Tavernier, B. (2013). Guidelines for perioperative haemodynamic optimization. *Annales Francaises d'Anesthésie et de Réanimation*, 32(10):e151–e158.

[110] Vennin, S., Li, Y., Willemet, M., Fok, H., Gu, H., Charlton, P., Alastruey, J., and Chowienczyk, P. (2017). Identifying Hemodynamic Determinants of Pulse Pressure: A Combined Numerical and Physiological Approach. *Hypertension*, 70(6):1176–1182.

[111] Vermeersch, S. J., Rietzschel, E. R., De Buyzere, M. L., Van Bortel, L. M., Gillebert, T. C., Verdonck, P. R., and Segers, P. (2009). The reservoir pressure concept: the 3-element windkessel model revisited? Application to the Asklepios population study. *Journal of Engineering Mathematics*, 64(4):417–428.

[112] Vincent, J. L., de Mendonça, A., Cantraine, F., Moreno, R., Takala, J., Suter, P. M., Sprung, C. L., Colardyn, F., and Blecher, S. (1998). Use of the SOFA score to assess the incidence of organ dysfunction/failure in intensive care units: results of a multicenter, prospective study. Working group on "sepsis-related problems" of the European Society of Intensive Care Medicine. *Critical care medicine*, 26(11):1793–1800.

[113] Weinbaum, S., Tarbell, J. M., and Damiano, E. R. (2007). The Structure and Function of the Endothelial Glycocalyx Layer. *Annual Review of Biomedical Engineering*, 9(1):121–167.

[114] Westerhof, N., Lankhaar, J.-W., and Westerhof, B. E. (2009). The arterial Windkessel. *Medical & Biological Engineering & Computing*, 47(2):131–141.

[115] Yancy, C. W., Jessup, M., Bozkurt, B., Butler, J., Casey, D. E., Drazner, M. H., Fonarow, G. C., Geraci, S. A., Horwich, T., Januzzi, J. L., Johnson, M. R., Kasper, E. K., Levy, W. C., Masoudi, F. A., McBride, P. E., McMurray, J. J., Mitchell, J. E., Peterson, P. N., Riegel, B., Sam, F., Stevenson, L. W., Tang, W. W., Tsai, E. J., and Wilkoff, B. L. (2013). 2013 ACCF/AHA Guideline for the Management of Heart Failure. *Journal of the American College of Cardiology*, 62(16):e147–e239.

[116] Zhou, S., Xu, L., Hao, L., Xiao, H., Yao, Y., Qi, L., and Yao, Y. (2019). A review on low-dimensional physics-based models of systemic arteries: application to estimation of central aortic pressure. *BioMedical Engineering OnLine*, 18(1):41.

[117] Zile, M. R. and Brutsaert, D. L. (2002). New Concepts in Diastolic Dysfunction and Diastolic Heart Failure: Part I: Diagnosis, Prognosis, and Measurements of Diastolic Function. *Circulation*, 105(11):1387–1393.

Part II

Estimation of left ventricular end diastolic pressure-volume relationship using a patient-specific biomechanical heart model

CHAPTER 2

Clinical motivations & overview of end-diastolic pressure-volume relationship

An impairment of the passive properties of the heart, also called diastolic dysfunction, is responsible for a clinical syndrome called heart failure. When heart failure decompensation suddenly occurs, patients may suffer from pulmonary oedema, a life-threatening condition associating major breathlessness and hypoxia. Left ventricular (LV) end-diastolic pressure P_{ed} is the most direct determinant of acute decompensated heart failure. Non-invasive clinical methods quantifying LVP_{ed} are lacking. However, there is a critical need as they could contribute to the diagnosis, quantification of severity and/or monitoring of the treatment effects. To address this concern, modelling the passive properties of the LV may help to fill the gap. Patient-specific biomechanical heart models may be used to estimate the end-diastolic pressure-volume relationship (EDPVR) which, in turn, can be useful for guiding therapy strategies. We propose a patient-specific framework for EDPVR estimation based on a complete biomechanical model of heart and vessels. This Chapter will discuss modelling issues, propose and evaluate a calibration procedure base on simple single-beat measurement of LV pressure and volume assessment. We will compare the proposed approach with existing methods.

2.1 Diastolic dysfunction assessment

Heart failure is a clinically defined syndrome as stated by the guidelines of the international societies of cardiology [27; 29]. It includes functional symptoms (*e.g.* breathlessness, ankle swelling or fatigue) that may be accompanied by physical symptoms (*e.g.* elevated jugular venous pressure, pulmonary crackles and peripheral oedema), that are caused by functional and/or structural cardiac abnormality. It results in a reduced cardiac output and/or elevated intracardiac pressure at rest or during stress. In these guidelines, the diastolic dysfunction is required to classify the patients into heart failure with preserved ejection fraction (HFpLVEF) entity. Echocardiography is the cornerstone complementary exam. It allows etiologic diagnosis, severity evaluation and classification within heart failure syndrome by assessing the impairment or the integrity of the systolic function. The HFpLVEF is subsequently defined as a heart failure syndrome associated with LVEF above 50% whereas the systolic heart failure is associated with a LVEF below 40%.

HFpLVEF is the clinical manifestation of the rise of the left ventricular (LV) end-diastolic pressure (P_{ed}) caused by a decompensation of the pathophysiological mechanism called diastolic dysfunction. Also, the high P_{ed} is responsible for the congestive symptoms, which are parts of the heart failure syndrome. However, diastolic dysfunction may be difficult to assess. Indeed, the acute rise of P_{ed} is a transient phenomenon, that may disappear quickly. The natural history of the diastolic dysfunction is composed by successive and transient decompensation episodes followed by compensated states. However, if the origin of the LV diastolic dysfunction is not identified and properly treated, the decompensation episodes will become more frequent, and may lead to definitive structural alterations on pulmonary circulation. Therefore, if diastolic heart failure is a clinical syndrome attesting the rise in LVP_{ed}, the diastolic dysfunction evaluation necessitates further complementary examinations, that aim 1) to confirm the rise in LVP_{ed}; 2) to assess structural alterations of the myocardium that can reveal diastolic dysfunction; 3) to identify the components of the diastolic function that are impaired (relaxation or passive filling), and ; 4) to identify aetiology (*e.g.* valvular diseases, myocardial hypertrophy or coronary heart disease). Because of the transient nature of the decompensation episodes, the preceding criteria may be missing. These analyses may be repeated in time or sensitised by exercise testing [27; 29].

The gold standard for LVP_{ed} assessment is the LV catheterisation. A LVP_{ed} above 16 mmHg is considered as an elevated LV filling pressure. It is the most sensitive indicator of acute diastolic dysfunction [31]. Even though the LV catheterisation is mandatory for direct measurement of P_{ed}, it limits its usage under routine clinical settings due to the invasiveness of the measurement. Therefore, LVP_{ed} as a prognostic information is obtained when the LV catheterisation is indicated for other reasons – typically acute coronary syndrome [2]. By contrast, indirect information regarding the LVP_{ed} may be obtained by performing right ventricle catheterisation. Indeed, the pulmonary capillary wedged pressure (PCWP) can be used to assess the elevated LVP_{ed}, as it reflects the left atrium pressure. Until the recent Berlin definition [28], a PCPW threshold of 18 mmHg was requested to identify the cardiogenic nature of the acute respiratory distress syndrome. The continuous nature of the right ventricular catheterisation may be interesting for the evaluation and the management of complex acute decompensation of HFpLVEF in intensive care. However, recent debates regarding the safety/usefulness balance of right heart catheterisation have diminished its usage [7]. Non-invasive estimations of P_{ed} are nowadays available by using echocardiography [25], which tend to replace the catheter measurement methods. Therefore, the functional key alterations assessed by transmitral flow velocity profile are recommended at first instance [27], while cardiac catheterisation is reserved for the most severe or complex cases. Indeed, the transmitral flow study helps to

classify the LV filling pressure to non-elevated or elevated. For example, an alteration of the ratio ($\frac{E}{e'}$) of early-diastolic transmitral flow velocity (E) over the early-diastolic mitral valve annulus velocity (e') has been associated with an elevated filling pressure [23]. International societies of echocardiography recommend a E/e' ratio > 12 to classify the filling pressure as increased [25] (Figure 2.1). Many other functional indicators can be derived from echocardiographic evaluation (*e.g.* longitudinal strain and tricuspid regurgitation velocity (TRV)), which helps to assess the LV filling pressure [25; 24]. However, despite being useful for a routine assessment of elevated or non elevated filling pressure, these procedures provide only a semi-quantitative assessment of LVP_{ed}.

Some statistical methods have also been described to estimate LVP_{ed} from pulmonary veins flows assessment [12; 26]. However, these methods require a high level of quality for echocardiography data acquisition, which is difficult to achieve in acute cares. Furthermore, none of the aforementioned indicators are superior to the direct measurement of LVP_{ed} for acute diastolic dysfunction diagnosis [31].

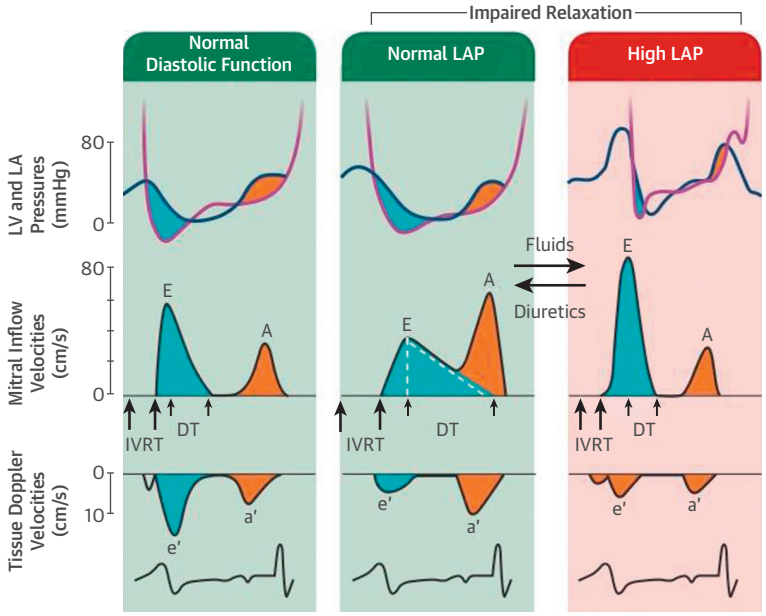

Figure 2.1 – Interpretation of transmitral flow patterns with respect to the left atrial pressure. **Left:** With normal diastolic function, left atrial pressure (LAP) and left ventricle (LV) pressure are normal with predominant early diastolic filling, short isovolumic relaxation time (IVRT), and deceleration time (DT). Mitral annulus early-diastolic velocity (e') exceeds mitral annulus late-diastolic velocity (a'). Onset of e' precedes onset of E. **Middle:** With impaired LV relaxation but normal LAP, early-diastolic transmitral pressure gradient is reduced, leading to reduced E and prolonged DT and IVRT. Due to increased LA volume before LA contraction, LA contractility increases, leading to increased late diastolic transmitral pressure gradient, increased mitral A velocity, and decreased E/A ratio. e' is delayed and reduced with increased a'. **Right:** With impaired LV relaxation but increased LAP, E increases with short DT and IVRT. Due to increased late diastolic LV pressures and LA afterload, mitral A velocity decreases, leading to an increased E/A ratio. e' is delayed and reduced with decreased a'. Increased intravascular volume in patients with grade I diastolic dysfunction leads to an increase in LAP and a pattern of predominant early LV filling (shift to right). Diuretics in patients with increased LAP shift mitral inflow pattern to one of predominant late diastolic filling. *Reproduced from [24]*

.

When an elevated LVP_{ed} cannot be proven, indirect morphological indices may be obtained by echocardiography, and may help to identify the patients at risk for decom-

pensation. Myocardial hypertrophy (left ventricular mass indexed to body surface area – LVMI > 115 g.m^{-2} for male and 95 g.m^{-2} for female), regional alteration of myocardium motion, left atrium dilation (indexed left atrium volume $\text{LAV}_\text{i} > 34$ mL.m^{-2}), aortic or mitral valvular diseases, systolic function alteration are usually associated with diastolic function alteration.

Quantitative and qualitative assessment of the active and passive components of the diastolic function may be also approximated. First, the LV relaxation is divided into two phases: the isovolumic period and the early filling period. The alteration of the isovolumic relaxation can be assessed by LV catheterisation, by the rate of LV pressure decay (the minimum $\frac{\text{dP}}{\text{dt}}$), which is altered when the relaxation is impaired. Also, the quantification of the time constant of the ventricular pressure decay (τ) by fitting a decreasing exponential function on the pressure waveform is the gold standard for assessment of LV relaxation [24]. An impaired LV relaxation may also be assessed using echocardiography, by quantifying the velocity of the mitral annulus during relaxation (e'), or by assessing the isovolumic relaxation time (the IVRT), between the end of the LV outflow and the beginning of transmitral inflow. Finally, the longitudinal/circumferential strain rate may be used for the assessment of relaxation [24]. Concerning the relaxation occurring during the LV filling, the minimal pressure (P_min), and the diastatic period (just before the atrial contraction, the $\text{P}_\text{pre-A}$) may be obtained in cathlab.

The passive properties of the LV are typically explored by the end-diastolic pressure volume relationship (EDPVR), which represents the LV P_ed at a varying end-diastolic volume (EDV) (Figure 2.2). However, not only simultaneous ventricular imaging and cardiac catheterisation are requested, but also invasive loading conditions manoeuvres are requested (in order to vary the preload). To characterise EDPVR, indices such as ratio between the P_ed over the EDV (P_ed/EDV), changes in pressure to changes in volume or diameter (ΔP/ΔV, ΔP/ΔD) and instantaneous changes in pressure and volume (dP/dV) were used to characterise the LV compliance at a given loading state [9; 13; 1]. Echocardiography allows to obtain some idea about LV compliance. A wave transit time and deceleration time of the E wave are usual indicators of the LV compliance (Figure 2.1). However, the compliance in the sense described above is given by the slope of the EDPVR at a given measurement point. It is therefore only a local measure of compliance and is not able to characterise the EDPVR globally.

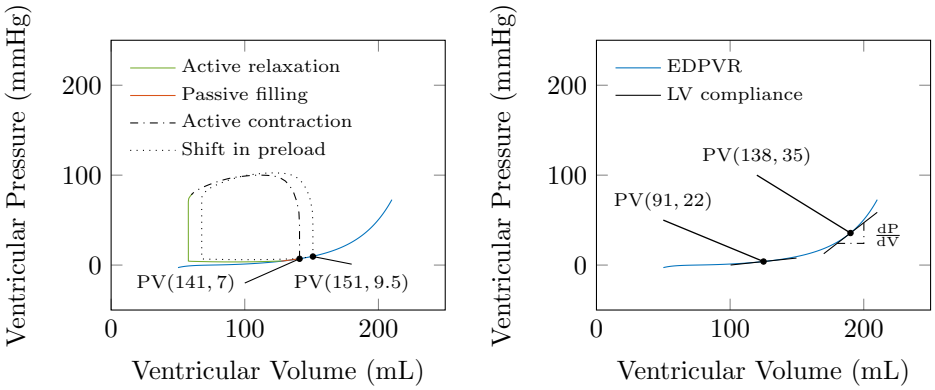

Figure 2.2 – Example of end-diastolic pressure volume relationship (EDPVR). **Left**: Decomposition of the PV loop with respect to the active and the passive period. **Right**: Example of the concept of left ventricle (LV) compliance, and dependancy with repect to the preload.

Since *in vivo* EDPVR measurement can not be performed in clinical settings or since non invasive indirect estimations are lacking, mathematical models have been proposed to

estimate the EDPVR.

2.2 Modelling presentation and issues

Since the early 1970's, it has been hypothesised that the passive properties of the heart behaved like a non-Hookean elastic material [10; 21; 8] (Figure 2.2). This hypothesis allowed to apply the physical principles of the continuum mechanics theory. The passive properties of the myocardium could therefore be described in terms of stress (τ_c)/strain (e) relationship, characterised by its tangent modulus $\left(\frac{d\tau_c}{de}\right)$ (*i.e* the elastic stiffness (E_s) for myocardium assessment). The exponential nature of the myocardial stress/strain relationship was theoretically proven [10], and experimentally demonstrated [18; 8].

Based on these observations, two types of model have emerged. On the one hand, to allow a more complete description of the data obtained during cardiac catheterisation, exponential functions were fitted to Pressure-Volume datapoints (*i.e.* to EDPVR) [19]. These phenomenological models allowed to developed single-beat methods of EDPVR estimation [17], with the potential toward non-invasive applications [12]. However, such phenomenological models do not allow explanatory introspection of physical phenomenon hidden in the EDPVR. Furthermore, the statistical approach used to determine the coefficients of these models decreases the patient-specificity of the estimation.

The other class of models of passive behaviour of the LV are based on continuum mechanics theory and allow a description of phenomena underlying the EDPVR, by taking into account physical, energetical, morphological, geometrical and physiological characteristics of the chamber, at micro- (*i.e.* down to molecular level) to macro-scale levels (*i.e.* up to organ level) [15; 6]. General formulations of these models can be turned into a patient-specific regime by the process of "model calibration", during which the parameters of the models are adjusted by using the data processed from a given patient. However, this calibration procedure often requests rich data information, that are difficult to obtain in routine clinical practice. Furthermore, the approach allows to use complex geometry (*i.e.* detailed three-dimensional (3D) geometry of heart). However, this increases the computational cost, preventing the implementation with standard computational resources in a time-frame compatible with anaesthesia and intensive care issues. In 2008, Caruel et al. [4] have proposed a simplified formulation of a complex 3D biomechanical model [6], the geometry being reduced to a sphere. This particular formulation is suitable to perform calibration with data routinely acquired during clinical procedures. It allows to simulate heartbeats close to real time – typically one heartbeat being computed in less than 30 seconds. It allows fast calibration procedures, which can be implemented on computers with standard resources.

2.2.1 Phenomenological models

During the early 70's, since progresses in the application of the continuum mechanics theory have led to describe the passive properties of the myocardium tissue as an hyperelastic material (See Figure 2.3), it has been hypothesised that PV relationship at end-diastole (EDPVR) and therefore the passive properties of the left ventricle can be described by an exponential function [11]:

$$P = Ae^{\alpha V} \tag{2.1}$$

A and α are the parameters to be estimated to fit the estimated curve on the measured data.

Originated in 1973, and summarised in 1990, Mirsky et al. demonstrated a link between the micro-scale level (the myocardial fibre) and the macro-scale level (left ventricle

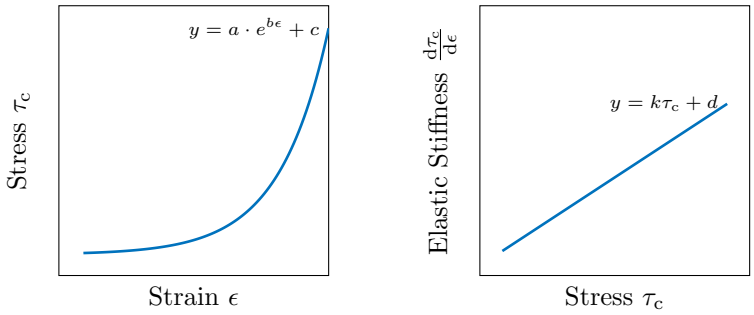

Figure 2.3 – **Left:** The stress (τ_c) strain (ϵ) relationship. **Right:** the elastic stiffness ($\frac{d\tau_c}{d\epsilon}$) as a function of stress. If the stress – strain relationship is of exponential form, then the elastic stiffness is a linear function of stress. *Reproduced from [21].*

pressure–volume relationship) by using a spherical or a cylindrical model of heart [21; 19; 20; 22]. By integrating stress-strain relationship over a cylindrical or spherical heart model, Mirsky and coworkers explained the exponential shape of the PV relationship by demonstrating the linear behaviour of what they called the chamber stiffness with respect to end-diastolic pressure (*i.e.* chamber stiffness $= \frac{dP}{dV}$ by analogy with the elastic or myocardial stiffness $E_s = \frac{d\tau_c}{d\epsilon}$) :

$$\frac{dP}{dV} = \frac{(4/9)\,\frac{d\tau_c}{d\epsilon} - P\,(V/V_w)}{V\,(1 + V/V_w)} \tag{2.2}$$

$E_s = \frac{d\tau_c}{d\epsilon}$ is the elastic or myocardial stiffness, τ_c and ϵ being respectively the stress and the strain applied to a myocardial fibre, V the end-diastolic ventricular volume, P the end-diastolic ventricular pressure and V_w the myocardial wall volume. They further demonstrated that, when normalising Equation (2.2) to volume, it yields:

$$\frac{dP}{dV/V} = V\left(\frac{dP}{dV}\right) = \frac{(4/9)\,E_s - P\,(V/V_w)}{(1 + V/V_w)} \tag{2.3}$$

which is directly related to myocardial stiffness.

They also demonstrated that when normalising equation (2.2) to myocardial volume V_w, it yields:

$$\frac{dP}{dV/V_w} = \frac{(4/9)\,E_s - P\,(V/V_w)}{(V/V_w)\,(1 + V/V_w)} \tag{2.4}$$

which indicates that the relationship $V_W\,(dP/dV)$ might yields an index of chamber stiffness.

By demonstrating the linearity of the chamber stiffness (described by Equation (2.2)) with respect to ventricular pressure, they justified the choice of exponential functions to curve fit Pressure–Volume data, as proposed by Gaasch et al. [11] (Equation (2.1)).

Therefore they proposed to fit Pressure-Volume data points by functions which are convenient to use to make links between observation and physics:

$$P = Ae^{\alpha\frac{V}{V_w}}\ ;\ P = BV^{\beta} \tag{2.5}$$

Indeed, when deriving Equation (2.5), it yields

$$\begin{cases} \frac{dP}{d(V/V_w)} = \alpha \cdot Ae^{\alpha\frac{V}{V_w}} = \alpha P \\ \frac{dP}{dV} \cdot V = \beta \cdot BV^{\beta} = \beta P \end{cases} \tag{2.6}$$

α and β being index of myocardial and chamber stiffness respectively.

From this formulation, we can interpret that P can be fitted by one or the other formulation depending on the type of data available. We can also deduced that β and α are interdependant. Two major issues of such approach have been discussed in the review written by Burkhoff and Mirsky [3]. First the shape of the exponential or polynomial functions is governed by two terms: A or B on one hand, α and β on the other hand. Such formulation makes comparison between patient difficult as each parameter in front of the exponent or polynomial can only be interpreted with the respective exponent or power term. Second, the choice of exponential function might be non ideal because as formulated on Equation (2.5), the function tends towards 0 pressure when $\frac{V}{V_w}$ tends toward $-\infty$. Indeed, it has been observed that the curve fit by such exponential or polynomial formulation is misleading for the lowest PV data measured.

Recently, Klotz et al. [17] used data obtained from 80 explanted hearts from various species: human, dogs and rats. He observed that after double normalisation (Equation (2.7)), the EDPVR demonstrates a common underlying shape across subjects and across species.

$$V_n = \frac{V - V_{ref}}{V_{30} - V_{ref}} \tag{2.7}$$

V_n being the ventricle volume normalised, V_{ref} and V_{30} respectively the volume at stress free configuration and the volume measured when the ventricular pressure reached 30 mmHg (Figure 2.4).

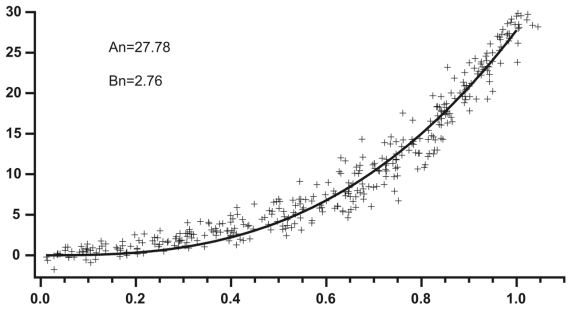

Figure 2.4 – Normalised end-diastolic pressure volume data point obtained for 80 explanted human hearts. A_n and B_n are the fitted coefficients. *Reproduced from Klotz et al.* [17]

The Klotz model is therefore written as follows:

$$P_{klotz} = A_n \cdot V_n{}^{B_n} \tag{2.8}$$

With A_n, B_n being the coefficients which were fit on normalised population data.

As was originally described, the procedure proposed by Klotz, allowed to calibrate the EDPVR from one single-beat measurement of pressure (P_m) and volume (V_m) by following these steps:

1) The estimation of V_{ref} from (V_m, P_m) [17] based on linear regression between volumes measured at different levels of pressure and V_{ref}:

$$V_{ref} = k \cdot V_m \tag{2.9}$$

With $k = 0.53$ for $P_m < 10$ mmHg, $k = 0.48$ for $10 \leq P_m < 15$ mmHg, $k = 0.46$ for $15 \leq P_m < 20$ mmHg and $kk = 0.43$ for $P_m > 25$ mmHg, in order to estimate V_{ref} from (V_m, P_m).

2) The estimation of V_{30}, derived from the combination of Equation (2.7) and Equation (2.8)

$$V_{30} = V_{ref} + (V_m - V_{ref})/(P_m/A_n)^{1/B_n} \tag{2.10}$$

and 3) The Estimation of EDPVR by combining Equation (2.7) and Equation (2.8):

$$P_{klotz} = \frac{A_n}{\left(\frac{V_{30}}{V_{ref}} - 1\right)^{B_n}} \cdot \left(\frac{V}{V_{ref}} - 1\right)^{B_n} \tag{2.11}$$

By using this procedure and the A_n and B_n parameters obtained by optimising the parameters of Equation (2.8) on the data provided in Figure 2.4, the work of Klotz et al. [17] was the first to propose a single-beat method for EDPVR estimation. This work has been widely adopted by the modelling community (*e.g.* used in [14]).

However, there are several limitations of such phenomenological models. Indeed, despite convenient applicability on patient data, they typically neglect important geometrical properties of the myocardium. Relying on the use of population-based coefficient to parametrise the model – namely A_n, B_n, V_{ref} and V_{30} is another limitation. It decreases the patient specificity of this approach.

2.2.2 Biomechanical models

The biomechanical models defined herein are based on physical description of mechanical response of myocardial tissue. The first biomechanical models described the passive law by transversely isotropic and hyperelastic constitutive equations [30] of the form:

$$W = Ce^{A_x E_x^2 + A_y E_y^2} \tag{2.12}$$

The hyperelastic potential (W) stands for the energy response to the strain (E_x and E_y), C and A_x and A_y being the coefficient to fit on the stress/strain data in x and y direction, respectively.

In the work of Humphrey and Yin [16], the equation (2.12) was composed of the sum of two exponential functions oriented in transversal direction:

$$W = c\left[e^{b(I_1-3)} - 1\right] + A\left[e^{a(\sqrt{I_4}-1)^2} - 1\right] \tag{2.13}$$

where c, b, A and a are pseudoelastic material parameters, and $I_1 = \mathrm{tr}\left(\underline{\underline{C}}\right)$ and $I_4 = \underline{\tau_1} \cdot \underline{\underline{C}} \cdot \underline{\tau_1}$ the first and fourth invariants of the left Cauchy-Green tensor ($\underline{\underline{C}} = \underline{\underline{F}}^T\underline{\underline{F}}$, where $\underline{\underline{F}}$ is the deformation gradient). Each term of Equation (2.13) denotes respectively the isotropic, and transversely isotropic energy in fibre direction (τ_1), respectively.

In 2009, Holzapfel and Ogden published an advanced version of these models, based on structural approach [15]. The three-dimensional orthotropic model depends on a hyperelastic potential described by a limited number of parameters. This has the advantage to describe the passive property of a piece of myocardium, taking into account the orthotropic fibre direction and the shear inside the myocardium, independently of the global geometry of the heart model. This hyperelastic potential is written as follows:

$$W = \frac{a}{2b}e^{b(I_1-3)} + \sum_{i=f,s}\frac{a_i}{2b_i}e^{b_i(I_{4i}-1)^2} - 1 + \frac{a_{fs}}{2b_{fs}}\left(e^{b_{fs}I_{fs}^2} - 1\right) \tag{2.14}$$

where a, b coefficients related to I_1, I_4, I_{fs}.

The hyperelastic potential described by Equation (2.14) inspired the passive law used in the model described by Chapelle et al. [6], and modified by Caruel et al. [4]. The hyperelastic potential is written as:

$$W_e = C_0 \cdot e^{C_1(J_1-3)^2} + C_2 \cdot e^{C_3(J_4-1)^2}, \tag{2.15}$$

where $J_1 = I_1 \cdot {I_3}^{-\frac{1}{3}}$ and $J_4 = I_4 \cdot {I_3}^{-\frac{1}{3}}$, being the reduced invariants of the Cauchy-Green strain tensor, $I_3 = \det\left(\underline{\underline{C}}\right)$ and (C_0, C_1, C_2, C_3) the parameters of the hyperelastic potential. We remark that in [14], the authors demonstrated that the form of hyperelastic potential (2.15) has in addition advantage of a good identifiability of parameters.

Assuming spherical geometry, the stress expression can be written as (see [4]):

$$\Sigma_{\text{sphere}}\left(e_{\text{fib}}\right) = 4\left(1 - C^{-3}\right)\frac{\partial W_e}{\partial J_1} + 2\frac{\partial W_e}{\partial J_4} \tag{2.16}$$

with $C = (1 + e_{\text{fib}})^2$ the circumferential component of the Cauchy-Green strain tensor and e_{fib} the fibre extension.

We further modified the spherical model described in [4] by implementing a wall thickening model:

$$\begin{cases} R = R_{\text{ref}} \cdot (1 + e_{\text{fib}}) \\ d = d_{\text{ref}} \cdot (1 + e_{\text{fib}})^{-2} \end{cases} \tag{2.17}$$

R and R_{ref}, and d and d_{ref} being respectively the radius until mid-wall thickness of the sphere and the diameter of the myocardium at any position and at stress free reference configuration. The volume of the sphere is therefore calculated using the following formula:

$$V = \frac{4\pi}{3}\left(R - \frac{d}{2}\right)^3 \tag{2.18}$$

Substituting R and d from Equation (2.17) into Equation (2.18), it yields

$$\begin{cases} V = \frac{4\pi}{3}{R_{\text{ref}}}^3 \cdot \left(1 + e_{\text{fib}} - \frac{\epsilon}{2}(1 + e_{\text{fib}})^{-2}\right)^3 \\ V_{\text{ref}} = \frac{4\pi}{3}{R_{\text{ref}}}^3 \cdot \left(1 - \frac{\epsilon}{2}\right)^3 \end{cases} \tag{2.19}$$

With $\epsilon = \frac{d_{\text{ref}}}{R_{\text{ref}}}$.

At equilibrium, the ventricular pressure can be written as a function of the fibre extension e_{fib}, of the constitutive tissue stiffness parameters C_i ($i \in 0, \ldots, 3$) and of the thickness of the sphere at stress-free reference configuration attested by ϵ (adapted from [5]):

$$P_{0_D} = \epsilon \cdot \Sigma_{\text{sphere}}\left(e_{\text{fib}}\right) \cdot \left(1 + e_{\text{fib}}\right)\left(1 + e_{\text{fib}} - \frac{\epsilon}{2}(1 + e_{\text{fib}})^{-2}\right)^{-2}\left(1 + \epsilon\,(1 + e_{\text{fib}})^{-3}\right)^{-1} \tag{2.20}$$

The main advantage of the models based on continuum mechanics approach is due to their underlying physical and physiological bases since they incorporate physical and physiological assumptions. However, turning the model into patient-specific regime (*e.g.* by calibrating the model, or automatically assimilating data into the model) is a challenging task of the biomechanical modelling community. Despite their interesting potential applications, their use have not yet spread to clinical communities for routine patient's care.

By using the model described by Equation (2.20), we propose a calibration method that allow patient-specific modelling of EDPVR with data acquired routinely in operating theatre.

2.3 Working hypothesis and objectives

Our hypothesis is to propose a framework reuniting the pragmatic approach of the phenomenological models with the rigorous approach of the biomechanical models. We propose a fast single-point EDPVR estimation method, which is underlied by the passive law

derived from the 0D model described in [4] (Equation (2.20)). In the subsequent chapters, we will first describe and study the EDPVR behaviour generated by our framework, and we will compare its performance with the single-beat estimation method described in the paper of Klotz et al. [17], to fit EDPVR data.

Bibliography

[1] Barry, W. H., Brooker, J. Z., Alderman, E. L., and Harrison, D. C. (1974). Changes in Diastolic Stiffness and Tone of the Left Ventricle During Angina Pectoris. *Circulation*, 49(2):255–263.

[2] Brienesse, S. C., Davies, A. J., Khan, A., and Boyle, A. J. (2018). Prognostic Value of LVEDP in Acute Myocardial Infarction: a Systematic Review and Meta-Analysis. *Journal of Cardiovascular Translational Research*, 11(1):33–35.

[3] Burkhoff, D. (2005). Assessment of systolic and diastolic ventricular properties via pressure-volume analysis: a guide for clinical, translational, and basic researchers. *AJP: Heart and Circulatory Physiology*, 289(2):H501–H512.

[4] Caruel, M., Chabiniok, R., Moireau, P., Lecarpentier, Y., and Chapelle, D. (2014). Dimensional reductions of a cardiac model for effective validation and calibration. *Biomechanics and Modeling in Mechanobiology*, 13(4):897–914.

[5] Caruel, M. and Truskinovsky, L. (2018). Physics of muscle contraction. *Reports on Progress in Physics*, page 50.

[6] Chapelle, D., Le Tallec, P., Moireau, P., and Sorine, M. (2012). Energy-preserving muscle tissue model: formulation and compatible discretizations. *International Journal for Multiscale Computational Engineering*, 10(2).

[7] Connors, A. F., Speroff, T., Dawson, N. V., Thomas, C., Harrell, F. E., Wagner, D., Desbiens, N., Goldman, L., Wu, A. W., Califf, R. M., and others (1996). The effectiveness of right heart catheterization in the initial care of critically III patients. *Jama*, 276(11):889–897.

[8] Demiray, H. (1976). Stresses in Ventricular Wall. *Journal of Applied Mechanics*, 43(2):194.

[9] Diamond, G. and Forrester, J. S. (1972). Effect of Coronary Artery Disease and Acute Myocardial Infarction on Left Ventricular Compliance in Man. *Circulation*, 45(1):11–19.

[10] Fung, Y. (1967). Elasticity of soft tissues in simple elongation. *American Journal of Physiology-Legacy Content*, 213(6):1532–1544.

[11] Gaasch, W. H., Battle, W. E., Oboler, A. A., Banas, J. S., and Levine, H. J. (1972). Left Ventricular Stress and Compliance in Man: With Special Reference to Normalized Ventricular Function Curves. *Circulation*, 45(4):746–762.

[12] Gayat, E., Mor-Avi, V., Weinert, L., Yodwut, C., and Lang, R. M. (2011). Noninvasive quantification of LV elastance and ventricular-arterial coupling using 3D echo and arterial tonometry. *AJP: Heart and Circulatory Physiology*, 301(5):H1916–H1923.

[13] Grossman, W., Stefadouros, M. A., Mclaurin, L. P., Rolett, E. L., and Young, D. T. (1973). Quantitative Assessment of Left Ventricular Diastolic Stiffness in Man. *Circulation*, 47(3):567–574.

[14] Hadjicharalambous, M., Chabiniok, R., Asner, L., Sammut, E., Wong, J., Carr-White, G., Lee, J., Razavi, R., Smith, N., and Nordsletten, D. (2015). Analysis of passive cardiac constitutive laws for parameter estimation using 3d tagged MRI. *Biomechanics and modeling in mechanobiology*, 14(4):807–828.

[15] Holzapfel, G. A. and Ogden, R. W. (2009). Constitutive modelling of passive myocardium: a structurally based framework for material characterization. *Phil. Trans. R. Soc. A: Mathematical, Physical and Engineering Sciences*, 367(1902):3445–3475.

[16] Humphrey, J. and Yin, F. (1989). Biomechanical experiments on excised myocardium: Theoretical considerations. *Journal of Biomechanics*, 22(4):377–383.

[17] Klotz, S., Hay, I., Dickstein, M. L., Yi, G.-H., Wang, J., Maurer, M. S., Kass, D. A., and Burkhoff, D. (2006). Single-beat estimation of end-diastolic pressure-volume relationship: a novel method with potential for noninvasive application. *AJP: Heart and Circulatory Physiology*, 291(1):H403–H412.

[18] Mirsky, I. (1976). Assessment of passive elastic stiffness of cardiac muscle: Mathematical concepts, physiologic and clinical considerations, directions of future research. *Progress in Cardiovascular Diseases*, 18(4):277–308.

[19] Mirsky, I., Cohn, P. F., Levine, J. A., Gorlin, R., Herman, M. V., Kreulen, T. H., and Sonnenblick, E. H. (1974). Assessment of Left Ventricular Stiffness in Primary Myocardial Disease and Coronary Artery Disease. *Circulation*, 50(1):128–136.

[20] Mirsky, I., Janz, R. F., Kubert, B. R., Korecky, B., and Taichman, G. C. (1976). Passive elastic wall stiffness of the left ventricle: A comparison between linear theory and large deformation theory. *Bulletin of Mathematical Biology*, 38(3):239–251.

[21] Mirsky, I. and Parmley, W. W. (1973). Assessment of Passive Elastic Stiffness for Isolated Heart Muscle and the Intact Heart. *Circulation Research*, 33(2):233–243.

[22] Mirsky, I. and Pasipoularides, A. (1990). Clinical assessment of diastolic function. *Progress in Cardiovascular Diseases*, 32(4):291–318.

[23] Mulvagh, S., Quiñones, A., M., Kleiman, S., N., Cheirif, B., J., and Zoghbi, A., W. (1992). Estimation of left ventricular end-diastolic pressure from doppler transmitral flow velocity in cardiac patients independent of systolic performance. *Journal of the American College of Cardiology*, 20(1):112–9.

[24] Nagueh, S. F. (2019). Left Ventricular Diastolic Function. *JACC: Cardiovascular Imaging*, page S1936878X19302530.

[25] Nagueh, S. F., Appleton, C. P., Gillebert, T. C., Marino, P. N., Oh, J. K., Smiseth, O. A., Waggoner, A. D., Flachskampf, F. A., Pellikka, P. A., and Evangelisa, A. (2008). Recommendations for the Evaluation of Left Ventricular Diastolic Function by Echocardiography. *European Journal of Echocardiography*, 10(2):165–193.

[26] Olariu, A. (2003). Non-invasive estimation of left ventricular end-diastolic pressure by pulmonary venous flow deceleration time. *European Journal of Echocardiography*, 4(3):162–168.

[27] Ponikowski, P., Voors, A. A., Anker, S. D., Bueno, H., Cleland, J. G. F., Coats, A. J. S., Falk, V., González-Juanatey, J. R., Harjola, V.-P., Jankowska, E. A., Jessup, M., Linde, C., Nihoyannopoulos, P., Parissis, J. T., Pieske, B., Riley, J. P., Rosano,

G. M. C., Ruilope, L. M., Ruschitzka, F., Rutten, F. H., and van der Meer, P. (2016). 2016 ESC Guidelines for the diagnosis and treatment of acute and chronic heart failure: The Task Force for the diagnosis and treatment of acute and chronic heart failure of the European Society of Cardiology (ESC)Developed with the special contribution of the Heart Failure Association (HFA) of the ESC. *European Heart Journal*, 37(27):2129–2200.

[28] The ARDS definition task force (2012). Acute respiratory distress syndrome: The berlin definition. *JAMA*, 307(23).

[29] Yancy, C. W., Jessup, M., Bozkurt, B., Butler, J., Casey, D. E., Drazner, M. H., Fonarow, G. C., Geraci, S. A., Horwich, T., Januzzi, J. L., Johnson, M. R., Kasper, E. K., Levy, W. C., Masoudi, F. A., McBride, P. E., McMurray, J. J., Mitchell, J. E., Peterson, P. N., Riegel, B., Sam, F., Stevenson, L. W., Tang, W. W., Tsai, E. J., and Wilkoff, B. L. (2013). 2013 ACCF/AHA Guideline for the Management of Heart Failure. *Journal of the American College of Cardiology*, 62(16):e147–e239.

[30] Yin, F. C., Strumpf, R. K., Chew, P. H., and Zeger, S. L. (1987). Quantification of the mechanical properties of noncontracting canine myocardium under simultaneous biaxial loading. *Journal of biomechanics*, 20(6):577–589.

[31] Zile, M. R., Gaasch, W. H., Carroll, J. D., Feldman, M. D., Aurigemma, G. P., Schaer, G. L., Ghali, J. K., and Liebson, P. R. (2001). Heart Failure With a Normal Ejection Fraction. *Circulation*, page 4.

CHAPTER 3

Description of the behaviour of the biomechanical passive law

In this Chapter, we define a framework to calibrate our biomechanical passive law from a limited availability of pressure-volume datapoints. Our method is original as the identification of the parameters necessary for patient-specific calibration in other biomechanical heart models is difficult in a clinical setting. We propose an original method based on a complete analysis of the physiological behaviour of the passive law calibrated on a reference patient. We describe a procedure to reduce the number of parameters to be adjusted, comparatively to this reference patient. We proved that the passive law described in Chapter 2, deviates as a homothetical transformation from the reference configuration, when modifying intrinsic stiffness C_i or stiffness associated with geometrical organisation of myocardial fibre – *i.e.* associated with the wall thickness in the reference configuration. Therefore we describe a framework to estimate the parameters associated with the deviation from the reference configuration. One of the advantages of our approach lies in the fact that these parameters can be seen directly as either a stiffness or either a volume information, and can be physiologically interpreted. In particular, the proposed method allows to compare between various patients, while quantifying the passive tissue stiffness of their myocardium. Another advantage lies in the setup of a single-beat estimation method, which would allow to use our framework in clinical scenarios.

In this Chapter, we will describe the behaviour of the passive law introduced in Chapter 2, Section 2.2. From a reference configuration calibrated on a patient's dataset obtained in vivo during general anaesthesia, we will first optimise the C_i parameters using the normalised data from the paper of Klotz et al. [3]. Then we will analyse the sensitivity of the passive law when deviating the ϵ, and the V_{ref} parameters. Finally we will propose and study a numerical method to estimate model parameters from measured PV datapoints.

3.1 Numerical study of the passive law behaviour

3.1.1 Patient's data

Data were obtained in a reference patient who was anaesthetised for neuroradiological procedure. The data collection procedure is described in details elsewhere (see Chapter 1, Section 1.5.2.9). In brief, after general anaesthesia induction, a transoesophageal Doppler probe was inserted into the oesophagus of the patient. A continuous measurement of arterial pressure was obtained using a radial artery cannula. A transthoracic echocardiography (TTE) was also performed in order to obtain geometrical and functional information (see Table 3.1). During the neuroradiological procedure, the radiologist inserted arterial guidewire through femoral puncture up to cerebral arteries. The aortic pressure was recorded when the guidewire was located inside the ascending aorta. The patient was orally informed that we used the acquired data for research purpose and agreed with using his/her data for research purposes. The ethical committee (CE SRLF 14-34) waived the need for written consent. Indeed, the research protocol described above was non interventional, all the invasive procedures were performed for medical reasons. The patients could withdraw their consent at any time.

We estimated the LV end-diastolic volume (V_{ed} or V_m) from the apical 4-cavity chambers view of transthoracic echocardiography (TTE) (Figure 3.1), by using the revolution of the LV end-diastolic surface and long axis. We isolated the LV wall thickness and estimated the LV wall volume in order to estimate the LV mass. We also used the transmitral pulsed Doppler velocity waveform to classify the filling pressure of the LV between low or high, according to the European guidelines [6]. In the patient studied, the filling pressure was found low. We therefore prescribed the level of 7 mmHg pressure for LVP_{ed} (P_m).

3.1.2 Passive law calibration

In order to calibrate the spherical heart model to the patient's data, we used the following procedure:

3.1.2.1 Estimation of V_{ref}, R_m, d_m and ϵ parameters

First, from (V_m, P_m), we estimated V_{ref} according to the method used in Klotz et al. [3] (See Chapter 2, Section 2.2.1).

Secondly, we estimated the radius (R_m) and the thickness (d_m) of the sphere:

$$R_m = \left(\frac{3}{4\pi}V_m\right)^{\frac{1}{3}} + \frac{d_m}{2} \tag{3.1}$$

d_m being estimated by the combination of Equation (2.18), and Equation (3.2):

$$LV_{mass} = V_{total} - V_{inner} \tag{3.2}$$

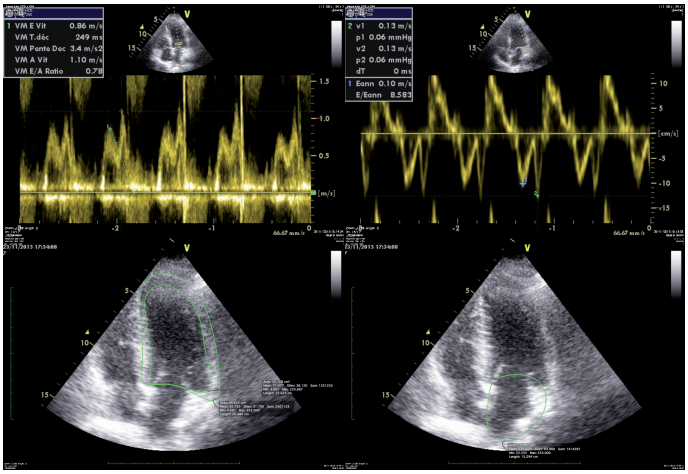

Figure 3.1 – Example of echocardiographic Data measurement. **Upper Left**: Semiquantitative left ventricular (LV) end-diastolic pressure (P_{ed}) measurement. Apical 4-cavity view; Pulsed Doppler; Transmitral flow velocity signal; **Upper Right**: Semiquantitative LVP_{ed} measurement. Apical 4-cavity view; Tissular Pulsed Doppler; Mitral annulus velocity signal; **Lower Left**: LV end-diastolic volume (V_{ed}) measurement. Apical 4-cavity view; 2D echography; **Lower Right**: Atrial end-diastolic surface measurement. Apical 4-cavity view; 2D echography;

Table 3.1 – Data obtained in the reference Patient 11, and corresponding geometrical parameters.

	Patient 11
Patient's Data	
LVV_{ed} (mL)	133
LWPW (cm)	9.8
E wave ($cm.s^{-1}$)	86
A wave ($cm.s^{-1}$)	110
DT (ms)	249
E' wave ($cm.s^{-1}$)	10
LA surface (cm^2)	18
LV mass (g)	103
Model parameters	
V_{ref} (mL)	70.49
R_{ref} (cm)	3.01
d_{ref} (cm)	0.9
ϵ	0.2980
LVP_{ed} (mmHg)	7

LVV_{ed}: Left ventricular end-diastolic volume; LWPW: Left ventricular posterior wall; DT: Deceleration time; LA: Left atrium; V_{ref}: End-diastolic LV volume at reference configuration; R_{ref}: End-diastolic LV diameter at reference configuration; d_{ref}: End-diastolic LV wall thickness at reference configuration; $\epsilon = \frac{d_{ref}}{R_{ref}}$; LVP_{ed}: LV end-diastolic pressure.

V_{total} and V_{inner} ($= V_m$) being respectively the maximal volume of the sphere and the volume inside the cavity. These volumes and LV_{mass} were estimated using the method described in Section 3.1.1.

It yields:

$$d_m = \left(\frac{3}{4\pi}\left(V_m + LV_{mass}\right)\right)^{\frac{1}{3}} - \left(\frac{3}{4\pi}V_m\right)^{\frac{1}{3}} \tag{3.3}$$

Third, in Equation (3.1) and (3.3), we replaced V_m by V_{ref} to obtain d_{ref} and R_{ref}, and we estimated ϵ by using the following equation:

$$\epsilon = \frac{d_{ref}}{R_{ref}} \tag{3.4}$$

3.1.2.2 Optimisation of the C_i coefficients parameters by using normalised data

We hypothesised that the C_i coefficients parameters could be optimised in order to fit the normalised Data available in the paper of Klotz et al. [3] and described in Section 2.2.1.

First, we estimated V_{ref} from the patient's single measured point (V_m, P_m), by using the Klotz algorithm, described in section 2.2.1. We further calculated V_{30} by using Equation (2.10) with the previously calculated V_{ref}, the given coefficient ($A_n = 27.78$ and $B_n = 2.76$), and V_m.

Second, for parameters estimation, we defined a variable $e_{fib} = [0 : 0.01 : 0.2]$, which is the variable of the passive law defined by Equation (2.20). In order to compare our passive law, written as a function of e_{fib}, with Klotz model described by Equation (2.11), we had to perform a variable transformation:

$$\left(\frac{V}{V_{ref}}\right)^{\frac{1}{3}} = \frac{1 + e_{fib} - \frac{\epsilon}{2}\left(1 + e_{fib}\right)^{-2}}{\left(1 - \frac{\epsilon}{2}\right)}. \tag{3.5}$$

Therefore, V can be approximated by a function of e_{fib}, V_{ref}, and ϵ, by using Newton's algorithm for a nonlinear equation.

Third, we minimised the following criterion by using a gradient descent method, to get an initial guess on C_i (C_i^{init})

$$J\left(C_i^{init}\right) = \sum_{n=1}^{N}\left(P_{klotz}^n\left(\frac{V^n}{V_{ref}}, V_{30}, A_n, B_n\right) - P_{0_D}^n\left(\frac{V^n}{V_{ref}}, \epsilon, C_i^{init}\right)\right)^2 \tag{3.6}$$

N being the length of the vector e_{fib}, $P_{0_D}^n$ the solution of Equation (2.20), and P_{klotz}^n the solution of Equation (2.11).

Fourth, we extracted the volume-normalised PV data ($P_{data}, V_{(data,n)}$) provided in Figure 3 of the publication [3] (see section 2.2.1 and Figure 2.4 for details). We used Equation (2.7) to calculate $\frac{V_{data}}{V_{ref}}$, which was translated into $e_{fib_{data}}$ using Equation (3.5). Therefore, we were able to estimate the C_i coefficients that minimise the following equation:

$$J_{data}\left(C_i\right) = \sum_{n=1}^{N_{data}}\left(P_{data}^n - P_{0_D}^n\left(\frac{V^n{}_{data}}{V_{ref}}, \epsilon, C_i\right)\right)^2 \tag{3.7}$$

N_{data} being the number of PV datapoints.

Finally, we estimated the passive law associated with the optimised C_i parameters, by using the variable $e_{fib}{}^N$ and the ϵ parameter derived from the reference patient's data. We compared the passive law (P_{0_D}) and the Klotz function (P_{klotz}) with the P_{data}.

Figure 3.2, shows the result of the optimisation process. The root mean squared error (RMSE) was lower when using the proposed passive law (P_{0_D}) compared with Klotz procedure (P_{klotz}) (1.52 mmHg vs 1.61 mmHg). Qualitative comparison suggests that the biggest difference between the two models is in the the initial part of the EDPVR.

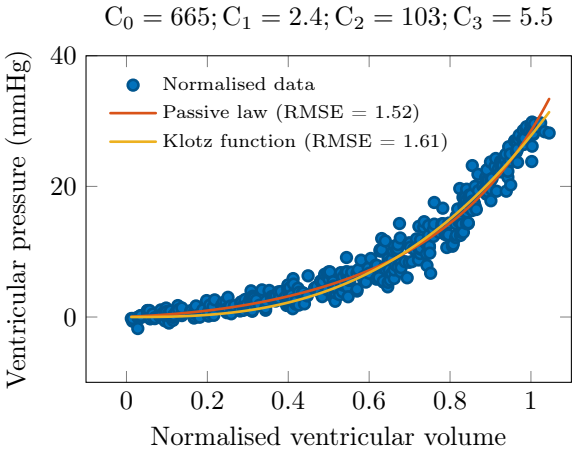

Figure 3.2 – Result of the optimisation procedure. Comparison between passive law and Klotz function in normalised space

The optimised parameters in our subject were found as follows: $[C_0 = 665, C_1 = 2.4, C_2 = 103$ and $C_3 = 5.5]$.

3.1.3 Description of the behaviour of the passive law with respect to parameters changes

3.1.3.1 Parametric deviation with respect to V_{ref} parameter

We see from Equation (2.20), for a given ϵ and C_i, that the pressure only depends on e_{fib}. Therefore, through the variable transformation written in Equation (3.5) a modification of e_{fib} is translated into a change in V_{ref}. Furthermore, the relationship between e_{fib} and the normalised volume V_n can be obtained by combining Equation (2.7) and Equation (3.5). It yields:

$$V_n = \left[\left(\frac{1 + e_{fib} - \frac{\epsilon}{2}(1 + e_{fib})^{-2}}{1 - \frac{\epsilon}{2}} \right)^3 - 1 \right] \cdot \left(\frac{V_{30}}{V_{ref}} - 1 \right)^{-1} \tag{3.8}$$

The ratio $\frac{V_{30}}{V_{ref}}$ is constant and does not depend on V_{ref}. Indeed, the extension fibre ${e_{fib}}^{30}$ is univocally defined from Equation (2.20) taking the pressure $P_{30} = 30$ mmHg. In particular, according to Equation (3.5), ${e_{fib}}^{30}$ does not depend on V_{ref} but rather on the ratio $\frac{V_{30}}{V_{ref}}$. To satisfy Equation (3.5) for $e_{fib} = {e_{fib}}^{30}$, a relative change in V_{ref} is necessarily associated with the same relative change in V_{30}. Figure 3.3 shows example of the effect of isolated change in V_{ref} on the passive law.

3.1.3.2 Parametric deviation with respect to C_i parameters

In Equation (2.11), the stiffness of the tissue is governed by the ratio of parameters $\frac{V_{30}}{V_{ref}}$. A modification of $\frac{V_{30}}{V_{ref}}$ by a factor k_{klotz} leads to a simple rescaling of the P_{klotz} function:

$$P_{klotz}\left(k_{klotz} \cdot \frac{V_{30}}{V_{ref}}, \frac{V}{V_{ref}} \right) = \alpha_{klotz} \cdot P_{klotz}\left(\frac{V_{30}}{V_{ref}}, \frac{V}{V_{ref}} \right) \tag{3.9}$$

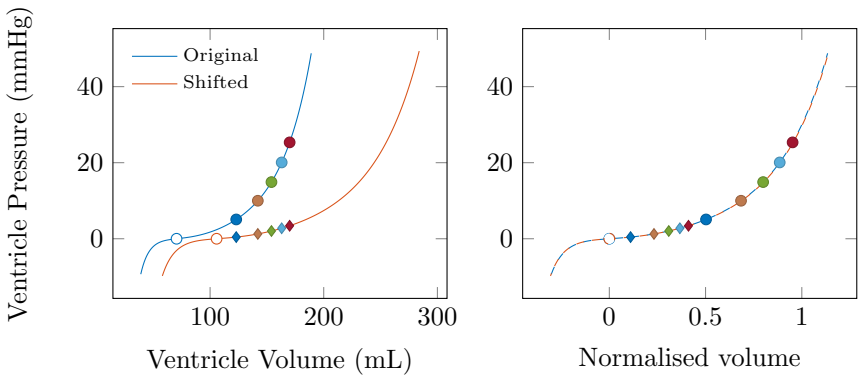

Figure 3.3 – Example of the effect of the variable transformation on the passive law. **left**: Volume space. We see two passive laws for whom only the V_{ref} parameter is different (coloured circles). The coloured dots and diamonds are the respective pressure associated with 5 different volumes; **Right**: Normalised-volume space. The two passive laws are also displayed but are over-imposed. The only difference stands in the location of the pressure points on the variable (V_n) axis.

It is then possible to calculate the proportional factor α_{klotz} that is associated with the modification of $\frac{V}{V_{ref}}$ parameter.

$$\alpha_{klotz} = \left[\left(\frac{V_{30}}{V_{ref}} - 1 \right) / \left(k_{klotz} \cdot \frac{V_{30}}{V_{ref}} - 1 \right) \right]^{B_n} \tag{3.10}$$

In the 0_D model, it is possible to apply the proportional factor $\alpha_{0_D} = \alpha_{klotz}$ to the passive law. We can see from Equations (2.15) and (2.20) that a simple rescaling of the passive law by a factor α_{0_D}, *i.e.* a homothety of $P_{0_D}\left(C_i, \epsilon, \frac{V}{V_{ref}}\right)$, is directly applied on the parameters $(C_0,\ C_2)$:

$$\alpha_{0_D} \cdot P_{0_D}\left(C_i, \epsilon, \frac{V}{V_{ref}}\right) = P_{0_D}\left(\alpha_{0_D} \cdot (C_0, C_2), \epsilon, \frac{V}{V_{ref}}\right) \tag{3.11}$$

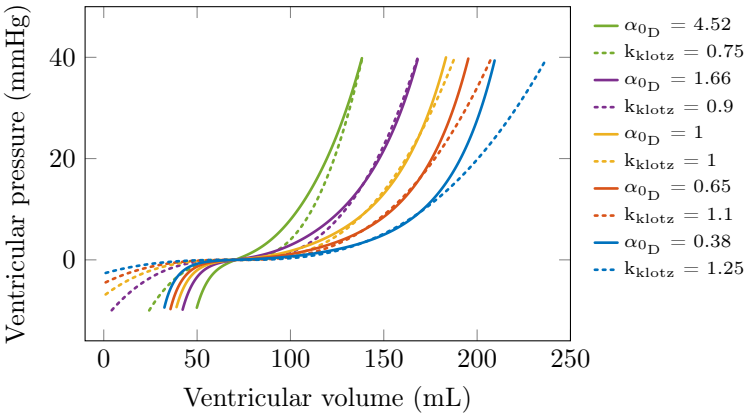

Figure 3.4 – Effect of stiffness modification. Comparison of EDPVR between Klotz function and passive law, when varying stiffness (α_{0_D}, k_{klotz}).

Figure 3.4 demonstrates the differences in passive law and Klotz relation when modifying the respective stiffness of each model ($\frac{V_{30}}{V_{ref}}$ or C_i) by the same magnitude. When we normalised the volume according to the Klotz algorithm (described in section 2.2.1), we observed in Figure 3.5 that: 1) Klotz relation stays fitted on the average population

data points, and 2) the passive law demonstrated deviations from the original passive law associated with the original C_i parameters (described in Section 3.1.2.2).

The Klotz function described by Equation (2.11) is based on the regression of the PV data points (P_{data}) in normalised space, that is parameterised by the population-based coefficient A_n and B_n. Therefore, to use the Klotz procedure (described in Section 2.2.1) to estimate the EDPVR from a single PV point will lead to over-impose the original Klotz relation in normalised space, whatever is the stiffness modification. However, we see from the P_{data} dataset, that there exists a patient-specific dispersion around this relation (Figure 3.5, right panel). On the contrary, our model allows patient-specific stiffness particularities in the normalised space as demonstrated by Figure 3.5, left panel. We can also see that for a significant variation of the tissue stiffness, the modified passive laws were all within the ranges of the P_{data} dataset.

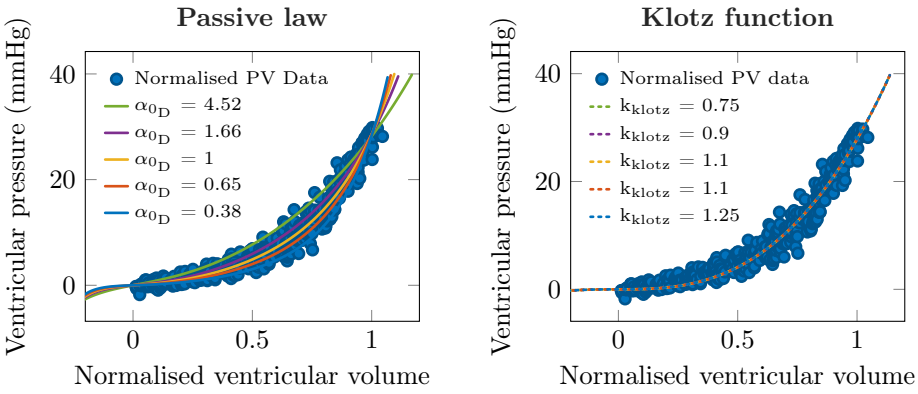

Figure 3.5 – Effect of stiffness parameters modification on passive law (**Left**) or Klotz (**right**) function in normalised space.

Using the optimisation procedure described in Section 3.1.2.2, we were able to calibrate the C_i parameters for a given subject. However, Equation (2.15) includes two terms, the first term represents the hyperelastic potential related to stretch applied in radial direction, the second term related to fibre oriented in orthogonal direction. This poses a question about the sensitivity of the first term with respect to the second term, under this calibration conditions, where only one direction is present (*i.e* increase/decrease in volume). Figure 3.6 shows the results of the sensitivity analysis of C_2, when sequential modification of C_0 was applied.

Comparable RMSEs demonstrate that the problem is not well conditioned with respect to C_0 and C_2. To decide about the optimal combination of (C_0, C_2), we would need some additional experimental data, typically of bi-axial stretch. In sequel, we will use the values C_i presented in section 3.1.2.2.

3.1.3.3 Parametric deviation wrt ϵ

In the Klotz model (Equation (2.11)), the information about the wall thickness is hidden in the V_{30} parameter. There is no direct correspondence between Klotz relation and 0_D model, with respect to ϵ. We propose to study the behaviour of the passive law with respect to variations in ϵ.

First, the passive law (Equation (2.20)) can be re-written as:

$$P_{0_D}(C_i, \epsilon, e_{fib}) = (1 + e_{fib}) \cdot g(\epsilon, e_{fib}) \cdot \epsilon \cdot \Sigma_{sphere} \tag{3.12}$$

Where the dependency in ϵ is driven by two terms : 1) a linear term (*i.e.* ϵ itself), and

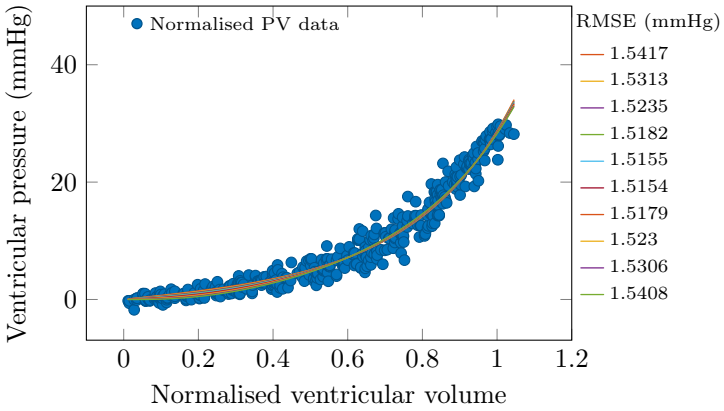

Figure 3.6 – Sensitivity analysis. The C_0 parameter is fixed and sequentially modified [120, 40, 360, 480, 600, 720, 840, 960, 1080, 1200] and the C_2 parameter is optimised to fit the normalised data [219, 193, 168, 142, 117, 91, 66, 41, 15, -10]. The passive law corresponding to each couple (C_0,C_2) is represented.

2) a nonlinear term (*i.e.* $g(\epsilon, e_{fib})$), and where $g(\epsilon, e_{fib})$ is written as follows:

$$g(\epsilon, e_{fib}) = \left((1+e_{fib}) - \frac{\epsilon}{2}\cdot(1+e_{fib})^{-2}\right)^{-2} \cdot \left(1+\epsilon\cdot(1+e_{fib})^{-3}\right)^{-1} \tag{3.13}$$

Therefore, if we assume that the nonlinear relation (3.13) is close to 1, Equation (2.20), modified in Equation (3.12), shows a linear dependency on epsilon. To verify this hypothesis, we posed the following Equation (3.14):

$$\frac{P_{0_D}}{\epsilon} = (1+e_{fib})\cdot g(\epsilon, e_{fib}) \cdot \text{sphere} \tag{3.14}$$

We tested the effect of changes in ϵ (*i.e.* between 0.15 and 0.45) on that nonlinear term. We demonstrated in Figure 3.7 that the nonlinear ϵ dependency has a little impact on the solution of Equation (3.14), for acceptable ranges of ϵ. We can then write:

$$\frac{P_{0_D}(C_i, \epsilon\cdot k_\epsilon, e_{fib})}{\epsilon\cdot k_\epsilon} \simeq \frac{P_{0_D}(C_i, \epsilon, e_{fib})}{\epsilon} \tag{3.15}$$

And so:

$$P_{0_D}(C_i, \epsilon\cdot k_\epsilon, e_{fib}) \simeq k_\epsilon \cdot P_{0_D}(C_i, \epsilon, e_{fib}) \tag{3.16}$$

with $k_\epsilon = \frac{\epsilon+\delta\epsilon}{\epsilon}$.

Equation (3.16) shows that a modification of ϵ leads to a simple rescaling of P_{0_D}, by a factor k_ϵ, where e_{fib} is the variable. When renormalising on V_{30} and V_{ref}, we observed a similar behaviour as for C_i variations (Figure 3.8).

Finally, we propose to study the combined effects of modification of stiffness and ϵ. If we start from a reference parametrisation noted

$$\begin{cases} P_{0_D}(\overline{C_i}, \overline{\epsilon}, e_{fib}) = \overline{\alpha_{0_D}}\cdot\overline{\epsilon}\cdot f(\overline{C_i}, \overline{\epsilon}, e_{fib}) \\ f(\overline{C_i}, \overline{\epsilon}, e_{fib}) = (1+e_{fib})\cdot\Sigma_{sphere}\cdot g(\overline{C_i}, \overline{\epsilon}, e_{fib}) \end{cases} \tag{3.17}$$

with $\overline{\alpha_{0_D}} = 1$, $\overline{\epsilon} = 0.298$ and $\overline{C_i} = [665,\ 2.4,\ 103,\ 5.5]$, then P_{0_D} for another configuration can be written:

$$P_{0_D}(C_i, \epsilon, e_{fib}) = \alpha_{0_D}\cdot\frac{\epsilon}{\overline{\epsilon}}\cdot P_{0_D}(\overline{C_i}, \overline{\epsilon}, e_{fib}) \tag{3.18}$$

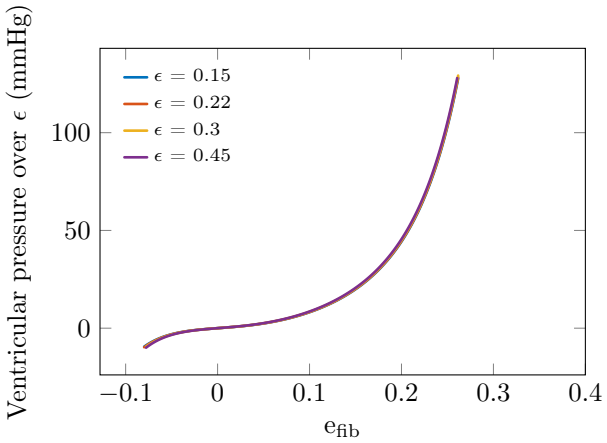

Figure 3.7 – Effect of geometry modification. Effect of the ϵ value on the non-linear ϵ dependency of the passive law.

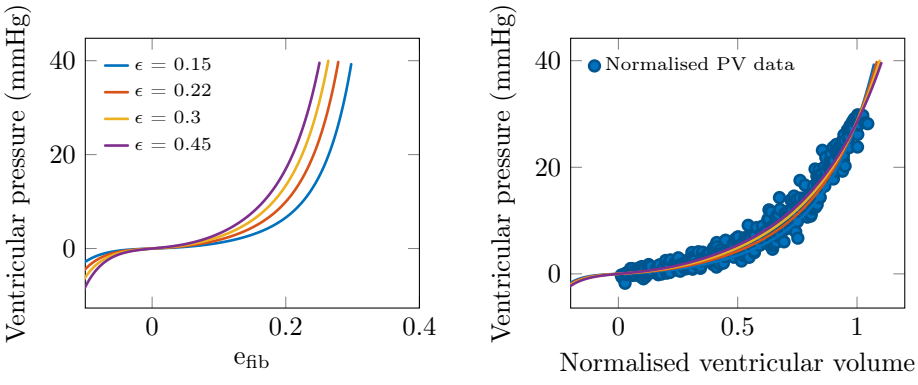

Figure 3.8 – Modification of ϵ and subsequent effect on the normalised space

We therefore defined

$$\beta = \alpha_{0_D} \cdot \frac{\epsilon}{\overline{\epsilon}} \tag{3.19}$$

β being the proportional factor that contains the global stiffness deviation from the reference configuration (*i.e.* the optimised configuration presented in section 3.1.2.2), and is composed from the intrinsic fibre stiffness associated with C_i (α_{0_D}), and the stiffness associated with wall thickness $\left(\frac{\epsilon}{\overline{\epsilon}}\right)$.

3.2 Description of a simplified calibration procedure for ED-PVR estimation based on a biomechanical model

3.2.1 Polynomial function

First, for code optimisation purposes, we fit, for $\epsilon = \overline{\epsilon}$ and $C_i = \overline{C_i}$, a 7^{th} order polynomial on the passive law function, and propose to study for reasonable range this polynomial function, and verify that it behaves as the optimised passive law (2.20).

$$P^{pol}(e_{fib}) = \sum_{i=0}^{7} a_i \left[\phi(e_{fib})\right]^i \tag{3.20}$$

with $a = [-21.3394, 0.1672 * 1 \cdot 10^6, 0.0811 * 1 \cdot 10^6, 0.3312 * 1 \cdot 10^6, 0.9557 * 1 \cdot 10^6, 1.2413 * 1 \cdot 10^6, -0.6922 * 1 \cdot 10^6, 0.1870 * 1 \cdot 10^6]$.
Figure 3.9 shows the results of the polynomial fit between reasonable ranges of pressure (P=[0 - 40] mmHg). The RMSE demonstrated that the fit was excellent. However, before we use this polynomial for operational calibration procedure, we verified that the proportional constraints imposed by the passive law behaviour was respected. We therefore started from reference configuration and modified the α_{0_D} parameter sequentially. It was subsequently applied on the passive law (Equation (3.18)) and on the polynomial (Equation (3.20)).

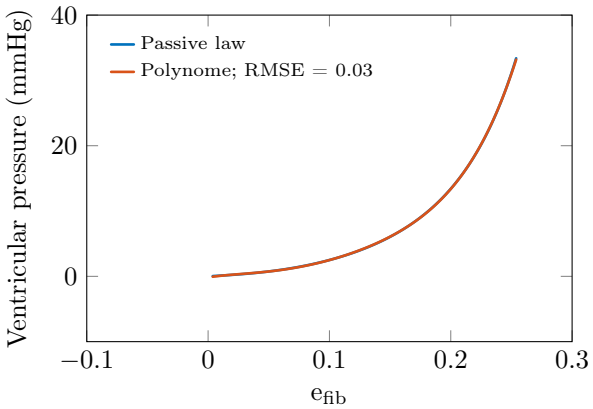

Figure 3.9 – Comparison between the passive law function and the polynomial fit ($P^{pol}(e_{fib})$)

Figure 3.10 demonstrates that for reasonable ranges of stiffness modification, the polynomial did not deviate significantly from the passive law. A deviation is however observed for a very compliant configuration, and only in high pressures. We performed a similar analysis regarding the stiffness related to the sphere thickness. We can see in Figure 3.11, that the deviation observed is even less significant than for the deviation observed for intrinsic stiffness.

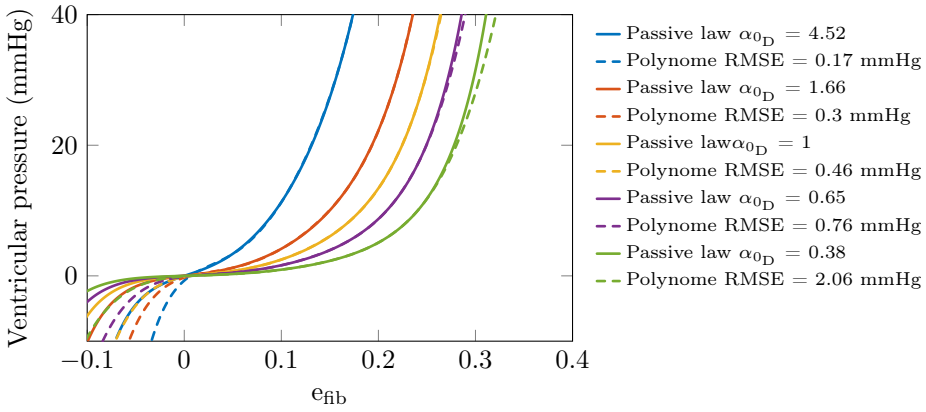

Figure 3.10 – Behaviour of the polynomial compared to the passive law when modifying the C_i. The RMSE is calculated for positive values of e_{fib} and for pressure below 40 mmHg

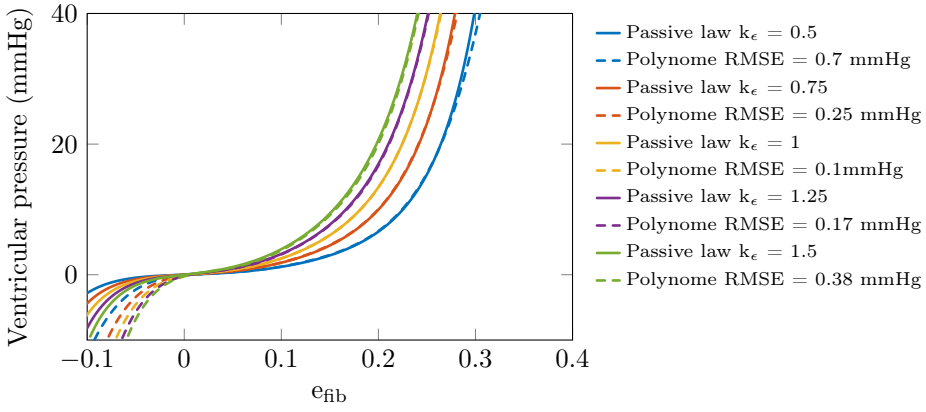

Figure 3.11 – Behaviour of the polynomial compared to the passive law when modifying the ϵ. The RMSE is calculated for positive values of e_{fib} and for pressure below 40 mmHg.

3.2.2 Minimisation problem

The objective of this algorithm is to estimate from a known set of PV data points (V_m, P_m), the global stiffness deviation factor β from the optimised configuration, along with estimation of V_{ref}. We posed the following minimisation problem:

$$J = \sum_{i=1}^{N} \left({P_{data}}^{i} - \beta \cdot P^{pol} \left(e_{fib} \left(V_{data}^{i}, V_{ref}, \bar{\epsilon} \right) \right) \right)^2 \tag{3.21}$$

with $\bar{\epsilon} = 0.298$

Figure 3.12 shows the root mean of the solution of Equation (3.21) (RMSE), obtained for different values of β and V_{ref}. In this example, P_{data}^{i} are simulated by choosing a passive law (Equation (2.20)) parametrised by: $C_i = \overline{C_i}$, $\epsilon = \bar{\epsilon}$ and $V_{ref} = 56$ mL. We determined P_{data}^{i} by calculating the i^{th} pressure points (50 points) associated with ${e_{fib}}^{i}$ and we add a random error to each calculated pressure data point (maximum 3 mmHg). We observed that this problem is ill-posed, especially in β direction. We therefore introduced regularising terms that use the information from the pathophysiological knowledge we can obtain from the geometry information of the heart [4]. The minimisation problem is then written as follows:

$$J = \sum_{i=1}^{N} \left(\frac{\left({P_{data}}^{i} - \beta \cdot P^{pol} \left(e_{fib}(V_{data}^{i}, V_{ref}, \bar{\epsilon}) \right) \right)}{sd^{error}} \right)^2 + \left(\frac{V_{ref} - {V_{ref}}^{\mu}}{{V_{ref}}^{\sigma}} \right)^2 + \left(\frac{\beta - \beta^{\mu}}{\beta^{\sigma}} \right)^2 \tag{3.22}$$

The minimisation criterion (J) is now a-dimensioned, as written in the Equation (3.22), by

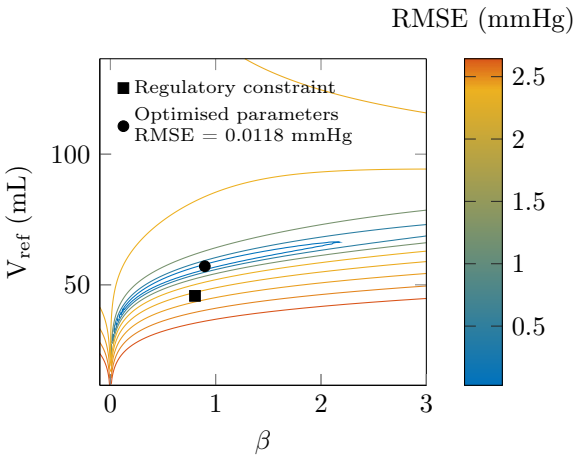

Figure 3.12 – Example of a results of the optimisation procedure, and effect of the regularising terms. The diagram displays the root mean square error (RMSE) between synthetic data (P_{data}) and the pressure associated with the passive law parameterised by (e_{fib}, $\overline{C_i}$, $\bar{\epsilon}$, $V_{ref} = [-5.6 : 0.8736 : 168]$ mL and $\beta = [-0.8 : 0.0125 : 2.4]$). The P_{data} data were generated as follows: we randomly chose a set of 50 e_{fib} and calculated the pressure given by the passive law parameterised by (e_{fib}, $\overline{C_i}$, $\bar{\epsilon}$, $V_{ref} = 56$ mL and $\beta = 1$). We finally add a random error on these pressure-e_{fib} points (maximum 3 mmHg) in order to obtain P_{data}. The dark square corresponds to the RMSE calculated with the passive law associated with the population-defined ($\beta = 0.8$, $V_{ref} = 45$ mL). The dark dot corresponds to the RMSE calculated with the passive law associated with the parameters estimated using the final optimisation procedure.

dividing the Equation (3.21) by the standard deviation of error in pressure measurement, by setting ${V_{ref}}^{\mu}$ and β^{μ} as the mean reference volume and stiffness we would expect for a predefined population, and by setting ${V_{ref}}^{\sigma}$ and β^{σ} as the standard deviation of β and

V_{ref} we would expect in this population. In the end, the solution of the Equation (3.22) is obtained by using the fminsearch solver of the Matlab software (MathWorks, Natick, Massachussetts, USA). In our example, the population values are represented by the square, and the result of the optimisation procedure is represented by the dot.

In order to define the values for ${V_{ref}}^{\mu}$ and ${V_{ref}}^{\sigma}$, we used the classes defined in the recommendations for cardiac chamber quantification by echocardiography in adults [4], giving thresholds values for left ventricle dimensions (see table 3.2). According to the class in which the patient belongs, we defined the population regulatory term ${V_{ref}}^{\mu}$ as half the mean end-diastolic volume given for the appropriate class population and ${V_{ref}}^{\sigma}$ as half the interquartile range of the end-diastolic volume for the same class population.
The α parameter coding the relative fibre stiffness with respect to the optimised patient described in section 3.1.2.2 was supposed not to be altered by magnitude of dilation nor hypertrophy, it was assumed to be constant through all classes. After preliminary tests, we set the α_{factor} parameter to 0.8 times the value of the optimised patient. The β parameter being composed by the fibre stiffness and the stiffness associated with the wall thickness, we defined a hypertrophy factor based on the class definitions found in Table 3.2. This factor was applied to α_{factor} to define β^{μ}.

Finally, we performed an analysis to identify the value of β^{σ} that was associated with good optimisation performance. Figure 3.13 shows the results of this analysis with the regularising terms defined by the "normal" class (Table 3.22). We generated data according to the procedure described briefly in the beginning of this section and in details in Section 4.1.1. The parameters $(\beta^{\sigma}, {V_{ref}}^{\sigma})$ were also chosen in the "normal" class. We randomly chose V_{ref} within a normal law parametrised by ($\mu = 45$ and $\sigma = 17.5$ mL), and β within a normal law parameterised by ($\mu = 0.8$ and $\sigma = 0.4$). In the end we performed 50 simulations, and Figure 3.13 shows the mean root mean of the solution of Equation (2.20) (RMSE) for the 50 simulations. The choice for β^{σ} was determined by identifying a compromise between the algorithm performance and the regularising value of ${V_{ref}}^{\sigma}$, given by population knowledge (Table 3.2). We further performed similar analysis for mild to severe classes using increasing value of V_{ref} and verified that the performance of the algorithm when using $\beta^{\sigma} = 0.4$ was good in the four classes.

3.3 Discussion

In this chapter, we aimed at describing a patient-specific calibration method of the passive law introduced in Chapter 2. We first described a procedure to calibrate the parameters of the passive law to the data measured using transthoracic echocardiography information performed on a reference patient. From these geometrical and functional information, and using the normalised data provided in the work of Klotz et al. [3], we obtained a reference estimation of the coefficient parameters C_i that contained the tissue stiffness information. From that reference configuration, we described a particular behaviour of the passive law. When deviating the reference passive law by a proportional homothetic factor α, it preserved the normalised data constrained characteristic of the EDPVR. We described further how the parameters V_{ref}, ϵ and C_i affected this homothetic factor α. This finding paved the way of the description of the simplified calibration method. From couples of PV data points (V_m^i, P_m^i), and estimation of ϵ, we developed a method that allows to estimate the V_{ref} and α parameters of the passive law associated to the PV data points.

This approach is original because it allows from a very limited data availability, to calibrate a passive law fully derived from the continuum mechanics theory. Indeed, to turn this model into patient-specific regime we succeeded to reduce the parametric space

Table 3.2 – Class definition according to the magnitude of dilation and hypertrophy, and corresponding values for regulatory terms parameters. *Reproduced from Lang et al.* [4]

	normal			mild			moderate			severe		
	♂	♀	–	♂	♀	–	♂	♀	–	♂	♀	–
Thresholds												
EDV	⩽150	⩽106	⩽113	⩽174	⩽120	⩽148	⩽200	⩽130	⩽181	>200	>130	>181
EDVI	⩽74	⩽61	⩽67.5	⩽89	⩽70	⩽81	⩽100	⩽81	⩽90	>100	>81	>90
WT	⩽1	⩽0.9	⩽0.95	⩽1.3	⩽1.2	⩽1.25	⩽1.6	⩽1.5	⩽1.55	>1.6	>1.5	>1.55
Parameters												
$V_{ref}{}^{\mu}$	53	38	45	81	57	69	94	63	78.5	120	80	100
$V_{ref}{}^{\sigma}$	22	14	17.5	39	21	39	33	24	33	49	30	49
WT_{factor}		1			1.1			1.2			1.3	
α_{factor}		0.8			0.8			0.8			0.8	
β^{μ}		0.8			0.88			0.96			1.04	
β^{σ}		0.4			0.4			0.4			0.4	

EDV: End-diastolic volume in mL; EDVI: End-diastolic volume indexed to body surface area in $mL.m^{-2}$; WT: Wall thickness in cm; $V_{ref}{}^{\mu}$: Mean reference volume in the population class in mL; $V_{ref}{}^{\sigma}$: Interquartile range for the reference volume in the population class in mL; β^{μ}: Mean β in the population class; β^{μ}: Interquartile range for β in the population class; ♂: Men; ♀: Women; –: Unknown gender.

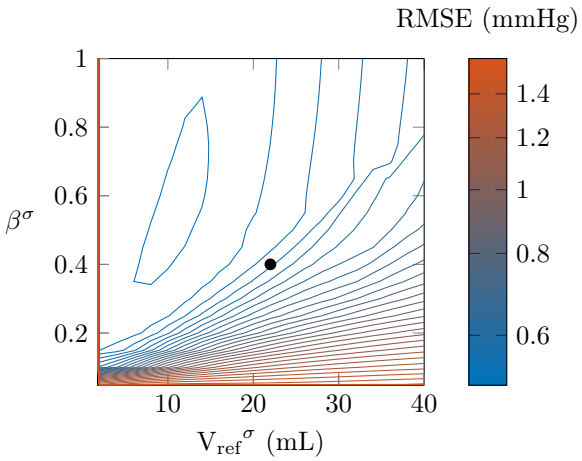

Figure 3.13 – Effect of regularisation on the result of the optimisation procedure. We generated synthetic P_{data} by using the passive law (Equation (2.20)) with the following parameters ($\overline{C_i}$, $\bar{\epsilon}$). We randomly chose V_{ref} within a normal law parametrised by ($\mu = 45$ and $\sigma = 17.5$ mL), and β within a normal law parameterised by ($\mu = 0.8$ and $\sigma = 0.4$). Fifty e_{fib} were randomly chosen and pressure was generated for the 50 data points. We add a random error to the pressure points generated (maximum 3 mmHg) to obtain P_{data}. Then we applied the optimisation procedure for given values of $\beta^{\sigma} = [0 : 0.05 : 1]$ and $V_{ref}{}^{\sigma} = [0 : 0.1606 : 40]$ mL. We performed this procedure 50 times and display on the diagram the mean RMSE between P_{data} and the pressure points associated with the passive law estimated, with respect to each $(\beta^{\sigma}, V_{ref}{}^{\sigma})$.

to 3 parameters α, V_{ref} and ϵ. If the original passive law is driven by 6 parameters (*i.e.* (C_0, C_1, C_2, C_3), V_{ref} and ϵ), the relative passive law can be described as a deviation of a previously optimised configuration. The normalised data provided in the work of Klotz et al. [3] were therefore used in this context, and allowed us to fix this reference configuration. We may observe that our method warrants patient-specificity also in this normalised space, which is not the case for the Klotz method. Indeed, when deviating passive law parameters from the reference, we can see that the normalised passive law is different from the original, but stands in the limits given by the normalised data points. Our procedure allows therefore between subjects comparison. This characteristic is a finding that may improve cardiac physiology understanding. Indeed, EDPVR data point are difficult to obtain because its measurements are associated with invasive manoeuvre (see Chapter 2). Therefore, models have emerged in order to estimate EDPVR [5; 2]. However, the lack of identifiability of the parameters given the available data in routine practice prevent these models to allow between subject or between conditions comparison [1]. Furthermore, our framework allows to give sense to our parameters. The parameter β represents a global stiffness, because it is composed by the parameters that contains the tissue stiffness information (α, itself proportionally related to (C_0, C_2) parameters), and by the stiffness associated with the geometrical conformation of the sphere (*i.e.* associated with ϵ).

Our framework is based on several approximations. The reference configuration was calibrated by using existing methods, on a normalised dataset. It is not obvious that the true passive law for this reference patient would be really the passive law that minimises the criteria $J(C_i)$ of Equation (3.22). Indeed, if we had chosen different patient for reference configuration, the result of the optimisation procedure would lead to an estimated EDPVR that would also minimise the criteria $J(C_i)$, with respect to the normalised data, and that would be close to the EDPVR that is presented in Figure 3.3. However, our method does not claim to provide an absolute value for the passive law (which would be challenged against experimental dataset), but rather to provide a way to compare EDPVR within and between subjects. Also, we used a 7^{th} order polynomial approximation to build our optimisation framework. That may introduce errors in parameters estimation. However, we studied the behaviour of the polynomial compared with the passive law, and we saw that the error caused by this approximation is not significant for the ranges of PV data we may observe in clinical practices. More important is the ill-posedness of the problem in β direction (Figure 3.12). It was the reason to introduce regulatory terms into Equation (3.22). We used population-based information that were published in european guidelines of echocardiography [4], to fit the $V_{ref}{}^{\mu}$ parameter. The $V_{ref}{}^{\sigma}$ and β^{σ} parameters were found by performing well in numerical tests. We allow different values for these parameters with respect to various class of heart size provided in Table 3.2. The β^{μ} parameter was set by applying a stiffness factor depending on hypertrophy characteristic of the studied heart. Indeed, if structural intrinsic tissue stiffness would not be modified by the size of the LV, the remodelling of the heart would lead to concentric or excentric hypertrophy. Parameter β aggregates both the aforementioned constituents and is impacted by the size of the LV. Even though these choices could have introduced bias, their effects on the solution of our least-square problem is however interesting. In Figure 3.12 we can see that the point corresponding to the regulatory parameters $V_{ref}{}^{\mu}$ and $\beta\mu$ is not located in the valley of the criteria, but the solution is. We can deduce that the effect on the solution is small, but tend to locate the solution of the algorithm in the valley, not far from an average population-based value. Also, if the data is noisy, or with few data points, the sd^{error} term releases weight on PV data measurement, and gives more weight on the population-based *a priori*. Therefore, if the data is aberrant, our algorithm may

detect it and may give more confidence in population-based value.

The following chapter will focus on the performance of the simplified calibration method.

Bibliography

[1] Burkhoff, D. (2005). Assessment of systolic and diastolic ventricular properties via pressure-volume analysis: a guide for clinical, translational, and basic researchers. *AJP: Heart and Circulatory Physiology*, 289(2):H501–H512.

[2] Holzapfel, G. A. and Ogden, R. W. (2009). Constitutive modelling of passive myocardium: a structurally based framework for material characterization. *Phil. Trans. R. Soc. A: Mathematical, Physical and Engineering Sciences*, 367(1902):3445–3475.

[3] Klotz, S., Hay, I., Dickstein, M. L., Yi, G.-H., Wang, J., Maurer, M. S., Kass, D. A., and Burkhoff, D. (2006). Single-beat estimation of end-diastolic pressure-volume relationship: a novel method with potential for noninvasive application. *AJP: Heart and Circulatory Physiology*, 291(1):H403–H412.

[4] Lang, R. M., Badano, L. P., Mor-Avi, V., Afilalo, J., Armstrong, A., Ernande, L., Flachskampf, F. A., Foster, E., Goldstein, S. A., Kuznetsova, T., Lancellotti, P., Muraru, D., Picard, M. H., Rietzschel, E. R., Rudski, L., Spencer, K. T., Tsang, W., and Voigt, J.-U. (2015). Recommendations for Cardiac Chamber Quantification by Echocardiography in Adults: An Update from the American Society of Echocardiography and the European Association of Cardiovascular Imaging. *Journal of the American Society of Echocardiography*, 28(1):1–39.e14.

[5] Mirsky, I., Janz, R. F., Kubert, B. R., Korecky, B., and Taichman, G. C. (1976). Passive elastic wall stiffness of the left ventricle: A comparison between linear theory and large deformation theory. *Bulletin of Mathematical Biology*, 38(3):239–251.

[6] Nagueh, S. F., Appleton, C. P., Gillebert, T. C., Marino, P. N., Oh, J. K., Smiseth, O. A., Waggoner, A. D., Flachskampf, F. A., Pellikka, P. A., and Evangelisa, A. (2008). Recommendations for the Evaluation of Left Ventricular Diastolic Function by Echocardiography. *European Journal of Echocardiography*, 10(2):165–193.

CHAPTER 4

Estimation of end-diastolic pressure-volume relationship using biomechanical model

This Chapter presents and discusses the evaluation of the end-diastolic pressure-volume relationship (EDPVR) single-beat estimation method from biomechanical model compared with existing estimation methods. By generating synthetic data of left ventricular (LV) end-diastolic pressure and volume, we analyse the effect of the quality of the data available on our single-beat estimation of EDPVR. Furthermore, we are able to demonstrate that the biomechanical method allows for a better fit with the data, along with a more stable estimation of V_{ref} the end-diastolic volume at stress-free reference configuration. We confirme this results by comparing the single-beat biomechanical and the existing procedures using 23 invasive end-diastolic pressure and volume sets of measurements that were extracted from previously published papers. Our approach provides a simple and easy to use method for EDPVR estimation which allows for better fit, identification of parameters, and link with physiology, than the previously available phenomenological methods.

In this chapter, we will study the performance of the estimation method of EDPVR based on the biomechanical model described in Chapter 3. By generating synthetic data we will study the effect of the noise in the data and of the number of data points on the parameters estimation. Then, we will compare the ability of the estimation of the passive law parameters method as compared with the Klotz et al. [4] method calibrated using in vivo data obtained in experimental papers.

4.1 Data

4.1.1 Synthetic Data generation

In order to explore the performance of the optimisation method, we generated synthetic data as follows:

1. **Passive law selection.** The synthetic data were generated by setting up a predefined passive law. We selected the V_{ref}, ϵ and β parameters by using the characteristics of the class population described in section 3.2.2. First, ϵ was prescribed between 0.2 and 0.4. Then, we defined a normal distribution with the mean $V_{ref}{}^{\mu}$ and the standard deviation $V_{ref}{}^{\sigma}$ (See Table 3.2), and picked a V_{ref} within this normal distribution. We applied a similar procedure to choose the β parameter.

2. **Selection of the e_{fib} points.** The e_{fib} points were selected randomly by using normal distribution with mean $\mu = 0.15$ and $\sigma = 0.075$.

3. **Introduction of error in measurement.** The passive law was then generated using Equation (2.20), applying the V_{ref} and β parameters and the e_{fib} variable selected by the aforementioned procedure. We then applied an error defined by a normal law centred by the pressure value, and dispersed by the prescribed error in pressure unit as the standard deviation (see example in Figure 4.1).

4.1.2 In vivo Data

We used in vivo human dataset of EDPVR from Klotz et al. [4]; ten Brinke et al. [6]; Gaasch et al. [2]; Fester and Samet [1] and Kawaguchi [3]. We extracted the data points by using the GraphClick software (Arizona, Switzerland), which allowed to digitise semi-automatically the data.

In the paper of Klotz et al. [4], additionally to the normalised data, we reproduced the data from Figure 7, representing the EDPVR obtained in vivo in human, in which a transient inferior vena caval occlusion was performed while performing pressure and volume measurements.

In the paper of ten Brinke et al. [6], we reproduced the data from Figure 1 and 2 representing examples of EDPVR obtained in vivo in patients with pre/post coronary artery bypass graft, pre/post restrictive mitral annuloplasty or pre/post surgical ventricular restoration procedures, by using a transient vena caval occlusion method.

In the paper of Gaasch et al. [2], we reproduced the data from Figures 2, 3, 4 and 5 representing the EDPVR in body surface area (BSA) indexed volume space, for patients with congestive cardiomyopathy, LV hypertrophy, coronary artery disease and mitral stenosis, in which we deindexed the volume by using the BSA information available in Table 1.

In the paper of Fester and Samet [1], we reproduced the EDPVR example data reported in Figure 2. Patients in this study underwent cardiac catheterisation procedure for valvular or a possible coronary artery disease.

In the paper of Kawaguchi [3], we reproduced the EDPVR example from Figure 3, obtained during inferior vena caval occlusion. The patients in this study underwent cardiac catheterisation for assessment of HFpLVEF.

4.2 Passive law testing

4.2.1 Effect of the data noise

We chose the passive law according to the procedure described in section 4.1.1 and modified the synthetic data generated by this passive law (n = 1,000 assays) by randomly modifying the e_{fib} and error values. We set the number of points to 50. We compared the RMSE representing the difference between the prescribed and the estimated passive law. Then we estimated a Klotz model and calculated the RMSE representing the difference between the optimised Klotz algorithm and the prescribed passive law.

4.2.2 Effect of the number of data point

We chose a passive law according to the procedure described in section 4.1.1, and we modified the data generated from this prescribed passive law (n = 1,000 assays) by randomly changing the e_{fib}. We set the data noise to 3 mmHg. We then reduced the number of points used for the parameters estimation. Again, we compared the RMSE representing the difference between the prescribed and the estimated passive law and between the RMSE calculated from optimised Klotz algorithm and the prescribed passive law.

4.2.3 Estimation of V_{ref} and β

We aimed at evaluating the robustness of V_{ref} and β estimation when varying the parameters of the passive law, corresponding to various left ventricle size or thickness. We generated synthetic data by applying the parameters corresponding to the 4 classes of LV dilation and/or hypertrophy, provided in Table 3.2 [5]. We set the error to 3 mmHg and the number of points to 50. The regulatory parameters ($V_{ref}{}^{\mu}$, $V_{ref}{}^{\sigma}$, β^{μ} and β^{σ}) were set according to the procedure described in Section 3.2.2, for each class respectively.

We compared the value of the estimated V_{ref} and β with the prescribed parameters by using our estimation method. We compared the estimation of V_{ref} by using our and the Klotz estimation method.

4.2.4 Single-beat EDPVR estimation of EDPVR

As the next task, we tested the single-beat estimation method performance by using the in vivo human data described in Section 4.1.2. From the provided data (ventricular pressure and volume), we selected one PV pair and used it for a single-beat estimation of the EDPVR. We compared the single-beat estimated passive law with the available data points. Then, we compared it with the passive law that has been generated from the multiple-beat estimation (by using all the points available). We calculated the RMSE between passive law single beat and data points and passive law multiple beat and compared these results with the RMSEs obtained with the Klotz algorithm.

Wilcoxon rank sum test was used to compare the RMSEs obtained with the aforementionned methods. We used the R statistical software (The R Foundation for Statistical Computing, Vienna, Austria) for statistical analysis.

4.3 Algorithms for EDPVR estimations

For passive law estimation method we used the algorithm described in details in Section 3.2.2, which minimises the following equation (3.22):

$$\mathrm{J}(\beta, \mathrm{V_{ref}}) = \sum_{\mathrm{i=1}}^{\mathrm{n}} \left(\frac{\mathrm{P^i_{data}} - \beta \cdot \mathrm{P^{pol}} \left(\mathrm{e_{fib}} \left(\mathrm{V^i_{data}}, \mathrm{V_{ref}}, \bar{\epsilon} \right) \right)}{\mathrm{sd^{error}}} \right)^2 + \left(\frac{\mathrm{V_{ref}} - \mathrm{V_{ref}}^{\mu}}{\mathrm{V_{ref}}^{\sigma}} \right)^2 + \left(\frac{\beta - \beta^{\mu}}{\beta^{\sigma}} \right)^2$$

For the Klotz method, we estimated the parameter $\mathrm{V_{30}}$ and $\mathrm{V_{ref}}$ by minimising least-squared problem written in Equation (4.1).

$$\mathrm{J}\left(\mathrm{V_{30}}, \mathrm{V_{ref}}\right) = \sum_{\mathrm{i=2}}^{\mathrm{n}} \left(\mathrm{P^i_{data}} - \mathrm{P_{klotz}} \left(\frac{\mathrm{V_{30}}}{\mathrm{V_{ref}}}, \frac{\mathrm{V^i_{data}}}{\mathrm{V_{ref}}} \right) \right)^2 \tag{4.1}$$

Note that i ranges from 2 to n, because this algorithm was used only for estimation procedures that do not involve single PV data point. Indeed, a dedicated procedure is available. Therefore, when we compared the single beat estimation methods, we used the complete procedure described in details in Section 2.2.1 and in Klotz et al. [4].

For both the algorithms, the PV data ($\mathrm{P^i_{data}}$, $\mathrm{V^i_{data}}$) were either the synthetic data generated ($\mathrm{P^{synth}_{data}}$) or the human data obtained from the publications [4; 6; 2; 1; 3].

4.4 Performance of the simplified calibration method

4.4.1 Effect of the data noise

Figure 4.1 shows an example of the effect of the introduction of data noise in the estimation of the parameters of the passive law. The RMSE calculated from the estimated procedure was lower than than from the Klotz procedure ($p<0.001$, for $1,000$ assays).

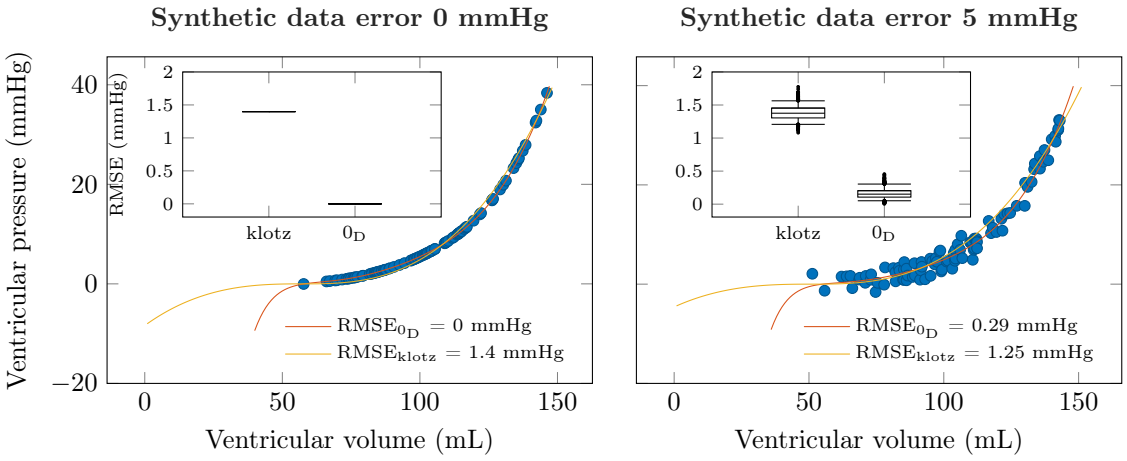

Figure 4.1 – Effect of the data noise on the passive law estimation and comparison with the Klotz procedure. The RMSE displayed in this figure is related to the prescribed passive law used to generate the data and not with the synthetic data itself. The comparison of the RMSE obtained with the passive law and the Klotz procedure was statistically significant ($p<0.001$).

4.4.2 Effect of the number of data point

Figure 4.2 shows examples of the effect of the number of points in the estimation of the parameters of the passive law. As for the noise analysis (Section 4.4.1), the RMSE

between the estimated procedure and the prescribed passive law was lower than for the RMSE evaluating the difference with the Klotz procedure ($p<0.001$, for $1,000$ assays).

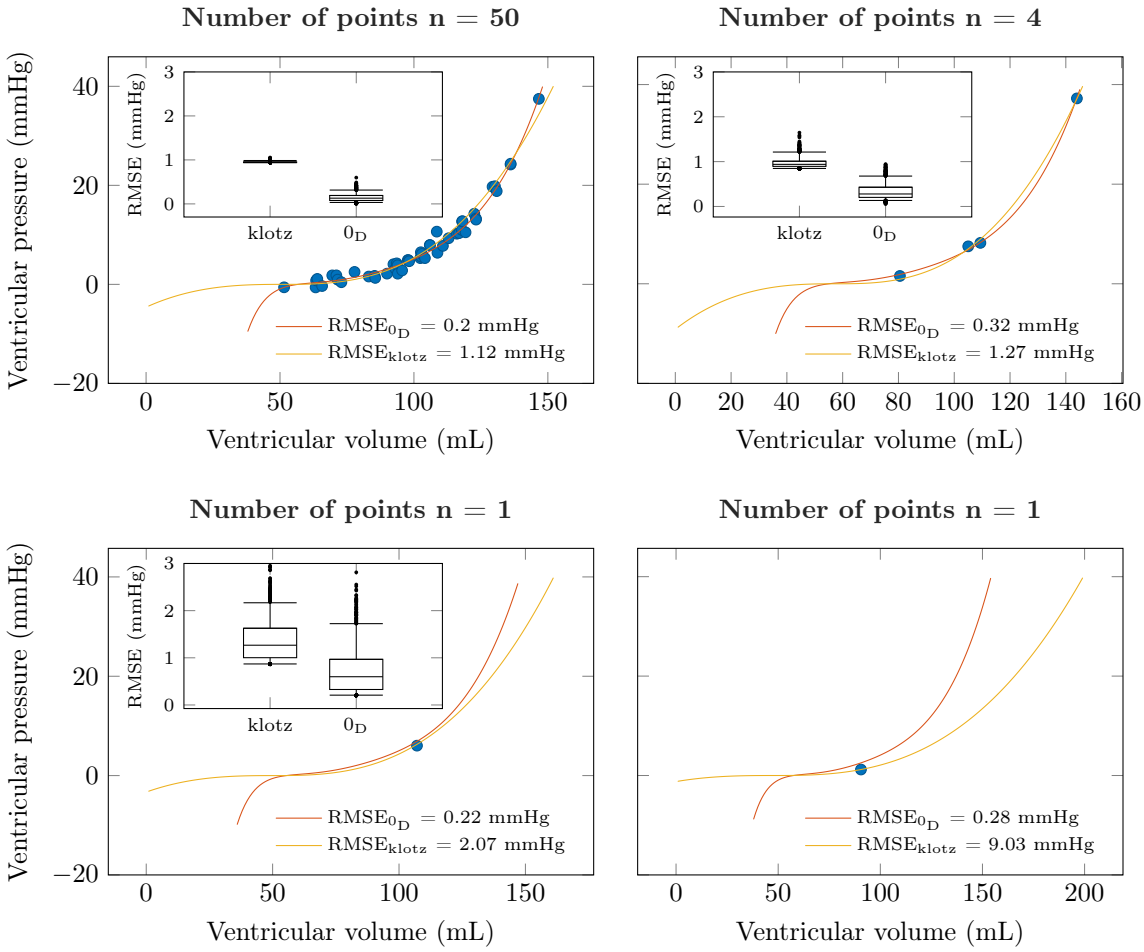

Figure 4.2 – Effect of the number of points on the passive law estimation and comparison with the Klotz procedure. The prescribed passive law parametrised to generate the synthetic data is used as the reference for comparison (root mean squared error RMSE) and not the synthetic data itself. The comparison of the RMSEs obtained with the passive law and with the Klotz procedure is statistically significant $p<0.001$. The bottom right panel is an illustration of the single-point effect and of the regulatory action of our regulatory terms included in our framework. The blue datapoint is flawed as compered to the passive law from which it has been generated. The algorithms which use no *a priori* knowledge on that datapoint would be importantly influenced by the measurement error. On the contrary, algorithms which use an *a priori* knowledge will detect that the datapoint is flawed with respect to the passive law from which it has been generated. Increasing the number of point will reinforce the confidence in the data and will release the population-based knowledge regularisation.

4.4.3 Effect of error in ϵ determination

In our analyses, we set $\epsilon = \bar{\epsilon}$. Since $\beta = \alpha_{0_D} \cdot \frac{\epsilon}{\bar{\epsilon}}$, if the true ϵ associated with a heart is different from the $\bar{\epsilon}$, we might misestimate the α_{0_D} factor and therefore the relative constitutive stiffness of this new heart. Furthermore, to modify the value of ϵ in Equation (3.22) could alter the result of the optimisation process and therefore the performance of the β and V_{ref} estimation. This issue is discussed in Chapter 5.

4.4.4 Estimation of V_{ref} and β

In this Section, we generated 1,000 synthetic EDPVR from passive laws parameterised by V_{ref} and β chosen using normal laws centred by ${V_{ref}}^{\mu}$ or β^{μ} with ${V_{ref}}^{\sigma}$ or β^{σ} as dispersion parameters. The V_{ref} and β parameters values were stratified by the class defined in Section 3.2.2, Table 3.2 (normal, mild, moderate, severe).

We minimised the single-beat criterion (3.22) using the synthetic data generated and the ${V_{ref}}^{\mu}$ and the β^{μ} parameters as initial guesses. We applied the Klotz procedure for simgle-beat estimation method (see Section 2.2.1).

The RMSE for overall V_{ref} estimation with the passive law was lower than for Klotz estimation (1.6±2.3 mmHg versus 21.7±25.9 mmHg; p< 0.001, respectively) (see Table 4.1). Furthermore, for each class of LV volumes the passive law estimation of V_{ref} was closer to the prescribed V_{ref}, as compared to the V_{ref} estimated from Klotz algorithm. Table 4.1 also provides the results of β estimation.

Figure 4.3 shows the relationship between prescribed and estimated V_{ref}, for passive law and Klotz method, for various classes of LV volumes. Figure 4.4 shows the results for β estimation by our algorithm.

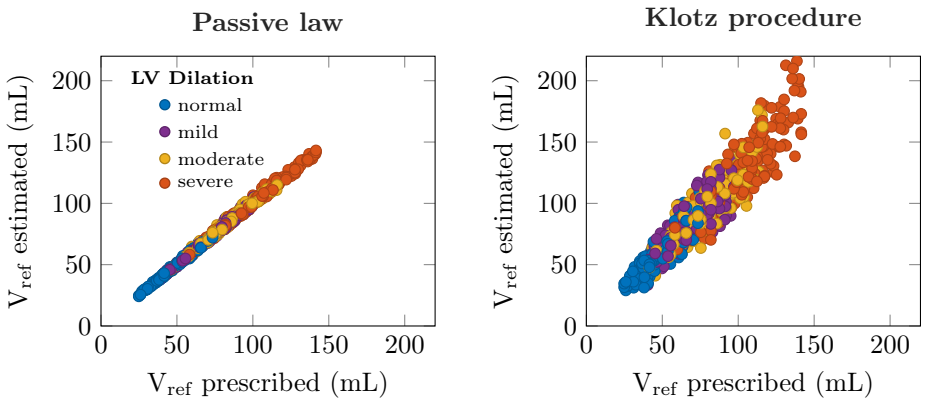

Figure 4.3 – Relationship between prescribed and estimated V_{ref}. **Left**: With the passive law; **Right**: With the Klotz relation. We performed subgroup analysis in 4 classes of left ventricles (LV) [5] (See Chapter 3 Table 3.2). Synthetic data were generated for this analysis

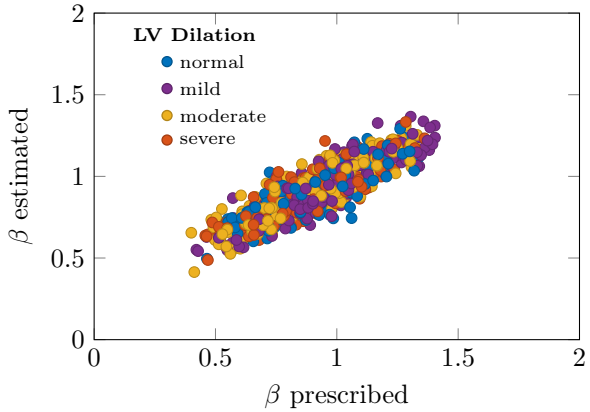

Figure 4.4 – Relationship between prescribed and estimated β. We performed subgroup analysis in 4 classes of Left Ventricles (LV) [5] (See Chapter 3 Table 3.2). Synthetic data were generated for this analysis

Table 4.1 – Difference between prescribed and estimated parameters performed on 1,000 synthetic EDPVR generated. t-test was used for data comparison

Parameters		Passive	Klotz	P–Value
V_{ref} (mL)	$(n = 1,000)$	1.6 ± 2.3	21.7 ± 25.9	< 0.001
normal	$(n = 236)$	1 ± 1.3	13.7 ± 15	< 0.001
mild	$(n = 281)$	1.3 ± 1.9	19.5 ± 20.5	< 0.001
moderate	$(n = 246)$	1.7 ± 2.4	22.4 ± 24.5	< 0.001
severe	$(n = 237)$	2 ± 2.7	28.9 ± 32.1	< 0.001
β	$(n = 1,000)$	0.1 ± 0.12	–	–
normal	$(n = 236)$	0.11 ± 0.12	–	–
mild	$(n = 281)$	0.1 ± 0.11	–	–
moderate	$(n = 246)$	0.1 ± 0.12	–	–
severe	$(n = 237)$	0.1 ± 0.11	–	–

4.4.5 Single beat EDPVR estimation of EDPVR

Figure 4.5 shows an example comparing the single- and multiple-beat estimation methods. The example also provides the results of the multiple-beat estimation. For the 23 cases, the RMSE demonstrating the differences between EDPVR estimation and data, was higher when using the Klotz algorithm than when using the 0D multiple beat method. However, no statistical difference have been observed when comparing RMSE from both the single-beat estimation methods. The bottom right panel of Figure 4.5, demonstrating the RMSE calculated when the comparator was the multiple-beat method, shows that a statistical trend exists toward difference between the two single-beat estimation methods.

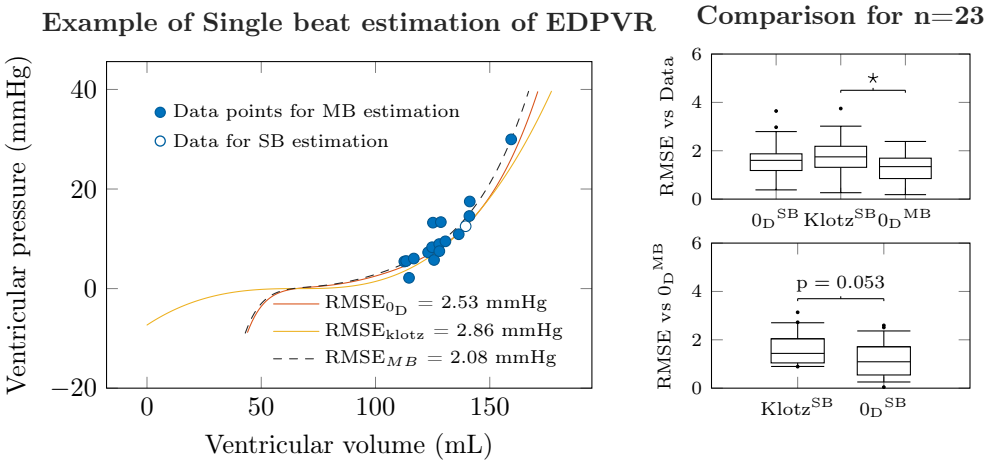

Figure 4.5 – Single-beat estimation of EDPVR. **Left**: Example of a single beat estimation of V_{ref}, β and EDPVR. The blue dots are the points used for RMSE calculation, and were also considered for multiple-beat estimation procedure. The white dot is the point use for the single-beat estimation methods (Klotz and biomechanical). **Upper Right**: Boxplot summarising the RMSE between the multiple PV datapoints and the estimation methods for the 23 cases. 0_D^{SB}: RMSE with the single-beat estimation method from biomechanical model; 0_D^{MB}: RMSE with the multiple-beat estimation method from biomechanical model; Klotz^{SB}: RMSE with the single-beat estimation method from Klotz method. **Lower Right**: Boxplot summarising the RMSE between the multiple-beat estimation method from biomechanical model and the single-beat estimation methods.

4.5 Discussion

In this chapter, we aimed at evaluating the performance of the estimation method derived from the passive biomechanical law into a framework described in Chapter 3. By using synthetic data generated from a prescribed passive law, we described the robustness of our framework to estimate the parameter of prescribed the passive law with respect to the data quality and/or richness. We quantified the error made in EDPVR estimation and demonstrated that this error was lower with our framework as compared to the method derived from Klotz et al. [4] procedure. We also evaluated the performance of our framework in a single beat estimation setting. We used in vivo human data originated from 23 cases published in Klotz et al. [4]; ten Brinke et al. [6]; Gaasch et al. [2]; Fester and Samet [1]; Kawaguchi [3]. We applied the single beat estimation algorithm of our framework and compared its performance with the single beat estimation method Klotz et al. [4].

Indeed, our results suggest that our framework allows better identification of V_{ref} parameter than the Klotz procedure, even for a low number of PV data points available or even if the error in data measurement is important, or even for a large ranges of heart size. This can be explained by the characteristic of the solution of the minimisation problem (Equation (3.22) exemplified in Figure 3.12), which demonstrated a steep valley close to V_{ref} solution. This confers to our method a better performance for V_{ref} estimation than the Klotz procedure (Figure 4.3). This may explain the better results observed for EDPVR estimation as demonstrated by the lower RMSE as compared to the Klotz method. However, we did not measure the V_{ref} as a gold standard. Our ground truth was a prescribed passive law. For this reason, our algorithm is supposed to have better chances to find the exact solution. Measurement of volume at stress-free reference configuration would have been stronger comparator for validation purposes. However, the experiment would suffer from accuracy problems. Indeed, it involves measurement of the volume of a balloon inflated within the LV at 0 mmHg pressure. It is not obvious that the structure and/or the stiffness of the ballon has no impact of this measurement. Furthermore, we were unable to perform this experiment that involves explanted hearts. However, even if we see better estimation by using our framework, we see that the results obtained with Klotz algorithm are also excellent. We may suppose that the error we made in choosing our ground truth is small, and our results may still be be valid. Another comment we can make with respect to the estimation of the passive law parameters is related to the better performance in V_{ref} as compare with the β estimation. This is caused by the lower identifiability of the β parameter, as discussed in Section 3.3. Indeed, if we quantify the deviation from the original prescribed parameter, an approximately 10% deviation is observed for the estimation of β, that is lower than the 2% for V_{ref} estimation (Table 4.1). This can be seen in Figure 3.12 and may be explained. A small error in V_{ref} estimation would lead to a significant compensatory deviation of β parameter estimation, to warrantee a good fit of the data.

As discussed in Section 3.3, the choice we made for tuning the parameters of the regulatory terms of Equation (3.22) may have introduced error in person-specific EDPVR estimation. In this chapter, we confirmed that the effect is small. Indeed, when testing our algorithm in various classes of LV size, the performance of our algorithm to estimate the parameters was good, especially for V_{ref}, and better than the Klotz estimate. More important, we suggested that the introduction of these regulatory terms could have beneficial effects when the accuracy of PV data point measurement was questioned. We can observe this effect on the example provided in Figure 4.2 bottom right panel. The yellow curve (representing the EDPVR estimation of Klotz algorithm) is more impacted by the data point than the red curve, representing the passive law estimation. If we look at

the RMSEs quantifying the deviation from the passive law prescription, we can observe that the accuracy of the result is really impacted by the error in data point. This ”single point effect” may have been attenuated by the implementation of these regulatory terms. This observation also demonstrated a significant limitation of the single beat estimation methods of EDPVR estimation, and if in the example our method allows to correct this effect, the width of the boxplot provided in the subfigure of the bottom left panel of Figure 4.2 demonstrates that our framework suffers also from this effect. However, our final results, testing our single beat estimation method on in vivo data against the Klotz method suggest that our framework may be better in EDPVR estimation.

Bibliography

[1] Fester, A. and Samet, P. (1974). Passive Elasticity of the Human Left Ventricle. *Circulation*, 50(3):609–618.

[2] Gaasch, W. H., Cole, J. S., Quinones, M. A., and Alexander, J. K. (1975). Dynamic determinants of letf ventricular diastolic pressure-volume relations in man. *Circulation*, 51(2):317–323.

[3] Kawaguchi, M. (2003). Combined ventricular systolic and arterial stiffening in patients with heart failure and preserved ejection fraction: Implications for systolic and diastolic reserve limitations. *Circulation*, 107(5):714–720.

[4] Klotz, S., Hay, I., Dickstein, M. L., Yi, G.-H., Wang, J., Maurer, M. S., Kass, D. A., and Burkhoff, D. (2006). Single-beat estimation of end-diastolic pressure-volume relationship: a novel method with potential for noninvasive application. *AJP: Heart and Circulatory Physiology*, 291(1):H403–H412.

[5] Lang, R. M., Badano, L. P., Mor-Avi, V., Afilalo, J., Armstrong, A., Ernande, L., Flachskampf, F. A., Foster, E., Goldstein, S. A., Kuznetsova, T., Lancellotti, P., Muraru, D., Picard, M. H., Rietzschel, E. R., Rudski, L., Spencer, K. T., Tsang, W., and Voigt, J.-U. (2015). Recommendations for Cardiac Chamber Quantification by Echocardiography in Adults: An Update from the American Society of Echocardiography and the European Association of Cardiovascular Imaging. *Journal of the American Society of Echocardiography*, 28(1):1–39.e14.

[6] ten Brinke, E. A., Burkhoff, D., Klautz, R. J., Tschope, C., Schalij, M. J., Bax, J. J., van der Wall, E. E., Dion, R. A., and Steendijk, P. (2010). Single-beat estimation of the left ventricular end-diastolic pressure-volume relationship in patients with heart failure. *Heart*, 96(3):213–219.

CHAPTER 5

Main issues & future perspectives on biomechanical modelling of EDPVR

In the previous chapters, End-diastolic pressure-volume relationship (EDPVR) estimation methods based on biomechanical modelling were described and evaluated against existing phenomenological procedures. Even if our approach allows to interpret our EDPVR estimation method from a physiological standpoint, some issues have been raised. Especially, we defined a β parameter, which is related to the global stiffness of the ventricle and which aggregates the intrinsic stiffness of the myocardium (C_i parameters) and the stiffness associated with the wall thickness of the myocardium (ϵ parameter). The identifiability of those two parameters is difficult to assess unless another information is known. By using echocardiographic data measurement, we provide a method to improve the ϵ estimation. Finally, our work is exploratory and necessitates further clinical studies to evaluate the usefulness of a therapeutical strategy based on EDPVR estimations.

Despite interesting for the monitoring and the understanding of pathophysiological processes occurring during heart failure caused by diastolic dysfunction, the EDPVR analysis is not used in routine clinical practices. Indeed, since EDPVR measurement requests cardiac catheterisation performed under various loading conditions, it has been used almost exclusively for research purposes. For this reason modelling the passive properties of the left ventricle may represent an interesting alternative. Two approaches are available. If the models based on continuum mechanics theory are attractive because of their underlying physical properties, they have to face several limitations. Among them, data measurements availability for model calibration purposes is probably the most limiting. On the contrary, the phenomenological approach uses the data already available into more simplistic models. This allows to perform patient-specific calibration [6; 4], but it prevents comparisons to be performed between subjects [1]. For these reasons, the potential for application of EDPVR modelling in clinical practice is limited.

By setting a method based on a biomechanical model of left venticle to estimate patient-specifically the EDPVR from data available in routine clinical practice, we reunited the pragmatic phenomenological with the rigorous biomechanical approaches. Indeed, we used a complete multi-scale biomechanical model [3] simplified by its spherical conformation, described in details in Caruel et al. [2]. The description of the passive properties of this model is derived from the original publication of Holzapfel and Holzapfel and Ogden [5], in which they described a transversely isotropic model characterised by an hyperelastic potential and geometrical properties. However, even if the models derived from that approach reduces the parametric space to at least 6 parameters, the calibration necessitates a fine testing of the tissue and can note be used in vivo in patient-specific regime. We solved this issue by using the observation made by Klotz et al. [6]. Under a double-normalisation condition (*i.e.* with respect to V_{ref} and V_{30}), they observed that the EDPVR for various subjects can be approximated by a unique averaged master EDPVR curve. We used this properties to calibrate the parameters of the hyperelastic potential of a reference passive law, all the other geometrical information being obtained non invasively using transthoracic echocardiography imaging in an anaesthetised patient. The originality of this approach stands in the fact that we successfully described the physiological behaviour of this passive law when deviating its geometrical or stiffness parameters from the reference configuration. Indeed, the reference passive law have to be modified in an homothetic manner in order to stay within the ranges of the EDPVR given by the double-normalised measured PV data. Consequently, we reduced the parametric space to 3 parameters (*i.e.* V_{ref}, β and ϵ). Therefore, we described a framework that allows to estimate all the 3 parameters from patient-specific data obtained non-invasively by TTE. We first studied the robustness of this framework on synthetic data by reducing the number of PV points available for EDPVR estimation, or by increasing the noise in the PV points. We also evaluated the performance of our framework in a single-beat setting against the Klotz single-beat method, for parameters and EDPVR estimation from 23 cases obtained in vivo in patients originated from previous publication. We demonstrated that the results of the two methods were close, even if the results in EDPVR estimation obtained by our framework tended to be better than the results obtained by Klotz estimation method. Furthermore, the biomechanical nature of our model confers advantages over phenomenological model, even though the performance may be equivalent. First, the parameters of our model can be interpreted directly as intrinsic tissue stiffness, tissue stiffness associated with wall thickness, and the reference configuration (the volume at stress free configuration) of the LV. Second, our framework allows not only comparison within subject (*e.g.* from a previously calibrated configuration, if concentric hypertrophy is evolving, an adaptation of the ϵ parameter would predict the effect on the EDPVR, without the

need for measuring new PV datapoint), but also between subjects, in a magnitude that is proportional to the reference EDPVR optimised from the reference patient. Third, by adding population-based regulatory term, we allows the framework to deviate from PV data if the solution of Equation (3.22) is too far from the result we would expect in this population. This can have an effect only if the number of data available is small – typically for single-beat estimation – in order to prevent the "single-beat effect" described in Section 4.5.

Our framework suffers from several limitations. Indeed, even though the calibration is fully patient-specific, the interpretation of the parameters and EDPVR estimation can only be performed relatively to the reference patient. Even if it is easy to find back the raw parameters as we provided the value for optimised C_i in the reference patients, the value for β and α parameters, and more importantly their between subject comparative potential for tissue stiffness information is conditioned by their link to this reference patient. If one would use another reference calibration parameters, then the value for α and β would be difficult to compare with the results obtained in our study. Also, the data measured in reference patient may be subject to controversies. We used a fully non invasive method to estimate both the volume (V_m) end pressure (P_m) at end diastole. The error in volume measurement by echocardiography can be significant as it is operator-dependant. We also used approximation in pressure measurement because we use semi-quantitative analysis of trans-mitral flux as a surrogate of filling pressure, as recommended by european society of echocardiography [7]. We arbitrarily advocated a 7 mmHg pressure in our patients because our analysis concluded that this patient did not have elevated filling pressure. The measurement of (V_m, P_m) in this patient was necessary to estimate the V_{ref} from Klotz method. We observed that a small error in V_{ref} estimation has an important impact on the values of the C_i parameters. However it has no effect on the fit with respect to normalised data. Therefore, our framework allows only a stiffness evaluation relatively to the reference patient, the interpretation of the C_i parameters as absolute stiffness information being difficult. The same limitation and advantage may be advanced for Klotz parameter $\frac{V_{30}}{V_{ref}}$ which quantifies the dilation of the heart, relatively to the reference configuration, to reach 30 mmHg pressure. The signification for this parameter may be close to the signification of the β parameter. Additionally to this information, our method allows to differentiate between intrinsic stiffness of the myocardium (α) and the stiffness associated with the wall thickness (ϵ). This differentiation is however subject to approximation in ϵ. Indeed, when measuring or estimating the PV data point, we did not have an *a priori* knowledge on the fibre extension with respect to the reference configuration (R_{ref}, d_{ref}). Consequently, we set a fixed value for this parameter ($\overline{e_{fib}}^m = 0.15$, Equation (5.2)), which necessarily introduced error. This error may have no direct impact on β estimation, because it is estimated from the PV data points, but rather on α parameter, or on V_{ref} estimation. Since we did not have access to the true V_{ref} measurement we were unable to quantify the error it introduced. However, as the results obtained were close to Klotz approximation, we believe that the error related to this approximation is small.

Future research on our framework may improve the technique. Indeed, in our validation study, we used only PV data obtained from literature. We did not have access to wall thickness information. We estimated β and V_{ref} but we had to define a value for ϵ. We chose a 0.2980 value, which corresponds to the optimised reference patient, for all patients. It seems reasonable to advance that since the β parameter is estimated from the data, and since β is a function of α and ϵ, an error in ϵ relatively to the true value would lead to a misestimation of α, without any effect on β and therefore on the final passive law. This approximation was tested on a sensitivity analysis, in which we applied the optimisation procedure for P_{data}^{synth} generated using the following parameters

($\beta = 0.8, \mathrm{V_{ref}} = 58$ mL, $\epsilon_{\mathrm{true}} = 0.298$). In the optimisation procedure, we modified sequentially ϵ ($\epsilon_{\mathrm{prescribed}} = [0.1192 : 0.0596 : 0.5960]$) and calculated the RMSE between the $\mathrm{P}_{\mathrm{data}}^{\mathrm{synth}}$ and the passive law estimated (Figure 5.1).

We observed differences in estimated passive laws and $\mathrm{P}_{\mathrm{data}}^{\mathrm{synth}}$ which is at the order of magnitude of the error prescription in our optimisation algorithm (less than 3 mmHg), . However, if we look at the estimated parameters (β, $\mathrm{V_{ref}}$), the error may be important relatively to the delta between ϵ_{true} and $\epsilon_{\mathrm{prescribed}}$ (Figure 5.1).

To estimate ϵ properly may be difficult. If we analyse Figure 3.12 in Section 3.2.2 we see that the optimisation problem is ill-posed in β direction. To identify α and ϵ from β would necessitate another information. However, our monitoring configuration involves to obtain morphological information. Indeed, for a complete calibration, the end-diastolic volume is requested. The inner radius ($\mathrm{R_{in}}$) of the sphere may be estimated from this information. If the myocardial volume can be measured, it is possible to obtain the wall thickness ($\mathrm{d_m}$) of the sphere. Therefore, the $\mathrm{R_m}$ can be obtain

$$\mathrm{R_m} = \mathrm{R_{in}} + \frac{\mathrm{d_m}}{2} \tag{5.1}$$

However, ϵ can be written as a function of $\mathrm{R_m}$ and $\mathrm{d_m}$

$$\epsilon = \frac{\mathrm{d_m}}{\mathrm{R_m}} \left(1 + {\mathrm{e_{fib}}}^{\mathrm{m}}\right)^3 \tag{5.2}$$

Furthermore, by combining Equation (3.4) with Equation (5.2), we can write the relationship between $\mathrm{e_{fib}}$ and $\frac{\mathrm{V}}{\mathrm{V_{ref}}}$ as a function of $\mathrm{d_m}$ and $\mathrm{R_m}$:

$$\left(\frac{\mathrm{V_m}}{\mathrm{V_{ref}}}\right)^{\frac{1}{3}} = \frac{1 + {\mathrm{e_{fib}}}^{\mathrm{m}} - \frac{\omega}{2}\left(1 + {\mathrm{e_{fib}}}^{\mathrm{m}}\right)}{1 - \frac{\omega}{2}\left(1 + {\mathrm{e_{fib}}}^{\mathrm{m}}\right)^3} \tag{5.3}$$

with $\omega = \frac{\mathrm{d_m}}{\mathrm{R_m}}$. Therefore, if ω is known by data measurement, and $\mathrm{V_{ref}}$ estimated by replacing Equation (3.5) by Equation (5.3), we will be able to estimate ϵ using Equation (3.4). Consequently, we would be able to calculate the α coefficient. Further work are requested to verify this hypothesis.

Another approach may help to estimate ϵ through iterative process. Starting from an estimated set of parameters ($\mathrm{V_{ref}}$ and β), obtained by a procedure in which ϵ was prescribed arbitrarily, it is possible to calculate a new ϵ by using Equation (5.2). First, from a first round of optimisation process, it is requested to estimate ${\mathrm{e_{fib}}}^{\mathrm{m}}$, by using Equation (3.5) and the knowledge relatively to $\mathrm{d_m}$ and $\mathrm{R_m}$. Then ${\mathrm{e_{fib}}}^{\mathrm{m}}$ is used in Equation (5.2), with $\mathrm{d_m}$ and $\mathrm{R_m}$. The new ϵ can be used as initial guess for iterative optimisation procedure. Figure 5.1 demonstrates the effect of this iterative process on parameters estimation. Figure 5.2 displays the effect of the correction with $\frac{\mathrm{d_m}}{\mathrm{R_m}}$ information on ϵ estimation. We observed that it allows for a good ϵ estimation, along with an improvement in $\mathrm{V_{ref}}$ estimation. The effect of the iterative ϵ estimation process also allow for more stability in β estimation, even if the dispersion around the mean estimation is wide. We also observed that the fit in the data is worsened, which suggests a potential data overfitting when not using the $\frac{\mathrm{d_m}}{\mathrm{R_m}}$ correction.

Also, PV Data is difficult to obtain. A non-invasive technique, based on elastography principle may be interesting for gathering stress-strain relationship that may be fitted by our framework [8; 9]. Rather than using conventional echocardiography for the ($\mathrm{V_m}$, $\mathrm{P_m}$) assessment, this technique is based on the propagation of shear waves originated from dedicated echocardiographic probes. The speed velocity of the shear waves in response to mechanic stimulus caused by high frequency Doppler beam was related to tissue stiffness.

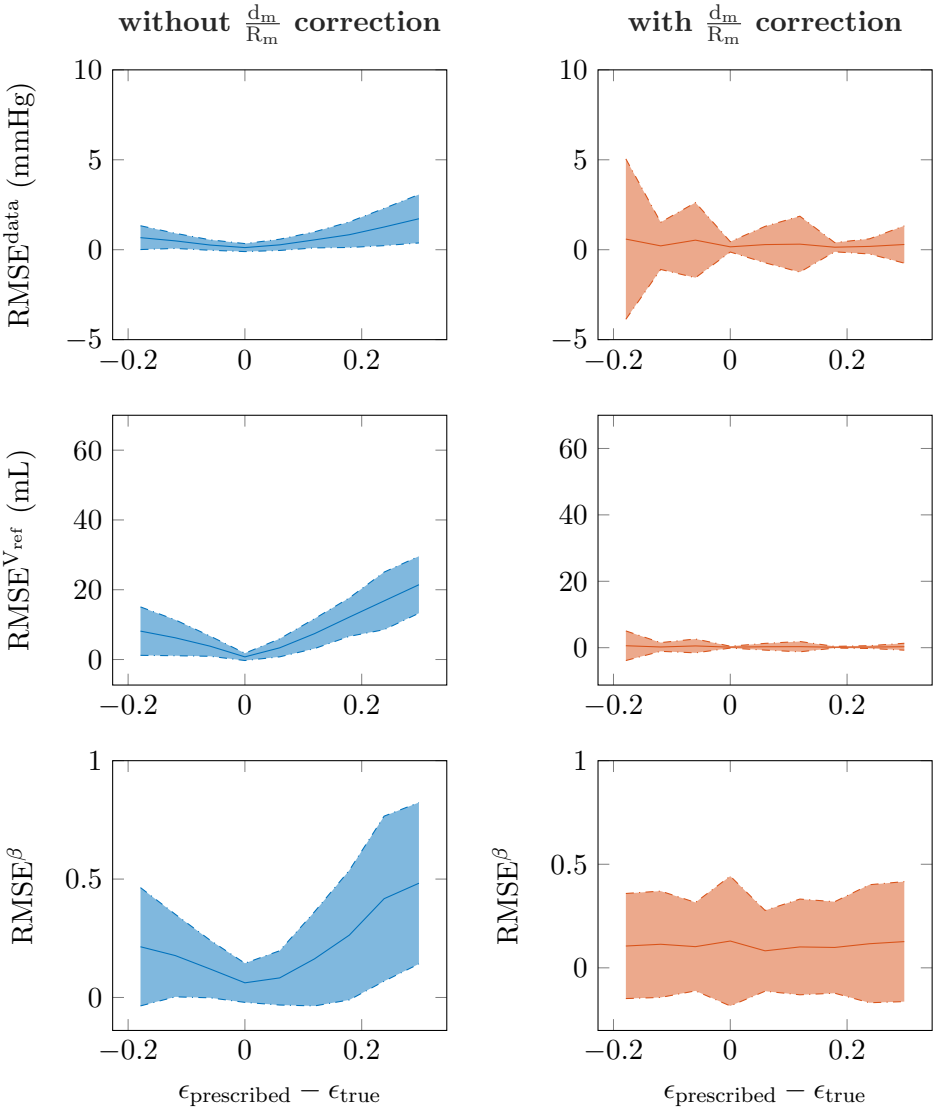

Figure 5.1 – Difference between synthetic data and estimated passive law. The data are generated using the following parameters ($\beta = 0.8, V_{ref} = 58$ mL, $\epsilon_{true} = 0.298$), with 30 e_{fib} points. The optimisation procedure is performed with normal dilation and hypertrophied class parameters and with sequential increase in ϵ prescription ($\epsilon_{prescribed} = [0.1192 : 0.0596 : 0.5960]$). The RMSE between data and the pressure generated by the passive law estimated is displayed against the difference between the $\epsilon_{prescribed}$ and the ϵ_{true} without **(upper left)** and with correction using $\frac{d_m}{R_m}$ **(upper right)**. Difference between estimated and prescribed V_{ref} **(middle)** and β **(bottom)** parameters without **(left)** and without **(right)** $\frac{d_m}{R_m}$ correction, with respect to error made in ϵ in optimisation procedure is also displayed. The solid line represents the mean of 100 simulations. The dash dotted lines represent the 95% confidence interval of the 100 simulations.

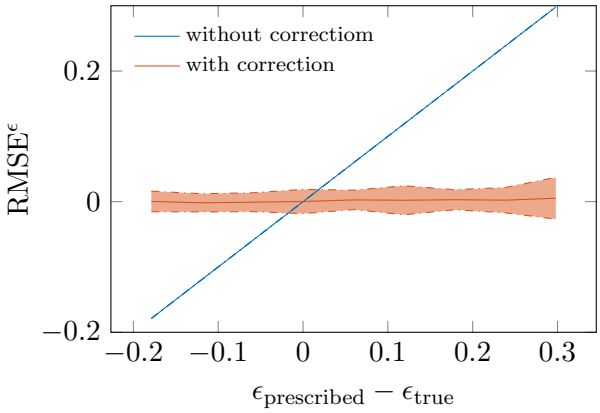

Figure 5.2 – Performance of the ϵ estimation using the iterative process with geometrical knowledge about the wall thickness and the radius of the sphere. The data are generated using the following parameters ($\beta = 0.8, \mathrm{V_{ref}} = 58$ mL, $\epsilon_{\text{true}} = 0.298$), with 30 $\mathrm{e_{fib}}$ points. The optimisation procedure is performed with normal dilation and hypertrophied class parameters and with sequential increase in ϵ prescription ($\epsilon_{\text{prescribed}} = [0.1192 : 0.0596 : 0.5960]$). The initial condition is the ϵ prescribed. Using the optimisation procedure described in Section 3.2.2, we estimated $\mathrm{V_{ref}}$ and β. We further estimated $\mathrm{e_{fib}}^{\mathrm{m}}$ from $\mathrm{V_{ref}}$, $\mathrm{d_m}$ and $\mathrm{R_m}$, using equation (5.3). We used $\mathrm{e_{fib}}^{\mathrm{m}}$ in Equation (5.2) to estimate a new ϵ which is subsequently used in the estimation procedure of $\mathrm{V_{ref}}$ and β.

Therefore, it may be used to test our method in various population. It may also be used for testing the optimisation of the $\mathrm{C_i}$ parameters on another population than the one provided in the publication of Klotz et al. [6].

Experimental bi-axial stretch test would be interesting to perform, as in the study of Yin et al. [10], to explore in detail the signification of the optimised $\mathrm{C_i}$ parameters.

Finally, experimental Data may be interesting for the validation of the $\mathrm{V_{ref}}$ estimation. However as discussed in Section 4.5, the accuracy of the measurement of $\mathrm{V_{ref}}$ is questionable. Proper experimental design should be set up prior to perform such a study.

Clinical studies may be designed for further validation of our framework. Non invasive $\mathrm{LVP_{ed}}$ estimation by our framework could be interesting to evaluate in intensive care unit, especially in monitoring condition. At the moment $\mathrm{P_{ed}}$ can be monitored by using Pulmonary Capillary Wedge Pressure, from a pulmonary arterial catheter, but this techique is invasive. Semi-quantitative transmitral Doppler flux analysis may help to classify between low or high filling pressure of the LV but does not provide absolute EDP estimation. Pulmonary Veins flow decelerating time has also been linked to EDP by phenomenological approach [4], but is technically difficult to obtain in mechanically ventilated patients. Comparison of the above-mentioned indicator would be interesting to perform especially when using therapeutical drugs, such as vasodilators or inotropic drugs, in order to estimate the shift in EDP. Also, straightforward EDPVR determination may be used in a more exhaustive cardiovascular modelling framework, in which the active properties of the heart could be implemented (See Chapter 7 and 10).

By describing a single-beat EDPVR estimation method based on biomechanical modelling, we connected continuum mechanic theories applied to cardiac physiology with approaches based on data availability allowing already approximated patient-specific estimation. The novelty of our framework stands in the fact that by describing the behaviour of the passive law based on biomechanics, relatively to a properly calibrated reference patient, we succeeded to reduce the parametric space requested for subsequent calibration to 3 parameters, which can be estimated by routinely acquired data. We validated our single-beat estimation method on in vivo PV measurements, against the original single-

beat estimation method described by Klotz et al. [6]. The potential for application of this method exists and may be useful for clinical cares in anaesthesia, intensive care or cardiology, when considering left ventricle compliance pathologies. This framework allows also to use a patient-specific EDPVR on a more complete left ventricle model, which may be helpful in fluid-responsiveness status determination under critical care situations for example.

Bibliography

[1] Burkhoff, D. (2005). Assessment of systolic and diastolic ventricular properties via pressure-volume analysis: a guide for clinical, translational, and basic researchers. *AJP: Heart and Circulatory Physiology*, 289(2):H501–H512.

[2] Caruel, M., Chabiniok, R., Moireau, P., Lecarpentier, Y., and Chapelle, D. (2014). Dimensional reductions of a cardiac model for effective validation and calibration. *Biomechanics and Modeling in Mechanobiology*, 13(4):897–914.

[3] Chapelle, D., Fragu, M., Mallet, V., and Moireau, P. (2013). Fundamental principles of data assimilation underlying the Verdandi library: applications to biophysical model personalization within euHeart. *Medical & Biological Engineering & Computing*, 51(11):1221–1233.

[4] Gayat, E., Mor-Avi, V., Weinert, L., Yodwut, C., and Lang, R. M. (2011). Noninvasive quantification of LV elastance and ventricular-arterial coupling using 3D echo and arterial tonometry. *AJP: Heart and Circulatory Physiology*, 301(5):H1916–H1923.

[5] Holzapfel, G. A. and Ogden, R. W. (2009). Constitutive modelling of passive myocardium: a structurally based framework for material characterization. *Phil. Trans. R. Soc. A: Mathematical, Physical and Engineering Sciences*, 367(1902):3445–3475.

[6] Klotz, S., Hay, I., Dickstein, M. L., Yi, G.-H., Wang, J., Maurer, M. S., Kass, D. A., and Burkhoff, D. (2006). Single-beat estimation of end-diastolic pressure-volume relationship: a novel method with potential for noninvasive application. *AJP: Heart and Circulatory Physiology*, 291(1):H403–H412.

[7] Nagueh, S. F., Appleton, C. P., Gillebert, T. C., Marino, P. N., Oh, J. K., Smiseth, O. A., Waggoner, A. D., Flachskampf, F. A., Pellikka, P. A., and Evangelisa, A. (2008). Recommendations for the Evaluation of Left Ventricular Diastolic Function by Echocardiography. *European Journal of Echocardiography*, 10(2):165–193.

[8] Pernot, M., Lee, W.-N., Bel, A., Mateo, P., Couade, M., Tanter, M., Crozatier, B., and Messas, E. (2016). Shear Wave Imaging of Passive Diastolic Myocardial Stiffness. *JACC: Cardiovascular Imaging*, 9(9):1023–1030.

[9] Villemain, O., Correia, M., Mousseaux, E., Baranger, J., Zarka, S., Podetti, I., Soulat, G., Damy, T., Hagège, A., Tanter, M., Pernot, M., and Messas, E. (2019). Myocardial Stiffness Evaluation Using Noninvasive Shear Wave Imaging in Healthy and Hypertrophic Cardiomyopathic Adults. *JACC: Cardiovascular Imaging*, 12(7):1135–1145.

[10] Yin, F. C., Strumpf, R. K., Chew, P. H., and Zeger, S. L. (1987). Quantification of the mechanical properties of noncontracting canine myocardium under simultaneous biaxial loading. *Journal of biomechanics*, 20(6):577–589.

Part III

End-systolic pressure-volume relationship: From time-varying elastance concept to biomechanically-derived time-varying elastance modelling

CHAPTER 6

Time-varying elastance concept: from physiology to time-varying elastance model

In this chapter, we will give an overview of the concept of time-varying elastance (E(t)). Since its first description in the 70's, the E(t) concept was extensively studied. It consists in a simple local linearisation of the end-systolic pressure-volume relationship (ESPVR). It offered the opportunity to simplify cardiac physiology and allowed to obtain, with minimal invasiveness, useful information regarding cardiac properties *in vivo*. Indeed, although pressure-volume relationship analysis requires invasive intraventricular placement of pressure catheter, improvement of E(t) concept based methods has led to propose fully non invasive methods for end-systolic elastance (E_{es}) estimation, which was linked to the contractile state of the myocardium, and helped to analyse in vivo the effect of therapeutic drugs. Furthermore, the E(t) concept is also useful for modelling community as its simple design allows both easy identification of its parameter and its use as a surrogate for cardiac mechanics. Cardiac models based on E(t) functions allowed to perform complete pressure-volume (PV) loop analyses non-invasively. Therefore, even though the E(t) concept is a local approximation of physiological ESPVR, 50 years later, it is still a useful description of the cardiac complexity which helps to access clinical information with minimal invasiveness.

6.1 Introduction

Since the original works performed by Suga et al. [31] and Sagawa et al. [21], there has been a growing interest regarding the time-varying elastance concept. Indeed, by using linearisation of end-systolic pressure-volume relationship (ESPVR), of arterial elastance, and introducing the concept of ventricular arterial coupling, they paved the way to access interesting information about patients cardiac physiology.

First of all, they studied the concept of linearisation of the ESPVR. This linearisation gives a local approximation of the Starling relation linking the LV end-systolic volume and pressure at a given end-diastolic state [28]. As described in chapter 1, this linearisation is characterised by its slope (E_{es}) and its volume intercept (V_0) (Figure 6.1). E_{es} has been

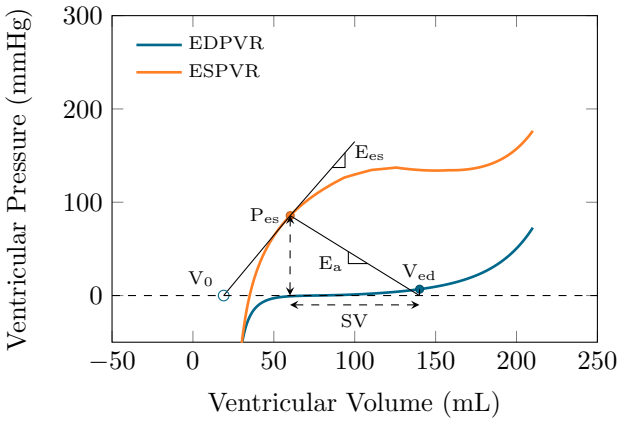

Figure 6.1 – Linearisation of the end-systolic pressure volume relationship (ESPVR) and description of ventricular-arterial coupling (V_{va}) concept. The linearised ESPVR is described by its slope E_{es} (first derivative of the ESPVR at the end-systolic pressure-volume point (P_{es})) and its volume intercept V_0. The arterial elastance (E_a) corresponds to the ratio between ESP and the stroke volume (SV), itself being the difference between the end-diastolic (V_{ed}) and the end-systolic volume (V_{es}). The V_{va} is the ratio between E_a and E_{es}. For an efficient system, V_{va} is supposed to be found between 0.6 and 1.2.

found to be associated with inotropic state and could represent a surrogate of contractile property of the whole LV [31; 8; 15; 10]. Indeed, experimental studies observed that E_{es} does not vary with loading conditions (load-independent) but does vary when administering positive or negative inotropic drugs [31; 8; 15; 10]. Also, heart rate has been found to be associated with myocardial contractility (the "*Bowditch effect*") [19]. This question is however complex and seems to be related to intracellular calcium distribution. It have raised many debates in cardiac physiology community [13]. In 1985, Maughan et al. [16] also found a linear association between heart rate and E_{es} over a heart rate range from 60 to 120 beats per minutes, in an isolated canine heart preparation.

Furthermore, they introduced the concept of ventricular-arterial coupling (V_{va}). The LV, seen as an elastic chamber, is characterised by its elastance E_{es}, producing output driven by contractile forces into the arterial system, which is also characterised by its elastic stiffness – the so-called arterial elastance. As for the ESPVR, the arterial elastance can be approximated by linearisation at the end-systolic state. It is characterised then by its slope (E_a), and its volume intercept – the end-diastolic volume (EDV). The two linearisations cross at the end-systolic pressure volume point, and their ratio $\frac{E_a}{E_{es}}$ is called the ventricular-arterial coupling (V_{va}). Experimental studies have linked the value of V_{va} to the optimal myocardial oxygen consumption or cardiac efficiency of the heart [6; 26] (Figure 6.2).

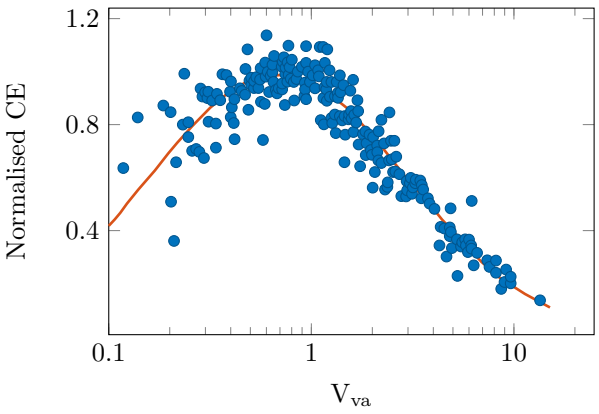

Figure 6.2 – Optimal ventricular-arterial coupling (V_{va}). Pooled data from 26 experimental runs in 8 explanted dogs' hearts. CE: Cardiac efficiency measured as the LV stroke work divided by the myocardial oxygen consumption. The results are normalised by the average maximal CE. The red line represents a normal law fitted on the data to find the V_{va} which maximises CE. In this experiment ${V_{va}}^{optim} = 0.638\,(CI_{95}$ 0.6 to 0.68) *Reproduced from [6]*

They further developed the concept by introducing the time-varying elastance of the LV. The linearisation of the ESPVR allows to estimate V_0. This "volume-at-zero-pressure" intercept has been found to be consistent across wide preload or afterload ranges and across inotropic states [16; 30]. Therefore, the following equation can be used to derive the time-varying elastance curve representing the ventricular elastance throughout the contraction period of the cardiac cycle:

$$E(t) = \frac{P\,(t)}{V\,(t) - V_0} \tag{6.1}$$

An example of a time varying elastance curve is provided in Figure 6.3. Another interesting feature of this concept relies on the normalisation of E(t). Indeed, when normalised to E_{es} and to t_{max} – which represents the time to reach E_{es} – Equation (6.2), the time-varying elastance curve has been found to be consistent within and across subjects [31; 23].

$$E^N\left(t^N\right) = \frac{E\left(\frac{t}{t_{max}}\right)}{E_{es}} \tag{6.2}$$

This finding paved the way for non invasive E_{es} estimation methods [23; 4; 24; 7], in which all of the components required for estimation can be approximated from clinical measurement. Indeed, in 1992, Kelly et al. observed that a phenomenological estimation of ventricular end-systolic pressure (P_{es}) demonstrated very good performance [12], with $P_{es} = 0.9 \times P_s$, P_s being the brachial systolic pressure. Therefore, both the components of V_{va}, E_a and E_{es} can be approximated by routine clinical measurements. These methods allow an easy and non-invasive access to V_{va}, and indirect access to contractile properties of the LV, to myocardial energetic expenditure or to cardiac efficiency throughout a cardiac cycle.

However, this approach is based on approximations which limit the concept validity. First it has been shown in animal experimental models that the ESPVR is not linear [2; 17; 32]. In canine ventricle, Burkhoff et al. [2] showed that the ESPVR expressed various curvatures, depending on the inotropic state (Figure 6.4). Mirsky et al. [17] also observed that a good data fit can be obtained by using non-linear models (Figure 6.5) in canine experimental models. Consequently, E_{es}, which is a local linearisation of ESPVR, should vary with respect to the operating condition on the ESPVR curve, and

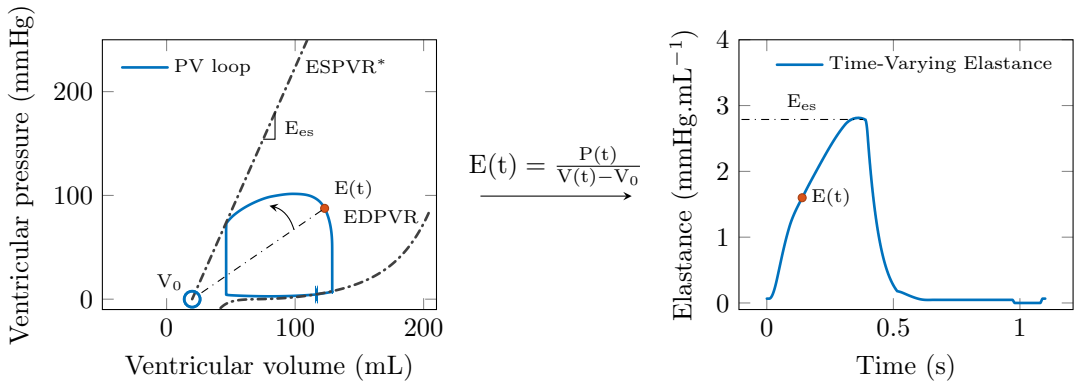

Figure 6.3 – Pressure-volume (PV) loop and time-varying elastance concept. **Right:** The time-varying elastance curve is derived from the PV loop (**Left**). The local linearisation of the ESPVR around the end-systolic PV point is characterised by its slope (E_{es}) and its intercept (V_0). The time course of the slope characterised by the red E(t) point correspond to the time-varying elastance curve.

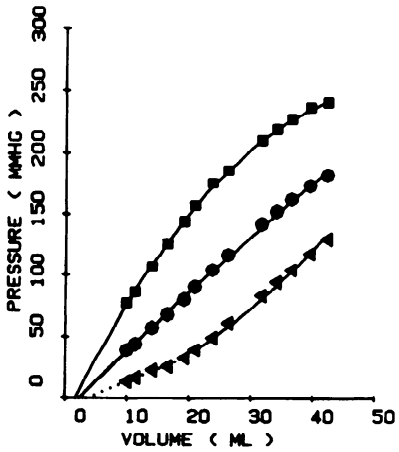

Figure 6.4 – End systolic pressure volume relations. Solid circles, control data; triangles, extrasystolic data; squares, postextrasystolic data. Solid lines are best-fit quadratic relations (P, = aVL +b, + c) to data as determined by nonlinear regression analysis. Dotted line is linear regression to data on extrasystolic beat obtained below 20 ml. *Reproduced from Burkhoff et al. [2]*

becomes load-independent only for small changes in after- or pre- loads. The position of V_0 could therefore be under-estimated if determined by using the linearisation method (See Figure 6.5). However, the V_0 placement is crucial for E(t) determination as written in Equation (6.1). A significant error in V_0 estimation may lead to an error in E(t) estimation.

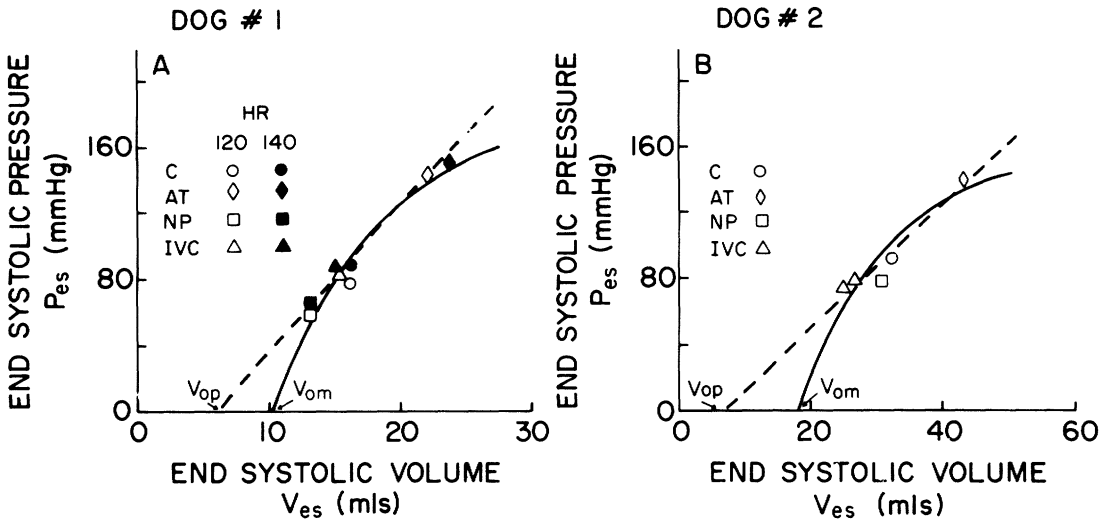

Figure 6.5 – End-systolic pressure-volume relations based on the maximum myocardial stiffness and maximum ventricular elastance concepts. The solid curve represents the relation obtained from the maximum myocardial stiffness concept and is clearly non linear. The dotted straight line is the end-systolic pressure-volume relation obtained from the maximum ventricular elastance concept. The isolated points represent the measured pressures and volumes at the time of maximum ventricular elastance. V_{0m} = zero stress - volume obtained from the present theoretical model ; V_{0P} = zero stress - volume obtained by linear extrapolation of the maximum elastance points. Linear extrapolation may lead to spurious results for V_{0P}. Afterload was altered from control(C) with nitroprusside (NP), angiotensin I(AT), and IVC occlusion (IVC) at constant heart rates of 120, 140 beats/min. In all cases there was no significant difference in the slopes (max Eav) of these relationships at heart rates from 120 to 140 beats/min. *Reproduced from [17]*

Second, the non-invasive E_{es} estimation methods described in Senzaki et al. [23]; Chen et al. [4], are based on the principle of unicity/consistency across subjects of normalised time-varying elastance curve. However, we will discuss in Chapter 7 the sensitivity of these estimation methods to measurement errors. These limitations decreased the usefulness of this approach at a patient-specific level.

6.2 Time-Varying Elastance models

The time-varying elastance curve has been used for modelling purposes. Indeed, through Equation (6.1), if E(t) is known, a link with ventricular pressure and volume is established. There has been a growing interest in substituting the mechanical behaviour of the heart with the time-varying elastance curve, which contains information about cardiac mechanics. Therefore, attempts have been made to reproduce the E(t) curve by using many methods.

6.2.1 Existing methods for E(t) estimation

In 2002, Heldt et al. [9] proposed an electrical analogous model

$$E(t) = \begin{cases} \frac{E_s - E_d}{2} \cdot \left[1 - \cos\left(\pi \cdot \frac{t}{T_s}\right)\right] + E_d & \text{if } 0 \leq t \leq T_s \\ \frac{E_s - E_d}{2} \cdot \left[1 + \cos\left(2\pi \cdot \frac{t - T_s}{T_s}\right)\right] + E_d & \text{if } T_s \leq t \leq \frac{3}{2}T_s \\ E_d & \text{if } \frac{3}{2}T_s \leq t \leq T \end{cases} \tag{6.3}$$

in which E_s and E_d correspond to the end-systolic and diastolic elastances, respectively; t denotes the time measured with respect to the onset of ventricular contraction; T_s, the systolic time interval, is defined by the Bazett formula $T_s(n) \approx 0.3 \cdot \sqrt{T(n-1)}$ [1], with T(i) denotes the cardiac cycle length of the i^{th} beats. The authors compared the time-varying elastance curve originated by this model to the data provided in Senzaki et al. [23] (see Figure 6.6).

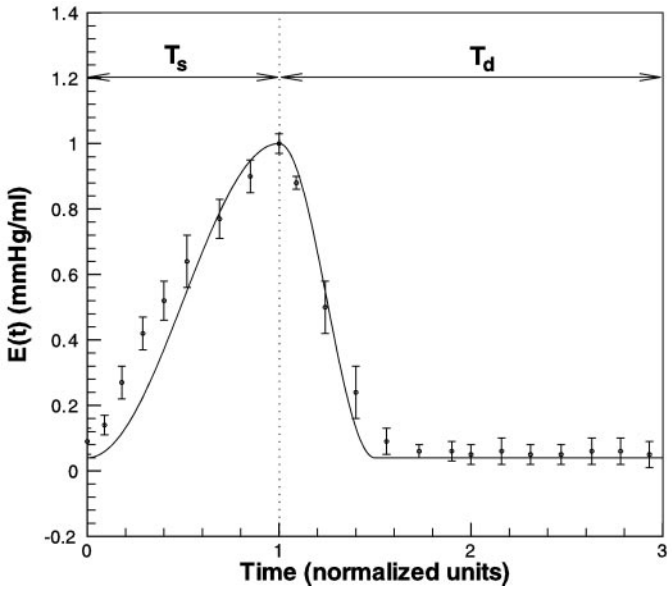

Figure 6.6 – Time-varying elastance, E(t), of the left ventricle during 1 cardiac cycle (solid line) compared with experimental data (*data reproduced from Senzaki et al. [23]*). T_s, systolic time interval, T_d, diastolic time interval.

A simplified version of this model was proposed by Chen et al. [5] (Figure 6.7):

$$E(t) = \begin{cases} \frac{E_s - E_d}{T_s}t + E_d & \text{if } 0 \leq t \leq T_s \\ 2 \cdot \frac{E_d - E_d}{T_s}t + 3E_s - 2E_d & \text{if } T_s \leq t \leq \frac{3}{2}T_s \\ E_d & \text{if } \frac{3}{2}T_s \leq t \leq T \end{cases} \tag{6.4}$$

E_s and E_d correspond to the end-systolic and diastolic elastances, respectively. T_s, the systolic time interval, is defined to be one-third of the cycle period T, *i.e.* $T_s = \frac{1}{3}T$. The authors used parameters provided in litterature in [9] for model calibration.

In 2003 Oommen et al. [20] attempted to represent the time-varying elastance function using a simple harmonic oscillator (SHO) (Figure 6.8) in the form:

$$\begin{cases} m \cdot y(t) + c \cdot y(t) + k \cdot (y(t) - y_L) = F(t) \\ F(t) = F_0 + F_1 \cos(\omega t) \end{cases} \tag{6.5}$$

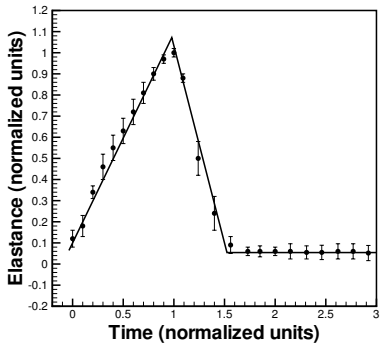

Figure 6.7 – Piecewise linear function vs. experimental elastance (*data reproduced from Senzaki et al. [23]*).

with y(t), and F(t) being respectively the displacement and the force applied to the oscillator. m represents the inertia of the lumped system, c the damping constant to account for all sources of viscosity, k the spring constant accounting for lumped chamber stiffness, y_L the slack length of the oscillator, F_0 the mean value of applied force, F_1 the amplitude of the applied force, and ω the frequency of the applied force.

The in vivo left ventricle operating under steady state physiological conditions is viewed as a forced, damped SHO, having a frequency equal to the heart rate. In this model, the analogues of the instantaneous ventricular pressure and volume are the force and length (displacement) of the SHO, respectively. Although ventricular pressure is generated by chemical and elastic forces, such as the contractile force generated by the heart muscle during systole, and mechanical ventricular suction generated by the extracellular matrix and titin during diastole, all these forces are lumped into the forcing term F(t) for simplicity.

Considering

$$\omega_0 = \sqrt{\frac{k}{m}} \text{ and } \gamma = \frac{c}{2\sqrt{km}} \tag{6.6}$$

the model (6.5) can be written in the form:

$$\begin{cases} E(t) = \frac{F(t)}{y(t)-y_c} \\ E(t) = k\frac{1+\cos(\omega t)}{1+\frac{\cos(\omega t+\varphi)}{\cos\sqrt{\left(1-(\omega/\omega_0)^2\right)^2+4\gamma^2(\omega/\omega_0)^2}}} \end{cases} \tag{6.7}$$

with $y_c = y_L + y_0$ describing the time-independent component of y(t), $y_0 = \frac{F_0}{k}$ and φ the phase angle of the cosine function.

Another approach was to use a double-Hill equation, originally described for time-varying elastance application in Stergiopulos et al. [27]:

$$E(t) = \alpha \cdot E_{max} \cdot \left[\frac{\left(\frac{t}{\tau_1}\right)^{n_1}}{1+\left(\frac{t}{\tau_1}\right)^{n_1}}\right] \cdot \left[\frac{1}{1+\left(\frac{t}{\tau_2}\right)^{n_2}}\right] + E_{min} \tag{6.8}$$

This curve is parameterised by E_{max}, E_{min}, which represent the amplitude of the curve, τ_1, τ_2 which denote the relative fraction of the heartbeat duration with respect to the time from end-diastole to reach E_{max} and α, n^1 and n^2 which are dimensionless parameters that control the curvature of the time-varying elastance curve.

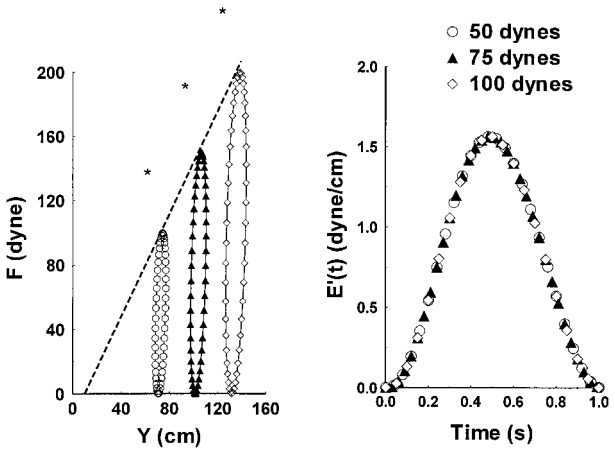

Figure 6.8 – **Left:** Force–length (F–y) loops with different values of forcing function: F0 = F1 = 50 dyn (small loop); F0 = F1 = 75 dyn (mid-size loop); F0 = F1 = 100 dyn (large loop). **Right:** Instantaneous E(t) curves corresponding to loops shown on the left. The frequency of the forcing function for both loops is the same ($\omega = 2\pi$). The point of maximal elastance is marked with an asterix (*). The other model parameters are $y_L = 10\text{cm}, c = 583\text{dyns/cm}, k = 1600\text{dyn/cm}$, m = 1g. *Reproduced from Oommen et al. [20]*

6.2.2 Application of E(t) as a substitute for cardiac mechanics

Mathematical modelling of the E(t) function was used to replace cardiac mechanics in heart models. In the study of Oommen et al. [20], authors used the E(t) function described by Equation (6.7). Using invasive LV pressure and volume measurements, y(t) was determined by using the first (dominant) term of the Fourier series approximation of the volume waveforms. F(t) was defined by fitting the cosine to the first (dominant) term of the Fourier series approximation of the pressure waveforms. The other model parameters (c, k, m and y_L) were optimised by using a Levenberg-Marquardt algorithm. The outputs of this model is displayed in Figure 6.9. Even though it does not consider isovolumic contraction/relaxation phases, and even though the associated PV loops are ellipsoidal and therefore mimic more or less the cardiac physiology, it catches one component that was neglected by original works on time-varying elastance concept: The non linear behaviour of ESPVR.

Another E(t) curve determination method was used for cardiac modelling purposes (see Equation (6.8)) under clinical settings. For example, the authors in Stergiopulos et al. [27], used this double-Hill equation in an electrical analogous model of cardiovascular system, in which the estimated E(t), representing the cardiac mechanics, is coupled with an arterial linear 3-element Windkessel model and with both a mitral and aortic valve models, parametrised by their respective resistances (R_v and R_c) which represent mitral and aortic valves (Figure 6.10). They posed the following problem:

$$\begin{cases} P_s = F_1\left(R_c, R_p, C, T, E_{max}, E_{min}, P_v, V_0, T_p\right) \\ P_d = F_2\left(R_c, R_p, C, T, E_{max}, E_{min}, P_v, V_0, T_p\right) \\ SV = F_3\left(R_c, R_p, C, T, E_{max}, E_{min}, P_v, V_0, T_p\right) \end{cases} \tag{6.9}$$

with P_s, P_d the aortic systolic and diastolic pressure respectively, SV the stroke volume, C the total arterial compliance, T_p the time to reach peak contraction, E_{max}, E_{min} the maximum and minimum time-varying elastance respectively and P_v the venous pressure.

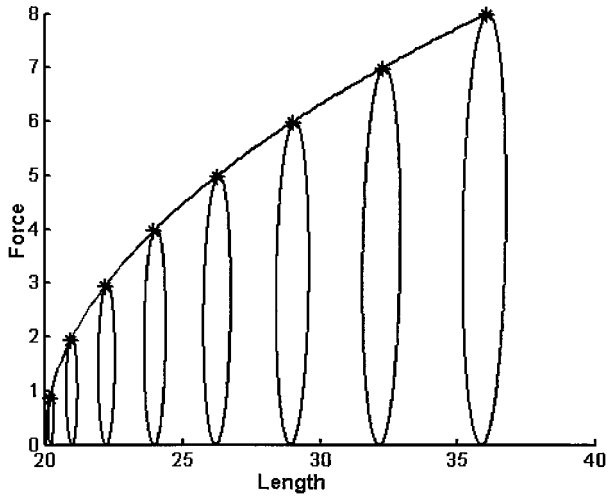

Figure 6.9 – Force–length loops obtained with several values of F0 ranging from 0.5 to 4 dyn. The spring constant k is load-dependent, defined as k = 1/F0. The '*' marks the points of maximal elastance (Eq. (11)) for each loop. *Reproduced from Oommen et al. [20]*

Finally, F_{1-3} are functions which are further determined by using dimensional method [14], and non-linear fit with data obtained invasively in cats. It yields:

$$\begin{cases} \frac{P_s}{P_v} = b_1 \cdot \frac{E_{max}}{E_{min}} \left(1 + b_2 \frac{R_c}{R_p}\right) (b_3 CE_{max})^{-b4+b_5 R_c/R_p} \cdot \left(b_6 \frac{R_p C}{T}\right)^{b_7 - b_8/(CE_{max})} \\ \frac{P_d}{P_v} = c_1 \cdot \frac{E_{max}}{E_{min}} \left[1 - c_2 e^{-c_3 (R_p C)/T}\right] (c_4 CE_{max})^{-c_5 + c_6 (R_p C)/T} \\ \frac{SV}{V_0} = d_1 \cdot \frac{P_v}{E_{min}} \cdot e^{-[d_2 (R_p C)/T + d_3/(CE_{max}) + d_4 R_p/(TE_{max})]} \end{cases} \tag{6.10}$$

with T the heart period. The values of the coefficients b_i (i = 1,...,8), c_i (i = 1,...,6), and d_i (i = 1,...,4) were empirically determined in humans. Finally, the authors used Equation (6.10) to estimate SV, P_s, and P_d.

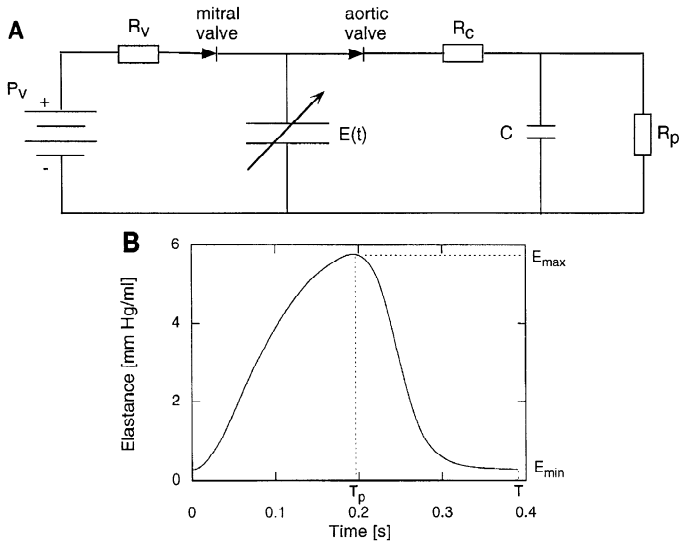

Figure 6.10 – Model presentation as described in Stergiopulos et al. [27]. **A:** electrical representation of model of heart and arterial system. P_v is venous pressure and R_v a (small) resistor over which filling takes place. E(t) is time-varying elastance. Three parameters of Windkessel (R_c, characteristic resistance; R_p, peripheral resistance; and C, total arterial compliance) are indicated. **B:** waveform of time-varying elastance with its minimum(E_{min}), maximum (E_{max}), and peak time (T_p) values pertaining to cat heart

Seemann et al. [22] also used the double-Hill function (Equation (6.8)) as a substitute for cardiac mechanics in a heart model. By using 875 time-varying elastance curves obtained in pigs, they optimised the α, τ_1, τ_2, n^1 and n^2 parameters. Therefore, Equation (6.8) becomes dependant only to E_{max} and E_{min}. They further defined a patient-specific estimation of E_{max} and E_{min}:

$$\begin{cases} E_{max} = \frac{LVP_{systole}}{V(T_{LVP,max}) - V_0} \\ E_{min} = \frac{LVP_{diastole}}{V(T_{ED}) - V_0} \end{cases} \tag{6.11}$$

with $LVP_{systole} = \frac{2}{3}SBP + \frac{1}{3}DBP$, SBP and DBP being respectively systolic and diastolic blood pressure measured by cuff a sphygmomanometer. They fixed $LVP_{diastole}$ to 5 mmHg and V_0 to the origin. The volume curve V(t) was obtained by cardiovascular magnetic resonance imaging, which allows to solve for Equation (6.11). P(t) was finally reconstruct using the following:

$$P(t) = E(t)(V(t) - V_0) \tag{6.12}$$

They used this framework on 41 human subjects and were able to build and interpret the patient-specific PV loops simulated using the time-varying elastance model approximated by the double-Hill function (Figure (6.11)).

Another similar approach using double-Hill equation (Equation (6.11)) was used to represent the cardiac chamber of a more complex cardiovascular system model, by Casas et al. [3]. They performed their experiments in 8 healthy volunteers, in which E_{max} and E_{min} were also estimated using Equation (6.11), with $LVP_{systole} = 0.9 \cdot SBP$, as described in Kelly et al. [12]. V_0 was estimated using the method described by Chen et al. [4], based on the linearity of the ESPVR, and the uniqueness of population averaged normalised time-varying elastance (see Chapter 7). The other parameters of this modelling framework were optimised with a Levenberg-Marquardt algorithm, using data obtained in the volunteers,

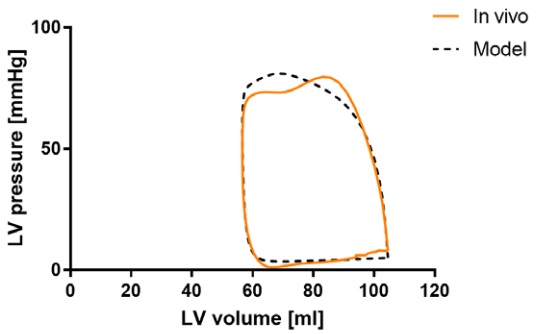

Figure 6.11 – An example of a left ventricular (LV) pressure-volume loop measured in vivo in pigs in orange and simulated by the proposed model as a dashed black line. This example was provided to illustrate the experimental validation procedure. *Reproduced from Seemann et al. [22].*

by using the sum squared error between the flow waveforms obtained from the 4D flow MRI data and those generated by the model.

All the above-mentioned cardiovascular models used an E(t) substitute for cardiac mechanics, demonstrating the feasibility of using simple time-varying elastance curve for cardiac modelling purposes. This approach allows to simulate patient-specific cardiac physiology with models using limited number of parameters. However, a major limitation lies in the approximations made in E(t). Furthermore, the need for invasive and/or advanced imaging pressure and/or data measurement are also required for model calibration, which limits its applicability under clinical monitoring settings in anaesthesia and/or critical cares.

6.2.3 Biomechanically-derived time-varying elastance model

We propose an original framework of heart and vessel modelling in which the E(t) curve, further used as a surrogate for cardiac mechanics, is first derived from a full and patient-specific biomechanical heart and vessel model. For a detailed description of the biomechanical model used in this part, see Chapter 1.

6.2.3.1 Biomechanical model calibration

In brief we used the geometrical information obtained from transthoracic echocardiography (TTE) performed in patients undergoing general anaesthesia (see Chapter 1, Section 1.5.2.9). The LV volume and thickness were estimated using the 4 chamber view. We estimated the LV end diastolic pressure by using the semi-quantitative method provided in Nagueh et al. [18]. According to the method described in Chapter 1, Section 1.5.2.5, and based on Equation (2.20), we calibrated the passive law.

We also measured on patients the aortic pressure and aortic flow velocity which allowed us to calibrate a 2 elements Windkessel model, by imposing the aortic flow and tuning sequentially the distal and proximal resistance and capacitance to fit the aortic pressure.

The timing properties of the 0D model were adjusted by using an activation law calibrated by using the characteristic ECG timing (PQ, QRS and ST segments). The cardiac cycle duration was also adjusted by using the heart rate.

Finally we set the contractility of the calibrated heart model step by step in order to fit the measured aortic flow.

6.2.3.2 Determination of V_0

The first issue was to determine V_0. In chapter 7, we propose a method in which the original experimental condition [28; 29; 25; 11] was reproduced *in silico*, allowing to identify both V_0 and E_{es}. In further experiments, we observed that this method may not be ideal. Chapter 8 presents the rationale, method and results concerning this specific topic, which is a prerequisite for E(t) function determination.

6.2.3.3 Determination of the time varying-elastance function

The time-varying elastance function was defined by Equation (6.1):

$$E(t) = \frac{P(t)}{V(t) - V_0}$$

V_0 is defined by the above-mentioned method, and P(t) and V(t) are the outputs of the original patient-specific calibrated version of our modelling framework. Therefore, E(t) is patient-specific and fully derived by using a complete biomechanical heart and vessel model.

6.2.3.4 Biomechanically derived time varying-elastance function as a surrogate for cardiac mechanics

This derived time-varying elastance curve was used subsequently as the active part of our time-varying elastance model. This curve contains information regarding the systole. It also contains information about the relaxation of the LV (the decrease of the time-varying elastance curve) until the PV reaches the passive law. During the systole, the mechanics of our model is given by the time-varying elastance curve. During the passive filling of the LV, the mechanics of the model is given by the passive law (2.20). The model is therefore written as:

$$\begin{cases} P(t) = E(t) + \eta_V^s \dot{V}(t) & \text{during systole} \\ P(t) = EDPVR(t) + \eta_V^d \dot{V}(t) & \text{during diastole} \end{cases} \tag{6.13}$$

with $\eta_V^s \dot{V}(t)$ and $\eta_V^d \dot{V}(t)$ denote a penalty terms for numerical stability respectively for systole and diastole.

6.3 Working hypothesis

We hypothesise that the model derived from time-varying elastance estimation, obtained by calibrating a full biomechanical heart and vessel model, could be used under reasonable ranges of varying conditions instead of the complete 0D model. This procedure aims to target a real-time, biomechanical model augmented, cardiovascular monitoring, during surgical intervention or during ICU stay.

Bibliography

[1] Bazett, H. C. (1997). AN ANALYSIS OF THE TIME-RELATIONS OF ELECTROCARDIOGRAMS. *Annals of Noninvasive Electrocardiology*, 2(2):177–194.

[2] Burkhoff, D., Sugiura, S., Yue, D. T., and Sagawa, K. (1987). Contractility-dependent curvilinearity of end-systolic pressure-volume relations. *American Journal of Physiology-Heart and Circulatory Physiology*, 252(6):H1218–H1227.

[3] Casas, B., Lantz, J., Viola, F., Cedersund, G., Bolger, A. F., Carlhäll, C.-J., Karlsson, M., and Ebbers, T. (2017). Bridging the gap between measurements and modelling: a cardiovascular functional avatar. *Scientific Reports*, 7(1).

[4] Chen, C.-H., Fetics, B., Nevo, E., Rochitte, C. E., Chiou, K.-R., Ding, P.-A., Kawaguchi, M., and Kass, D. A. (2001). Noninvasive single-beat determination of LV end-systolic elastance in humans. *JACC*, 38(7):2028–2034.

[5] Chen, J., Heldt, T., Verghese, G., and Mark, R. (2003). Analytical solution to a simplified circulatory model using piecewise linear elastance function. In *Computers in Cardiology, 2003*, pages 45–48, Thessaloniki Chalkidiki, Greece. IEEE.

[6] De Tombe, P. P., Jones, S., Burkhoff, D., Hunter, W. C., and Kass, D. A. (1993). Ventricular stroke work and efficiency both remain nearly optimal despite altered vascular loading. *American Journal of Physiology-Heart and Circulatory Physiology*, 264(6):H1817–H1824.

[7] Gayat, E., Mor-Avi, V., Weinert, L., Yodwut, C., and Lang, R. M. (2011). Noninvasive quantification of LV elastance and ventricular-arterial coupling using 3D echo and arterial tonometry. *AJP: Heart and Circulatory Physiology*, 301(5):H1916–H1923.

[8] Grossman, W., Braunwald, E., Mann, T., McLaurin, L. P., and Green, L. H. (1977). Contractile state of the left ventricle in man as evaluated from end-systolic pressure-volume relations. *Circulation*, 56(5):845–852.

[9] Heldt, T., Shim, E. B., Kamm, R. D., and Mark, R. G. (2002). Computational modeling of cardiovascular response to orthostatic stress. *Journal of Applied Physiology*, 92(3):1239–1254.

[10] Kass, D. A., Maughan, W. L., Guo, Z. M., Kono, A., Sunagawa, K., and Sagawa, K. (1987). Comparative influence of load versus inotropic states on indexes of ventricular contractility: experimental and theoretical analysis based on pressure-volume relationships. *Circulation*, 76(6):1422–1436.

[11] Kass, D. A., Yamazaki, T., Burkhoff, D., Maughan, W. L., and Sagawa, K. (1986). Determination of left ventricular end-systolic pressure-volume relationships by the conductance (volume) catheter technique. *Circulation*, 73(3):586–595.

[12] Kelly, R. P., Ting, C. T., Yang, T. M., Liu, C. P., Maughan, W. L., Chang, M. S., and Kass, D. A. (1992). Effective arterial elastance as index of arterial vascular load in humans. *Circulation*, 86(2):513–521.

[13] Koch-Weser, J. and Blinks, J. R. (1963). The Influence Of The Interval Between Beats On Myocardial Contractility. *Pharmacological Reviews*, 15:601–652.

[14] Langhaar, H. (1951). *Dimensional analysis and theory of models*. John WIley & Sons Ltd.

[15] Lee, J.-D., Tajimi, T., Widmann, T. F., and Ross, J. (1987). Application of end-systolic pressure-volume and pressure-wall thickness relations in conscious dogs. *Journal of the American College of Cardiology*, 9(1):136–146.

[16] Maughan, W. L., Sunagawa, K., Burkhoff, D., Graves, W. L., Hunter, W. C., and Sagawa, K. (1985). Effect of heart rate on the canine end-systolic pressure-volume relationship. *Circulation*, 72(3):654–659.

[17] Mirsky, I., Tajimi, T., and Peterson, K. L. (1987). The development of the entire end-systolic pressure-volume and ejection fraction-afterload relations: a new concept of systolic myocardial stiffness. *Circulation*, 76(2):343–356.

[18] Nagueh, S. F., Appleton, C. P., Gillebert, T. C., Marino, P. N., Oh, J. K., Smiseth, O. A., Waggoner, A. D., Flachskampf, F. A., Pellikka, P. A., and Evangelisa, A. (2008). Recommendations for the Evaluation of Left Ventricular Diastolic Function by Echocardiography. *European Journal of Echocardiography*, 10(2):165–193.

[19] Noble, M. I. M. (1988). An introduction to modern work on the Bowditch phenomenon. *Cardiovascular Research*, 22(8):586–586.

[20] Oommen, B., Karamanoglu, M., and Kovács, S. J. (2003). Modeling Time Varying Elastance: The Meaning of "Load-Independence". *Cardiovascular Engineering*, 3(4):123–130.

[21] Sagawa, K., Maughan, L., Suga, H., and Sunagawa, K. (1988). Cardiac contraction and the pressure volume relationship. In *Cardiac contraction and the pressure volume relationship*. Oxford University Press.

[22] Seemann, F., Arvidsson, P., Nordlund, D., Kopic, S., Carlsson, M., Arheden, H., and Heiberg, E. (2019). Noninvasive Quantification of Pressure-Volume Loops From Brachial Pressure and Cardiovascular Magnetic Resonance. *Circulation: Cardiovascular Imaging*, 12(1).

[23] Senzaki, H., Chen, C.-H., and Kass, D. A. (1996). Single-Beat Estimation of End-Systolic Pressure-Volume Relation in Humans: A New Method With the Potential for Noninvasive Application. *Circulation*, 94(10):2497–2506.

[24] Shishido, T., Hayashi, K., Shigemi, K., Sato, T., Sugimachi, M., and Sunagawa, K. (2000). Single-Beat Estimation of End-Systolic Elastance Using Bilinearly Approximated Time-Varying Elastance Curve. *Circulation*, 102(16):1983–1989.

[25] Sodums, M. T., Badke, F. R., Starling, M. R., Little, W. C., and O'Rourke, R. A. (1984). Evaluation of left ventricular contractile performance utilizing end-systolic pressure-volume relationships in conscious dogs. *Circulation Research*, 54(6):731–739.

[26] Starling, M. R. (1993). Left ventricular-arterial coupling relations in the normal human heart. *American Heart Journal*, 125(6):1659–1666.

[27] Stergiopulos, N., Meister, J. J., and Westerhof, N. (1996). Determinants of stroke volume and systolic and diastolic aortic pressure. *American Journal of Physiology-Heart and Circulatory Physiology*, 270(6):H2050–H2059.

[28] Suga, H. (1969). Time course of left ventricular pressure-volume relationship under various enddiastolic volume. *Japanese Heart Journal*, 10(6):509–515.

[29] Suga, H. (1970). Time Course of Left Ventricular Pressure-Volume Relationship under Various Extents of Aortic Occlusion. *Japanese Heart Journal*, 11(4):373–378.

[30] Suga, H. and Sagawa, K. (1974). Instantaneous Pressure-Volume Relationships and Their Ratio in the Excised, Supported Canine Left Ventricle. *Circulation Research*, 35(1):117–126.

[31] Suga, H., Sagawa, K., and Shoukas, A. A. (1973). Load Independence of the Instantaneous Pressure-Volume Ratio of the Canine Left Ventricle and Effects of Epinephrine and Heart Rate on the Ratio. *Circulation Research*, 32(3):314–322.

[32] van der Velde, E. T., Burkhoff, D., Steendijk, P., Karsdon, J., Sagawa, K., and Baan, J. (1991). Nonlinearity and load sensitivity of end-systolic pressure-volume relation of canine left ventricle in vivo. *Circulation*, 83(1):315–327.

CHAPTER 7

Minimally-invasive estimation of patient-specific end-systolic elastance using a biomechanical heart model

The end-systolic elastance (E_{es}) – the slope of the end-systolic pressure-volume relationship (ESPVR) at the end of ejection phase – has become a reliable indicator of myocardial functional state. The estimation of E_{es} by the original multiple-beat method is invasive, which limits its routine usage. By contrast, non-invasive single-beat estimation methods, based on the assumption of the linearity of ESPVR and the uniqueness of the normalised time-varying elastance curve $E^N\left(t^N\right)$ across subjects and physiology states, have been applied in a number of clinical studies. It is however known that these two assumptions have a limited validity, as ESPVR can be approximated by a linear function only locally, and $E^N\left(t^N\right)$ obtained from a multi-subject experiment includes a confidence interval around the mean function. Using datasets of 3 patients undergoing general anaesthesia (each containing aortic flow and pressure measurements at baseline and after introducing a vasopressor noradrenaline), we first study the sensitivity of two single-beat methods –- by Sensaki et al. and by Chen et al. –- to the uncertainty of $E^N\left(t^N\right)$. Then, we propose a minimally-invasive method based on a patient-specific biophysical modelling to estimate the whole time-varying elastance curve $E^{model}(t)$. We compare E_{es}^{model} with the two single-beat estimation methods, and the normalised varying elastance curve $E^{N,model}(t)$ with $E^N\left(t^N\right)$ from published physiological experiments.

This chapter was published as a paper in the proceedings of the Functionnal Imaging and Modelling of the Heart conference (FIMH 2019)

Minimally-invasive estimation of patient-specific end-systolic elastance using a biomechanical heart model

Arthur Le Gall[1,2,3], Fabrice Vallée[1,2,3], Dominique Chapelle[1,2], Radomír Chabiniok[1,2,4]

[1] Inria, Paris-Saclay University, Palaiseau, France, [2]LMS, École Polytechnique, CNRS, Paris-Saclay University, Palaiseau, France, [3] Anaesthesia and Intensive Care department, Lariboisière hospital, Paris, France, [4] School of Biomedical Engineering & Imaging Sciences (BMEIS), St Thomas Hospital, King's College London, UK

FIMH, DOI:10.1007/978-3-030-21949-9_29

Abstract

The end-systolic elastance (E_{es}) – the slope of the end-systolic pressure-volume relationship (ESPVR) at the end of ejection phase – has become a reliable indicator of myocardial functional state. The estimation of E_{es} by the original multiple-beat method is invasive, which limits its routine usage. By contrast, non-invasive single-beat estimation methods, based on the assumption of the linearity of ESPVR and the uniqueness of the normalised time-varying elastance curve $E^N\left(t^N\right)$ across subjects and physiology states, have been applied in a number of clinical studies. It is however known that these two assumptions have a limited validity, as ESPVR can be approximated by a linear function only locally, and $E^N\left(t^N\right)$ obtained from a multi-subject experiment includes a confidence interval around the mean function. Using datasets of 3 patients undergoing general anaesthesia (each containing aortic flow and pressure measurements at baseline and after introducing a vasopressor noradrenaline), we first study the sensitivity of two single-beat methods –- by Sensaki et al. and by Chen et al. –- to the uncertainty of $E^N\left(t^N\right)$. Then, we propose a minimally-invasive method based on a patient-specific biophysical modelling to estimate the whole time-varying elastance curve $E^{model}(t)$. We compare E_{es}^{model} with the two single-beat estimation methods, and the normalised varying elastance curve $E^{N,model}(t)$ with $E^N\left(t^N\right)$ from published physiological experiments.

Keywords— Time-varying elastance, End-systolic elastance estimation, Patient-specific biophysical modelling

7.1 Introduction

The relation between ventricular pressure (P) and volume (V) at the end of ejection is described by the preload and afterload independent end-systolic pressure-volume relationship (ESPVR). The slope of ESPVR – the so-called end-systolic elastance, E_{es} – and its volume intercept (V_0) allow to derive the time-varying elastance $E(t) = P(t)/(V(t) - V_0)$, see Fig. 7.1. Under physiological loading ranges, the E_{es} is known to be closely related to the active properties of the myocardium [1; 13], and is assumed to be itself preload and afterload independent, and so the ESPVR to be linear. Even though the load dependency

of E_{es} has been experimentally shown [1], the linear approximation of ESPVR and the subsequent analysis of its derived indicators have been proven to be clinically useful for performance assessment and monitoring of failing hearts, and for studying the interaction between the heart and vasculature (e.g. by assessing the so-called ventricular-arterial coupling, $V_{va} = E_{es}/E_a$, with E_a being the arterial elastance [13]).

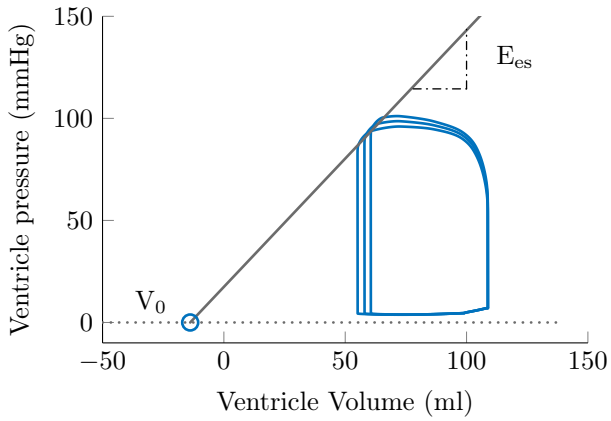

Figure 7.1 – Example of the model-based determination of E_{es}, V_0 and E(t)

Originally, E_{es} and ESPVR were obtained using a multiple-beat measurement technique. A linear regression was fitted on the end-systolic P-V points measured at different loading conditions (*e.g.* by inferior vena cava occlusion, or administration of vasopressors), during cardiac catheterisation. The associated technical issues led to a development of single-beat methods [14; 15], which allow to estimate E_{es} and ESPVR non-invasively [5; 7]. We hypothesised that the estimation of E_{es} using such methods is, however, too sensitive to their parameters to obtain a reliable patient-specific result.

By calibrating a biomechanical model of heart and vasculature [2; 4] using aortic pressure and flow data, we can simulate the entire P-V loop and reproduce minimally-invasively the original multiple-beat measurement method. We aimed at comparing the E_{es} obtained by the single-beat methods or obtained by a method based on patient-specific biophysical modelling. Furthermore, we evaluated the properties of the derived time-varying elastance after spatial-temporal normalisation [16].

7.2 Methods

7.2.1 Data and models

7.2.1.1 Patients and procedures

Three patients undergoing general anaesthesia (GA) for neuroradiological intervention, for whom a continuous arterial pressure and cardiac output monitoring were indicated, were included in the presented observational study, approved by the ethical committee of the Société de Réanimation de Langue Française (CE-SRLF 14-356). The data collection is described in detail in [10]. Briefly, after GA induction, a transthoracic echocardiography (TTE) was performed to obtain cardiac geometry information. A transoesophageal Doppler probe (Deltex Medical, Chichester, UK) was inserted into the oesophagus in order to continuously measure the aortic flow. During the procedure, the anaesthetist could need to raise blood pressure using intravenous administration of 5μg of noradrenaline (NOR). The neuroradiologist cannulated aorta through femoral puncture, and inserted a

guidewire. A fluid-filled mechanotransducer was connected to obtain the aortic pressure waveform.

7.2.1.2 Biomechanical model of heart and vasculature

The model used in this study was a combination of a biomechanical heart and Windkessel circulation models connected together to represent the cardiovascular system. The heart model was derived from a previously validated complete three-dimensional (3D) model [4] by model reduction [2]. While the entire geometry was reduced to a sphere, all the passive and active properties were kept as in the 3D model. The passive part of myocardium was modelled according to Holzapfel and Ogden [8], and adjusted using experimental data [11]. The active contraction was based on Huxley's sliding filament theory [9]. The circulation was represented by a 2-stage Windkessel model connected in series (proximal and distal capacitances and resistances). In turning the model into patient-specific regime, see also [3; 12], first the Windkessel model parameters were calibrated by imposing the measured aortic flow and tuning the resistance and capacitance parameters, in order to fit the simulated and measured aortic pressure. Then, geometry and passive myocardial properties were calibrated using TTE data. The timing of the electrical activation was adjusted using ECG timings (in particular, the action potential duration in line with the ST interval). Finally, the myocardial contractility was tuned to minimise the difference between the simulated and measured aortic flow and pressure. The model calibration as described above was performed in two different conditions – at baseline and at maximal effect of NOR – to explore comparatively the cardiovascular effect of NOR. Data processing and signal analysis were performed in Matlab, (Natick, Massachussets, USA) in which the model [2] was implemented into a library named CardiacLab.

7.2.2 Single-beat estimation of E_{es}

7.2.2.1 Method by Senzaki et al. [14]

The method is based on the characteristics of the time-varying elastance E(t) described in detail by Suga et al. [16]. In brief, the normalised E(t) – with respect to the time at end-systole (t_{max}) and maximal elastance value (E_{es}), i.e. $E^N(t) = \frac{E(t/t_{max})}{E_{es}}$ – was found to be consistent across subjects and across varying loading conditions [16]. This principle therefore allows to identify a particular time-point on the subject and physiology independent "universal" $E^N(t)$, if the ratio $\frac{t}{t_{max}}$ is known.

To estimate E_{es}, the following values need to be obtained: 1) the end of isovolumic contraction (t_{ed}) assessed by TTE; 2) ventricular pressure at the opening of aortic valve (measured by aortic catheter) (P_{aod}); 3) ejection time (from end-diastole to end-systole) by TTE; and 4) ventricular volumes (end-diastole and end-systole), accessed by TTE. We can then apply the formula by Senzaki et al. [14]:

$$E_{es}{}^{senzaki} = \left(\frac{P_{aod}}{E^N_{ed}} - P_{es} \right) / SV, \tag{7.1}$$

where $E^N_{ed} = E^N(t_{ed})$, P_{es} being the aortic end-systolic pressure, SV the stroke volume.

Table 7.1 – Patients characteristics at baseline. LVEDV: left ventricular end-diastolic volume; SV: stroke volume; P_{aod}: end-diastolic aortic pressure; P_{es}: end-systolic aortic pressure; t_{ed}: pre-ejection time; t_{max}: ejection time.

Patient	Age yo	Weight kg	Height cm	LVEDV ml	SV ml	P_{aod} mmHg	P_{es} mmHg	t_{ed} ms	t_{max} ms
Patient 16	40	58	160	109	71	61	77	107	329
Patient 21	15	58	158	140	91	56	79	84	283
Patient 69	58	88	178	81	45	55	72	77	321

7.2.2.2 Method by Chen et al. [5]

This method is derived from the original method of Senzaki by optimising the following linear regression to estimate E_{ed}^{N}:

$$E_{ed}^{N,modified} = 0.0275 - 0.165 \cdot EF + 0.3656 \cdot \frac{P_{aod}}{P_{es}} + 0.515 \cdot E_{ed}^{N}, \tag{7.2}$$

EF being the ejection fraction measured by TTE as the ratio between SV and the end-diastolic volume. Finally, $E_{ed}^{N,modified}$ is used in Eq. (7.1) to estimate $E_{es}{}^{chen}$. We used the methods of Senzaki and Chen to predict E_{es}.

7.2.3 Estimation of E_{es} using biomechanical heart model

7.2.3.1 Model-based E_{es} and time-varying elastance curve estimation

The original multiple-beat technique involves first a construction of ESPVR, which is given by linear regression performed on the consecutive End-Systolic Pressure-Volume points obtained in PV loops measured in different loading conditions. Then the slope and the intercept of the ESPVR with the volume axis represent E_{es} and V_0, respectively. To reproduce this procedure in silico using the calibrated patient-specific model described in Section 7.2.1.2, we modified sequentially the afterload by varying Windkessel model parameters. We obtained 5 P-V loops with varying loading conditions and identified the end-systolic pressure-volume point of every P-V loop (corresponding to the aortic valve closing). We performed a linear regression to obtain E_{es}^{model} and V_0, and computed the simulated varying elastance $E^{model}(t) = P(t)/(V(t) - V_0)$ (see Fig. 7.1).

7.2.3.2 Study of the simulated time-varying elastance

The simulated and normalised time-varying elastances $E^{N,model}(t)$ were compared with the $E^{N}\left(t^{N}\right)$ obtained experimentally by Suga et al. [16].

7.3 Results

Table 7.1 shows the main characteristics of patients and data indicators at baseline obtained from the three patients included in the study.

Table 7.2 – Results of the end-systolic elastance E_{es} (in $mmHg.ml^{-1}$) estimation using the method of Senzaki et al. [14], Chen et al. [5], and the biophysical model [2].

Method	Challenge	Patient 16	Patient 21	Patient 69
$E_{es}^{senzaki}$	*Baseline*	2.88 [1.65 – 4.83]	3.45 [1.85 – 6.76]	6.17 [3.5 – 12.5]
	Noradrenaline	4.68 [2.66 – 8.3]	3.39 [1.86 – 6.17]	7.95 [4.28 – 15.02]
E_{es}^{chen}	*Baseline*	1.59 [1.23 – 1.94]	1.58 [1.22 – 1.93]	2.51 [2 – 3.08]
	Noradrenaline	2.12 [1.68 – 2.55]	1.83 [1.39 – 2.27]	3.71 [2.83 – 4.57]
E_{es}^{model}	*Baseline*	2.42	3.35	3.64
	Noradrenaline	5.82	3.05	5.51

7.3.1 Sensitivity analysis of the existing methods

To assess the sensitivity of the Senzaki method, we used the $E^N\left(t^N\right)$ curve from the study of Suga et al. [16]. We generated an interpolation of all the outliers of the curve, to be able to evaluate the effect of the error in measuring E_{ed}^N on the $E_{es}^{senzaki}$ estimation (see Fig. 7.2, left). We can see in the right panel of Fig. 7.2 that the standard deviation in estimating E_{ed}^N had a significant impact on the predicted $E_{es}^{senzaki}$. When considering the standard deviation in the $E^N\left(t^N\right)$ data, the value of E_{es} is ranging between half and twice times the predicted value, for all 3 patients.

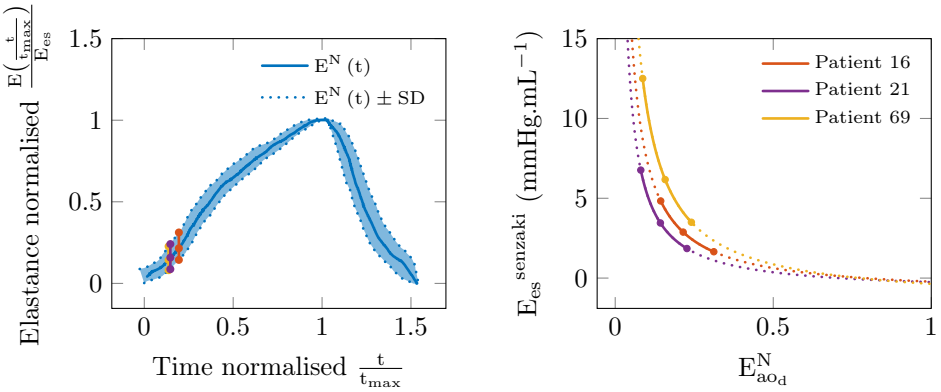

Figure 7.2 – Normalised elastance curve and effect of the standard deviation (SD) of E_{ed}^N on $E_{es}^{senzaki}$ estimation [14]. **Left:** Normalised elastance curve (reproduced from Suga et al. [16]) and E_{ed}^N prediction (colored dots) using $\frac{t_{ed}}{t_{max}}$ as obtained by TTE. **Right:** $E_{es}^{senzaki}$ estimation as function of E_{ed}^N, for the data obtained in the 3 patients. The plain lines represent the $E_{es}^{senzaki}$ for E_{ed}^N inside the ranges given by Suga et al. The dashed line represent the extrapolation of the $E_{es}^{senzaki}$ for E_{ed}^N outside these ranges.

In order to appreciate the consistency between the method of Senzaki and the method of Chen, we compared the values of E_{es} given by the two methods at baseline and at maximum effect of NOR. The results are presented in Table 7.2.

7.3.2 Method from biomechanical model

For the 3 subjects, we were able to calibrate the biomechanical model and obtain the P-V loop at baseline and after the administration of NOR (see example of calibration in Fig. 7.3).

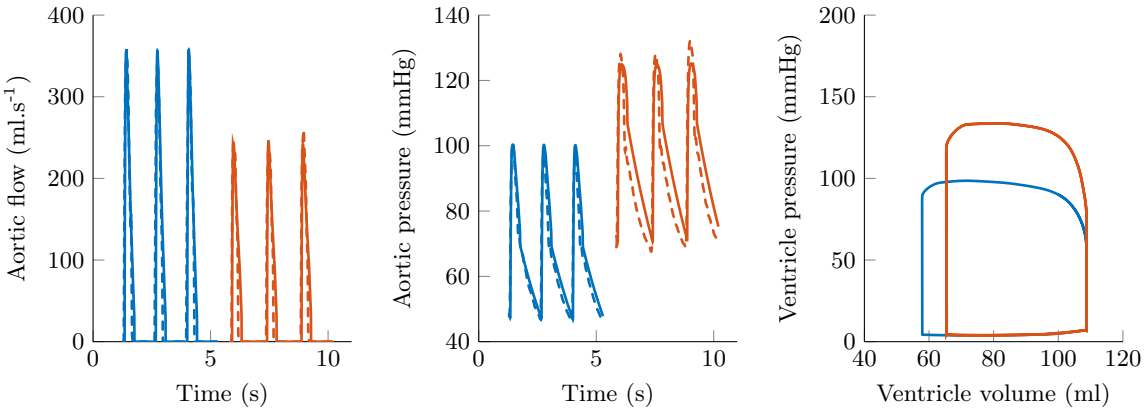

Figure 7.3 – Example of a calibrated model. **Left** and **Middle** panels display respectively the aortic blood flow and pressure at baseline (blue) and at maximal effect of noradrenaline(orange). The simulations (bold) are calibrated using patient's measured data (dashed). **Right** panel displays pressure-volume loops generated using the results of the aforementioned calibrated simulations at baseline (blue) and at maximal effect of noradrenaline (orange).

Table 7.2 shows the patient-specific E_{es} prediction from the $E_{es}^{senzaki}$, E_{es}^{chen} and E_{es}^{model}. We can see that E_{es}^{model} is close to $E_{es}^{senzaki}$ for Patients 16 and 21, and located within the ranges given in Suga et al. [16] for all 3 subjects. We can also see that the usage of NOR was associated with an increase of $E_{es}^{senzaki}$ and in E_{es}^{model} except for Patient 21, in whom all methods suggested no change in E_{es}.

Out of uncertainties in the estimated E_{es}^{model}, we performed a sensitivity analysis with respect to the error in measuring the input parameters for the model, specifically the error in the wall thickness. The wall thickness was varied by ±50% from the measured value, and the passive and active properties of the model were calibrated accordingly. Table 7.3 displays the results in E_{es}^{model} estimation for each wall thickness.

Fig. 7.4 demonstrates that the biomechanical model was able not only to estimate E_{es}, but did provide the overall time-varying elastance curve. This example shows that the $E^{model}(t)$ was higher when using noradrenaline (Fig.7.4 left panel), according to the expected effect of noradrenaline (enhancement of contractility). Furthermore, when $E^{model}(t)$ curves were normalised as described in Sec. 7.2.2 (see Fig. 7.4 right panel), both the time-varying elastance curves (baseline and NOR) were within the physiological ranges described by Suga et al. [16].

7.4 Discussion

In this paper, we described a mini-invasive multi-beat method to estimate patient-specific time-varying and end-systolic elastance by using biomechanical modelling. As originally described, the E_{es} estimation involves a multiple-beat measurement of P-V loop. For

Table 7.3 – Sensitivity analysis for E_{es} estimation to relative change in wall thickness, for the Patient 16. The measured wall thickness is in bold.

Wall thickness	(% of measured value)	60	80	**100**	120	150	avg (SD)
E_{es}^{model}	($mmHg^{-1}$)	2.56	2.38	**2.42**	2.73	3.09	2.64 ± 0.29

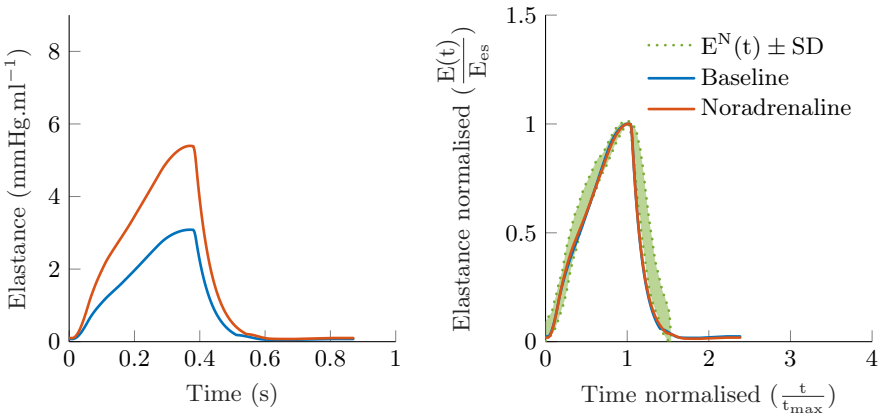

Figure 7.4 – Example of a patient-specific model-derived time-varying elastance curve. **Left:** Time-varying elastance at baseline and after NOR administration. **Right:** Normalised time-varying elastance curve at baseline and after NOR administration, plotted against experimental data (reproduced from [16]).

technical concerns, single-beat estimation methods were developed. These methods assume the ESPVR being linear with constant slope of E_{es}, which is extrapolated from the end-diastolic measurement point. However, the slope of the real ESPVR is decreasing when approaching the end-diastolic point [1], deviating the estimated E_{es}. Our method allows to modify loading conditions in order to estimate E_{es} around the measured end-systolic P-V point, where the linearity of ESPVR can be assumed. Furthermore, we demonstrated a very high sensitivity of the single-beat estimation method by Senzaki et al. [14] to E_{ed}^N parameter. Then, we demonstrated a limited accuracy of the method by Chen et al. [5], which introduced some phenomenological terms to the equation (7.1). Indeed, no concordance with the method of Senzaki et al. [14] could have been observed, the mean values and confidence intervals for E_{es}^{chen} estimation falling outside the ranges of $E_{es}^{senzaki}$. The reproducibility of the results obtained in the validation studies [14; 5] is therefore questioned. To address these issues, we would have to compare our results against invasive P-V loop measurements, which were not available in our study. Despite the aforementioned limitations, we used the $E_{es}^{senzaki}$ estimation as a comparator for an indirect validation of our method. We verified that our simulated E_{es}^{model} at least fell within the ranges of the outliers of the $E_{es}^{senzaki}$, and that the normalised time-varying elastance $E^{N,model}(t)$ was consistent with the $E^N\left(t^N\right)$ from Suga et al. [16], in all three subjects even when varying physiology (baseline vs. administration of NOR). We remark in addition that neglecting the standard deviation of the experimentally obtained $E^N\left(t^N\right)$ in the single-beat estimations of E_{es} effectively means decreasing the individuality of the considered subject. We showed, however, that the specificity of patients had a great impact on the E_{es} estimation by these methods. Our framework – based on patient-specific biomechanical modelling – allows a more detailed personalisation. The output of the model is the actual P-V loop and the entire time-varying elastance curve – both being important when considering management of individual patients. Additionally to study the sensitivity of the $E^N\left(t^N\right)$ given by the the range of values in the experiments [16], we could have also explored the sensitivity of the single-beat estimation methods to the accuracy of time measurement. Clearly, during the steepest part of the $E^N\left(t^N\right)$ curve, a small error on the t_{ed} measurement will have a significant impact on the E_{ed}^N, and therefore on the estimation of E_{es}. Finally, the model-derived elastance would be as well a subject of analysis of sensitivity to the parameters of the model. In this paper, we considered only an example of the uncertainty in ventricular wall thickness, see Table 7.3. A thorough

sensitivity analysis including other input parameters remains to be done in the future.

Our study suffers from several limitations. Indeed, while the Chen's method, allows a non-invasive estimation of E_{es}, our presented framework involves aortic pressure measurement. This preliminary setup will be improved by the methods of transferring the peripheral arterial pressure – practically always available during GA – into the central aortic pressure [6]. Also, the $E^N\left(t^N\right)$ curve was reproduced manually from the study of Suga et al. [16], involving experimental setup from dogs. In the study of Senzaki et al. [14], the authors presented an $E^N\left(t^N\right)$ curve from human data. They showed an absence of variability during the pre-ejection period supporting their final results regarding the reproducibility of their method. This lack of variability is however questioned by Shishido et al. [15]. In a preliminary *in silico* study (data not shown), we also observed a great variability in $E^N\left(t^N\right)$ during the pre-ejection period. For this reason, we did not use the human data made available by Senzaki et al. [14]. We could have compared our method with the method by Shishido et al. [15] aiming at considering the patient's variability of E^N_{ed} estimation, by using a bilinear interpolation of the $E^N\left(t^N\right)$ curve. The comparison with our modelling framework will be explored in the future.

7.5 Conclusion

By using a patient-specific modelling framework, we proposed a method to estimate E_{es} and the entire time-varying elastance curve, considering individual normalised time-varying elastance variability, at the expense of minimally invasive data measurements. This method provides patient-specific time-varying curve and estimates the value of maximum elastance. Our proposed method could be used both clinically – to assess the patients' heart function – and in cardiac modelling community to provide patient-specific input for simplified models of the heart contraction.

Acknowledgment

We acknowledge Prof. Alexandre Mebazaa, and Prof. Etienne Gayat (Anaesthesiology and Intensive Care department, Lariboisière hospital, Paris, France) for their support in conducting the study. In addition, we would like to acknowledge Dr. Philippe Moireau, Inria research team MDISIM, for the development of the cardiac simulation software CardiacLab used in this work.

Bibliography

[1] Burkhoff, D.: Assessment of systolic and diastolic ventricular properties via pressure-volume analysis: a guide for clinical, translational, and basic researchers. AJP: Heart and Circulatory Physiology **289**(2), H501–H512 (Aug 2005)

[2] Caruel, M., Chabiniok, R., Moireau, P., Lecarpentier, Y., Chapelle, D.: Dimensional reductions of a cardiac model for effective validation and calibration. Biomechanics and Modeling in Mechanobiology **13**(4), 897–914 (Aug 2014)

[3] Chabiniok, R., Moireau, P., Kiesewetter, C., Hussain, T., Razavi, R., Chapelle, D.: Assessment of atrioventricular valve regurgitation using biomechanical cardiac modeling. In: Proc. of FIMH 2017. pp. 401–411. Springer (2017)

[4] Chapelle, D., Le Tallec, P., Moireau, P., Sorine, M.: Energy-preserving muscle tissue model: formulation and compatible discretizations. International Journal for Multiscale Computational Engineering **10**(2) (2012), http://www.dl.begellhouse.com/journals/61fd1b191cf7e96f,42f1beba0b405e70,2491c81155ff42d6.html

[5] Chen, C.H., Fetics, B., Nevo, E., Rochitte, C.E., Chiou, K.R., Ding, P.A., Kawaguchi, M., Kass, D.A.: Noninvasive single-beat determination of LV end-systolic elastance in humans. JACC **38**(7), 2028–2034 (2001)

[6] Gaddum, N., Alastruey, J., Chowienczyk, P., Rutten, M.C., Segers, P., Schaeffter, T.: Relative contributions from the ventricle and arterial tree to arterial pressure and its amplification: an experimental study. American Journal of Physiology-Heart and Circulatory Physiology **313**(3), H558–H567 (2017)

[7] Gayat, E., Mor-Avi, V., Weinert, L., Yodwut, C., Lang, R.M.: Noninvasive quantification of LV elastance and ventricular-arterial coupling using 3D echo and arterial tonometry. AJP: Heart and Circulatory Physiology **301**(5), H1916–H1923 (2011)

[8] Holzapfel, G.A., Ogden, R.W.: Constitutive modelling of passive myocardium: a structurally based framework for material characterization. Phil. Trans. R. Soc. A: Mathematical, Physical and Engineering Sciences **367**(1902), 3445–3475 (2009)

[9] Huxley, A.F.: Muscular contraction. The Journal of Physiology **243**(1), 1–43 (1974)

[10] Joachim, J., Vallée, F., Le Gall, A., Matéo, J., Lenck, S., Millasseau, S., Houdart, E., Mebazaa, A., Gayat, É.: Velocity–pressure loops for continuous assessment of ventricular afterload: influence of pressure measurement site. Journal of Clinical Monitoring and Computing (Nov 2017)

[11] Klotz, S., Hay, I., Dickstein, M.L., Yi, G.H., Wang, J., Maurer, M.S., Kass, D.A., Burkhoff, D.: Single-beat estimation of end-diastolic pressure-volume relationship: a novel method with potential for noninvasive application. AJP: Heart and Circulatory Physiology **291**(1), H403–H412 (Feb 2006)

[12] Ruijsink, B., Zugaj, K., Pushparajah, K., Chabiniok, R.: Model-based indices of early-stage cardiovascular failure and its therapeutic management in fontan patients. In: Proc. of FIMH 2019. p. accepted. Springer (2019)

[13] Sagawa, K., Maughan, L., Suga, H., Sunagawa, K.: Cardiac contraction and the pressure volume relationship. In: Cardiac contraction and the pressure volume relationship. Oxford University Press (1988)

[14] Senzaki, H., Chen, C.H., Kass, D.A.: Single-Beat Estimation of End-Systolic Pressure-Volume Relation in Humans: A New Method With the Potential for Noninvasive Application. Circulation **94**(10), 2497–2506 (Nov 1996)

[15] Shishido, T., Hayashi, K., Shigemi, K., Sato, T., Sugimachi, M., Sunagawa, K.: Single-Beat Estimation of End-Systolic Elastance Using Bilinearly Approximated Time-Varying Elastance Curve. Circulation **102**(16), 1983–1989 (Oct 2000)

[16] Suga, H., Sagawa, K., Shoukas, A.A.: Load Independence of the Instantaneous Pressure-Volume Ratio of the Canine Left Ventricle and Effects of Epinephrine and Heart Rate on the Ratio. Circulation Research **32**(3), 314–322 (Mar 1973)

CHAPTER 8

Estimation of V_0, E_{es} and time-varying elastance function using a biomechanical heart and vessel models

The time-Varying elastance concept (E(t)) was extensively studied since the original work performed by Suga, Sagawa, Sunagawa and colleagues in the 70's. Indeed, it allows for clinical evaluation of cardiac physiology, and may be used as a surrogate of cardiac mechanics for cardiac modelling purposes. However, E(t) function description necessitates an accurate estimation of the derivative of the end-systolic pressure-volume relationship (ESPVR), the so-called E_{es}, and of its 0-pressure intercept, V_0. In this Chapter, we propose and evaluate a biomechanical framework to estimate E(t) and V_0, comparatively with other available methods. The proposed static-isopressure method – a method derived from biomechanical approach – was found to allow for the most stable estimations of V_0 and E_{es} across various ranges of varying physiological conditions, as compared with the other methods tested. Our framework allows for clinical translation of E(t) concept to bedside as it necessitates only data that are routinely measured in anaesthesia and/or intensive care settings. Furthermore, it paves the way for E(t) modelling based on biomechanical principles.

8.1 Introduction

8.1.1 Motivations for V_0, E_{es} and E(t) estimations

Since the pioneering works performed by Suga, Sagawa, Sunagawa et al. [27; 37], the study of instantaneous pressure and volume (PV) relationship within the left ventricle has shifted from cardiac cath-labs towards numerical modelling, decreasing in the same time the invasiveness of PV analyses. Indeed, recent studies have been published, in which various patient-specific models were used to analyse the PV properties of patients' heart [26; 33; 5; 28; 12; 8]. Most of the heart models presented in these studies are based on the concept, also introduced by Suga, Sagawa, Sunagawa and colleagues, called "Time-varying elastance" (see chapter 6). In brief, the time-varying elastance function E(t) (see Equation (8.1)) can be used as a surrogate for cardiac mechanics.

$$E(t) = \frac{P(t)}{V(t) - V_0} \tag{8.1}$$

Indeed, the usage of this function is very convenient for cardiac modelling purposes. Substituting E(t) as cardiac mechanics, in a more global heart and circulation model, allows to access the PV relationships and the cardiac bioenergetic associated with a specific patient within specific conditions, in a minimally-invasive fashion, without the need for a full, complex, three-dimensional biomechanical model.

Therefore, efforts have been made to model E(t) [26; 33; 12; 8] (see Chapter 6 Section 6.2.1). However, most of these methods require at least the prescription of the maximum elastance E_{max} (or end-systolic elastance E_{es} which should be equivalent), and the time to reach E_{es}, t_{max}, to calibrate the function E(t) to a specific patient. In our approach, we propose to use the reduced formulation [4] of a full three-dimensional biomechanical model [6], calibrated on patients' data, to simulate patient-specific PV relationship. This methods allows us to access the P (t) and V (t) terms of Equation (8.1). A straightforward estimation of V_0 is further required to derive E(t) function from our biomechanical modelling approach. In other words, estimation of E_{es} and/or V_0 is important to solve for issues associated with E(t) modelling.

8.1.2 Issues with existing estimation methods

8.1.2.1 E_{es} and V_0 measurements

End-systolic elastance E_{es} corresponds to the slope of a local linearisation of the end-systolic pressure-volume relationship. It has been originally described by Suga [34], and was extensively studied. On canine experimental models, E_{es} has been associated with left ventricular (LV) inotropy [37; 24], and is seen as a surrogate of maximal contractile properties of the LV. These results have been reproduced in humans [10; 32]. Secondly, E_{es} has been experimentally shown to be independent of external loading conditions [37]. However, the linear characteristic of E_{es} may be true only for small variation of preload or afterload, as suggested by the experimental work performed by Burkhoff et al. [2] (See Chapter 6 Figure 6.4).

V_0 is the intercept at zero pressure of the locally linearised ESPVR. Although it should be theoretically independent either on loading conditions and inotropic state, experimental studies demonstrated that V_0 might not be consistent across preload, afterload and/or inotropy [2] (See Chapter 6 Figure 6.4). Indeed, although local linearisation of the ESPVR could be a reasonable approximation for clinical purposes, the ESPVR is not linear as emphasized by the work performed by Burkhof et al. Burkhoff et al. [2]. Also, one important

issue with V_0 lies in its measurement inability. We should imagine an experimental setting in which despite the fact that the heart is maximally contracted, the intraventricular pressure would be zero. V_0 is only a theoretical quantity, derived from a model which is wrong theoretically and experimentally [2]. Therefore, no ground truth exist for V_0 assessment.

Traditional methods for time-varying elastance analyses involve on the one hand an intraventricular placement of a high fidelity microtip manometer pressure transducer, on the other hand a ventriculography, MRI aquisition or the use of a conductance catheter to record intraventricular volume, and finally require to record PV loops at various loading conditions. The pioneering works were performed on explanted canine hearts [35]. Improvements in experimental settings allowed to performed time-varying elastance assessment in conscious dogs [25; 31; 15] and later in humans [21; 14] by using a transient *inferior vena cava* occlusion manoeuvre. The invasive requirement of these methods limited the translation of the time-varying elastance concept to clinical settings.

8.1.2.2 E_{es} estimation methods

Mathematical modelling helped to improve the experimental setting in order to withdraw the requirement for multiple-beats measurement method. For example, authors simulated the theoretical ventricular pressure that would be developed if no ejection would occur, by fitting a cosine [38] or a fifth-order polynomial [17; 39] function on the isovolumic contraction and relaxation pressure, which allowed to estimate E_{es} from a single-beat PV measurement. These methods still required invasive measurement of pressure and volume in the left ventricle. However, Senzaki et al. [29] proposed a single-beat E_{es} and V_0 estimation method, which paved the way for fully non-invasive single-beat estimation frameworks of E_{es} and V_0 [30; 7; 9].

The most recent methods are based on a particular characteristic of the E(t) function. In 1973, Suga Suga et al. [37] observed that the normalisation of E(t) with respect to E_{es} and t_{max} was consistent across subjects (explanted canine hearts). [29] confirmed this observation in humans. As Takeuchi et al. [38] and Kjørstad et al. [17], Senzaki et al. [29] aimed at extrapolating the maximal pressure the left ventricle is able to reach if no ejection would occur (P_{max}) (see Figure 8.1). They use the "unicity" property of normalised E(t) ($E^N\left(t^N\right)$) to derive P_{max}:

$$P_{max} = \frac{P_{aod}}{E^N\left(t^N_{ao_d}\right)}, \tag{8.2}$$

the ratio between E^N obtained at end-diastolic time $t^N_{ao_d}$ () and E_{es} (= 1 in normalised space) being equal to the ratio between P_{max} and the aortic end-diastolic pressure (P_{aod}).

E_{es} being:

$$E_{es} = \left(P_{max} - P_{es}\right)/SV \tag{8.3}$$

and combining Equation (8.2) and (8.3), it yields:

$$E_{es} = \left(\frac{P_{aod}}{E^N_{ao_d}} - P_{es}\right)/SV. \tag{8.4}$$

Considering that $E^N\left(t^N\right)$ is unique, therefore is only related to $t^N_{ao_d}$. Investigators would only need to measure t_{ao_d}, t_{max}, P_{aod}, P_{es} and SV to have access to E_{es}, all of which being quantities that are easily available under routine clinical situations. However, as discussed in Chapter 7, and emphasised by the authors in their original publication [29], the sensitivity to either inter-individual variability of E^N and/or either timings determination is important. Indeed, as illustrated in Figure 8.2, the relationship between and E_{es} is not linear, a small measurement error in t_{ao_d}, t_{max}, or the systematic uncertainty caused by

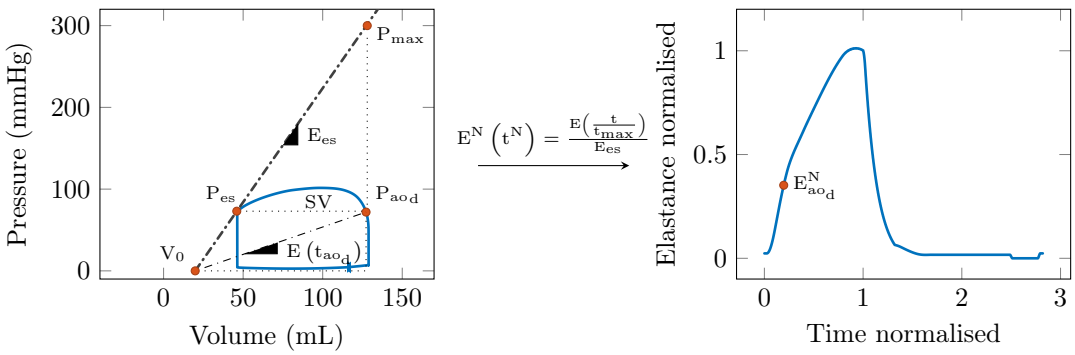

Figure 8.1 – Determination of end-systolic elastance (E_{es}) using the method by Senzaki et al. [29]. **Left:** Graphical method to estimate P_{max} from pressure-volume diagram. **Right:** Transformation of E(t) into the normalised space $E^N(t^N)$. P_{es}: End-systolic elastance; P_{ao_d}: Diastolic aortic pressure; P_{max}: Maximal pressure that would reach the left ventricle in case of complete isovolumic contraction; E_{es}: End-systolic elastance; V_0: Volume intercept of linearisation of ESPVR; SV: Stroke volume; $E(t_{ao_d})$: Elastance at opening of the aortic valves; Normalised elastance at the opening of the aortic valve; t: Time; t_{max}: Time to maximal elastance

the inter individual variability that is not considered when using the "master" E^N curve, would lead to a clinically significant error in E_{es} estimation.

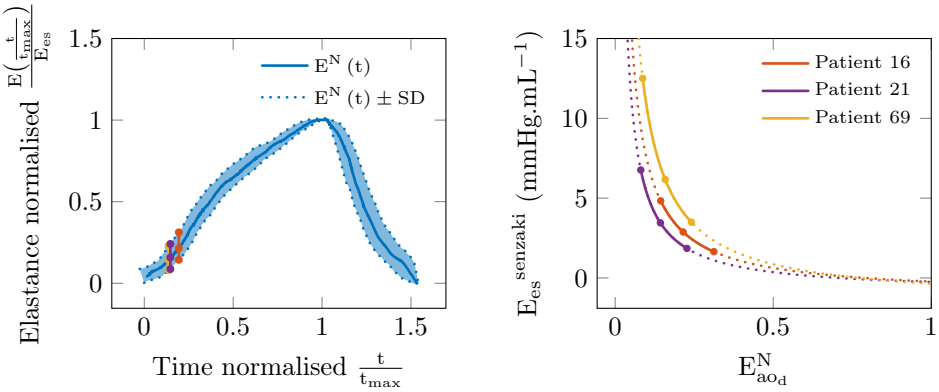

Figure 8.2 – Normalised elastance curve and effect of the standard deviation (SD) of on $E_{es}^{senzaki}$ estimation [29]. **Left:** Normalised elastance curve (reproduced from Suga et al. [37]) and prediction (colored dots) using $\frac{t_{ed}}{t_{max}}$ as obtained by trans-thoracic echocardiography, for 3 patients. **Right:** $E_{es}^{senzaki}$ estimation as function of , for the data obtained in the 3 patients. The plain lines represent the $E_{es}^{senzaki}$ for inside the ranges given by Suga et al. The dashed line represent the extrapolation of the $E_{es}^{senzaki}$ for outside these ranges.

Shishido et al. [30] proposed an adapted version, by approximating the ascending part of the E(t) with two linear functions. It yields:

$$E_{es} = \left[P_{aod} + \frac{(P_{aod} - P_{ed})}{ICT} \cdot ET \cdot \alpha - P_{es} \right] / SV \tag{8.5}$$

where P_{aod} is the pressure value at the end of the isovolumic contraction time (ICT) *i.e.* the opening of the aortic valves, and P_{ed} the pressure value at the end of the diastole. ET is the ejection time between the opening and the closing of the aortic valves. α is the ratio between the slope of the two linear functions and was estimated using the following:

$$\alpha = -0.210 + 1.348 \cdot EF + 0.682 \cdot \frac{ICT}{ICT + ET} \tag{8.6}$$

with EF being the ejection fraction.

In 2001, Chen et al. [7] improved also the method described by Senzaki in order to reduce the E_{es} sensitivity to measurement errors, by introducing phenomenological terms linked somehow to cardiac function:

$$E_{ao_d}^{N,modified} = 0.0275 - 0.165 \cdot EF + 0.3656 \cdot \frac{P_{ao_d}}{P_{es}} + 0.515 \cdot E_{ao_d}^{N}, \tag{8.7}$$

EF being the ejection fraction measured by transthoracic echocardiography (TTE) as the ratio between SV and the end-diastolic volume. Finally, $E_{ao_d}^{N,modified}$ is used in Equation (8.4) to estimate E_{es}.

8.1.2.3 V_0 estimation methods

The methods presented in the previous Section 8.1.2.2 assume a linearisation of ESPVR, and therefore, V_0 can be easily extrapolated from Equation (8.8)

$$V_0 = V_{es} - \frac{P_{es}}{E_{es}} \tag{8.8}$$

E_{es}, P_{es} and V_{es} being the elastance, pressure and volume at end-systole, respectively.

However, as discussed earlier, the linearisation of ESPVR is a wrong theoretical model by essence, that has been confirmed by experiments [2]. To take into account the non-linear characteristic of the ESPVR, Mirsky et al. described a non-linear method to fit end-systolic pressure-volume data [23; 22]. They introduce the concept of maximum systolic stiffness, focusing the model at the myocardium level. From myocardial stress-strain relationships in three-dimensional space integrated over an ellipsoidal model of heart, Mirsky et al. [23], demonstrated that pressure at end-systole was a non-linear function of end-systolic volume:

$$P_{es} = k_m \frac{\gamma}{G} \cdot \max\left(E_{avg}\right) \cdot \log \frac{V_{es}}{V_0} \tag{8.9}$$

with k_m being a constant which depends on the midwall short and long axis of the LV, γ a curve-fit parameter, G the slope of the relation between myocardial stress and end-systolic pressure (P_{es}), G being approximated by a linear function of the end-systolic volume V_{es}, and E_{avg} the average systolic myocardial stiffness.

In their work, they observed differences in V_0 estimation when calculated solving for equation (8.9) or Equation (8.1) (see Figure 8.3).

8.1.3 Non-invasive estimation of E_{es} and V_0 from phenomenological models

Even though the concept of time-varying elastance suffers from theoretical limitations related to its linear end-systolic pressure-volume relationship description which is non-linear by essence [2; 23; 22], it helped clinicians, physiologists and modellers to access global systolic properties of the left ventricle, withdrawing the requirement for invasive pressure and volume measurement acquired during extreme variations of loading conditions. Indeed, in original publications by Chen et al. [7] and Gayat et al. [9], the authors used non invasive estimation of the term we called P_{ao_d} in Equations (8.4) and (8.7), that was replaced by P_d which simply accounted for brachial diastolic pressure. They also used the method provided by Kelly et al. [16] to estimate P_{es} from systolic brachial pressure P_s by using $P_{es} = 0.9 \times P_s$.

Therefore non-invasive estimation of not only E_{es} and V_0, but E_a and V_{va} were rendered available for anaesthetists and intensivists, from simple clinical measurements [11], the

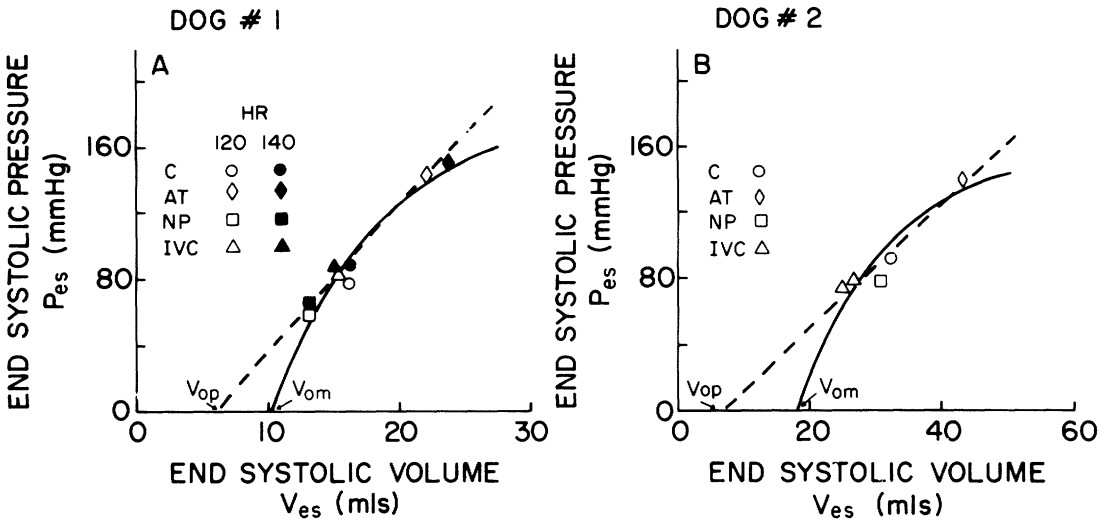

Figure 8.3 – End-systolic pressure-volume relations based on the maximum myocardial stifness and maximum ventricular elastance concepts. The solid curve represents the relation obtained from the maximum myocardial stifness concept and is clearly non-linear. The dotted straight line is the end-systolic pressure-volume relation obtained from the maximum ventricular elastance concept. The isolated points represent the measured pressures and volumes at the time of maximum ventricular elastance. V_{0m} =zero stress-volume obtained from the present theoretical model;V_{0P} =zero stress-volume obtained by linear extrapolation of the maximum elastance points. Linear extrapolation may lead to spurious results for V_{0_p}. IVC: *inferior vena cava* occlusion; C: Control; AT: Angiotensine II; NP: nitrorusside.

latter being associated with ventricular-arterial coupling and so forth myocardial energetic expenditure.

8.1.4 Theoretical biomechanical model of ESPVR

As presented in Chapter 2 The hyperelastic potential used in the model was described by Chapelle et al. [6], and modified by Caruel et al. [3]. The hyperelastic potential is written as:

$$W_e = C_0 \cdot e^{C_1(J_1-3)^2} + C_2 \cdot e^{C_3(J_4-1)^2}, \tag{8.10}$$

where $J_1 = I_1 \cdot {I_3}^{-\frac{1}{3}}$ and $J_4 = I_4 \cdot {I_3}^{-\frac{1}{3}}$, being the reduced invariants of the Cauchy-Green strain tensor, $I_3 = \det\left(\underline{\underline{C}}\right)$ and (C_0, C_1, C_2, C_3) the parameters of the hyperelastic potential.

Assuming spherical geometry and a maximum tension the heart can develop, the stress expression can be written as (see [3]):

$$\Sigma_{\text{sphere}}\left(e_{\text{fib}}\right) = \frac{n_0\left(e_{\text{fib}}\right) \cdot \tau_0}{1 + e_{\text{fib}}} + 4\left(1 - C^{-3}\right)\frac{\partial W_e}{\partial J_1} + 2\frac{\partial W_e}{\partial J_4} \tag{8.11}$$

with n_0 and τ_0 being respectively the Starling effect associated with the fibre extension e_{fib} and the contractility when the heart is maximally contracted, and $C = (1 + e_{\text{fib}})^2$ the circumferential component of the Cauchy-Green strain tensor.

At equilibrium, the ventricular pressure can be written as a function of the fibre extension e_{fib}, the constitutive tissue stiffness parameters C_i ($i \in 0, \ldots, 3$) and of the thickness of the sphere at stress-free reference configuration attested by ϵ (adapted from [4]):

$$P_{0_D} = \epsilon \cdot \Sigma_{\text{sphere}}(e_{\text{fib}}) \cdot (1 + e_{\text{fib}}) \left(1 + e_{\text{fib}} - \frac{\epsilon}{2}(1 + e_{\text{fib}})^{-2}\right)^{-2} \left(1 + \epsilon\,(1 + e_{\text{fib}})^{-3}\right)^{-1} \quad (8.12)$$

Also, our geometrical model allows to write e_{fib} as a function of ventricular volume (V) (See Chapter 2 Equation (2.19)).

8.1.5 Aim of the chapter

We propose a method in which E(t), E_{es}, and V_0 are fully derived by our biomechanical model (See Chapter 1). Our objectives are 1/ to evaluate the sensitivity of our method with respect to changes in preload, afterload and contractility; 2/ to compare the variability of our method as compared to the methods proposed by Senzaki et al. [29],. Chen et al. [7] and Shishido et al. [30] and; 3/ to verify that the E(t) generated using our framework fulfills the normalisation criteria observed in Suga et al. [37].

8.2 Method

8.2.1 Proposed procedures to estimate E_{es} and V_0

We used the datasets of 5 patients extracted from the database described in details in Chapter I. From the patient-specific models, we first identified E_{es} and subsequently V_0, by using the phenomenological and the biomechanical methods.

We sequentially modified *in silico* the loading conditions in order to modify the stroke volume (SV) and/ or the end-systolic pressure (P_{es}) by ± 10%. We decreased/increased either the preload or either the distal resistances of the biomechanical model in order to reach the 10% changes of SV or P_{es}. From these new conditions, we applied our biomechanical and phenomenological estimation methods. We finally compared the variability of the E_{es} and V_0 obtained between the estimation methods available.

We also modified the contractility of the biomechanical model in order to operate a ± 10% change in SV, and we compared the E_{es} values obtained with the different methods, and the V_0 variability.

We finally verified that the E(t) obtained with the biomechanical method were within the normalised time-varying elastance ranges provided by Suga et al. [37].

8.2.1.1 From phenomenological models

The data used for calibration of the biomechanical model were also used for the estimation of E_{es} and V_0 from the phenomenological models and are described in detailed in chapter 1:

- From trans-thoracic echocardiography we evaluated the isovolumic contraction time (ICT), as the time between the end of the auricular contraction, assessed by the end of the A wave on the mitral Doppler flux, and the beginning of the ejection, as assessed by the beginning of the aortic Doppler flux evaluated on the left ventricular outflow tract.
- the ejection time (ET) was evaluated as the duration of ejection, as evaluated on the aortic Doppler flux;
- the end-systolic pressure (P_{es}) was obtained on the simulated ventricular pressure as the maximal distance between the ventricular pressure signal and a straight line traced between maximum and minimum ventricular pressure (method derived from [19]) (See figure 8.4);

- the aortic end-diastolic pressure (P_{aod}) was obtained as the local minimum of the simulated aortic pressure;
- the SV was computed as the difference between the maximal and the minimum ventricular volume (simulated);
- the ejection fraction (EF) as the ratio between SV and the end-diastolic volume (V_{ed});
- $E^N_{ao_d}$ was estimated using the normalised time-varying elastance curve obtained in [36], and the ICT.

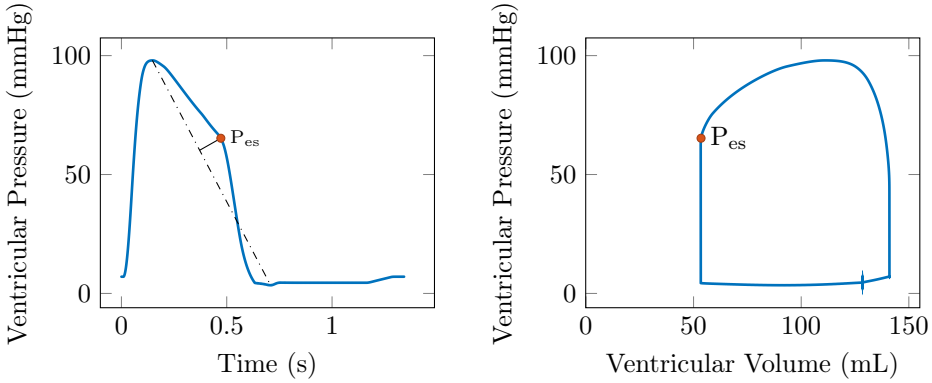

Figure 8.4 – Example of the method used to identify end-systolic pressure (P_{es}). **Left:** Pressure signal from which is identified the end-systolic pressureP_{es} point. The local minimum and maximum of the pressure signal is identified. The maximal distance from the pressure signal to the straight line drawn from the local minimum and maximum corresponds to the P_{es}. **Right:** Equivalence in pressure-volume loop space.

Using these informations, we were able to solve for Equations (8.4), (8.5) and (8.7). As the sensitivity to $E^N_{ao_d}$ has already been studied in Chapter 7, we estimated $E^N_{ao_d}$ only once (when ETT measurements were available), all the other parameter values being obtained using the results of the simulation performed with the biomechanical model at different loading and contractile state.

8.2.1.2 From biomechanical model

As discussed in Section 8.1.4, the theoretical ESPVR can be calculated statically at maximal contraction (Equation (8.12)). However, in dynamic simulations, the static maximal contraction may not be reached (see Figure 8.5). In other words, the relaxation begins before the maximal contraction occurs.

For a given afterload, the rate at which the contraction occurs is governed by determinants of the Force - Velocity relationship of the model – namely the amplitude and the rate of activation of the myocardium, the rate of attachment and destruction of the actin-myosin cross bridges, and the viscous active component (See Chapter , Section 1.5.2.6 and Figure 1.21). Finally, the destruction rate of the actin-myosin cross-bridges is governed in our model by a parameter α_{0_D} (See Equation (1.31)). The calibration of α_{0_D} was discussed in Figure (8.6).

The latter parameter may help to get dynamically closer to the theoretical static ESPVR. However, experiments suggests that this behaviour may be non-physiological (See Figure 8.6).

No physiological experiment was performed in intact human samples at 37°C. We therefore chose an $\alpha_{0_D} = 12$ as the results provided in Figure 8.6, suggest better fit with mammalian data.

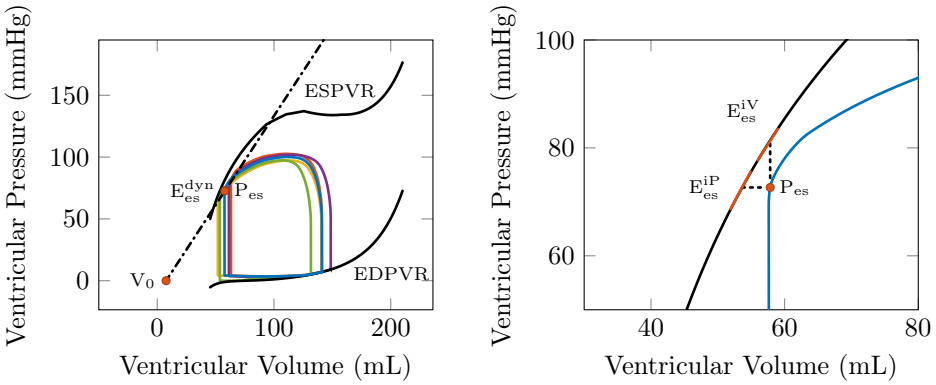

Figure 8.5 – End-systolic elastance (E_{es}) Estimation methods. **Left:** Dynamic method. The PV loop are obtained under various loading conditions (preload and afterload variations). We can observe that the end-systolic pressure-volume point (P_{es}) does not reach the theoretical end-systolic pressure-volume relationship (ESPVR). The end-systolic elastance is estimated using the Dynamic estimation method (E_{es}^{dyn}). **Right:** Zoom around the P_{es} point where the static isovolume (E_{es}^{iV}) and isopressure (E_{es}^{iP}) methods are displayed. The V_0 is subsequently calculated after E_{es} estimation. ESPVR: end-systolic pressure-volume relationship; EDPVR: End-diastolic pressure-volume relationship

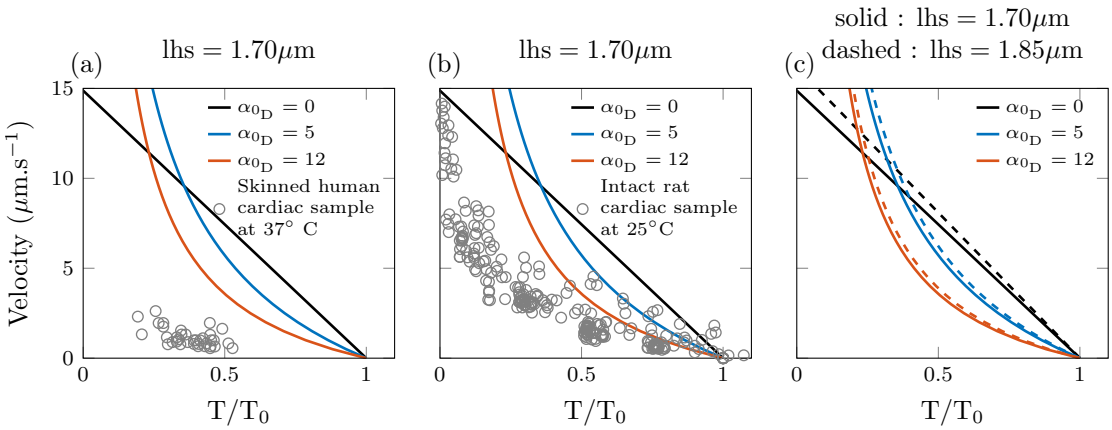

Figure 8.6 – Force-Velocity relationship. **(a)** Data from human cardiac cells sample at 37° C. The calibration of the active part of the model was performed using different destruction rate (α_{0_D} = 0, 5 or 12). **(b)** Data from rat cardiac tissue at 25° C. **(c)** Simulation performed with different sarcomere length. lhs: length of half-sarcomere; T/T_0: Stress variation, relative to stress at reference configuration. *Data reproduced from Land et al. [18].*

We designed three methods to estimate E_{es}, all of which being evaluated (Figure 8.5).

- **Dynamic estimation of E_{es} – (E_{es}^{dyn}).** The method relies on an *in silico* reproduction of the original experimental method described by Suga [34]. From the calibrated model, we varied the preload and afterload and simulated the PV loop, in order to obtain 5 different conditions. We identified the P_{es} point by using the method described in Section 8.2.1.1, and performed a linear regression. The slope and the intercept of the linear regression correspond to our estimated E_{es} and V_0.
- **Static estimation of E_{es} – Isopressure (E_{es}^{iP}).** The method is based on the statical description of the ESPVR. We first identify the P_{es} point by using the method described in Section 8.2.1.1. We further identified the isopressure point on the ESPVR and solve for first derivative of Equation (8.12). The slope of the tangent corresponds to the E_{es}.
- **Static estimation of E_{es} – Isovolume (E_{es}^{iV}).** The procedure is similar as presented for isopressure but rather than fixing an isopressure, we identified the isovolume point on the ESPVR, the tangent on this point corresponding to the E_{es}

We calculated the intercept (*i.e.* V_0), of the linear function characterised by the slope E_{es} passing through P_{es} point. We further applied Equation (8.1) to estimate E(t) function, with the simulated P (t) and V (t), and the estimated V_0.

8.2.2 Outcomes

We evaluated the variability of the estimated V_0 with respect to the loading conditions and with respect to the contractility. From the original calibrated condition, we estimated the original V_0 for all the six methods – namely dynamic, static isopressure, static isovolume, Senzaki, Chen and Shishido. We varied the preload, afterload and contractility of the biomechanical model until we reached a P_{es} (for afterload variation) or SV (for preload and contractility variations) variation between 10 to 15 % the original P_{es} or SV value.

For each new condition, we estimated E_{es} and V_0 for all 6 estimation methods. In theory, the E_{es} and V_0 is not affected by changes in preload and afterload. Therefore, we expected the E_{es} and the V_0 to be close to the original calibrated estimations. The same hypothesis is made concerning changes in contractility and stability of V_0 estimation.

We calculated the root mean squared error (RMSE) between the original estimations of E_{es} and V_0 obtained for the 5 patients at baseline and after Noradrenaline administration, and estimations obtained, from the aforementioned original conditions, after variation in $\pm 10 - 15\%$ the original SV and/or P_{es} obtained by manipulating preload, afterload or contractility, for each method (dynamic, static isopressure, static isovolume, Senzaki, Chen and Shishido) as follows:

$$\mathrm{RMSE}_{V_{0\mathrm{method}}} = \frac{1}{N}\sqrt{\sum_{i=1}^{N}\left(V_{0}{}^{i}_{\mathrm{original}} - V_{0}{}^{i}_{\mathrm{method}}\right)^2} \tag{8.13}$$

with i = 1,...N; N being at maximum 6 combinations of changing conditions (n varying conditions = 2 – $\pm 10 - 15\%$ the original SV and/or P_{es}) × (n parameters = 3 – Preload, Afterload, Contractility) for 10 calibrated datasets (n patients = 5) × (n challenges = 2 – Baseline and Noradrenaline), and

$$\mathrm{RMSE}_{E_{es\mathrm{method}}} = \frac{1}{N}\sqrt{\sum_{i=1}^{N}\left(E_{es}{}^{i}_{\mathrm{original}} - E_{es}{}^{i}_{\mathrm{method}}\right)^2} \tag{8.14}$$

with i = 1,...N; N being at maximum 4 combinations of changing conditions – (n varying conditions = 2 – $\pm 10 - 15\%$ the original SV and/or P_{es}) × (n parameters = 2 – Preload, Afterload) for 10 calibrated datasets (n patients = 5) × (n challenges = 2 – Baseline and Noradrenaline). We considered each dataset independently.

8.2.3 Statistical analysis

The results are provided as median [IQR – interquartile ranges] or number (%). A p was considered statistically significant beyond 0.05.

8.3 Results

Physiological analysis of Noradrenaline effects

The parameters calibrated for the 5 patients at baseline and at peak effect of Noradrenaline are provided in Table 8.1. The haemodynamic indicators used for phenomenological estimations and biomechanical calibration are provided in Table 8.2.

Table 8.1 – Patient-specific main parameters before and after Noradrenaline administration.

	R_{ref}	d_{ref}	cycle length	C_i	P_{ed}	τ_0	R_d	C_d	R_p
Patient12									
Baseline	3	0.83	1.34	[637,2.4,99,5.5]	7	85	1.18	1.82	1.76
Noradrenaline	–	–	1.39	–	–	95	2.83	0.86	2.31
Patient16									
Baseline	2.8	0.84	0.93	[635,2.4,98,5.5]	7	75	1.65	0.73	1.32
Noradrenaline	–	–	0.99	–	–	95	2.93	0.58	2.86
Patient18									
Baseline	3.1	0.86	1.19	[1272,2.4,198,5.5]	14	85.5	1.28	1.09	3.52
Noradrenaline	–	–	1.29	–	–	105	1.74	0.74	4.4
Patient21									
Baseline	3.1	0.9	0.77	[635,2.4,99,5.5]	7	110	0.7	1.49	1.98
Noradrenaline	–	–	0.91	–	–	110	1.49	0.99	1.43
Patient69									
Baseline	2.6	0.85	0.87	[636,2.4,99,5.5]	7	75	1.4	1.16	1.64
Noradrenaline	–	–	0.99	–	–	100	2.62	0.63	3.08

R_{ref}: Radius at stress-free configuration (cm); d_{ref}: Wall thickness at stress-free configuration (cm); cycle length: (s); C_i: Stiffness parameters; P_{ed}: End-diastolic pressure (Preload) (mmHg); τ_0: Contractility (kPa); R_d: Distal resistance ($1e^{08}$Pa.s.m^{-3}); C_d: Distal capacitance ($1e^{-08}$m^{-3}.Pa^{-1}); R_p: Proximal resistance ($1e^{07}$Pa.s.m^{-3})

Table 8.2 – Patients haemodynamic data at Baseline and after Noradrenaline administration used for phenomenological estimations and biomechanical model calibration.

		P_{aod}	P_{aos}	SV	EF	E^N_{aod}	ICT	ET	t_{max}
Patient12	Baseline	47	73	83	59	0.12	160	415	579
	Noradrenaline	77	115	57	41	0.12	158	428	586
Patient16	Baseline	54	88	51	47	0.08	144	595	737
	Noradrenaline	82	123	40	37	0.08	146	720	872
Patient18	Baseline	43	97	65	44	0.06	91	570	661
	Noradrenaline	53	122	62	42	0.05	86	578	664
Patient21	Baseline	50	101	81	58	0.05	69	435	504
	Noradrenaline	85	121	68	49	0.08	92	450	544
Patient69	Baseline	53	72	50	61	0.07	78	453	533
	Noradrenaline	82	117	42	52	0.08	83	445	529

P_{aod}: Diastolic aortic pressure (mmHg); P_{aos}: Systolic aortic pressure (mmHg); SV: Stroke volume (mL); EF: Ejection fraction (%); E^N_{aod}: Normalised elastance at end-diastole; ICT: Isovolumic contraction time (ms); ET: Ejection time (ms); t_{max}: time to maximum elastance (ms)

Figure 8.7 shows the results of E_{es} and V_0 estimations using the 6 different methods described in Section 8.2. We can observe that the interindividual variability of both E_{es} and V_0 is minimal with the static ${}_iP$ method, as compared with the other methods. Also, the difference in E_{es} estimated by the different methods is globally significant (p - value $= 0.01$). The difference in V_0 estimated by the different methods is globally significant (p - value < 0.001).

Furthermore, time-varying elastance theory states that V_0 should be loading and contractility independent. Noradrenaline has the potency to act both on loading conditions and on contractility. Table 8.1 and Table 8.2 demonstrated that the Noradrenaline administration was followed by important changes in loading conditions and in contractility, and the resulting effect on the end-systolic conditions was also significant. However, we observed that, even if the changes in physiological conditions are important, the V_0 remained stable from baseline to peak effect of Noradrenaline, only for static ${}_iP$ method (Figure 8.7).

If we consider ${E_{es}}^{iP}$ variation after Noradrenaline administration, intuitively, since Noradrenaline increases contractility, we would have expected E_{es} to increase. This is not the results we observed as ${E_{es}}^{iP}$ stays stable within our 5 patients. Noradrenaline is an α_1 and β_1 adrenoreceptor agonist, and even if an increase in contractility is expected with Noradrenaline administration, the effect on the "true" E_{es} caused by the increase in contractility might be counteracted by the tremendous increase in E_a which is closely dependent to the vascular conditions. However, if we look into details the results observed in our 5 patients, we observed that E_{es} decreased after Noradrenaline only in Patient 12, for whom V_0 estimation was also decreased, and in Patient 21, in which no increase in contractility has been observed. For the remaining three patients (16, 18, 69) the Noradrenaline was associated with an increase in E_{es} along with a relative stability of V_0 estimation (Table 8.3).

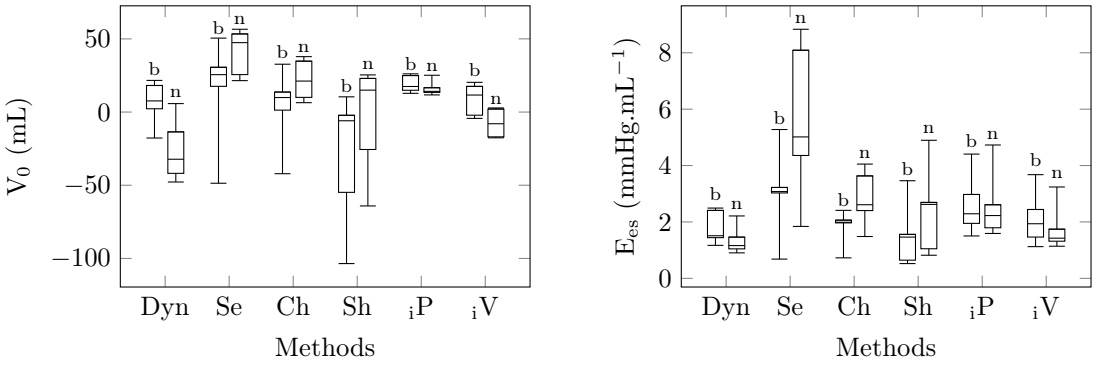

Figure 8.7 – V_0 and E_{es} estimations by methods before and after Noradrenaline administration. The boxplots represent the distribution of the estimated indicators for the 5 patients at calibration condition. **Left**: V_0 estimation; **Right**: E_{es} estimation. *b: Baseline; n: Noradrenaline; Dyn: dynamical, $_iP$: static-isopressure, $_iV$ static-isovolume, Se: Senzaki, Sh: Shishido, Ch: chen*

Table 8.3 – E_{es} and V_0 estimated from original condition before and after Noradrenaline administration, using the static isopressure method

	E_{es} mmHg.mL^{-1}	V_0 mL	τ_0 kPa
Patient12			
Baseline	2.29	26	85
Noradrenaline	1.59	11	95
Patient16			
Baseline	1.95	13	75
Noradrenaline	2.23	13	95
Patient18			
Baseline	1.5	17	85.5
Noradrenaline	1.79	17	110
Patient21			
Baseline	2.97	25	110
Noradrenaline	2.61	25	110
Patient69			
Baseline	4.41	15	75
Noradrenaline	4.73	14	100

Stability related to parametric deviations

Figure 8.8 demonstrates the results of the stability of V_0 and E_{es} estimations with respect to the variations of the physiological conditions (*i.e.* preload, afterload and contractility for V_0, preload and afterload for E_{es}). The method that offers the better V_0 and E_{es} stability is again the static isopressure method. This was evaluated on the 5 patients with and without Noradrenaline administration, for variations of ± 10-15% the original P_{es} and/or SV obtained after modification of the preload, afterload and/or contractility parameters. The RMSE is evaluated as the difference between the variation and the original condition (n = 60 and 40 respectively for V_0 and E_{es}). The between group differences is statistically significant (p - value < 0.001).

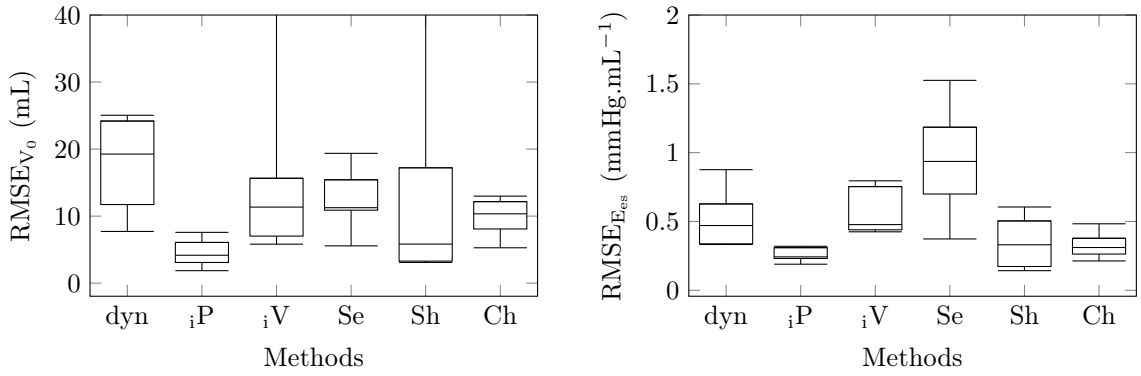

Figure 8.8 – Stability of V_0 and E_{es} with respect to the variations of haemodynamic condition after change of preload, afterload and/or contractility parameters, from original calibration. **Left:** The box plot represents the distribution of the root mean square error between the V_0 calculated from varying preload, afterload and contractility and the V_0 estimated from original configuration calibrated on 5 patients' data with and without Noradrenaline administration. Each parameter (preload, afterload contractility) was varied twice, increased or decreased in order to vary the P_{es} or the SV by 10 to 15%. **Right:** Same for E_{es}. Here the variation of contractility is not displayed as E_{es} is supposed to be very sensitive to this parameter. *Dyn: dynamical, $_iP$: static-isopressure, $_iV$ static-isovolume, Se: Senzaki, Sh: Shishido, Ch: chen.*

According to these results, in the rest of the document, we use the static isopressure method to estimate V_0 and E_{es} from biomechanical model.

Sensitivity of E(t) to V_0

In the previous Section, we evaluated the stability of V_0 to preload, afterload and contractility, when determined using various methods. The method which offers the more stable estimation of V_0 is the method called static isopressure. In this section, we aimed to evaluate the sensitivity of E(t) tracing to V_0 variations, and to verify that the E(t) normalisation according to E_{es} and t_{max} behaves in a similar manner than the $E^N\left(t^N\right)$ provided by Suga et al. [37].

We used the results of the calibrated simulation performed using the data from 5 patients (Patient 12, 16, 18, 21 and 69) at baseline (Table 8.1). We first used the static isopressure method to estimate V_0 for the calibrated condition. Second, we modified the preload and the afterload in order to deviates the P_{es} and/or the SV by 10 to 15% the original calibrated outputs, and we estimated the V_0 associated with the modified loading condition. It yields slightly different V_0 as compared with the original V_0 (the difference is in accordance with the values observed in Figure 8.7). As our objective is to evaluate the effect of an error in V_0 estimation, we used the modified V_0, associated with the original

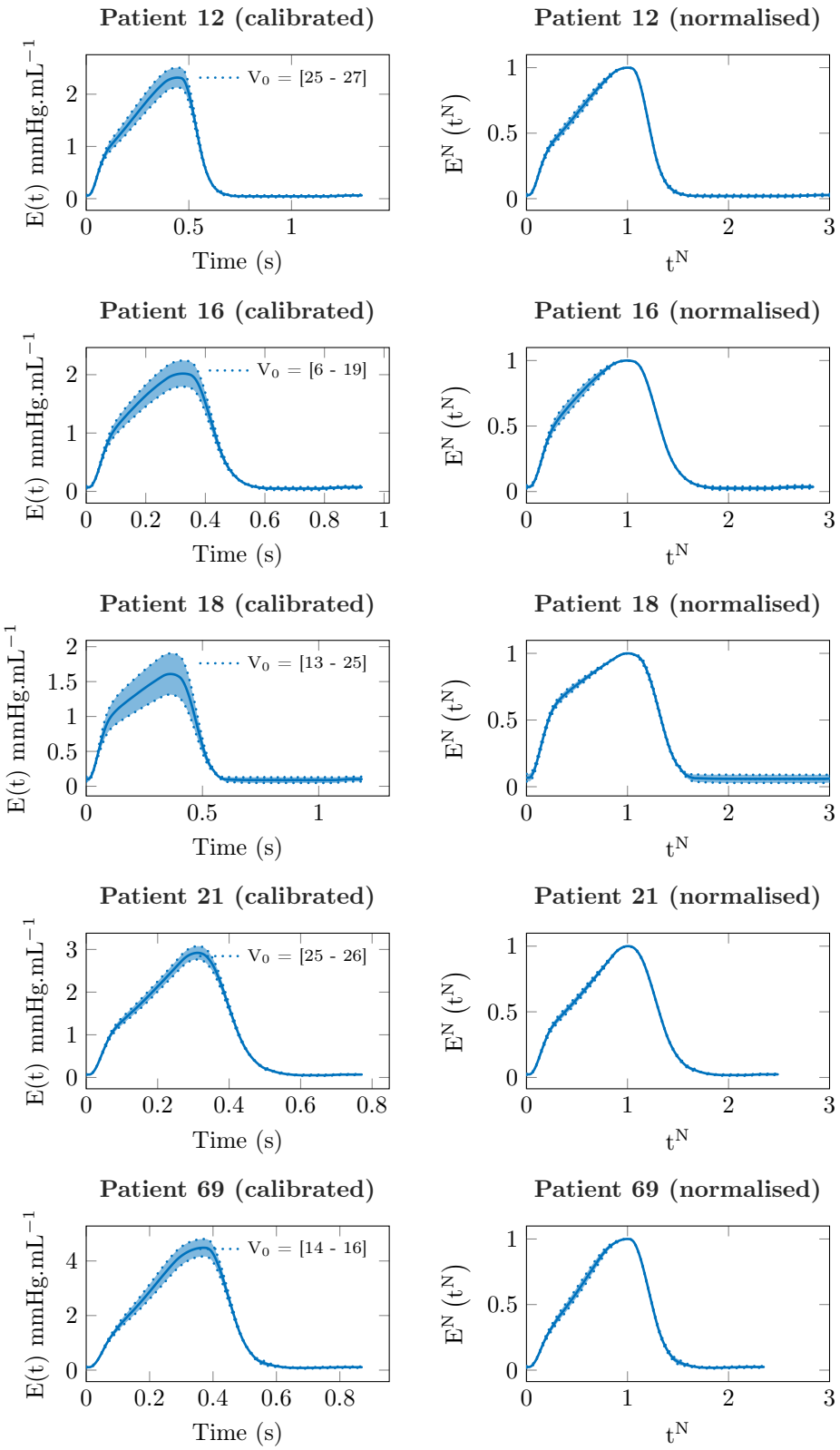

Figure 8.9 – **Left:** Effect of V_0 variations on E(t) and **Right:** on $E^N\left(t^N\right)$. The V_0 ranges were obtained by using the static isopressure method at different preload and afterload conditions, deviating from the calibrated original condition.

calibrated P (t) and V (t) values to estimate E(t). Figure 8.9 shows the effect of these errors in V_0 estimation on E(t) and on $E^N\left(t^N\right)$ tracings.

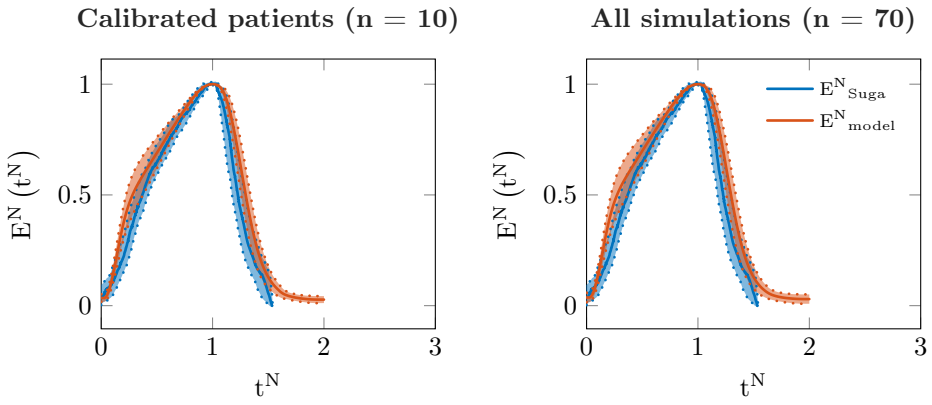

Figure 8.10 – Normalised elastance from data from Suga et al. [37] (blue) and from biomechanical model (red). **Left:** The red curve is the mean of the normalised E(t) obtained from original patient specific calibration performed on 5 patients at baseline and after Noradrenaline administration. **Right:** We simulated deviation from these original conditions by applying a change in preload, afterload, and contractility in the biomechanical model. The changes were prescribed in order both to increase and decrease the end-systolic pressure (P_{es}) (for afterload), and the stroke volume (SV) (for contractility or preload) by 10 to 15% the original P_{es} or SV. The dotted lines correspond to the standard deviation of the E^N curves used.

We can note that most of the difference is observed on the maximal elastance E_{es}, and to a lower extent on the second portion of the ascending curve of the E(t) function, for all 5 patients. A second observation relies on the fact that even if large differences as compared with the original calibrated condition can be observed in E(t) tracing (See Patient 18, Figure 8.10), it does not translate into important changes in normalised space. This reinforces our findings discussed in Chapter 7, in which we warn about the use of the master $E^N\left(t^N\right)$ curve to estimate accurately E_{es}. If the master $E^N\left(t^N\right)$ curve is used, as exemplified with the Patient 18, a small variation in $E^N\left(t^N\right)$ could lead to a great error in E_{es}.

Finally, we aimed to verify that our E(t) tracings using our static isopressure method reproduce the observations made by Suga et al. [37] concerning the within and between patient uniqueness of the $E^N\left(t^N\right)$ master curve. Figure 8.10 plots the normalisation of E(t) curves obtained by using the calibrated datasets (n = 10) and the results obtained after preload, afterload and contractility variations (n= 60), provided in Figure 8.9, against the results reproduced from Suga et al. [37].

8.4 Discussion

In this Chapter, we proposed a framework to estimate the V_0 parameter of the time-varying elastance concept, from a calibrated patient-specific biomechanical heart and vessel model. By systematically analysing the candidate methods, comparatively with the existing phenomenological methods, we demonstrated by using 5 patient cases that the method called static isopressure offers the V_0 estimation that is the most stable with respect to preload, afterload, and contractility variations. We also verified that the E(t) normalisation with respect to E_{es} and t_{max} behaved similarly to the normalised E(t) measured in experimental conditions by Suga et al. [37].

V_0 estimation is not a trivial task as no clinical or experimental setting allows for

measuring the "true" V_0. The time-varying elastance concept is based on the local linearisation of the non-linear end-systolic pressure-volume relationship. This linearised ESPVR is parametrised by its slope, E_{es} and its pressure intercept, V_0. As the time-varying elastance concept is a linear approximation of a non-linear physical phenomena, V_0 may be flawed and cannot be measured. It is however an important parameter to consider when manipulating time-varying elastance concept especially for modelling purposes. However, even if the time-varying elastance concept may be wrong, its use as a surrogate of cardiac mechanics may be convenient for modelling purposes. It may approximate adequately cardiac physiology, under clinical settings, without the need to design and parametrise a complex biomechanical model [26; 33; 5; 28; 12; 8]. Thereafter, the question of a proper estimation of V_0 is important, as it may influence the results of the E(t) modelling.

To assess the performance of the V_0 estimation method, we evaluated the stability of the V_0 estimation across various ranges of preload, afterload and contractility variations. Indeed, in theory, V_0 is supposed to be independent of all those 3 conditions [27]. We tested 6 candidate-methods for proper V_0 estimation, and evaluated all those 6 methods comparatively in order to choose the method which allowed for the most stable V_0 estimation. We evaluated 3 methods derived from our biomechanical approach, and three phenomenological methods already available [29; 30; 7]. The method which yields the most convincing results was the static isopressure method, as it warrants for V_0 estimation stability, expected physiological magnitude, and relative concordance with the inter- and intra-individual unicity of the normalised E(t) curve.

We also provided results regarding E_{es} stability analysis. Indeed, the linearisation of ESPVR allows for V_0 and E_{es} estimations. Although V_0 is supposed to be loading and contractile independent, E_{es} was used as a surrogate of contractile state experimentally [37; 10; 20; 13], and clinically [9; 11]. Therefore, the stability analysis of E_{es} was focused only on preload and afterload dependency. We observed even more stable results with E_{es} than for V_0 stability analysis, when choosing the static isopressure method. We may interpret this result as a surrogate for strong load-independence of both E_{es} and V_0 estimations, and a relative contractile-dependence of V_0 estimation. This result is consistent with experimental findings in which V_0 was found to be affected by change in contractile state induced by inotropic drugs. [2].

The interpretation of the results obtained when varying physiology with Noradrenaline is also interesting. We observed an intra-individual stability of V_0 estimation before and after Noradrenaline administration (Figure 8.7 and 8.3). This is consistent with the theoretical principle that V_0 may not be affected by changes in preload, afterload and contractility. In our results, even though the ESPVR is non-linear, the physiological changes consecutive to Noradrenaline administration were not followed by a modification in V_0 estimation. This is convenient for modelling purposes, but has to be discussed from a physiological perspective, as V_0 should be relatively dependent on the contractile state. One interpretation could be that the ESPVR portion in which operated our patients without and with Noradrenaline was located on stable region of the ESPVR with respect to its derivative. Also, another interpretation could be that the relative changes of inotropic state was not sufficient to translate into change in V_0 estimation. It should be interesting to evaluate our framework using drugs with more inotropic potency.

Concerning the effect of Noradrenaline on E_{es} estimation, no change have been observed. This result is surprising as we would have expected an increase in E_{es} following Noradrenaline administration. Noradrenaline demonstrates strong α_1 adrenoreceptor agonist effect and to a smaller extent, a β_1 adrenoreceptor agonist effect. The resulting effect would be *in vivo* a strong vasoconstriction with a small increase in contractility. However, it has been demonstrated that E_{es} could be associated with inotropic state [37; 10; 20; 13],

although it remains preload and afterload independent. Our first comment is physiological. We may imagine a situation in which, while contractility is slightly increasing and therefore, the ESPVR is slightly upscaled, a relatively bigger shift in operating physiological condition toward the gentler portion of the ESPVR occurs (supposing therefore a load-dependency). However, we stated earlier that E_{es} was found to be contractile-dependent and load-independent. These two statements may be discussed. Indeed, the contractile-dependency of E_{es} was observed experimentally by using inotropic drugs with more β_1 effect than Noradrenaline [37; 10; 20; 13]. In these studies, the specificity of E_{es} to inotropic state was assessed by demonstrating the absence of association with afterload or preload state. However, even if load-independence of E_{es} is strongly suggested by these studies, it has not be definitively demonstrated, and some experimental studies argued in the other direction [40; 20; 1]. For example, in the study of Lee et al. [20], E_{es} has been associated with contractile indicators that are also preload and/or afterload dependant. A reasonable compromise would be to say that the load-dependency of E_{es} is relatively small as compared to its strong association with inotropic state. Therefore, in light with this hypothesis, and since the α_1 effect of Noradrenaline is larger than the β_1 effect, then we may observe a shift of the end-systolic pressure-volume point toward a gentler portion of the upscaled ESPVR. The net effect could be either a decrease or no change in E_{es}, associated with a decrease in V_0. This may explain the results obtained in Patient 12 (See Figure 8.11). The last comment concerning this question comes from the results observed in clinical studies. Gayat et al. showed an association between E_{es} and Dobutamine infusion [9]. In 2017, Wong et al. [41] evaluated the haemodynamic response of a step increase of Dobutamine infusion from introduction to 10 to 20 mcg/kg/min, evaluated on invasive measurement of PV loop. E_{es} was found to be increased by the first Dobutamine infusion step, but remained stable from 10 to 20 mcg/kg/min. Recently, Guinot et al. [11] published a clinical study, evaluating the effect of Noradrenaline infusion in patients admitted in intensive care units using E_{es} estimation and ventricular-arterial coupling. They found that E_{es} was increased and the V_{va} improved, especially in patients for whom administration of Noradrenaline was followed by an increase in stroke-volume (the "SV-responders"). The authors conclude that their results demonstrate *in vivo* the gentle inotropic effect of Noradrenaline. In their study, both Gayat et al. [9] and Guinot et al. [11] used the Chen's algorithm. Our results are consistent with their observations, as we also observed a global increase in E_{es} if we used the Chen's algorithm (see Figure 8.7).

We also evaluated our V_0 estimation method from the perspective of the time-varying elastance transformation of the PV relationship. Especially, we verified that the normalised E(t) ($E^N\left(t^N\right)$) function calculated using our estimated V_0 was consistent with the observation made by Suga et al. [37] in which $E^N\left(t^N\right)$ was found very stable within and across subjects. We observed discrepancies between the $E^N\left(t^N\right)$ curve provided by Suga et al. [37] and our results. This can be explained by the different heart characteristics, as Suga et al. [37] involved explanted canine heart. We may expect differences related to different size of the canine as compared with human hearts. We may also hypothesised that our method tends to increase V_0 (as the isopressure method is the one which selected the steepest E_{es} for a given P_{es}), and in turn, increases globally E(t) (see Equation (8.1)). It may affect the ascending part of the $E^N\left(t^N\right)$ curve, which can in turn have impact on time-varying elastance modelling. This question has to be specifically addressed.

Also, the $E^N\left(t^N\right)$ curves analysis, reinforces the findings obtained in Chapter 7 as we observed that small errors in $E^N_{ao_d}$ may be translated into important errors in E_{es} estimation. In line with this results, we argued against the $E^N\left(t^N\right)$ curve-based E_{es} estimation methods.

Our results are limited by several factors. First, we did not use the reference method

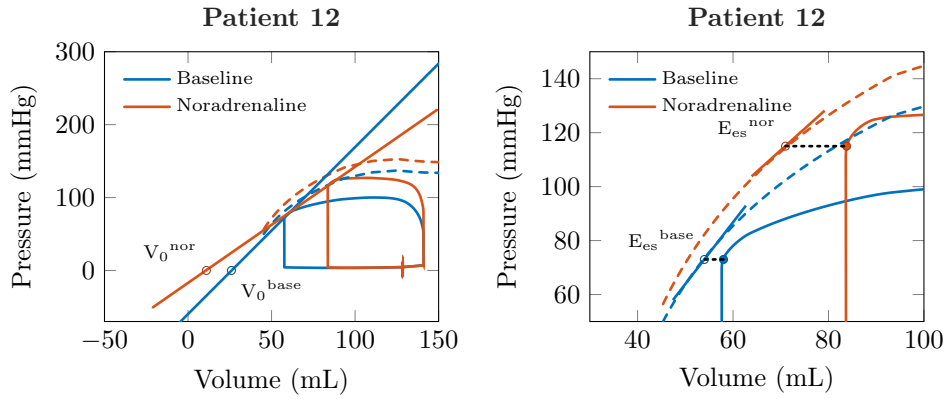

Figure 8.11 – Pathophysiological exploration of the effect of Noradrenaline on the V_0 and E_{es} estimations for Patient 12, using the static-isopressure method. **Left**: Pressure-volume (PV) loops (bold) plotted using calibrated simulations from the biomechanical model, the corresponding end-systolic pressure-volume relationship (ESPVR) (dashed), and their respective linearisation at the end-systolic pressure, before (base) and after the administration of Noradrenaline (nor). **Right**: A focus on the end-systolic PV point. In this patient Noradrenaline administration was followed by a 12% increased in contractility (τ_0), and a by a 140% increase in distal resistances (R_d). This translates into a slight upscaled of the ESPVR, and into a relatively more bigger shift of the operating end-systolic PV point to the right of the ESPVR. The net effect is a decrease both in V_0 (from 26 to 11 mL) and in E_{es} (from 2.29 to 1.59 mmHg.mL^{-1}). This is a demonstration of how E_{es} and V_0 may be dependent of the loading conditions. Even though an increase in inotropic state is observed, we observed a decrease in E_{es} because of its loading dependency. The balance between contractility variations and loading variations would probably be a better determinant of E_{es} rather than contractility variations alone.

for E_{es} and V_0 estimation method. This method involves invasive measurements performed in cardiac cathlab, as they require the measurement of the ESPVR. On top of the invasive intraventricular pressure and volume measurement, the ESPVR measurement necessitates invasive manoeuvres that modify preload (*e.g.* inflation of a balloon inside the *inferior vena cava*) [15], or afterload (*e.g.* tightening of aorta). This method is not suitable under clinical conditions. Second, our analysis was performed on a small subset of patients. It could have introduced selection bias, and our results should be confirmed in a larger study involving more patients. Third, our V_0 estimation method is not ideal since the slope of the linearised ESPVR (E_{es}) is derived directly from the theoretical ESPVR which is not reached during a cardiac cycle. The V_0 is found by shifting this slope to the P_{es} PV point. This may introduce inaccuracies with respect to the "true" E_{es} and the "true" V_0. However, E_{es} and V_0 are not physiological quantities, as they are constructed using the time-vaying elastance concept which is a geometrical description of the ESPVR rather than a physiological description. Therefore, no "true" E_{es} or V_0 can be measured, and their estimations are necessarily dependent on the approximations chosen for estimation.

8.5 Conclusion

This Chapter describes and evaluate the performance of a V_0 and E_{es} estimation method based on a calibrated biomechanical heart and vessels model. By using the derivative of the analytical description of the end-systolic pressure-volume relationship, we were able to defined E_{es} and the subsequent V_0. Our static-isopressure method was found to provide the most stable V_0 and E_{es} estimations as compared with the other five methods based on various biomechanical or phenomenological principles. By using our proposed method, we

were able to interpret the physiological effect of Noradrenaline, to estimate the complete E(t) function, and to verify the relative adequacy with the normalised E(t) observations made by Suga et al. [37]. Our method paved the way for a complete biomechanical description of a time-varying elastance model.

Bibliography

[1] Burkhoff, D. (2005). Assessment of systolic and diastolic ventricular properties via pressure-volume analysis: a guide for clinical, translational, and basic researchers. *AJP: Heart and Circulatory Physiology*, 289(2):H501–H512.

[2] Burkhoff, D., Sugiura, S., Yue, D. T., and Sagawa, K. (1987). Contractility-dependent curvilinearity of end-systolic pressure-volume relations. *American Journal of Physiology-Heart and Circulatory Physiology*, 252(6):H1218–H1227.

[3] Caruel, M., Chabiniok, R., Moireau, P., Lecarpentier, Y., and Chapelle, D. (2014). Dimensional reductions of a cardiac model for effective validation and calibration. *Biomechanics and Modeling in Mechanobiology*, 13(4):897–914.

[4] Caruel, M. and Truskinovsky, L. (2018). Physics of muscle contraction. *Reports on Progress in Physics*, page 50.

[5] Casas, B., Lantz, J., Viola, F., Cedersund, G., Bolger, A. F., Carlhäll, C.-J., Karlsson, M., and Ebbers, T. (2017). Bridging the gap between measurements and modelling: a cardiovascular functional avatar. *Scientific Reports*, 7(1).

[6] Chapelle, D., Le Tallec, P., Moireau, P., and Sorine, M. (2012). Energy-preserving muscle tissue model: formulation and compatible discretizations. *International Journal for Multiscale Computational Engineering*, 10(2).

[7] Chen, C.-H., Fetics, B., Nevo, E., Rochitte, C. E., Chiou, K.-R., Ding, P.-A., Kawaguchi, M., and Kass, D. A. (2001). Noninvasive single-beat determination of LV end-systolic elastance in humans. *JACC*, 38(7):2028–2034.

[8] Chen, J., Heldt, T., Verghese, G., and Mark, R. (2003). Analytical solution to a simplified circulatory model using piecewise linear elastance function. In *Computers in Cardiology, 2003*, pages 45–48, Thessaloniki Chalkidiki, Greece. IEEE.

[9] Gayat, E., Mor-Avi, V., Weinert, L., Yodwut, C., and Lang, R. M. (2011). Noninvasive quantification of LV elastance and ventricular-arterial coupling using 3D echo and arterial tonometry. *AJP: Heart and Circulatory Physiology*, 301(5):H1916–H1923.

[10] Grossman, W., Braunwald, E., Mann, T., McLaurin, L. P., and Green, L. H. (1977). Contractile state of the left ventricle in man as evaluated from end-systolic pressure-volume relations. *Circulation*, 56(5):845–852.

[11] Guinot, P.-G., Longrois, D., Kamel, S., Lorne, E., and Dupont, H. (2018). Ventriculo-Arterial Coupling Analysis Predicts the Hemodynamic Response to Norepinephrine in Hypotensive Postoperative Patients: A Prospective Observational Study. *Critical Care Medicine*, 46(1):e17–e25.

[12] Heldt, T., Shim, E. B., Kamm, R. D., and Mark, R. G. (2002). Computational modeling of cardiovascular response to orthostatic stress. *Journal of Applied Physiology*, 92(3):1239–1254.

[13] Kass, D. A., Maughan, W. L., Guo, Z. M., Kono, A., Sunagawa, K., and Sagawa, K. (1987). Comparative influence of load versus inotropic states on indexes of ventricular contractility: experimental and theoretical analysis based on pressure-volume relationships. *Circulation*, 76(6):1422–1436.

[14] Kass, D. A., Midei, M., Graves, W., Brinker, J. A., and Maughan, W. L. (1988). Use of a conductance (volume) catheter and transient inferior vena caval occlusion for rapid determination of pressure-volume relationships in man. *Catheterization and Cardiovascular Diagnosis*, 15:192–202.

[15] Kass, D. A., Yamazaki, T., Burkhoff, D., Maughan, W. L., and Sagawa, K. (1986). Determination of left ventricular end-systolic pressure-volume relationships by the conductance (volume) catheter technique. *Circulation*, 73(3):586–595.

[16] Kelly, R. P., Ting, C. T., Yang, T. M., Liu, C. P., Maughan, W. L., Chang, M. S., and Kass, D. A. (1992). Effective arterial elastance as index of arterial vascular load in humans. *Circulation*, 86(2):513–521.

[17] Kjørstad, K. E., Korvald, C., and Myrmel, T. (2002). Pressure-volume-based single-beat estimations cannot predict left ventricular contractility in vivo. *American Journal of Physiology-Heart and Circulatory Physiology*, 282(5):H1739–H1750.

[18] Land, S., Park-Holohan, S.-J., Smith, N. P., Kentish, J. C., and Niederer, S. A. (2017). A model of cardiac contraction based on novel measurements of tension development in human cardiomyocytes. *Journal of Molecular and Cellular Cardiology*, page 16.

[19] Le Gall, A., Laurin, A., Vallee, F., and Chemla, D. (2017). Comparison of Systolic Period Duration Using Aortic Flow or Pressure Based Methods in Anesthetized Patients. In *2017 Computing in Cardiology Conference*.

[20] Lee, J.-D., Tajimi, T., Widmann, T. F., and Ross, J. (1987). Application of end-systolic pressure-volume and pressure-wall thickness relations in conscious dogs. *Journal of the American College of Cardiology*, 9(1):136–146.

[21] McKay, R. G., Miller, M. J., Ferguson, J. J., Momomura, S.-I., Bs, P. S., Facc, W. G., and Facc, R. C. P. (1986). Assessment of left ventricular end-systolic pressure-volume relations with an impedance catheter and transient inferior vena cava occlusion: Use of this system in the evaluation of the cardiotonic effects of dobutamine, milrinone, posicor and epinephrine. *Journal of the American College of Cardiology*, 8(5):1152–60.

[22] Mirsky, I., Corin, W. J., Murakami, T., Grimm, J., Hess, O. M., and Krayenbuehl, H. P. (1988). Correction for preload in assessment of myocardial contractility in aortic and mitral valve disease. Application of the concept of systolic myocardial stiffness. *Circulation*, 78(1):68–80.

[23] Mirsky, I., Tajimi, T., and Peterson, K. L. (1987). The development of the entire end-systolic pressure-volume and ejection fraction-afterload relations: a new concept of systolic myocardial stiffness. *Circulation*, 76(2):343–356.

[24] Monge Garcia, M. I., Jian, Z., Settels, J. J., Hunley, C., Cecconi, M., Hatib, F., and Pinsky, M. R. (2018). Performance comparison of ventricular and arterial dP/dtmax for assessing left ventricular systolic function during different experimental loading and contractile conditions. *Critical Care*, 22(1):325.

[25] Olsen, C. O., Tyson, G. S., Maier, G. W., Spratt, J. A., Davis, J. W., and Rankin, J. S. (1983). Dynamic ventricular interaction in the conscious dog. *Circulation Research*, 1:20.

[26] Oommen, B., Karamanoglu, M., and Kovács, S. J. (2003). Modeling Time Varying Elastance: The Meaning of "Load-Independence". *Cardiovascular Engineering*, 3(4):123–130.

[27] Sagawa, K., Maughan, L., Suga, H., and Sunagawa, K. (1988). Cardiac contraction and the pressure volume relationship. In *Cardiac contraction and the pressure volume relationship*. Oxford University Press.

[28] Seemann, F., Arvidsson, P., Nordlund, D., Kopic, S., Carlsson, M., Arheden, H., and Heiberg, E. (2019). Noninvasive Quantification of Pressure-Volume Loops From Brachial Pressure and Cardiovascular Magnetic Resonance. *Circulation: Cardiovascular Imaging*, 12(1).

[29] Senzaki, H., Chen, C.-H., and Kass, D. A. (1996). Single-Beat Estimation of End-Systolic Pressure-Volume Relation in Humans: A New Method With the Potential for Noninvasive Application. *Circulation*, 94(10):2497–2506.

[30] Shishido, T., Hayashi, K., Shigemi, K., Sato, T., Sugimachi, M., and Sunagawa, K. (2000). Single-Beat Estimation of End-Systolic Elastance Using Bilinearly Approximated Time-Varying Elastance Curve. *Circulation*, 102(16):1983–1989.

[31] Sodums, M. T., Badke, F. R., Starling, M. R., Little, W. C., and O'Rourke, R. A. (1984). Evaluation of left ventricular contractile performance utilizing end-systolic pressure-volume relationships in conscious dogs. *Circulation Research*, 54(6):731–739.

[32] Starling, M. R. (1993). Left ventricular-arterial coupling relations in the normal human heart. *American Heart Journal*, 125(6):1659–1666.

[33] Stergiopulos, N., Meister, J. J., and Westerhof, N. (1996). Determinants of stroke volume and systolic and diastolic aortic pressure. *American Journal of Physiology-Heart and Circulatory Physiology*, 270(6):H2050–H2059.

[34] Suga, H. (1969). Time course of left ventricular pressure-volume relationship under various enddiastolic volume. *Japanese Heart Journal*, 10(6):509–515.

[35] Suga, H. (1970). Time Course of Left Ventricular Pressure-Volume Relationship under Various Extents of Aortic Occlusion. *Japanese Heart Journal*, 11(4):373–378.

[36] Suga, H. (1979). Total mechanical energy of a ventricle model and cardiac oxygen consumption. *American Journal of Physiology-Heart and Circulatory Physiology*, 236(3):H498–H505.

[37] Suga, H., Sagawa, K., and Shoukas, A. A. (1973). Load Independence of the Instantaneous Pressure-Volume Ratio of the Canine Left Ventricle and Effects of Epinephrine and Heart Rate on the Ratio. *Circulation Research*, 32(3):314–322.

[38] Takeuchi, M., Igarashi, Y., Tomimoto, S., Odake, M., Hayashi, T., Tsukamoto, T., Hata, K., Takaoka, H., and Fukuzaki, H. (1991). Single-beat estimation of the slope of the end-systolic pressure-volume relation in the human left ventricle. *Circulation*, 83:202–212.

[39] Ten Brinke, E. A., Klautz, R. J., Verwey, H. F., Van Der Wall, E. E., Dion, R. A., and Steendijk, P. (2010). Single-beat estimation of the left ventricular end-systolic pressure–volume relationship in patients with heart failure: Single-beat ESPVR in heart failure patients. *Acta Physiologica*, 198(1):37–46.

[40] van der Velde, E. T., Burkhoff, D., Steendijk, P., Karsdon, J., Sagawa, K., and Baan, J. (1991). Nonlinearity and load sensitivity of end-systolic pressure-volume relation of canine left ventricle in vivo. *Circulation*, 83(1):315–327.

[41] Wong, J., Pushparajah, K., de Vecchi, A., Ruijsink, B., Greil, G. F., Hussain, T., and Razavi, R. (2017). Pressure–volume loop-derived cardiac indices during dobutamine stress: a step towards understanding limitations in cardiac output in children with hypoplastic left heart syndrome. *International Journal of Cardiology*, 230:439–446.

CHAPTER 9

Time-varying Elastance model derived from biomechanical heart and vessel model

The time-varying elastance concept is useful for cardiovascular modelling as it allows to represent a surrogate of cardiac mechanics during systole, and to estimate the left ventricular (LV) pressure-volume (PV) relationship throughout a cardiac cycle. In this Chapter, we use a cardiovascular model based on E(t) function that was derived from a calibrated version of a full biomechanical model (0_D model). This framework, coupled with valve laws and Windkessel model allows to simulate cardiovascular physiology. We aimed to evaluate the properties of the E(t) model when varying conditions that could affect the cardio-vascular physiology. In *in silico* experiments performed from a patient dataset, we observed that the results of the E(t) model were consistent with those obtained with the 0_D model, even when we varied the preload, the afterload, the contractility and the heart rate. These results were confirmed by another *in silico* experiment in which we varied the stroke volume (SV) and the end-systolic pressure (P_{es}) by up to 50% the original quantities. We also performed *in silico* testing on 61 datasets obtained in 45 patients in which afterload and preload were varied by up to 20%. During each experiment, we observed that the differences observed between the E(t) and the 0_D models were small and clinically not relevant. We finally tested in *real life* conditions the performance of the E(t) model to reproduce the outputs of the 0_D model. On 5 patients in which two sets of calibration were available (at baseline and at peak effect of noradrenaline), we adjusted the parameters of the two models from baseline calibration to the new noradrenaline peak effect condition and observed again that the differences observed between the outputs of the two models were clinically not relevant. In other words, the clinical decision-making would be similar when interpreting the results of both models. Our study offers perspective to transfer biomechanical modelling into clinical settings, by improving the computational time close to real-time, a condition that is suitable for cardiovascular monitoring purposes during general anaesthesia or when treating life-threatened patients in critical care units.

9.1 Introduction

The purpose of this chapter is to present and analyse a framework composed by a time-varying elastance model fully derived by a complete and patient-specific biomechanical model of heart and vessels. In the previous Chapter 8, we proposed a method to estimate the E(t) function, from a calibrated version of our reduced order biomechanical model. In the present chapter, we will evaluate a modelling framework in which we replace the active part of the biomechanical model by the biomechanically-derived E(t) function. This time-varying elastance model will be compared against the complete biomechanical model. We will perform several experiments using up to 61 patients' datasets recorded during general anaesthesia in which the parameters of the models were deviated from original calibrated conditions. We will compare the outputs of the time-varying elastance model with the outputs of the biomechanical model for each tested condition.

9.2 Method

9.2.1 Calibration of the biomechanical model

We used patient-specific versions of the reduced order biomechanical heart model, described in Chapter 1, following the methodology described in details in Chapter 10. In brief, the complete biomechanical 3D model described in Chapelle et al. [3] was reduced assuming a spherical geometry for the heart cavities [2], keeping all the physical and biomechanical properties as in the 3D model. The parameters used in the simulations which will be modified in the sensitivity analysis are exemplified in table 8.1

We used many sets of calibration to perform our tests. From our database, we selected 1 patient (Patient 12) to perform the *in silico* qualitative testing (see below). The main patient specific parameters used for this patient are as follows:

- Geometry
  - Sphere radius = 3 cm
  - Sphere thickness = 0.83 cm
- Activation (see Chapter 1, Section 1.5.2.4 and Figure 1.20)
  - Activation time = [0.095 ; 0.38 ; 0.465 ; 0.475] seconds.
  - Amplitude = [-20 ; +35] μVolts.
- Passive properties
  - Passive law parameters = [637 ; 2.4 ; 99 ; 5.5].
- Active properties
  - Myosin head detachment rate = 12 kPa.s^{-1}
  - Contractility (τ_0) = 85 kPa
- Windkessel parameters
  - distal capacitance = 1.82e-08 cm^3.Pa^{-1}
  - proximal resistance = 1.76e07 Pa.s.cm^{-3}
  - proximal capacitance = 1.92e-10 cm^3.Pa^{-1}

To confirm the results in a larger population, we used the calibrated dataset originated from the complete 45 patients database among which 16 having 2 sets of calibration, at baseline and at maximum effect of Noradrenaline.

Finally, we used two sets of calibrated data at baseline and at peak effect of Noradrenaline originated from 5 patients (Patient 11, 16, 18, 21, 69) to perform a *real life* experiment.

9.2.2 Static-isopressure estimation of E_{es}, V_0, and $E(t)$

The method is described in details in Chapter 8. In brief, we used a method based on the local derivative of ESPVR to estimate E_{es}, which is subsequently used to estimate V_0. We identified the ESPVR point by looking for the end-systolic pressure-volume (PV) point on the PV loop. Thereafter, we looked for the isopressure point on the ESPVR. We finally calculated the first derivative of Equation (9.1) to estimate the end-systolic elastance E_{es}

$$\begin{cases} P_{0_D} = \epsilon \cdot \Sigma_{\text{sphere}}\left(e_{fib}\right) \cdot \left(1 + e_{fib}\right) \left(1 + e_{fib} - \dfrac{\epsilon}{2}(1 + e_{fib})^{-2}\right)^{-2} \left(1 + \epsilon\left(1 + e_{fib}\right)^{-3}\right)^{-1} \\ \Sigma_{\text{sphere}}\left(e_{fib}\right) = \frac{n_0(e_{fib}) \cdot \tau_0}{1 + e_{fib}} + 4\left(1 - C^{-3}\right) \frac{\partial W_e}{\partial J_1} + 2\frac{\partial W_e}{\partial J_4} \end{cases} \tag{9.1}$$

with P_{0_D} the theoretical pressure the heart model can reach for a given fibre extension e_{fib}, ϵ a geometrical term accounting for the myocardium thickness related to the radius of the sphere at reference configuration, Σ_{sphere} the maximal stress at e_{fib}, $n_0\left(e_{fib}\right)$ the Starling effect at e_{fib}, τ_0 the contractility, W_e the hyperelastic potential, $J_1 = I_1 \cdot {I_3}^{-\frac{1}{3}}$ and $J_4 = I_4 \cdot {I_3}^{-\frac{1}{3}}$, the reduced invariants of the Cauchy-Green strain tensor, $I_3 = \det\left(\underline{\underline{C}}\right)$, and $C = (1 + e_{fib})^2$ the circumferential component of the Cauchy-Green strain tensor.

Finally, we applied the estimated E_{es} at the end-systolic PV point P_{es} to estimate the intercept of the linear function – *i.e.* V_0. We calculated the complete time-varying elastance function from the original calibrated setting, using Equation (9.2):

$$E(t) = \frac{P(t)}{V(t) - V_0} \tag{9.2}$$

9.2.3 Modelling heart and vessels using biomechanically derived $E(t)$

In the time-varying elastance model, the active and passive components of the biomechanical model are substituted by the following laws:

$$\begin{cases} P(t) = E\left(t\right) \cdot \left[V\left(t\right) - V_0\right] - \eta_V^s \dot{V} & \text{(Systole)} \\ P(t) = \text{EDPVR}\left(V, t\right) + \eta_V^d \dot{V} & \text{(Diastole)} \end{cases} \tag{9.3}$$

with EDPVR representing the static pressure-volume relationship of a filled heart (described in details in Part II), $E(t)$ the Time-varying elastance function, $P(t)$, the ventricular pressure throughout a cardiac cycle, $V(t)$ the ventricular volume throughout a cardiac cycle, V_0 the intercept of the linearised ESPVR, and $\eta_V^s \dot{V}$ and $\eta_V^d \dot{V}$ a regularising terms accounting for cardiac viscosity.

The problem is solved by using the valve Law described by the following state equations (Figure 9.1):

$$\begin{cases} C_v \dot{P}_{0_D} = Q_v + Q_{at} - Q_{ao} \\ P_{at} - P_{0_D} = L_{at} \dot{Q}_{at} + \left(K_{at}{}^{\text{for/back}}\right)^{-1} Q_{at} \\ P_{0_D} - P_{ao} = L_{ar} \dot{Q}_{ao} + \left(K_{ao}{}^{\text{for/back}}\right)^{-1} Q_{ao} \end{cases} \tag{9.4}$$

with $Q_v = -\dot{V}$, the derivative in time of the ventricular volume, C_v the ventricular capacitance, Q_{at} and Q_{ao} respectively the atrial valve inflow and the aortic valve outflow, P_{at} and P_{ao} respectively the pressure at the entrance of the valve system and the output pressure of the model, L_{at} and L_{ar} respectively the inductance of the atrial and arterial valve, K_{at} and K_{ao} respectively the conductance of the atrial and arterial valve, and P_{0_D} the ventricular pressure.

Using this framework, we were able to vary the parameters to evaluate the correspondence with the biomechanical model when varying conditions.

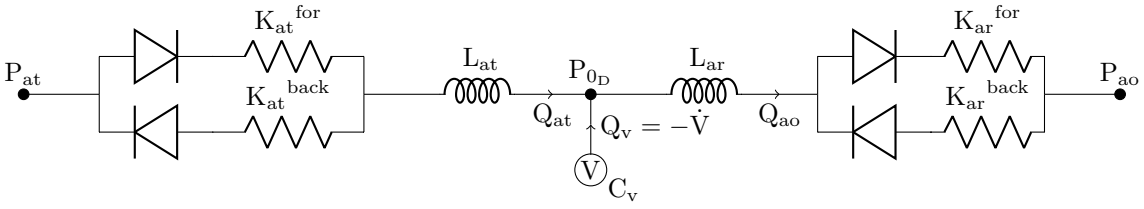

Figure 9.1 – Schematic representation of the valve law. $Q_v = -\dot{V}(t)$, *the derivative in time of the ventricular volume* V, C_v *the ventricular capacitance,* Q_{at} *and* Q_{ar} *respectively the atrial valve inflow and the arterial valve outflow,* P_{at} *and* P_{ar} *respectively the pressure at the beginning of the valve low and the output pressure of the model,* L_{at} *and* L_{ar} *respectively the inductance of the atrial and arterial valve,* K_{at} *and* K_{ar} *respectively the conductance of the atrial and arterial valve, and* $P(t)$ *the ventricular pressure.*

9.2.4 Experiments to evaluate models adequacy

We used the calibrated datasets described in Section 9.2.1. From these conditions, we estimated E_{es}, V_0 and E(t) according to the procedure described in Section 9.2.2.

First *in silico* experiments were performed using one patient calibrated dataset (Patient 12). We first verified the adequacy between the biomechanical and the time-varying elastance models at this reference condition. We subsequently evaluated the transition phase – the behaviour of both models to reach the equilibrium when a perturbation of initial condition (*e.g.* here the initial pressure) is applied. Third we modified the afterload, the preload, the contractility and the heart rate of both the biomechanical and the time-varying elastance models. The magnitude of change of initial parameters ranged between -40 to +40% the original parameters. At each step we compared the outputs of the two models.

Second *in silico experiment* was performed using the calibrated dataset originated from the complete database (n= 61 datasets). We used the calibrated datasets as the original condition and we deviated the preload and the afterload by ± 20%, in order to confirm the results obtained at the preceding stage.

Third, we realised a *real life* experiment in which we used the calibrated dataset originated from 5 patients at baseline. We estimated E(t) function for these 5 patients and applied the calibrated parameters obtained for peak effect of Noradrenaline condition. We upscaled the E(t) curve by the proportional factor that linked the contractility parameter of the biomechanical model at baseline and at peak effect of Noradrenaline. We compared the output of the calibrated biomechanical model with the outputs of the modified time-varying elastance model at peak effect of Noradrenaline.

9.2.5 Outcomes

In order to evaluate the adequacy between the models, we considered the following indicators: 1/ mean (P_{aom}), systolic (P_{aos}) and diastolic aortic (P_{aod}) aortic pressures; 2/ minimum (V_{es}) and maximum (V_{ed}) ventricular volumes; 3/ stroke volume (SV) and ejection fraction (EF); 4/ end-systolic pressure (P_{es}); 5/ end systolic elastance (E_{es}), arterial elastance (E_a), ventricular arterial coupling (V_{va}) and; 6/ internal work (I_w), external work (E_w), cardiac efficiency (CE).

9.2.6 Statistical analysis

The results are presented as median and interquartile ranges (IQR), or as number and percentage. The comparison between the outputs of the biomechanical and the time-varying elastance models was performed using a student t-test, with a p value below 0.05 considered as significant.

9.3 Results

9.3.1 Comparison between complete biomechanical biomechanical model and time-varying elastance derived model: Detailed analysis on 1 patient

9.3.1.1 Correspondence with biomechanical model at initial condition

We used the parameters obtained from the original calibrated condition described in Section 9.2.1.

We verified that for the original calibrated condition, the time-varying elastance model and the biomechanical model corresponded. This is shown in Figure 9.2. We observed small differences in the filling of the heart (upper right and bottom left panels of Figure 9.2). However, the end-systolic pressure, the systolic aortic and ventricular pressure, the aortic diastolic pressure, the stroke volume, and the mean aortic pressure are not distinguishable.

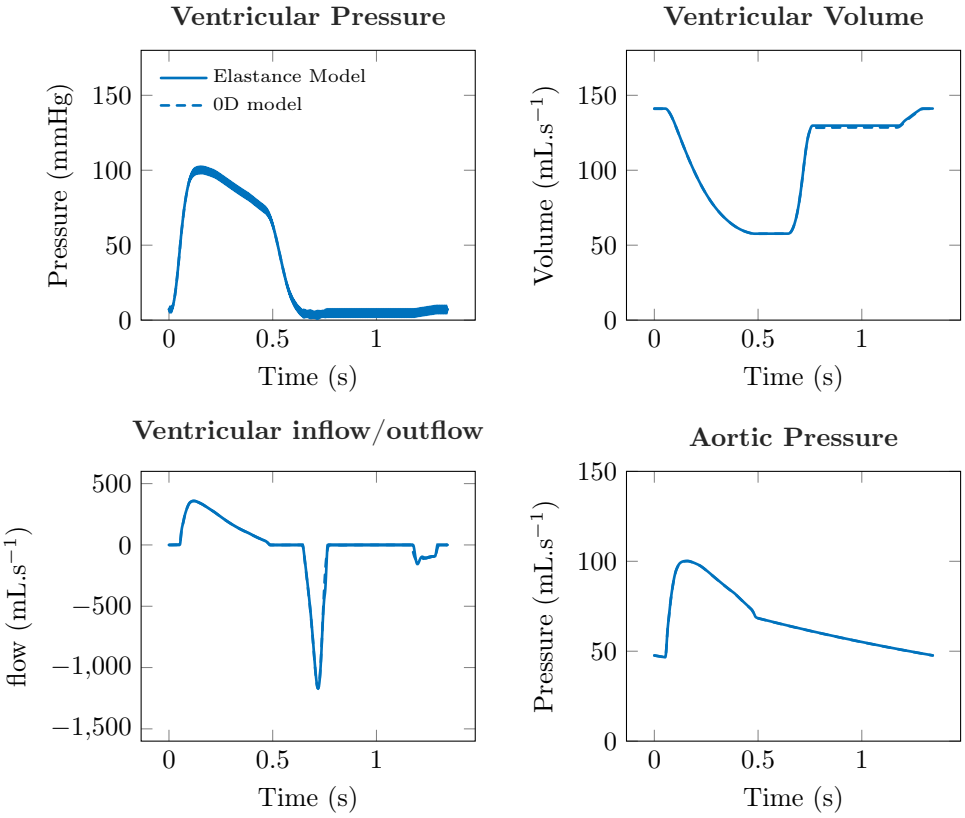

Figure 9.2 – Comparison between time-varying elastance and biomechanical models at equilibrium. Each panel represents outputs of both the time-varying elastance and the biomechanical model.

9.3.1.2 Initial pressure modification

In this section, we aimed to modify the initial condition of the previously calibrated configuration described in Section 9.2.1, in order to analyse the convergence rate of the two models.

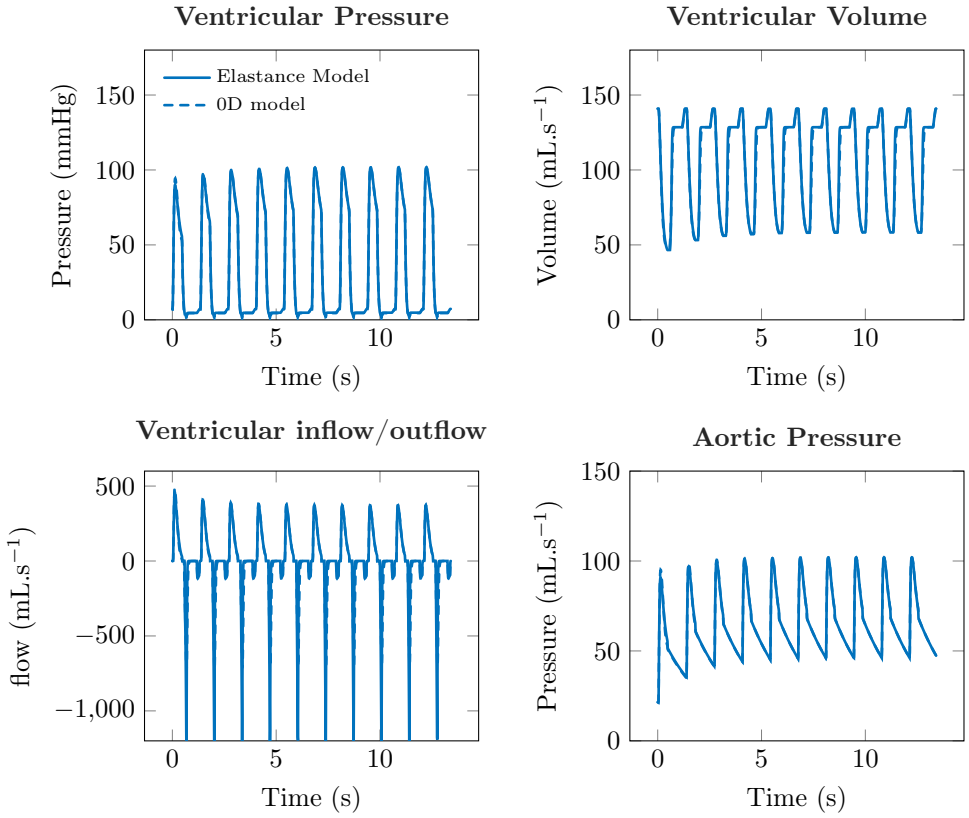

Figure 9.3 – Comparison between time-varying elastance and biomechanical models. The four panels represents the respective outputs of the two models at calibrated conditions, when decreasing the initial pressure by half the original configuration.

We chose to modify the initial pressure parameter, by increasing or decreasing it by half times the original value. The expected behaviour is a slow return to the results observed in Figure 9.2. Figure 9.3 demonstrated the effects of decreasing the initial pressure by half the original configuration. The results are similar when increasing the initial pressure from the original condition. As in Section 9.3.1.1, we observed in the end of the simulations, that the outputs are superimposed except when considering the filling rate of the ventricle. However, all the clinically pertinent information are not perturbated when using the time-varying elastance model as compared with the biomechanical model. Figure 9.3 showed also the transition time, during which the models equilibrate themselves. We observed that the convergence rates are similar for both models.

9.3.1.3 Afterload modification – Detailed analysis

In this section, we investigated the effect of afterload variation on the respective outputs of the two models. By definition, the time-varying elastance model should not be affected by afterload modification. However, its cardiac mechanics during systole is defined by the E(t) function, itself estimated by linearising end-systolic conditions. We demonstrated in Chapter 8 that our method to estimate E(t) was sensitive to loading condition (but to

a smaller extent than other available methods). To address this issue using time-varying elastance model, we aimed to evaluate the sensitivity of the outputs of the time-varying elastance model to afterload variations.

From the original calibrated condition, we sequentially modified the distal resistance parameter (R_d) from -40% to +40% the original R_d (1.184407e08 Pa.s.cm^{-3}). In order to maintain the diastolic time constant ($\tau = R_d \times C_d$), we also divided the distal capacitance (C_d) by the corresponding R_d modification factor.

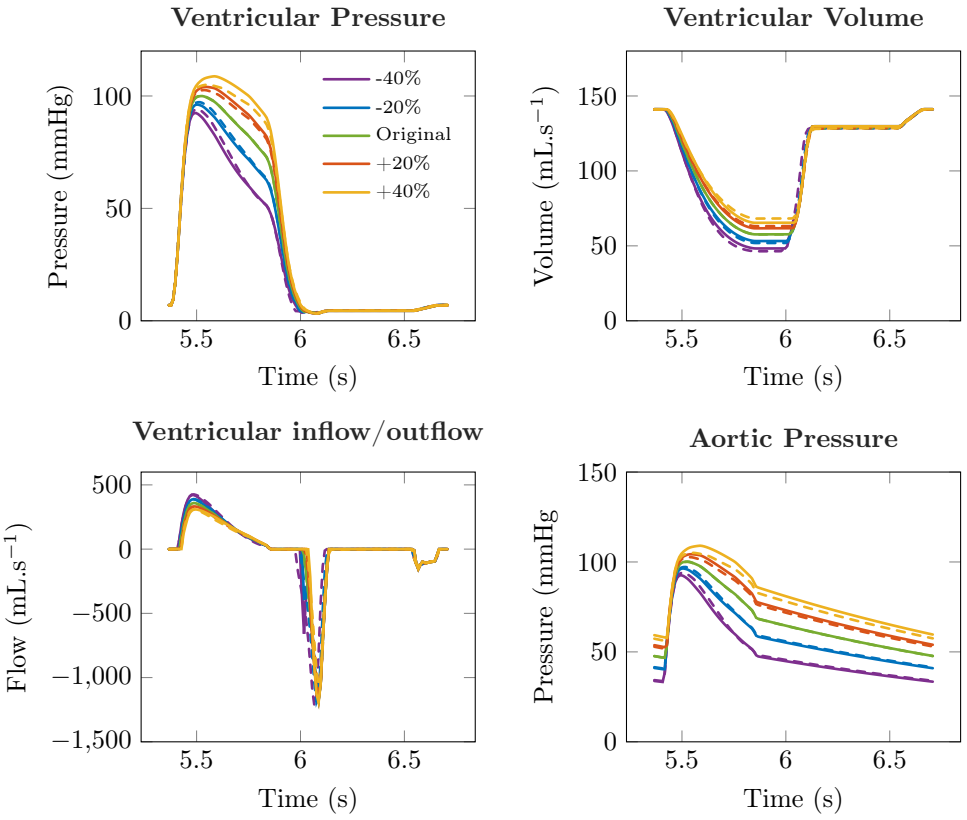

Figure 9.4 – Results of the *in silico* afterload variation experiment. The 4 panels show the final heartbeats of a 5-cycles simulation performed using the time-varying elastance (solid) and the biomechanical (dashed) models.

Figure 9.4 and Table 9.1 show the final five beats results of the *in silico* experiment. Only small discrepancies are observed, predominantly during maximal systole (P_{aos}). The filling rate of the LV also displays differences between the time-varying and the biomechanical models. However, when looking at the indicators that are clinically pertinent (P_{aom}, SV, P_{aod}) we could consider the two models consistent.

We investigated into details the reasons of these discrepancies. Figure 9.5 provides PV loop assessment, with the linearised ESPVR. Again, we observed that each PV loops, characterised by its end-systolic PV point, is located close to the linearised ESPVR. Most of the differences observed between the two models are held by differences in the dynamic of the cardiac contraction, and not by end-systolic characteristics. Indeed, the end-systolic conditions are not affected by afterload variations, for both models, when considering reasonable ranges of variation.

Table 9.1 – Comparison between biomechanical (0_D) and time-varying elastance (E(t)) models for various afterload. Original: the calibrated version of the models. The afterload was modified by changing distal resistance and capacitance in the Windkessel model by -40% to + 40%.

	Original		+20%		+40%		-20%		-40%	
	0_D	E(t)	0_D	E(t)	0_D	E(t)	0_D	E(t)	0_D	E(t)
Aortic Pressures										
P_{aom} (mmHg)	67	67	73	74	78	80	60	59	51	50
P_{aos} (mmHg)	100	100	103	104	105	109	97	96	94	93
P_{aod} (mmHg)	47	47	52	52	56	58	41	40	34	33
Systolic outputs										
SV (mL)	83	83	78	79	73	76	89	88	95	93
EF (%)	0.59	0.59	0.55	0.56	0.52	0.54	0.63	0.62	0.67	0.66
Ventricular outputs										
P_{es} (mmHg)	73	73	81	82	87	90	63	63	50	51
V_{es} (mL)	58	58	63	62	68	65	52	53	46	48
V_{ed} (mL)	141	141	141	141	141	141	141	141	141	141
Bioenergetics										
I_w (Joules)	0.28	0.28	0.37	0.36	0.45	0.43	0.2	0.2	0.12	0.13
E_w (Joules)	0.99	0.99	0.96	1	0.93	1.01	1	0.97	0.99	0.95
CE (%)	0.78	0.78	0.72	0.74	0.67	0.7	0.83	0.83	0.89	0.88
Ventricular arterial coupling										
E_{es} (mmHg.mL^{-1})	2.28	2.28	2.19	2.28	2.07	2.31	2.42	2.33	2.5	2.32
E_a (mmHg.mL^{-1})	1.26	1.26	1.29	1.32	1.28	1.38	1.21	1.19	1.09	1.06
V_{va}	0.55	0.55	0.59	0.58	0.62	0.6	0.5	0.51	0.44	0.46

P_{aom}: mean aortic pressure; P_{aos}: systolic aortic pressure; P_{aod}: diastolic aortic pressure; SV: stroke volume; EF: ejection fraction; P_{es}: end-systolic pressure; V_{es}: end-systolic-volume; V_{ed}: end-diastolic volume; P_{ed}: end-diastolic pressure; I_w: internal work; E_w: external work; CE: cardiac efficiency; E_{es}: end-systolic elastance; E_a: arterial elastance; V_{va}: ventricular-arterial coupling.

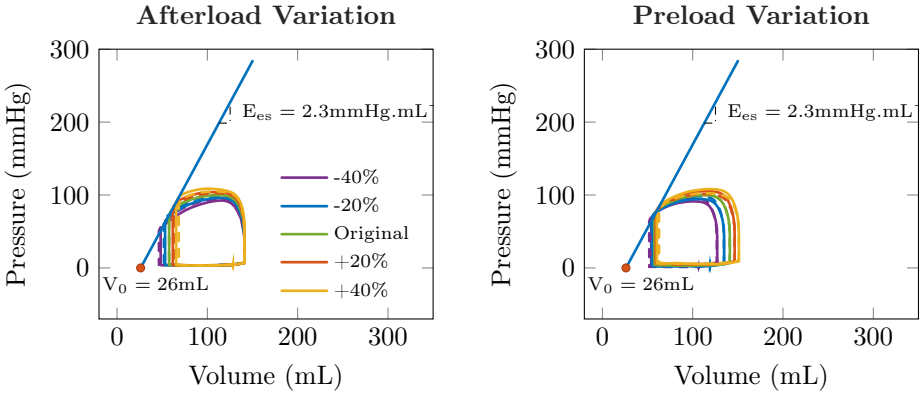

Figure 9.5 – Effect of afterload (**Left**) and of preload (**Right**) variations on the difference between the time-varying elastance and the biomechanical models. Pressure-volume loop representation.

9.3.1.4 Preload modification – Detailed analysis

In this section, we investigated the effect of changes in preload on the output observed with the time-varying elastance model, compared with the biomechanical model.

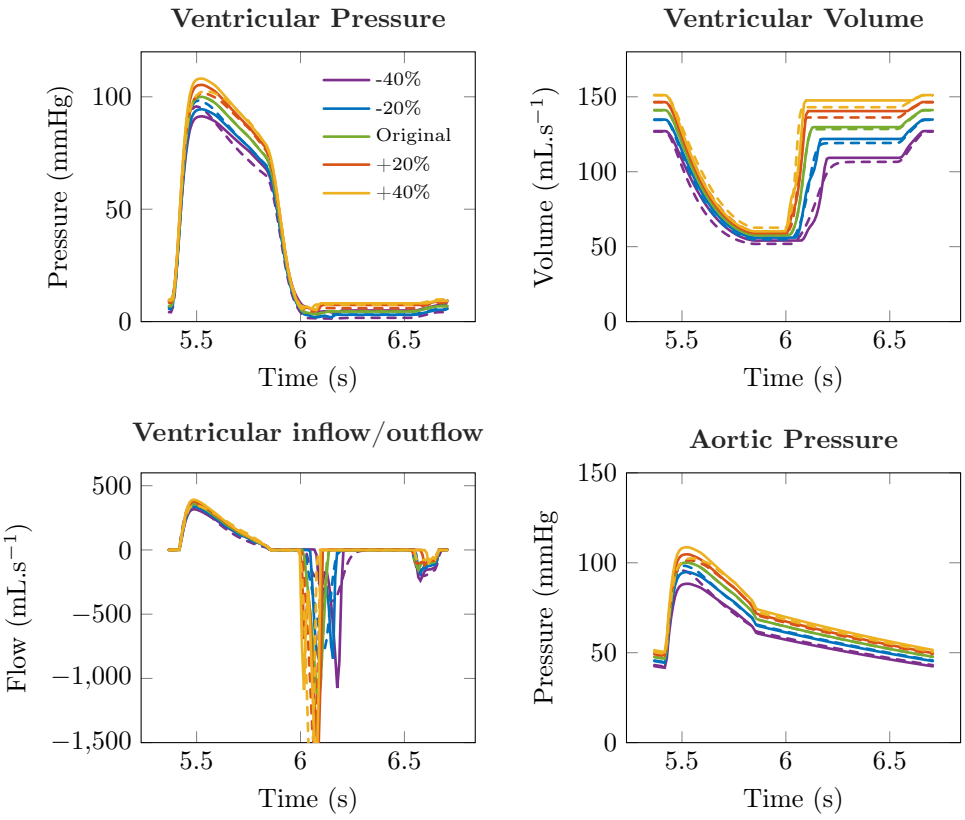

Figure 9.6 – Results of the *in silico* preload variation experiment. The 4 panels plot show the final heartbeat of a 5-cycles simulation performed using the time-varying elastance (solid) and the biomechanical (dashed) models.

Figure 9.6 and Table 9.2 demonstrates the results of the comparative simulations between the time-varying elastance and the biomechanical model for variations of prescribed preload ranging from -40 to +40% the original preload (7 mmHg). As expected, we observed small discrepancies between the time-varying elastance and the biomechanical models, concerning mostly the maximal pressures (ventricular or aortic). The filling rate of the ventricle is also affected, but with little effects on the pertinent clinical indicators (P_{aod}, P_{aom}, and SV).

We also investigated the differences observed in pressure-volume loop space. Figure 9.5 demonstrated the pressure-volume loops associated with the results presented in Figure 9.6. Again, we observed that most of the differences between the time-varying elastance and the biomechanical models are related to systolic pressures. Also, we can observe that for both the models the 5 PV loops are located on the same linearised ESPVR (with $V_0 = 26$ mL and $E_{es} = 2.3$ mmHg.mL^{-1}). This is an important result because, since that, the end-systolic conditions, and therefore the stroke volume, the mean pressures, the diastolic pressures, are consistent with respect to the time-varying elastance concept and across the two models used. Hence, the differences observed in maximal systole are mostly related to the characteristics of the cardiac contraction and therefore, caused by the biomechanical model as the cardiac mechanics of the time-varying elastance model is driven only by a unique E(t) function. These differences are probably caused by an ef-

Table 9.2 – Comparison between biomechanical (0_D) and time-varying elastance (E(t)) models for various preload. Original: the calibrated version of the models. The afterload was modified by changing distal resistance and capacitance in the Windkessel model by -40% to + 40%

	Original		+20%		+40%		-20%		-40%	
	0_D	E(t)	0_D	E(t)	0_D	E(t)	0_D	E(t)	0_D	E(t)
Aortic Pressures										
P_{aom} (mmHg)	67	67	69	70	70	72	64	63	61	59
P_{aos} (mmHg)	100	100	101	105	102	109	98	95	96	88
P_{aod} (mmHg)	47	47	48	49	49	50	45	44	42	42
Systolic outputs										
SV	83	83 (mL)	86	87	88	91	80	79	75	73
EF	0.59	0.59 (%)	0.59	0.6	0.58	0.6	0.59	0.59	0.59	0.57
Ventricular outputs										
P_{es} (mmHg)	73	73	76	76	78	80	69	70	64	68
V_{es} (mL)	58	58	60	59	63	60	55	56	52	54
V_{ed} (mL)	141	141	146	146	151	151	135	135	127	127
P_{ed} (mmHg)	7	7	8.4	8.4	9.8	9.8	5.6	5.6	4.2	4.2
Bioenergetics										
I_w (Joules)	0.28	0.28	0.31	0.3	0.34	0.32	0.25	0.26	0.21	0.24
E_w (Joules)	0.99	0.99	1.03	1.07	1.06	1.14	0.93	0.9	0.85	0.78
CE (%)	0.78	0.78	0.77	0.78	0.76	0.78	0.79	0.78	0.8	0.76
Ventricular arterial coupling										
E_{es} (mmHg.mL^{-1})	2.28	2.28	2.24	2.3	2.11	2.35	2.38	2.33	2.46	2.43
E_a (mmHg.mL^{-1})	1.26	1.26	1.27	1.29	1.24	1.33	1.25	1.25	1.23	1.26
V_{va}	0.55	0.55	0.57	0.56	0.59	0.57	0.53	0.54	0.5	0.52

P_{aom}: mean aortic pressure; P_{aos}: systolic aortic pressure; P_{aod}: diastolic aortic pressure; SV: stroke volume; EF: ejection fraction; P_{es}: end-systolic pressure; V_{es}: end-systolic-volume; V_{ed}: end-diastolic volume; P_{ed}: end-diastolic pressure; I_w: internal work; E_w: external work; CE: cardiac efficiency; E_{es}: end-systolic elastance; E_a: arterial elastance; V_{va}: ventricular-arterial coupling

fect of the loading condition on the velocity/length relationship of the cardiac contraction which depends on external loading conditions (see Chapter 8 Figure 8.6). This hypothesis should be studied in an extensive analysis of both models.

9.3.1.5 Contractility estimation

In this Section, we compared the outputs of the biomechanical with the outputs of the time-varying elastance models when we changed contractility ($\tau_0^{\text{original}} = 85$kPa). We modified in the biomechanical model the contractility by -40% to +40%. In the time-varying elastance model, we multiplied the whole E(t) function by -40% to +40%. Figure 9.7 shows the results of this *in silico* experiment. Figure 9.8 presented the results in a PV loop form.

In this experiment, we can observe that for small variation of contractility (-20% to +20%), which is a modification which is clinically pertinent for anaesthesia and/or intensive care purposes, the main behaviour of the time-varying elastance model looks similar to the biomechanical model. However, when deviating more from original condition, significant differences appeared. If we look qualitatively, most of the difference is held by maximum systolic condition. Systolic volume and pressure are lower with the biomechanical model as compared with the time-varying elastance model, when decreasing the

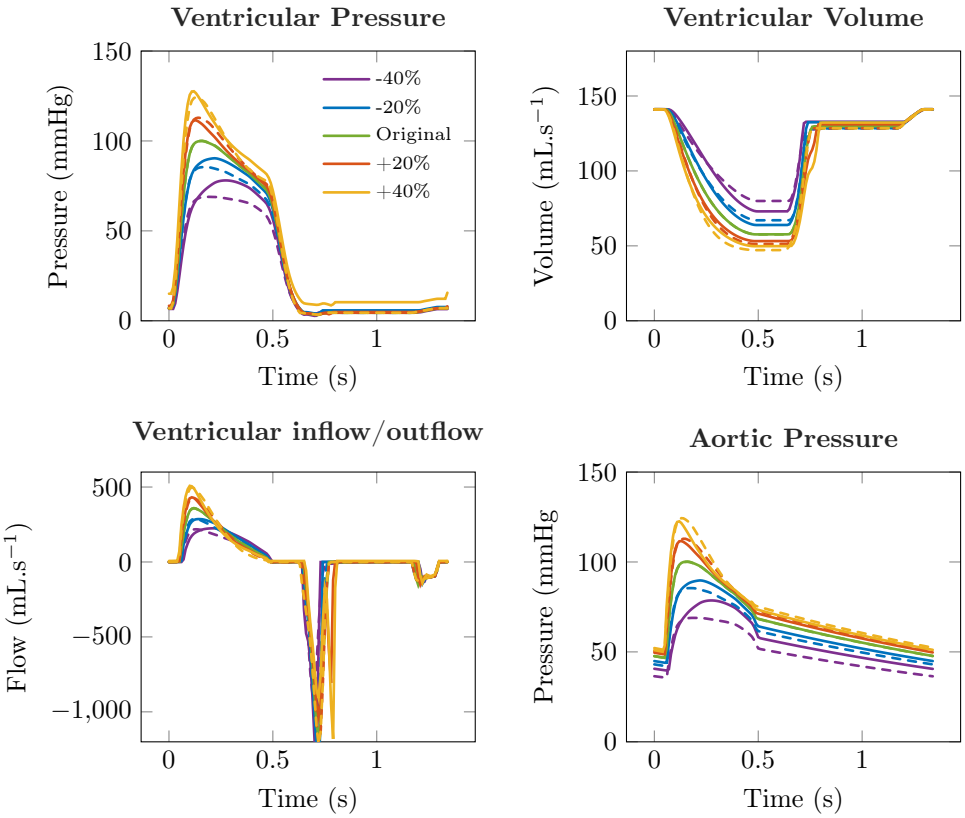

Figure 9.7 – Results of the *in silico* contractility variation experiment. The 4 panels show the final heartbeats of a 5-cycles simulation performed using the E(t) (solid) and the biomechanical (dashed) models.

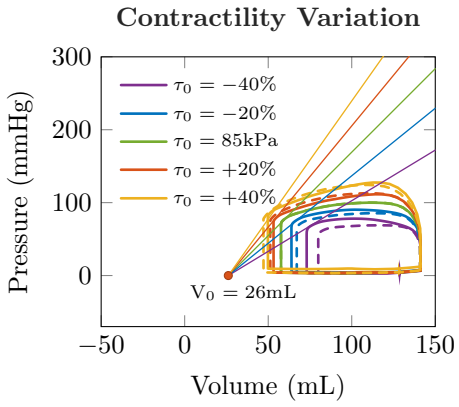

Figure 9.8 – Effect of the contractility variations on the difference between the time-varying elastance and the biomechanical models. Pressure-volume loop representation.

Table 9.3 – Comparison between biomechanical (0_D) and time-varying elastance (E(t)) models for various contractility. Original: the calibrated version of the models. The afterload was modified by changing distal resistance and capacitance in the Windkessel model by -40% to + 40%.

	Original		+20%		+40%		-20%		-40%	
	0_D	E(t)	0_D	E(t)	0_D	E(t)	0_D	E(t)	0_D	E(t)
Aortic Pressures										
P_{aom} (mmHg)	67	67	71	70	74	73	60	62	50	55
P_{aos} (mmHg)	100	100	113	112	124	123	85	90	69	79
P_{aod} (mmHg)	47	47	49	49	51	50	42	44	36	40
Systolic outputs										
SV (mL)	83	83	90	88	94	91	74	77	61	68
EF (%)	0.59	0.59	0.64	0.62	0.67	0.65	0.52	0.55	0.43	0.48
Ventricular outputs										
P_{es} (mmHg)	73	73	75	74	76	81	68	71	59	64
V_{es} (mL)	58	58	51	53	47	50	67	64	80	73
Bioenergetics										
I_w (Joules)	0.28	0.28	0.23	0.24	0.19	0.24	0.34	0.33	0.38	0.38
E_w (Joules)	0.99	0.99	1.18	1.13	1.35	1.25	0.76	0.83	0.5	0.63
CE (%)	0.78	0.78	0.84	0.82	0.88	0.84	0.69	0.72	0.57	0.62
Ventricular arterial coupling										
E_{es} (mmHg.mL^{-1})	2.28	2.28	3	2.74	3.62	3.38	1.66	1.87	1.09	1.43
E_a (mmHg.mL^{-1})	1.26	1.26	1.47	1.4	1.62	1.62	1.01	1.11	0.74	0.92
V_{va}	0.55	0.55	0.49	0.51	0.45	0.48	0.61	0.59	0.68	0.64

P_{aom}: mean aortic pressure; P_{aos}: systolic aortic pressure; P_{aod}: diastolic aortic pressure; SV: stroke volume; EF: ejection fraction; P_{es}: end-systolic pressure; V_{es}: end-systolic-volume; V_{ed}: end-diastolic volume; P_{ed}: end-diastolic pressure; I_w: internal work; E_w: external work; CE: cardiac efficiency; E_{es}: end-systolic elastance; E_a: arterial elastance; V_{va}: ventricular-arterial coupling

contractility or the E(t) function by 40%. The value for minored contractility is 51 kPa.

End-systolic conditions are also affected differently when looking at the PV representation. One explanation could be that to consider the increase in contractility, we had to modify the mechanics of the time-varying elastance model. We use a simple proportional change from the original E(t) function. Therefore, not only the maximal elastance was modified but the overall E(t) function. Concerning the biomechanical model, the increase in contractility may not be followed by a proportional increase in the E(t) function that would be determined from the outputs of the simulation. To further analyse this we should probably recompute the elastance with modified contractility and compare. Also, the change in contractility in the biomechanical models may affect the length-velocity relationship (Chapter 8 Figure 8.6). Therefore, discrepancies may arise in end-systole due to this phenomenon.

9.3.1.6 Heart rate

We explored the effect of the modification of the heart rate on the outputs of both the models. We sequentially decreased the heart beat duration parameter by [0, 10, 20, 30, 40] percent the original heart beat (44 beats.min^{-1}).

Figure 9.9 shows the results of the simulations. It represents the final heartbeat of a 5 heartbeats sequence simulated with 5 different heart rates. We can observe that for small heart rate variations, the two models correspond. However, when increasing the heart

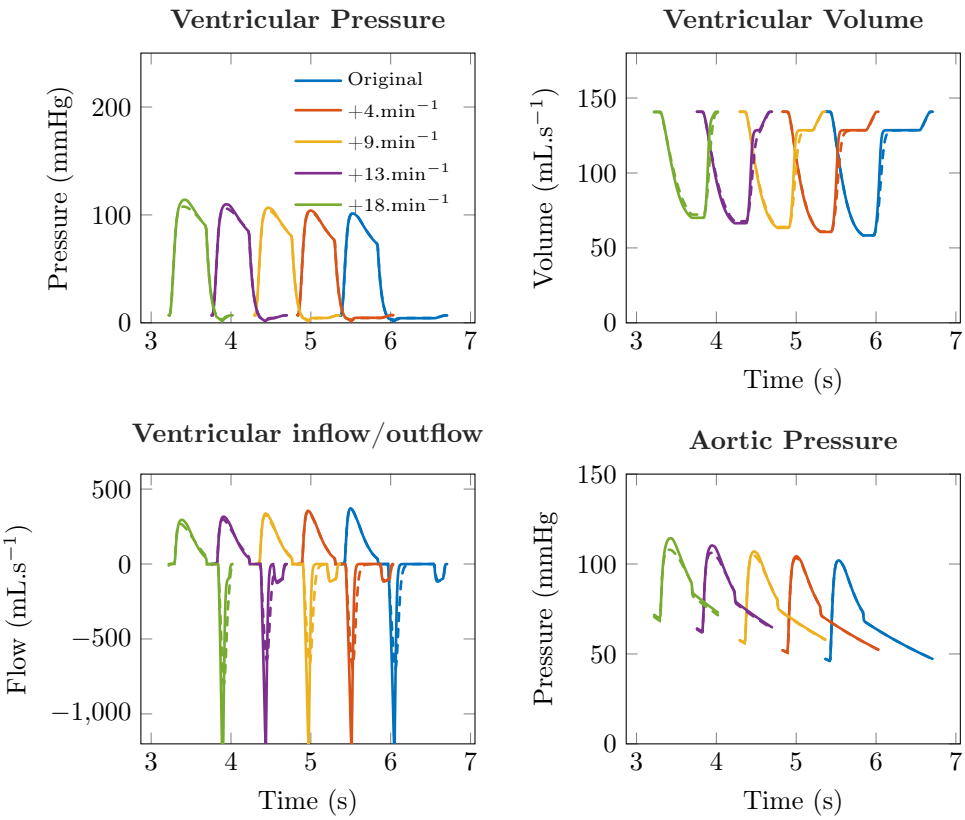

Figure 9.9 – Comparison between the time-varying elastance and the biomechanical models. The 4 panels represent the respective outputs of the two models when increasing the heart rate up to 40%.

rate more than 20%, we observed differences, mostly related to systolic ventricular and aortic pressure. For extreme variations (HR = 75 beat.min^{-1}), we also observed that the atrial contraction did not occur for both the time-varying elastance and biomechanical models (see bottom left panel of Figure 9.9). The discrepancy between the outputs of the two models might be explained by this loss of cardiac function. To overcome this issue we should consider a time adaptation of systolic period, in order to restore the atrial contraction.

However, even though the differences exist, the overall behaviour of the two models are similar. Importantly, the stroke volumes and the mean aortic pressures are similar, and the results may be interpreted in the same manner.

9.3.2 Comparison between the biomechanical biomechanical model and the time-varying elastance E(t) model: Quantitative analysis on 61 patients' dataset

In this Section we aimed to confirm the results obtained in the Patient's example (See Section 9.3.1.3 and 9.3.1.4), by reproducing the *in silico* experiment presented in the preceding section. We used the data obtained on 45 patients undergoing general anaesthesia on which we calibrated the biomechanical model. Sixteen patients necessitated administration of Noradrenaline to restore arterial blood pressure. We sequentially modified the calibration from the baseline condition of each of the 16 patients to adapt the biomechanical model to the arterial pressure and cardiac output following Noradrenaline administration. We obtained 61 sets of calibration on which we performed a sequential 20% increase and 20% decrease in preload and distal resistances parameters. Table 9.4 presents the results of the calibrated simulations for the 61 datasets and the effects of preload and afterload variations on the outputs of the biomechanical model.

Table 9.5 shows the outputs deviation from the biomechanical models when obtained by the time-varying elastance model, when varying preload and afterload.

Table 9.4 – Effect of preload and afterload modification on biomechanical model (0_D) outputs. The results are performed on 45 patients on whom 16 received Norarenaline (n = 61 calibration). The afterload and the preload were modified by changing distal resistance and capacitance in the Windkessel model or the preload by -20% to + 20%.

	Original	Preload		Afterload	
	0_D	decreased	increased	decreased	increased
Aortic Pressures					
P_{aom} (mmHg)	87 ± 14	-4 ± 3*	2 ± +3*	-9 ± 4*	6 ± 3*
P_{aos} (mmHg)	122 ± 20	-4 ± 3*	2 ± +2*	-5 ± 3*	4 ± 3*
P_{aod} (mmHg)	61 ± 11	-3 ± 4*	1 ± +4*	-8 ± 4*	5 ± 3*
Systolic outputs					
SV (mL)	71 ± 16	-3 ± 2*	2 ± 3*	6 ± 2*	-5 ± 3 *
EF (%)	55 ± 8	1 ± 2*	0 ± 2*	5 ± 2*	-4 ± 2 *
Ventricular outputs					
P_{es} (mmHg)	96 ± 18	-6 ± 4*	3 ± 5*	-10 ± 8*	8 ± 4 *
V_{es} (mL)	59 ± 18	-4 ± 2*	3 ± 3*	-6 ± 2*	5 ± 3 *
V_{ed} (mL)	130 ± 25	-7 ± 1*	5 ± 1*	0 ± 0	0 ± 0 *
Bioenergetics					
I_w (Joules)	0.46 ± 28	-0.06 ± 0.04*	0.04 ± 0.05*	-0.11 ± 0.06*	0.1 ± 0.06 *
E_w (Joules)	1.04 ± 0.31	-0.07 ± 0.04*	-.04 ± 0.03*	0.02 ± 0.04*	-0.03 ± 0.03 *
CE (%)	70 ± 13	2 ± 2*	1 ± -2*	-6 ±- 0.02*	5 ± -2 *
Ventricular arterial coupling					
E_{es} (mmHg.mL^{-1})	3.04 ± 1.23	0.22 ± 0.18*	-0.12 ± 0.12*	0.3 ± 0.42*	-0.17 ± 0.12 *
E_a (mmHg.mL^{-1})	1.75 ± 0.47	0.01 ± 0.08	-0.03 ± 0.07*	-0.02 ± 0.16	0.01 ± -0.05
V_{va}	0.62 ± 0.14	-0.03 ± 0.02*	0.01 ±- 0.02*	0.05 ± 0.02*	0.03 ± 0.02 *

P_{aom}: mean aortic pressure; P_{aos}: systolic aortic pressure; P_{aod}: diastolic aortic pressure; SV: stroke volume; EF: ejection fraction; P_{es}: end-systolic pressure; V_{es}: end-systolic-volume; V_{ed}: end-diastolic volume; P_{ed}: end-diastolic pressure; I_w: internal work; E_w: external work; CE: cardiac efficiency; E_{es}: end-systolic elastance; E_a: arterial elastance; V_{va}: ventricular-arterial coupling. $*$ $p<0.05$ as compared with original calibrated biomechanical model output.

* pvalue < 0.05 as compared with calibrated biomechanical model outputs.

Table 9.5 – Mean difference between outputs of time-varying elastance (E(t)) and of biomechanical (0_D) models for various preload and afterload. Results performed on 45 patients on whom 16 received Noradrenaline (n = 61 calibrations). The afterload and the preload were modified by changing distal resistance and capacitance in the Windkessel model or the preload by -20% to + 20%.

	Original	Preload		Afterload	
	E(t)	decreased	increased	decreased	increased
Aortic Pressures					
P_{aom} (mmHg)	+0 ± 1	-2 ± 1*	+3 ± 2*	-1 ± 1*	+2 ± 2*
P_{aos} (mmHg)	+0 ± 1	-4 ± 2*	+5 ± 3*	-1 ± 1*	+3 ± 3*
P_{aod} (mmHg)	+0 ± 1	-1 ± 1*	+2 ± 2*	+0 ± 1*	+2 ± 2*
Systolic outputs					
SV (mL)	+1 ±1*	-1 ± 1*	+2 ± 2*	-1 ± 1*	+2 ± 2*
EF (%)	+0 ± 0	-1 ± 1*	+1 ± 1*	-1 ± 1*	+1 ± 1*
Ventricular outputs					
P_{es} (mmHg)	+0 ± 2	+1 ± 4	+3 ± 6*	+0 ± 7	+2 ± 5*
V_{es} (mL)	+0 ± 0	+2 ± -1*	+1 ± 1*	+1 ± 1*	-1 ± 1*
V_{ed} (mL)	+1 ± 1*	+1 ± 1*	+1 ± 2*	+1 ± 1*	+1 ± 1*
Bioenergetics					
I_w ($1e^{-2}$Joules)	+0 ± 2	+2 ± 2*	+1 ± 5	+2 ± 4*	+0 ± 6
E_w ($1e^{-2}$Joules)	+1 ± 1*	-4 ± 3*	+8 ± 5*	-1 ± 4*	+13 ± 11*
CE (%)	+0 ± 0*	-2 ± 1*	1 ± 1*	-1 ± 2*	+1 ± 2*
Ventricular arterial coupling					
E_{es} ($1e^{-2}$mmHg.mL^{-1})	-1 ± 8	-17 ± 26*	+12 ± 16*	-24 ± 33*	+13 ± 12*
E_a ($1e^{-2}$mmHg.mL^{-1})	+0 ± 3	-4 ± 9*	+6 ± 9*	-6 ± 13*	+6 ± 6*
V_{va} ($1e^{-2}$)	+0 ± 0	+1 ± 1	+1 ± 0*	-1 ± 1*	-1 ± 1*

P_{aom}: mean aortic pressure; P_{aos}: systolic aortic pressure; P_{aod}: diastolic aortic pressure; SV: stroke volume; EF: ejection fraction; P_{es}: end-systolic pressure; V_{es}: end-systolic-volume; V_{ed}: end-diastolic volume; P_{ed}: end-diastolic pressure; I_w: internal work; E_w: external work; CE: cardiac efficiency; E_{es}: end-systolic elastance; E_a: arterial elastance; V_{va}: ventricular-arterial coupling.
* pvalue < 0.05 as compared with biomechanical model outputs.

9.3.3 *Real life* experiment: models comparison at peak effect of Noradrenaline

In this experiment, we analysed the biomechanical and time-varying elastance models adequacy in *real life* condition, when the haemodynamic state was modified by the administration of Noradrenaline. We selected 5 patients (Patients 12, 16, 18, 21 and 69) for whom both a calibration at baseline and at peak effect of Noradrenaline were available. We used the biomechanical model outputs as the ground truth. From the baseline calibrated biomechanical model, we estimated the E(t) function, as described in section 9.2.2. To consider the change in contractility (τ_0) induced by the Noradrenaline administration, we defined a $k_{\tau_0} = \frac{\tau_0^{peak}}{\tau_0^{base}}$ factor that is subsequently applied to the E(t) function.

At maximum peak effect of Noradrenaline, we deviated from the parameters value calibrated at baseline by -34 [-46 to -32]% for the distal capacitance, and by +86 [+77 to +114]% and by +23 [+12 to +27]% for the distal resistance and the contractility, respectively. The comparative results between the models are provided in Figure 9.10.

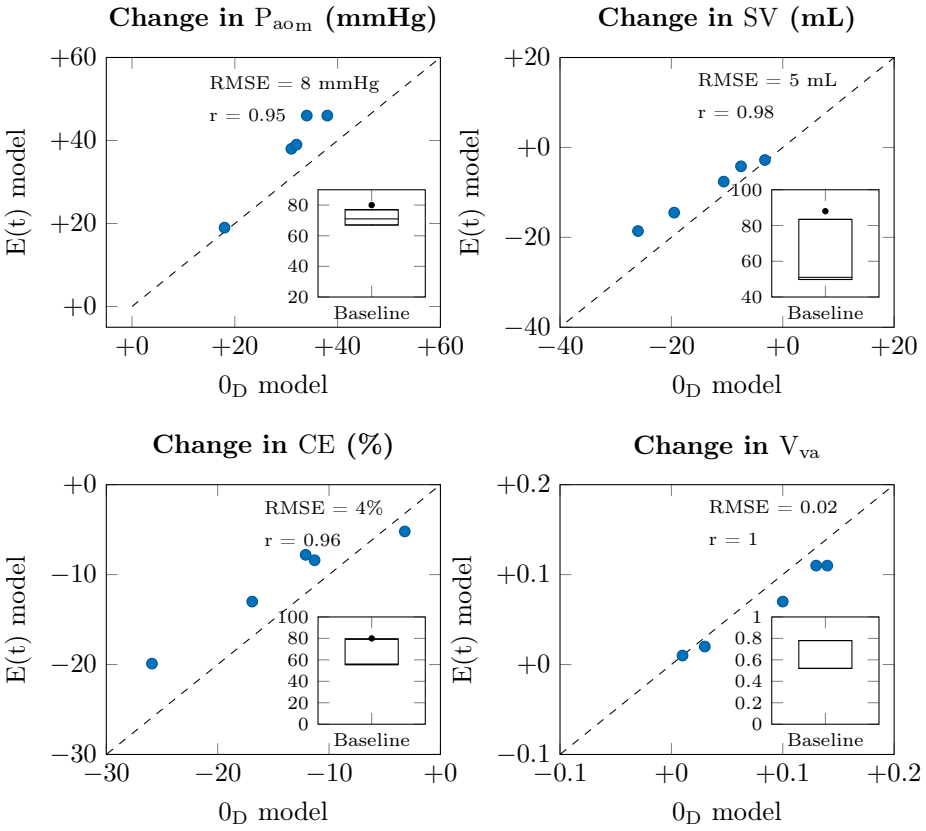

Figure 9.10 – Comparison of haemodynamic indicators obtained using the biomechanical and the time-varying elastance models after Noradrenaline administration. The results of the biomechanical model represent the ground truth as they are calibrated on the 5 patients' data. **Box plots**: The box plots represent the baseline value of the indicator obtained with the biomechanical model. **Large plots**: The blue dots represent the correlation between the results obtained with the biomechanical and the time-varying elastance models. The Pearson correlation coefficient is provided. The RMSE is the root mean squared error between the output of the time-varying elastance and the biomechanical model, the latter being considered as the ground truth.

9.4 Discussion

In this Chapter, we aimed to evaluate the ability of a biomechanically derived time-varying elastance model to represent the outputs of the biomechanical model from which it originates, when the external conditions applied to the models were modified. We conducted a step by step analysis, in which we compared the outputs of the time-varying elastance and the biomechanical models qualitatively for one patient. We also performed a quantitative analysis, by analysing the differential outputs of the models when varying preload and afterload by ± 20% from the original calibrated condition for 61 patients' dataset (n = 45 patients – 16 with baseline and Noradrenaline dataset). We finally compared the models outputs during a *real life* experiment in which the models were calibrated at baseline and at peak effect of Noradrenaline, for 5 patients.

In the qualitative analysis performed on the Patient 12, we observed that the time-varying elastance model reproduced the biomechanical model outputs almost exactly when the conditions which were used for E(t) function estimation were met. We verified also that equilibrium was reached as fast as with the biomechanical model. When we varied external conditions (*i.e.* preload, afterload and contractility), the time-varying elastance model behaves globally as the biomechanical model, for significant biomechanical model's output variations. Most of the differences observed in qualitative sensitivity analysis was observed on maximal systolic pressure (either ventricular and aortic). This deviation was observed for extreme variations of preload and contractility (± 40% the calibrated parameters), with an order of magnitude which may not be clinically relevant for anaesthesia and intensive care issues. The difference was less pronounced for change in afterload. The *in silico* experiments performed using the 61 patients' dataset confirm this observation.

Concerning preload and afterload variations, a reason why differences could exist, and why differences increased when increasing the magnitude of change in parameters value, lies in the approximation made by linearising the ESPVR, which is necessary for time-varying elastance concept. Indeed, the time-varying elastance model is based on a local linear approximation of ESPVR, which is not linear [1; 5]. This linearisation was performed at a calibrated condition, based on patients' data. When deviating from calibrated condition by actions on preload and afterload, the change of loading conditions could be responsible for changes in end-systolic pressure volume relationship condition for the biomechanical model. The time-varying elastance model by essence does not allow a deviation of its end-systolic pressure volume relationship. The effect of preload and afterload variations on the E(t) function was already studied in Chapter 8. Therefore, in our experiment, we could imagine extreme conditions in which the biomechanical model outputs are located on other regions of the ESPVR, the effect being a discrepancy between the outputs of the time-varying elastance and the biomechanical models. However, when looking at Figure 9.5, we observed that the end-systolic pressure volume PV points were close to the linearisation used to estimate E(t) function, even if differences in pressure outputs were observed. Another explanation may come from the dynamics of the models. Indeed, while the E(t) function is unchanging, the dynamics of the biomechanical model varies with external conditions.

Most importantly when interpreting the variations in preload and afterload, the mean arterial pressure did not change significantly between biomechanical and time-varying elastance models' output, even for significant changes in mean arterial pressure after parameter variations. Indeed, if we consider the differential model results from a clinical perspective, we would think about the differences that may lead to different therapeutical decisions. In our case, a 3-5 mmHg difference in arterial pressure would probably not trigger a differential clinical intervention according to the differential model results. Also, the

combination of indicators informs the clinician about the integrity of the cardiovascular system. An isolated difference in arterial pressure with maintained cardiac output would probably not lead to a change in medical decision. Therefore, if we consider from this clinical perspective the results of the time-varying elastance as compared with the biomechanical models, we may conclude that for reasonable change in preload and afterload, the two models behave the same and would probably lead the clinician to act similarly.

We also investigated the effect of the contractility changes on the outputs of the two models. The contractility τ_0 is a parameter which represent the theoretical maximal contraction a myofilament could exert under a given level of inotropy. In a pressure-volume relationship space, the effect of a contractility change would lead to a proportional transformation of the non-linear ESPVR by a factor $\Delta\tau_0$. The local derivative of the ESPVR at P_{es} pressure-volume point (*i.e.* E_{es}) should also be modified by the same factor $\Delta\tau_0$. However, this assumption holds not true if V_0 is fixed, as the the derivative of ESPVR at any point would lead to different zero pressure intercept. In Chapter 8, we observed that for various contractilities, the V_0 might be relatively different if we recalculated the derivative of the ESPVR. Our time-varying elastance model assumes a fixed V_0. This could explain the differences observed between time-varying elastance and biomechanical models observed when we varied contractility. Another explanation could be related to the force-velocity relationship of the myocyte contraction, as discussed in Chapter 8, Section 8.2.1.1. Some viscous effects, captured in the biomechanical model prevent the dynamic end-systolic pressure-volume condition to reach the maximal contraction condition, namely the theoretical ESPVR. The difference of the results obtained with the time-varying elastance model as compared with those obtained with the biomechanical models can be explained by this effect, as demonstrated by Figure 9.8, in which end-systolic pressure volume condition are different between the two models.

Another difference could be discussed when looking at the differential results between the two models. The filling of the heart models demonstrates differences both when varying preload and afterload, and when we varied contractility. This is probably related to the different dynamic of the models. In the biomechanical model, a change in parameter affects the dynamics of the model. In the time-varying elastance model, the dynamic is fixed by the original condition. For preload and afterload changes, only the external conditions are modified. The E(t) function is identical. If in the biomechanical model, the change in preload and afterload leads to a change in dynamics, therefore we could expect to observe a difference in the results of the two models. For contractility, in the time-varying elastance model, the scaling of the E(t) function is different as compared with the original E(t) function. It is a proportional change that affects the whole E(t) function, and therefore, which affects the dynamic of the model in early diastole (filling of the model). This aspect should be discussed further by complementary analysis, to refine the behaviour of the time-varying elastance model.

We also tested the heart rate effects on the differences between the two models. We reduced the heart beat duration of both the models and observed a difference in systolic pressure only for a large increase in heart rate. At the magnitude of change we applied, we only modified timings that reduced the diastolic timing. The difference we observed for the highest heart rate might be caused by the fact that the biomechanical model did not achieve its complete filling. An adaptation in the biomechanical model would be to reduce the systolic period duration. However, the manner to adjust the systolic and diastolic time is not trivial [6; 4]. The relative contribution of systolic time period to heart beat duration varies with loading conditions and contractility. Further research is needed to explore how to adapt models cardiac rhythm when modifying heart rate.

Finally, we compared in *real life* setting the outputs of the two models when haemody-

namic changes from a baseline condition were induced by Noradrenaline administration. We observed that for significant changes in contractility and afterload, the time-varying elastance model outputs were closely correlated to the outputs of the biomechanical model. The differences in P_{aom}, SV, CE, and V_{va} were small, allowing for the interpretation of the time-varying elastance model outputs as a surrogate of biomechanical model outputs.

Some perspectives may be considered from our findings. First, our fully biomechanically derived approach allows to consider a patient-specific time-varying elastance model with only few clinical data available. It necessitates only routine echocardiographic and monitoring measurements to calibrate the full biomechanical biomechanical model, from which we can define the time-varying elastance model. The time-varying elastance model can further be used as a monitoring tool to evaluate the cardiovascular function across reasonable ranges of deviation of preload, afterload, contractility and heart rate. As compared with the biomechanical model, the time-varying elastance model has the advantages to reduce computational time allowing to obtain simulation results in a time frame close to real time. This aspect needs to be evaluated with some performance computing tests. A practical approach to use this framework would be to imagine a setup in which the complete biomechanical calibration is performed only discontinuously when important deviations in physiological (monitored arterial pressure or cardiac outputs) signals are observed.

Some limitations can be discussed. We studied the ability of the time-varying elastance model to reproduce the results of the biomechanical model when varying conditions. We observed that the differences observed between the two models were small and clinically not relevant, even for significant parameter variations, for the Patient 12 testing. When looking at the results obtained on the 61 datasets, even if the parametric variation was close to $\pm$ 20%, the change in outputs of the biomechanical model were small and probably not clinically relevant, except for changes in afterload. One may argue that the absence of clinically pertinent differences observed between our models could be related to the absence of effective change in cardiovascular condition. However, the results obtained in the 5 *real life* cases, in which the Windkessel parameters were calibrated and in which the systolic dynamic parameters was adjusted using a simple proportional factor, suggested that the time-varying elastance model could be used as a surrogate of the biomechanical model. Further *real life* experiments should be tested before to conclude on this point.

9.5 Conclusion

This Chapter aimed to demonstrate the ability of the time-varying elastance model, derived from an original calibrated version of the complete biomechanical biomechanical model, to reproduce the outputs of the biomechanical model when varying physiology – namely, heart rate, preload, afterload and contractility. By using qualitative testing on one patient, we observed that the discrepancy between the two models were small, even for significant changes in model parameters. We confirmed this result by using a dataset obtained on 5 patients in which the SV and/or the P_{es} were modified by up to 50% the original quantities. We finally observed small differences between models in a 61 patients dataset in which the preload and afterload were modified by up to 20%. These results taken altogether, suggest a good performance of the time-varying elastance model to follow haemodynamic state, as the biomechanical model, for reasonable deviations from the calibrated condition in which the E(t) function was determined. In case of a profound change in cardiovascular physiology, we would recommend to perform a novel complete calibration of the biomechanical model to restore the adequacy between the two models.

Bibliography

[1] Burkhoff, D., Sugiura, S., Yue, D. T., and Sagawa, K. (1987). Contractility-dependent curvilinearity of end-systolic pressure-volume relations. *American Journal of Physiology-Heart and Circulatory Physiology*, 252(6):H1218–H1227.

[2] Caruel, M., Chabiniok, R., Moireau, P., Lecarpentier, Y., and Chapelle, D. (2014). Dimensional reductions of a cardiac model for effective validation and calibration. *Biomechanics and Modeling in Mechanobiology*, 13(4):897–914.

[3] Chapelle, D., Le Tallec, P., Moireau, P., and Sorine, M. (2012). Energy-preserving muscle tissue model: formulation and compatible discretizations. *International Journal for Multiscale Computational Engineering*, 10(2).

[4] Le Gall, A., Laurin, A., Vallee, F., and Chemla, D. (2017). Comparison of Systolic Period Duration Using Aortic Flow or Pressure Based Methods in Anesthetized Patients. In *2017 Computing in Cardiology Conference*.

[5] Mirsky, I., Tajimi, T., and Peterson, K. L. (1987). The development of the entire end-systolic pressure-volume and ejection fraction-afterload relations: a new concept of systolic myocardial stiffness. *Circulation*, 76(2):343–356.

[6] Weissler, A. M. (1983). Interpreting systolic time intervals in man. *Journal of the American College of Cardiology*, 2(5):1019–1020.

Part IV

Application & perspectives: Cardiovascular modelling for haemodynamic monitoring

CHAPTER 10

Cardiovascular modelling for haemodynamic monitoring

During general anaesthesia (GA), direct analysis of the arterial pressure or aortic flow waveforms may be inconclusive in complex haemodynamic situations. Patient-specific biomechanical modelling allows to simulate Pressure-Volume (PV) loops and obtain functional indicators of the cardiovascular (CV) system, such as ventricular-arterial coupling (V_{va}), cardiac efficiency (CE) or myocardial contractility. In this prospective observational study, a biomechanical model of heart and vasculature specific to each patient (n=45) undergoing GA was built, while using transthoracic echocardiography and aortic pressure and flow signals. If intraoperative hypotension (IOH) appeared, diluted noradrenaline (NOR) was administered and the model readjusted. The accuracy of simulated mean aortic pressure (MAP) and stroke volume (SV) were in accordance with the guidelines for the validation of new devices or reference measurement methods in all patients at baseline. After NOR administration, the percentage of concordance with 10% exclusion zone between measurement and simulation was $> 95\%$ for both MAP and SV. The modelling results showed a decreased V_{va} (0.64 ± 0.37 vs 0.88 ± 0.43; $p=0.039$), and an increased CE (0.8 ± 0.1 vs 0.73 ± 0.11; $p=0.042$) in hypotensive as compared with normotensive patients. After NOR administration, V_{va} increased by $92\pm101\%$, CE decreased by $13\pm11\%$ ($p<0.001$ for both) and contractility increased by $14\pm11\%$ ($p=0.002$). The work demonstrates the application of numerical models built for individual patients to estimate PV loops and functional indicators of CV system using clinical data readily available during GA and paves the way for model-augmented haemodynamic monitoring at operating theatres or intensive care units to enhance the information of patient-specific physiology.
This chapter was published as an original article in PLOS ONE journal in May 2020.
doi: https://doi.org/10.1371/journal.pone.0232830

doi: https://doi.org/10.1371/journal.pone.0232830

Monitoring of cardiovascular physiology augmented by a patient-specific biomechanical model during general anaesthesia. A proof of concept study.

Arthur Le Gall[1,2,3,4] MD, Fabrice Vallée[1,2,3,4] MD PhD, Kuberan Pushparajah[5] MD PhD, Tarique Hussain[6] MD PhD, Alexandre Mebazaa[3,4] MD PhD, Dominique Chapelle[1,2] PhD, Étienne Gayat[3,4] MD PhD, Radomír Chabiniok[1,2,5,6,7] MD PhD

[1] Inria, Palaiseau, 91120, France, [2]LMS, École Polytechnique, CNRS, Institut Polytechnique de Paris, Palaiseau, 91120, France, [3] Anaesthesiology and Intensive care department, Lariboisière – Saint Louis – Fernand Widal University Hospitals, Paris, 75010, France, [4] INSERM, UMR-S 942, Paris, 75010, France, [5] School of Biomedical Engineering & Imaging Sciences, St Thomas' Hospital, King's College London, SE1 7EH, UK, [6] Division of Pediatric Cardiology, UT Southwestern Medical Center Dallas, TX 75235-7701, USA, [7] Department of Mathematics, Faculty of Nuclear Sciences and Physical Engineering, Czech Technical University in Prague, Czech Republic

This chapter was published as an original article in PLOS ONE journal in May 2020.

Abstract

During general anaesthesia (GA), direct analysis of the arterial pressure or aortic flow waveforms may be inconclusive in complex haemodynamic situations. Patient-specific biomechanical modelling allows to simulate Pressure-Volume (PV) loops and obtain functional indicators of the cardiovascular (CV) system, such as ventricular-arterial coupling (V_{va}), cardiac efficiency (CE) or myocardial contractility. In this prospective observational study, a biomechanical model of heart and vasculature specific to each patient (n=45) undergoing GA was built, while using transthoracic echocardiography and aortic pressure and flow signals. If intraoperative hypotension (IOH) appeared, diluted noradrenaline (NOR) was administered and the model readjusted. The accuracy of simulated mean aortic pressure (MAP) and stroke volume (SV) were in accordance with the guidelines for the validation of new devices or reference measurement methods in all patients at baseline. After NOR administration, the percentage of concordance with 10% exclusion zone between measurement and simulation was > 95% for both MAP and SV. The modelling results showed a decreased V_{va} (0.64±0.37 vs 0.88±0.43; p=0.039), and an increased CE (0.8±0.1 vs 0.73±0.11; p=0.042) in hypotensive as compared with normotensive patients. After NOR administration, V_{va} increased by 92±101%, CE decreased by 13±11% (p<0.001 for both) and contractility increased by 14±11% (p=0.002). The work demonstrates the application of numerical models built for individual patients to estimate PV loops and functional indicators of CV system using clinical data readily available during GA and paves the way for model-augmented haemodynamic monitoring at operating theatres or intensive care units to enhance the information of patient-specific physiology.

Keywords— Translational research, cardiovascular modelling, model-augmented physiological monitoring, myocardial contractility, cardiac work, pressure-volume loop

Key points

- Biomechanical models of cardiovascular system specific to individual patients have the potential to augment non-invasively the information obtained by physiological monitoring, particularly in complex haemodynamic situations in which direct analysis of arterial pressure or aortic flow waveforms may be inconclusive.
- In a group of patients (n=45) undergoing a neuroradiological intervention under general anaesthesia, we showed that patient-specific models allowed to obtain functional indicators of the cardiovascular (CV) system, such as vascular resistance, ventricular-arterial coupling, cardiac efficiency or myocardial contractility. These quantities were compared between normotensive and hypotensive patients, and in the latter ones prior to and after administering vasoactive drugs.
- Identification of these factors is a valuable addition for physiological monitoring during general anaesthesia and potentially at intensive care units throughout medical specialisations. The work demonstrates the use of numerical models in such an application and paves the way for model-augmented haemodynamic monitoring to enhance the information of patient-specific physiology.

10.1 Introduction

Cardiac physiology is a delicate balance between extrinsic (e.g. preload or afterload) and intrinsic (e.g. contractility or electrical activation) properties of the heart. Cardiovascular (CV) failure is the third reason for entering the intensive care unit (ICU) and the second cause of the in-ICU death [25]. Furthermore, around 230,000,000 general anaesthesia (GA) are performed each year worldwide [47] and perioperative CV events remain the main cause of postoperative death [24]. CV management during GA or at critical care includes CV monitoring based on (and not limited to) arterial pressure and cardiac output (CO) measurement [12; 34]).

The simultaneous evaluation of the ventricular pressure and volume (PV loop) allows a functional interpretation of pathophysiological conditions, such as quantifying myocardial energetic expenditure or ventricular-arterial coupling [18], see Figure 10.1). In some complex cases, the PV loop analysis can bring an additional insight in understanding the situation [14]. However, as it requires invasive intraventricular pressure measurement, its usage is not convenient during monitoring.

Patient-specific CV modelling provides a numerical representation of the CV system in individual patients – a "numerical avatar" – which is becoming a powerful diagnostic or therapeutic tool. For example, it allows to access the PV loop [21; 37; 6], predict the success of cardiac resynchronisation therapy [38; 29], or estimate myocardial stiffness and contractility or vascular resistance under various conditions [15; 7; 46; 35], see also reviews [8; 45] and references therein. However, a request of fast analysis alongside with restricted data availability make its implementation within CV monitoring rather challenging.

In the present study, we aimed to evaluate the feasibility of using a monitoring framework augmented by a biophysical model to obtain and interpret the simulated PV loops and some CV functional quantities, while using only data readily-available during neuroradiological procedure.

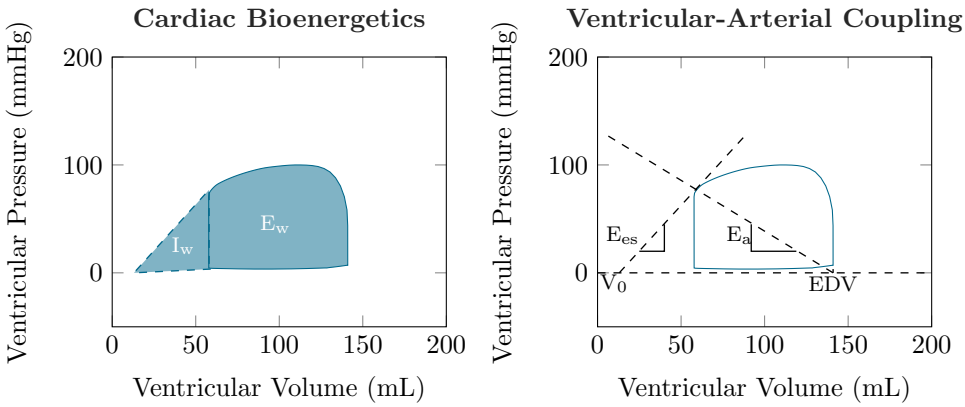

Figure 10.1 – Example of PV loop and its interpretation. Cardiac bioenergetics (left): internal work (I_w) associated with the potential energy or the energetic expenditure necessary to reach optimal conditions for ejection; external work (E_w) associated with the energetic expenditure of the ejection; cardiac efficiency (CE) defined as the ratio $CE = \frac{E_w}{E_w+I_w}$. Ventricular-arterial coupling (right): ventricular elastance E_{es} (slope of the end-systolic pressure-volume relationship, ESPVR, at end-systolic pressure-volume point); arterial elastance $E_a = \frac{ESP}{SV}$ with ESP being end-systolic pressure and SV = EDV − ESV the stroke volume (subtraction of end-diastolic and end-systolic volumes).

10.2 Methods

This prospective and non-interventional cohort study was held in a university hospital in Paris, and followed the STROBE guidelines for conducting observational studies.

10.2.1 Patients monitoring and data collection

Patients scheduled for intracranial endovascular procedures were selected for inclusion in this study. Only the patients, for whom continuous arterial pressure and CO monitoring was indicated for clinical purposes, were included. This study was approved by the appropriate Institutional Review Board – ethical committee of the Société de Réanimation de Langue Française (CE-SRLF 14-34) – which waived the need for written informed consent. Consequently, oral informed consent was obtained from all subjects after providing a protocol information letter. Every subject had the possibility to withdraw from the study at any time.

During neuroradiological procedure, GA was induced and maintained by using total intravenous anaesthesia (TIVA) using propofol (75-150 mg/kg/min) and remifentanil (0.2-0.5 μg/kg/min). Oro-tracheal intubation was facilitated using 0.5 mg/kg atracurium and followed, if needed, by continuous infusion of 0.5 mg/kg/h atracurium. After intubation, ventilation was established to reach an end-tidal CO_2 concentration of 35 - 38 cmH_2O using a tidal volume of 6-8 ml/kg of body weight.

After GA induction, the monitoring devices were installed. Transoesophageal Doppler probe (TOD) was inserted into the oesophagus and connected to the CombiQ monitor (Deltex medical, Chichester, UK). A transthoracic echocardiography (TTE) was performed in the beginning of the interventional procedure. A radiopaque wire was advanced from the femoral artery through the aorta up to cerebral arteries. Invasive arterial pressure was recorded by connecting a fluid-filled mechanotransducer (TruWave, Edwards Lifescience, Irvine, CA, USA), as previously described [19]. For research purposes, data were recorded when the pressure catheter was in the ascending aorta.

Our standard procedure for management of intraoperative arterial hypotension (IOH),

defined as the fall of mean arterial blood pressure by 20% as compared to the awake value, includes: 1) titration of saline isochloride by 250 ml step to optimise CO; and 2) in case of persistent IOH despite the fluid expansion, titration of diluted noradrenaline (NOR) (5μg/ml) by 5 μg steps to restore the blood pressure. This management was not modified for this research project. We separated a posteriori the population to hypotensive and normotensive groups according to whether they received NOR.

10.2.1.1 Validation group

In order to compare the PV loops obtained by the model to invasively acquired PV loops, we analysed four additional patients with intraventricular pressure and volume measured by pressure catheter and magnetic resonance imaging (MRI), respectively. Validation subjects #1-2 had a single-ventricular physiology (Fontan circulation) and underwent combined cardiovascular MRI and heart catheterisation procedure for progressive symptoms of exercise intolerance. Validation subjects #3-4 were patients with repaired tetralogy of Fallot who underwent cardiovascular MRI and catheterisation before pulmonary valve replacement.

All XMR exams were performed under GA. During catheterisation, pressure signals (aortic, ventricular, venae cavae, and pulmonary capillary wedge pressures) were obtained. Simultaneously, cardiac volumes and 2D flows (ascending and descending aorta) were acquired using cardiovascular MRI (CMR). The obtained CMR data were post-processed into 0D signals of time-vs-flow or time-vs-ventricular volumes.

The data collections in the patients with Fontan circulation were performed at Evelina London Children's Hospital, King's College London, under the ethical approval of institutional ethics committee, London UK (Ethics Number 09H0804062). The data collection in tetralogy of Fallot patients were performed at Children's hospital, UT Southwestern Medical Center Dallas, under the ethical approval UT Southwestern IRB (STU 032016-009).

10.2.2 Biomechanical model of cardiovascular system for monitoring purposes

The biomechanical model of heart and vasculature used in this study [5] is a combination of a biomechanical heart [9] and a Windkessel circulation model [48].

The passive component of the myocardium is inspired by [16] with a hyperelastic potential in the form:

$$\mathrm{W_e} = \mathrm{C_0 e^{C_1(J_1-3)^2}} + \mathrm{C_2 e^{C_3(J_4-1)^2}}, \tag{10.1}$$

with $\mathrm{J_1}$ and $\mathrm{J_4}$ being reduced invariants of the left Cauchy-Green tensor $\underline{\mathrm{C}}$, given by $\mathrm{J_1} = \mathrm{trace}\,(\underline{\mathrm{C}})\,(\det\,(\underline{\mathrm{C}}))^{-\frac{1}{3}}$ and $\mathrm{J_4} = \mathrm{fib}\cdot\underline{\mathrm{C}}\cdot\mathrm{fib}$

(with fib representing the myocardial fibre direction). We used the parameters $\mathrm{C_0} = 665$ Pa, $\mathrm{C_1} = 2.4$ Pa, $\mathrm{C_2} = 103$ Pa and $\mathrm{C_3} = 5.5$ Pa , which allows to fit the experimentally measured end-diastolic pressure volume relationship (EDPVR) [22] in a reference healthy human. The passive potential (Eq. 10.1)) is then multiplied by a "stiffness multiplication factor" – the only parameter used in adjusting the passive part of the model to a given patient (passive tissue stiffness). The active component of the model – representing actin-myosin interaction and formation of cross-bridges – is based on Huxley's sliding filament theory [17; 20], albeit with an extension allowing to represent the Frank-Starling mechanism [9]. The active stress τ_c and active stiffness $\mathrm{k_c}$ in sarcomeres with the extension $\mathrm{e_{fib}} = \frac{\mathrm{L}}{\mathrm{L_0}}$ (where L and $\mathrm{L_0}$ represents the actual and reference sarcomere lengths, respectively) generated in the sarcomere are given by

$$\begin{cases} \dot{k_c} &= -\left(|u| + \alpha\,|\dot{\mathrm{e}_{\mathrm{fib}}}|\right) k_c + n_0\left(\mathrm{e_{fib}}\right) k_0 |u|_+ \\ \dot{\tau_c} &= -\left(|u| + \alpha\,|\dot{\mathrm{e}_{\mathrm{fib}}}|\right) k_c + n_0\left(\mathrm{e_{fib}}\right) \sigma_0 |u|_+ + k_c \dot{\mathrm{e}_{\mathrm{fib}}}. \end{cases} \tag{10.2}$$

The asymptotic active stress σ_0 and stiffness k_0, generated by the sarcomere, are directly related to myocardial contractility, while taking into account the effect of actin-myosin overlap using a Frank-Starling law function $n_0(\mathrm{e_{fib}})$ with value between 0 and 1 (the maximum value for the optimal fibre extension and optimal overlap of actin and myosin chains), for details see [9]. The activation of the sarcomeres is modelled using an activation function u (positive when the tissue is electrically activated with the maximum value of $35s^{-1}$, which is given by the rate of active stress generation [4], $|u|_+$ is defined as $\max(u, 0)$. The parameter α governs the cross-bridge destruction rate due to rapid length changes.

The LV geometry was reduced to a thin-walled sphere as described in [5]. While the geometry and kinematics are simplified, all physical and physiological components are preserved. The model is then solved for an unknown displacement in the radial direction $\mathrm{y(t) = R(t) - R_{ref}}$, where $\mathrm{R(t)}$ and $\mathrm{R_{ref}}$ stands for the actual (at time t) and reference (stress-free) radii of the sphere (from the centre to the mid-wall), and unknown intra-ventricular pressure P (and active stiffness and stress as internal variables). Using the extension of the fibre ($\mathrm{e_{fib} = \frac{y}{R_{ref}}}$), the kinematics of the model can be rewritten to: $\mathrm{R = R_{ref}(1 + e_{fib})}$. Likewise, due to tissue incompressibility the thickness of the myocardium $\mathrm{d = d_{ref}(1 + e_{fib})^{-2}}$, with $\mathrm{d_{ref}}$ being the wall thickness at reference configuration. Ventricular volume is then given by $\mathrm{V = \frac{4}{3}\pi(R - d/2)^3}$.

The circulation is represented by a Windkessel model containing proximal and distal capacitances ($\mathrm{C_p}$ and $\mathrm{C_d}$) and resistances ($\mathrm{R_p}$ and $\mathrm{R_d}$) connected in series, with the distal part representing the majority of the vascular resistance – typically ten times higher than in the proximal part. The Windkessel model equations read:

$$\begin{cases} \mathrm{C_p \dot{P_{ao}} + \left(P_{ao} - P_d\right)/R_p} &= \mathrm{Q_{ao}} \\ \mathrm{C_d \dot{P_d} + \left(P_d - P_{ar}\right)/R_p} &= \mathrm{\left(P_{ve} - P_d\right)/R_d}, \end{cases} \tag{10.3}$$

with $\mathrm{P_{ao}, P_d, P_{ve}}$ representing aortic, distal arterial and venous pressures, respectively.

We remark that even though the geometry of the model used in this work is reduced to a sphere, the adjustment of the cavity size, myocardial mass and biophysical properties of the tissue allow to tailor the model to individual patients. Thanks to such a reduction of geometric complexity, the proposed formulation allows to use patient-specific cardiovascular modelling in close to real-time setting – a single heart beat being simulated within a few seconds – with standard computational resources.

10.2.3 Calibration of the model to data of individual patients

The generic model was turned into patient- and physiology-specific regime by a calibration procedure, during which the model parameters were manually adjusted according to the measured clinical data (see Table 10.1). The sequential calibration procedure consists of:

1. Adjustment of the parameters of Windkessel circulation model after imposing the flow in ascending aorta, with the objective the simulated aortic pressure matched the measurement. As the monitoring data contain only velocity in the descending aorta, this waveform was scaled by using stroke volume (SV) obtained by transthoracic echocardiography (TTE) in the beginning of the procedure, in order to obtain a surrogate of ascending aortic flow.

Table 10.1 – Imaging data procedure: Transthoracic echocardiography mesurements

Parasternal long axis	Left Ventricle Posterior Diameter	(LPWD)
	Aortic Root Diameter	(ARD)
	Septum Diameter	(SD)
	Left Ventricular End-Diastolic Diameter	(LVEDD)
Apical 4-chamber	E wave	
	A wave	
	E' wave (Tissue Doppler Imaging)	
	Left Ventricular End-Diastolic Surface	(LVEDS)
	Left Ventricular End-Systolic Surface	(LVESS)
	Left Atrial Surface	(LAS)
Apical 5-chamber	Velocity Time integral of Left Ventricular Outflow Tract	(VTI)

Table 10.2 – List of parameters used for calibration (in bold the parameters which were re-calibrated after noradrenaline administration according to the new physiology state).

Sphere radius at reference configuration
Sphere thickness at reference configuration
Atrial pressure
Heartbeat duration
Time of ventricular activation
Duration of electrical activation
Myocardial stiffness factor
Proximal Windkessel resistance
Distal Windkessel resistance
Distal Windkessel capacitance
Myocardial contractility

2. Adjustment of the left ventricular (LV) geometry (LV volume and myocardial mass) according to the TTE measurements taken at end-diastole. The assumed LV volume at zero pressure level (the so-called reference configuration), was set to 50% of the measured end-diastolic volume (EDV) [22].
3. Adjustment of the passive tissue stiffness of myocardium aiming at obtaining the EDV as in TTE while applying the ventricular end-diastolic pressure (EDP). Not having an access to the ventricular or atrial pressure, we used a semi-quantitative method to classify LV filling pressure as high or normal [27], and we arbitrarily advocated EDP value of 15 or 7 mmHg, respectively.
4. Adjustment of timing of the electrical activation by using the measured ECG.
5. Adjusting the myocardial contractility in the model to reach the stroke volume (SV) as in the data.

The model calibration was performed for all patients at baseline. If NOR was requested during GA, we re-adjusted only the parameters that are expected to be involved by NOR (i.e. Windkessel model, timing of heart activation and myocardial contractility, see Table 10.2).

Table 10.3 – Calculations of heart function indicators

Stroke Volume	$SV = \pi \frac{\mathrm{AOD}^2}{4} \cdot \mathrm{VTI}$
Left Ventricular End-Diastolic Volume	$\mathrm{LVEDV} = \sum_{i=1}^{n} \text{pixel spacing} \cdot \pi \frac{\mathrm{LVEDS}^2}{4}$
Left Ventricular End-Systolic Volume	$\mathrm{LVESV} = \sum_{i=1}^{n} \text{pixel spacing} \cdot \pi \frac{\mathrm{LVESS}^2}{4}$
Left Ventricular Ejection Fraction	$\mathrm{LVEF} = \frac{\mathrm{LVEDV}-\mathrm{LVESV}}{\mathrm{LVEDV}}$
Pulse Pressure	$\mathrm{PP} = \mathrm{SAP} - \mathrm{DAP}$
Cardiac Output	$\mathrm{CO} = \mathrm{SV} \cdot \mathrm{HR}$
Total Arterial Compliance	$\mathrm{C_{tot}} = \frac{\mathrm{SV}}{\mathrm{PP}}$
Systemic Vascular Resistance	$\mathrm{SVR} = \frac{\mathrm{MAP}}{\mathrm{CO}}$
Arterial Elastance	$\mathrm{E_a} = \frac{\mathrm{LVESP}}{\mathrm{SV}}$
Ventricular Elastance	$\mathrm{E_{es}} = \frac{\mathrm{LVESP}_{highPreload}-\mathrm{LVESP}_{lowPreload}}{\mathrm{LVESV}_{highPreload}-\mathrm{LVESV}_{lowPreload}}$
Ventricular-Arterial Coupling	$\mathrm{V_{va}} = \frac{\mathrm{E_a}}{\mathrm{E_{es}}}$
Internal Work	$\mathrm{I_w} = \frac{\mathrm{LVESP}(\mathrm{LVEDV}-\mathrm{V_{ref}})}{2}$
External work	$\mathrm{E_w} = \text{area under PV loop}$
Cardiac efficiency	$\mathrm{CE} = \frac{\mathrm{E_w}}{\mathrm{E_w}+\mathrm{I_w}}$

MAP, mean aortic pressure; SAP, systolic aortic pressure; DAP, diastolic aortic pressure; LVEDS, left ventricular end-diastolic surface; LVESS, left ventricular end-systolic surface; LVESP, left ventricular end-systolic pressure; AOD, Left ventricular outflow tract diameter; HR, heart rate; $\mathrm{V_{ref}}$, intersection of end-systolic pressure volume relationship with volume axis

10.2.4 Objectives

The first objective was to demonstrate that the calibrated models accurately represent the patients' data by conducting an equivalence study. The second objective was to employ the augmented haemodynamic monitoring to quantify the alterations of cardiovascular state during IOH and after administering NOR to restore blood pressure.

10.2.5 Judgement criteria

The primary endpoint was to test the equivalence between the simulated and measured aortic pressures and flow for the population. The mean (MAP), systolic (SAP), and diastolic (DAP) aortic pressures, and SV were used. The secondary endpoints were to compare the hypotensive and normotensive patients, and the hypotensive patients during restoration of blood pressure by NOR in the following sense: 1) Distal resistance ($\mathrm{R_d}$) and capacitance ($\mathrm{C_d}$) of the Windkessel model with the calculated systemic vascular resistance (SVR) and total arterial compliance ($\mathrm{C_{tot}}$), respectively; 2) myocardial contractility; 3) simulated indicators of ventricular-arterial coupling ($\mathrm{V_{va}}$); and 4) simulated indicators of heart bioenergetics (Table 10.3).

10.3 Statistics

We designed an equivalence study to validate the ability of our framework to reproduce the aortic pressure and CO. We followed the extended CONSORT guidelines for reporting equivalence and non-inferiority studies [32]:

1. Rationale and choice of equivalence margins: according to the guidelines for the validation of a new arterial pressure device [49], we set the equivalence margins for the simulated aortic pressure to 13 mmHg. By contrast, we set the percentage error

($\text{PE} = 100 \cdot 1.96 \cdot \frac{\text{SD}_{\text{sim-meas}}}{\text{Mean}_{\text{meas,sim}}}$) for CO estimation to lower than 30% with respect to the reference method [10]. The coefficient error ($\text{CErr} = \frac{\text{SD}}{\text{Mean}} \cdot \frac{1}{\sqrt{\text{nob}}}$, nob being the number of heart beats considered for calculation) was also calculated;

2. Sample size calculation: With a first-order error $\alpha = 0.025$ and a power $(1-\beta) = 0.99$, the number of patients requested to include in the equivalence study was 45;
3. Confidence interval analysis: We provided a Bland & Altman plot for repeated measurements to represent the bias with the reference method. We tested the equivalence between the simulation and the measurement using the Two One-Sided Test (TOST, [44]. This test postulates that accepting the H_0 hypothesis implies that there exists a difference between the two tested means, and accepting the H_1 hypothesis ($p < 0.05$) implies that the two tested means are equivalent.

We compared the characteristics of the normotensive group with the characteristics of the hypotensive group at baseline using the χ^2-test for categorical variables and Wilcoxon test for continuous variables. In the hypotensive group, we further analysed the variation of the parameters of the models and the results of the simulations from baseline to the maximum effect of NOR using the Wilcoxon test. Continuous variables were presented as mean ± standard deviation and categorical variables as count (%).

The simulations were performed using the CardiacLab library – an in-house implementation of the model in MATLAB (The MathWorks Inc, Natick, Massachusetts). The statistical analysis was performed using R (The R Foundation for Statistical Computing, Vienna, Austria).

10.4 Results

Between November 1st 2016 and October 30th 2017, 45 patients were included (Table 10.4). Among them, 16 patients (36%) received at least one NOR administration to treat IOH and were included in the hypotensive group. The remaining 29 (64%) patients stayed haemodynamically stable during the data recording and were included in the normotensive group. Main parameters of the models after calibrations to patients' data and the interpretation of PV loops are presented in Table 10.5. Figure 10.2 shows examples of the models confronted to the data. Figure 10.3 displays an example of simulated PV loop.

10.4.1 Equivalency of clinical data and the calibrated models

The Bland & Altman plots for repeated measurements in Figures 10.4 A) and 10.4 C) demonstrate that the simulated and the measured aortic pressure and flow were concordant. The simulated MAP, SAP, DAP, and SV were statistically equivalent to the measurements: -0.9 (95%-confidence interval $\text{CI}_{95} = -1.7$ to -0.1) mmHg for MAP, -1.2 (CI_{95}=-2.2 to -0.2) mmHg for SAP, 2.4 ($\text{CI}_{95} = 1.6$ to 3.2) mmHg for DAP and 0.1 ($\text{CI}_{95} = -0.9$ to 1.2) % of measured SV for SV ($p < 0.001$ for equivalence for all). Furthermore, the upper and the lower bounds of the confidence interval for the differences between measurements and simulations were within the predefined margins of equivalence (Figure 10.5). The percentage error for the MAP, SAP, DAP, and SV were 6, 5, 8, and 18 %, respectively. The coefficient error for simulation was 0.61, 0.29, 1.27, and 0.5 %, for MAP, SAP, DAP and SV, respectively. Finally, Figure 10.6 shows a statistically significant correlation between the measured and simulated indicators of arterial resistances and compliances.

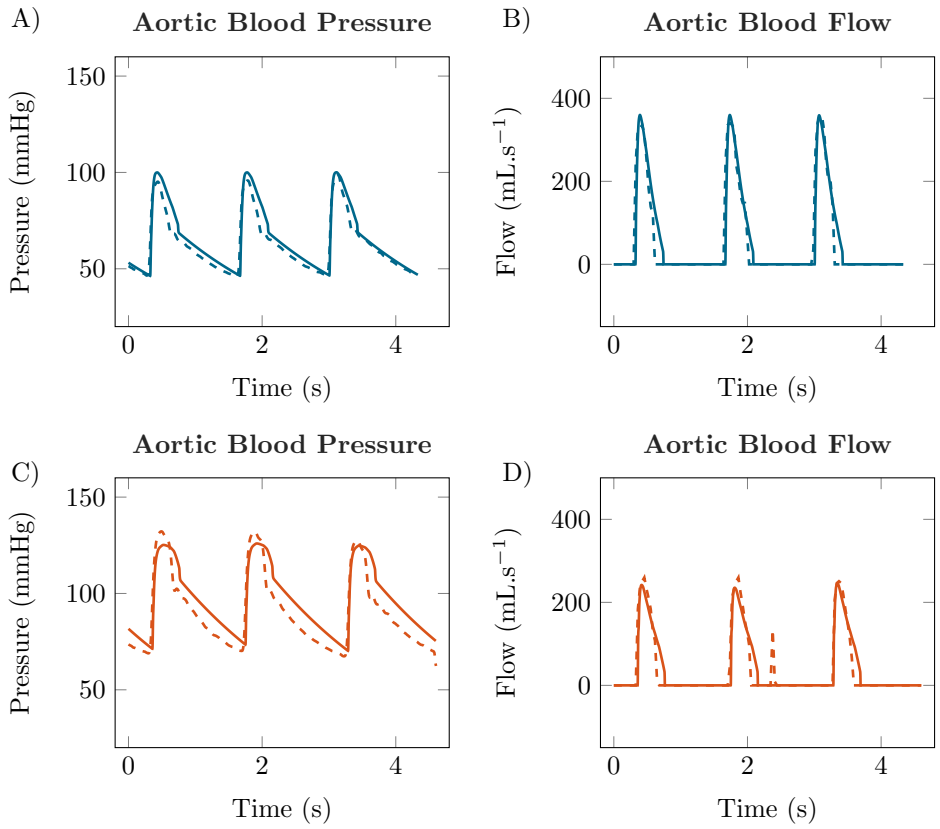

Figure 10.2 – Example of model calibration. Solid lines represent the result of the patient-specific simulation. Dashed lines represent measured data. Blue: Hypotensive. Orange: Maximum effect of noradrenaline.

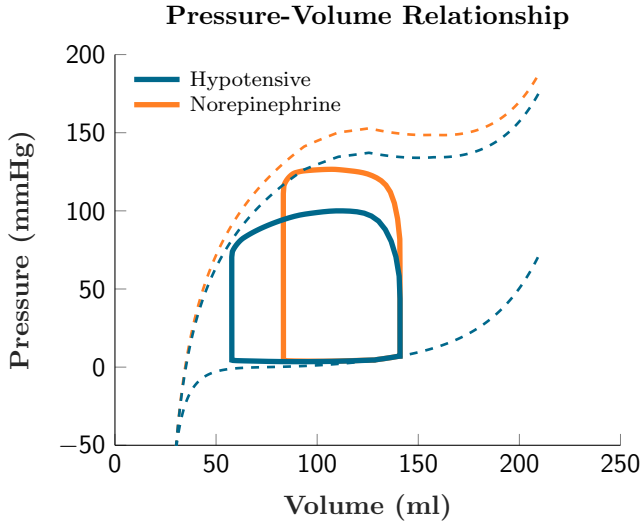

Figure 10.3 – Example of output of a patient-specific simulation for a hypotensive patient and at the maximum effect of noradrenaline: Solid lines represent the dynamic pressure-volume relationship, during a cardiac cycle – namely the Pressure-Volume Loop. Dashed lines represent the static pressure-volume relationships – namely the End-Diastolic Pressure-Volume Relationship (EDPVR) and the End-Systolic Pressure-Volume Relationship (ESPVR). The EDPVR characterises the ventricular volume for a given pressure at end-diastole. The ESPVR represents the ventricular pressure and volume at end-systole, prior to isovolumic relaxation. Note that the dynamic P-V loop does not necessarily reach the theoretical static ESPVR curve, typically when cardiac cycle is too short.

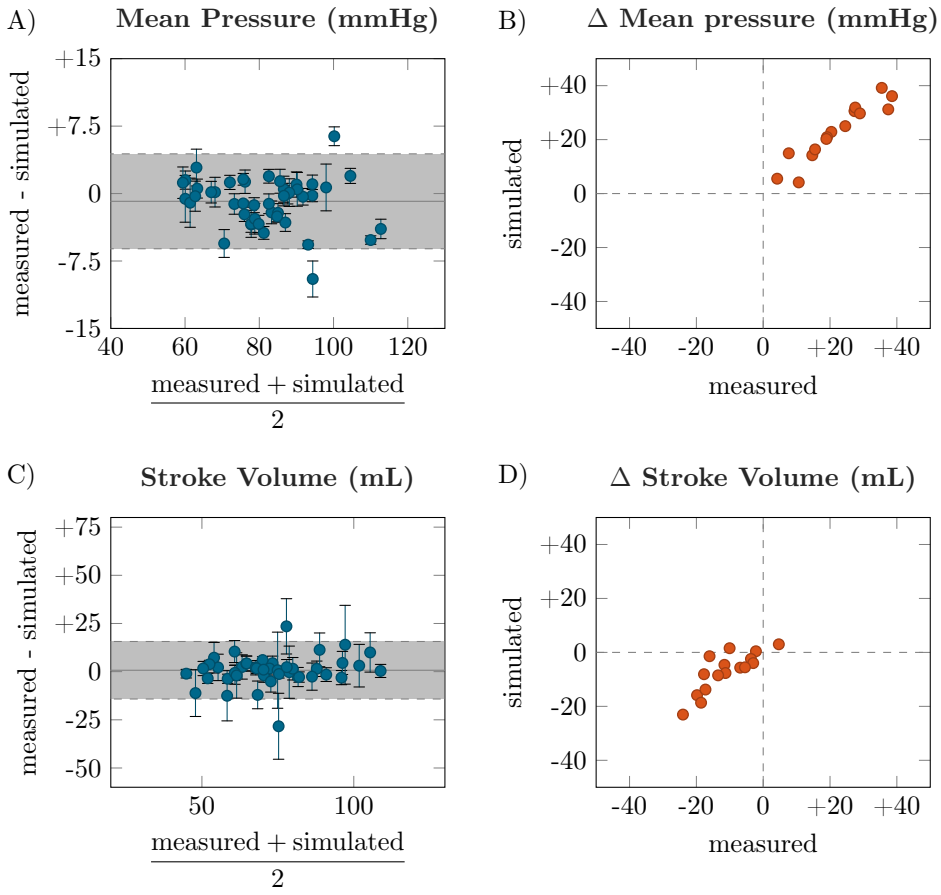

Figure 10.4 – Results of calibration. Left: Bland & Altman plots for repeated measurements representing dispersion of the difference between measurement and simulation (n = 45) over the averaged mean of these couples. Blue points represent couples averaged over 10 heart beats and blue bars represent standard deviations across the ten beats, for individual patients. Dotted horizontal lines represent the limit of agreement (±1.96 times Standard Deviation), and the horizontal grey line represents the bias or the mean difference between measurements and simulation. Values for bias and limits of agreements were $-1\,[-7{-}5]$ mmHg and $-1\,[-19{-}20]$ mL, respectively for mean arterial pressure and stroke volume. Right: 4-quadrant plots representing the variation of mean pressure and stroke volume from hypotension to maximum effect after administration of noradrenaline. Orange points represent mean of ten beats for the 16 patients that have received noradrenaline.

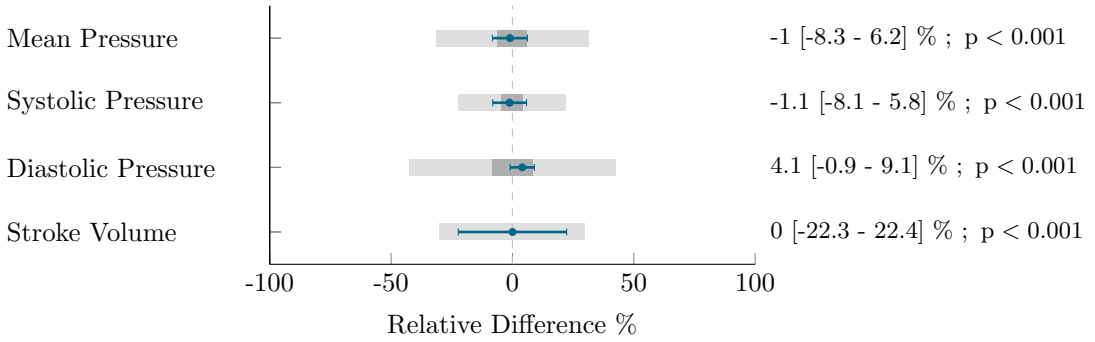

Figure 10.5 – Dark grey boxes represent the equivalence area for the mean difference estimation (in percentage of the measured indicator), light grey boxes represent the equivalence area for confidence intervals. Limits of equivalence were defined as ±8mm Hg for pressure and ±30% for stroke volume, as recommended by international guidelines. Blue lines represent the mean and the confidence interval for the difference between measurement and simulation.

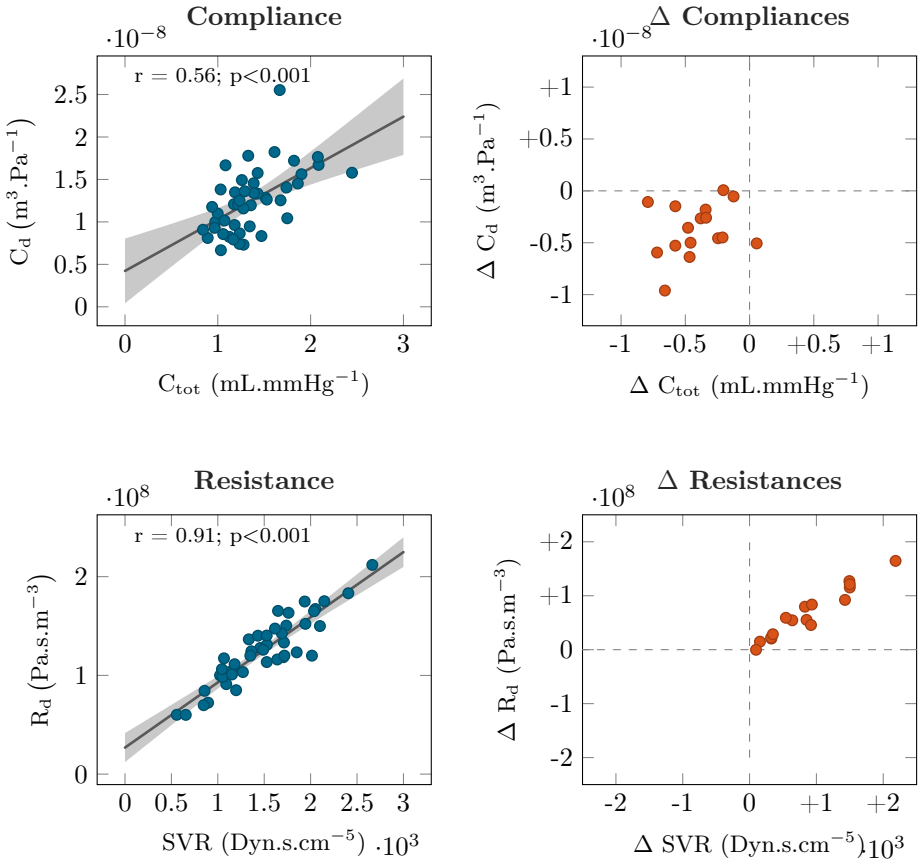

Figure 10.6 – Correlations between simulated and measured indicators. A: Correlation plot representing simulated capacitance (C_d) against measured total arterial compliance (C_{tot}=SV/PP). B: 4-quadrant plot representing ΔC_d against Δ C_{tot} for all 45 patients. C: Correlation plot representing simulated resistance (R_d) and systemic vascular resistance (SVR = $\frac{MAP}{CO}$); D: 4-quadrant plot representing the ΔR_d against the ΔSVR; from hypotension to maximum effect after administration of noradrenaline. Orange points represent mean of ten heartbeats for the 16 patients that have received noradrenaline. SV, stroke volume; PP, pulse pressure; MAP, mean aortic pressure.

Table 10.4 – Population characteristics and comparison between the normotensive and hypotensive group. Results are expressed as mean ± standard deviation or count (percentage).

Patient's data		**All**	**Normotensive**	**Hypotensive**	**P-val**
Demographic					
Age	(years)	51±13	53±14	49±12	0.315
Sex F	n (%)	21(46)	11(39)	10(63)	0.997
Weight	(kg)	73±15	76±17	69±11	0.292
Height	(cm)	168±9	169±10	166±8	0.329
Hypertension	n (%)	14(31)	10(39)	4(25)	0.957
Diabetes	n (%)	2(4)	1(4)	1(6)	0.516
Dyslipidemia	n (%)	5(11)	4(14)	1(6)	0.662
Myocardial infarction	n (%)	1(2)	1(4)	0(0)	0.468
Transthoracic echocardiography					
Ejection Fraction	(%)	59±9	57±9	61±8	0.127
Wall Thickness	(cm)	0.78±0.13	0.83±0.13	0.76±0.14	0.69
Aortic root diameter	(cm)	1.91±0.19	1.94±0.21	1.88±0.17	0.242
End-Diastolic Volume	(ml)	129±25	132±25	126±25	0.681
Left Atrial Volume	(ml)	54±5.4	56±3.8	52.4±7	0.682
E-wave	($cm.s^{-1}$)	76±24	70±21	82±26	0.105
A-wave	($cm.s^{-1}$)	61±18	64±18	59±15	0.432
E'-wave (TDI)	($cm.s^{-1}$)	12±5	11±3	13±5	0.352
Velocity-Time Integral	(cm)	23±5	23±5	23±5	0.86
Stroke Volume	(ml)	76±17	75±15	77±19	0.681
Hemodynamic					
Mean Pressure	(mmHg)	81±13	85±14	75±10	<0.001
Systolic Pressure	(mmHg)	114±19	118±20	109±16	<0.001
Diatolic Pressure	(mmHg)	60±10	62±11	56±7	<0.001
Stroke Volume (TOD)	(ml)	73±18	70±15	76±22	<0.001
Potassium	$mmol.l^{-1}$	4.1±0.4	4.1±0.5	4.1±0.3	0.962
Serum Creatinine	$\mu mol.l^{-1}$	70±16	73±18	65±12	0.242
Total Fluid Infusion	ml	1027±464	1079±417	950±612	0.475

10.4.2 PV loop interpretation in normotensive vs hypotensive groups

Characteristics of normotensive patients were not different from hypotensive, except for the haemodynamic conditions before the administration of NOR (Table 10.4). Specifically, the hypotensive patients had a lower blood pressure and a higher SV. The analysis of the values of the model parameters were consistent with these observations (see Table 10.5 and Figure 10.7), as the distal resistances were lower in hypotensive group (110±25 vs 133±35 $MPa{\cdot}s{\cdot}m^{-3}$; $p = 0.014$). At baseline, the PV loop analysis showed that the ventricular-arterial coupling (V_{va}) was lower for hypotensive than for normotensive group (0.64 ± 0.37 vs $0.88 \pm 0.43; p = 0.039$). The internal work (I_w) was lower and the cardiac efficiency (CE) was higher in the hypotensive group (0.23 ± 0.12 vs 0.38 ± 0.21 Joules; $p = 0.009$ and 0.8 ± 0.1 vs 0.73 ± 0.11; $p = 0.042$, for I_w and CE, respectively) (Table 10.5 and Figure 10.7).

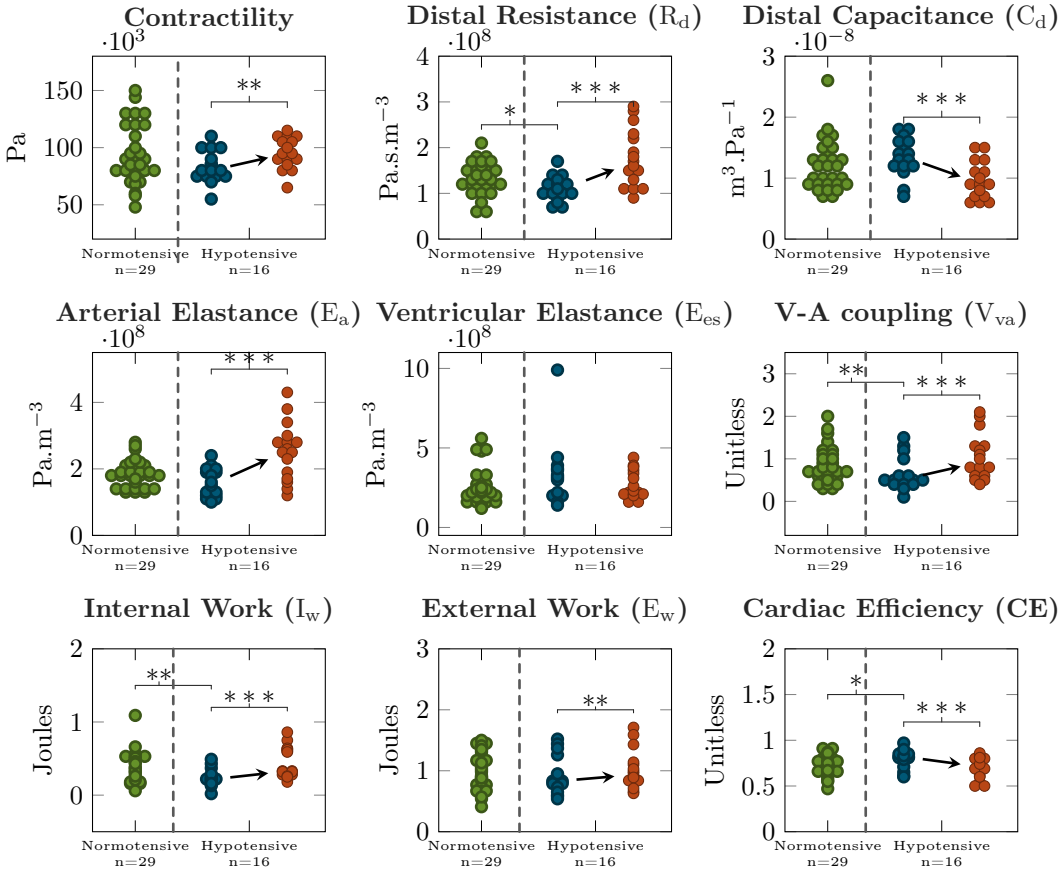

Figure 10.7 – Boxplots representing the parameters and the results of the simulation values. * p<0.05; ** p<0.01; *** p<0.001.

Table 10.5 – Results of calibration procedure for the entire population, and comparison between the normotensive and hypotensive group. Results are expressed as mean ± standard deviation.

		All	Normotensive	Hypotensive	P-val
Model parameters (at reference configuration)					
Ventricular volume	(ml)	69±14	70±14	66±13	0.581
Wall thickness	(cm)	0.96±0.17	0.93±0.15	1±0.19	0.404
Ventricular Radius	(cm)	3±0.2	3.01±0.19	3±0.21	0.842
Heartbeat duration	(ms)	9501±181	9621±182	9291±182	0.433
Distal Resistance	(10^8 Pa·s·m^{-3})	1.25±0.33	1.33±0.35	1.1±0.25	0.014
Distal Capacitance	(10^{-8} m^3· Pa^{-1})	1.25±0.38	1.2±0.4	1.35±0.31	0.09.
Contractility	(kPa)	91±23	94±27	84±14	0.302
Ventricular-arterial coupling					
E_a	(10^8 Pa· m^{-3})	1.76±0.45	1.86±0.42	1.59±0.45	0.095
E_{es}	(10^8 Pa· m^{-3})	2.76±1.52	2.52±1.15	3.2±1.99	0.182
V_{va}	(unitless)	0.8±0.4	0.88±0.43	0.64±0.37	0.039
Cardiac bioenergetics					
E_w	(Joules)	0.96±0.3	0.99±0.3	0.91±0.31	0.365
I_w	(Joules)	0.32±0.19	0.38±0.21	0.23±0.12	0.009
CE	(unitless)	0.75±0.11	0.73±0.11	0.8±0.1	0.042

E_a, arterial elastance; E_{es}, ventricular elastance; V_{va}, ventricular-arterial coupling; E_w, external work; I_w, internal work; CE, cardiac efficiency.

10.4.3 Interpretation of the noradrenaline effects in the hypotensive group

The effect of NOR was confirmed by the changes in measured pressures and flow (MAP, SAP and DAP increased by 30 ± 15, 23 ± 12 and $27 \pm 13\%$, respectively, whereas SV decreased by $14 \pm 9\%; p < 0.001$ for all). Figure 10.2 shows an example of the adjusted calibration after NOR administration in a hypotensive patient. The adequacy between the simulations and measurements was confirmed by the 4-quadrant plots (Figures 10.4 B) and 10.4 D) (> 95% concordance with 10% exclusion zone for MAP and SV, respectively). The 4-quadrant plots in Figure 10.6 shows the adequacy of the NOR-adjusted capacitance and resistance parameters with SVR and C_{tot}, respectively (> 95% concordance with 10% exclusion zone, for both). To adjust the calibration, we had to significantly increase R_d by $60 \pm 39\%(p < 0.001)$, contractility by $14 \pm 11\%(p = 0.002)$ and to decrease C_d by $27 \pm 16\%(p < 0.001)$.

When analysing the effect of blood pressure restoration by using the simulated PV loops (example in Figure 10.3), we observed an increase of E_w by $13 \pm 12\%(p = 0.001)$ and I_w by $141 \pm 161\%(p < 0.001)$, associated with a decrease of CE by $13 \pm 11\%(p < 0.001)$. We also observed an increase of V_{va} by $92 \pm 101\%$ caused by the increase of arterial elastance (E_a) by $59 \pm 37\%(p < 0.001$, for both). Figure 10.7 shows the absolute variation of PV loop functional indicators between the baseline and the maximal effect of NOR.

10.4.4 Validation group

The analysis of validation group confronts the simulated vs measured PV loops and demonstrates the sensitivity to using the flow in ascending vs descending aorta to calibrate the Windkessel model. While Figure 10.8 shows a visual comparison, Table 10.6 demonstrates that the errors between the simulated and measured ventricular pressures and the quantities obtained from PV loop analyses (E_w, CE and V_{va} coupling) are all $\leq 10\%$ in both types of recorded aortic flows.

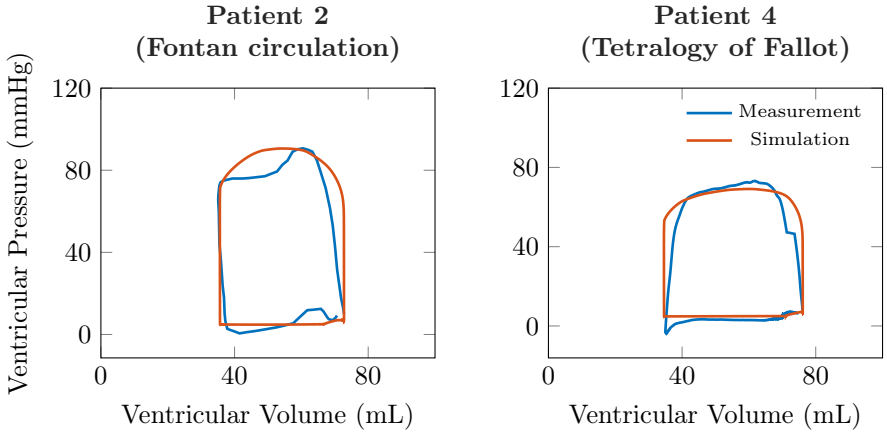

Figure 10.8 – Comparison of simulated PV loops and of the measurements in selected validation subjects once descending aortic flow was used (as in our clinical study) or when directly measured ascending aortic flow was used.

Table 10.6 – Relative error in simulation vs measurement (in %) in the validation group, first and second line in each subject when using flow in ascending, descending aorta, respectively.

Patient	measurement type	MP	SV	E_w	V_{va}	CE
Patient 1	ascending aorta	10	6	2	6	4
	descending aorta	5	3	5	6	4
Patient 2	ascending aorta	2	3	3	2	10
	descending aorta	2	2	3	5	10
Patient 3	ascending aorta	1	<1	4	2	1
	descending aorta	2	4	3	6	3
Patient 4	ascending aorta	1	3	10	2	8
	descending aorta	1	1	10	<1	8

MP, mean ventricular pressure; SV, stroke volume; E_w, external work; V_{va}, arterio-ventricular coupling; CE, cardiac efficiency.

10.5 Discussion

This study demonstrates the feasibility of employing biomechanical modelling to augment CV physiological monitoring. The proposed framework allowed to set up models for 45 patients while using standard data recorded during neuroradiological procedures (without cardiac catheterisation). The patient-specific models were subsequently used to quantify in vivo the CV consequences of IOH on cardiovascular system (including PV loop analysis)

as compared to normotensive population and the effects of restoration of blood pressure by NOR administration.

First, we verified that the models were adequately calibrated in the cohort of 45 patients. We performed an equivalence study between the measurements and simulations by analysing MAP, SAP, DAP and SV differences. The confidence interval of the differences did not exceed the equivalence margins. Moreover, we observed that the numerical values prescribed for the parameters were in accordance with the expected theoretical levels. The validation group confirmed that using the proposed calibration procedure, the simulated and measured PV loops were in accordance.

We therefore assumed that the calibrated models behaved as the CV systems of the patients, which allows to access an advanced cardiovascular picture of the individual patients. Specifically, we were able to observe from a cardiac energetics viewpoint, that the hypotensive group expressed more efficient hearts with better ventricular-arterial coupling. Despite the higher efficiency, the model revealed an anaesthetic drug-induced vasodilation. The restoration of blood pressure was required, as hypotension may worsen organ perfusion and lead to renal or myocardial ischemia [40; 43]. Optimising the cardiac energetic expenditure could be the main target, however, in other situations (e.g. failing hearts or malignant hypertension management [14].

Thirdly, we aimed to test the ability of our patient-specific model to quantify the changes in the CV system induced by a pharmacological challenge. NOR should enhance the myocardial contractility, increase systemic vascular resistance and decrease total arterial compliance [42; 41]. We can appreciate that, after NOR administration, both measured C_{tot} and distal capacitance C_d (model) varied in the expected direction, even though the correlation at baseline was mild. Measured SVR and distal resistance R_d (model) were significantly correlated at baseline and at the maximal effect of NOR. We observed that the contractility increased and that cardiac energetic expenditure and the V-A coupling worsened. This observation is compatible with the pharmacological effect of NOR.

It has been shown that the model-estimated contractility correlates with the maximum upslope of the ventricular pressure $(dp/dt)_{max}$ [38]. Moreover, close relationship has been found between the contractility changes and the changes of maximum ventricular elastance E_{es}, in response to inotropic drugs [3]. While both $(dp/dt)_{max}$ and E_{es} are only surrogate measures of contractility, which in addition require ventricular catheterisation, the estimated true myocardial contractility is likely to have a direct link to the energy needs of the cell.

Cardiovascular models combined with measured data have the potential to assist in diagnostic or therapeutic management by providing additional information not directly visible in the data. Patient-specific cardiovascular models are already available (e.g. [36; 1; 30; 28; 31; 2], however, they have not yet been tested for monitoring of physiological functions. In [6], the authors used lumped-parameter modelling framework calibrated using 4D flow MRI to compute PV loops in 8 healthy volunteers. MRI is however not suitable for monitoring. Popovic et al. [33] explored the effect of sodium nitroprusside on PV loops using a lumped-parameter model in 5 patients with decompensated heart failure. Their calibration involves a pulmonary artery catheter, which however narrows the applicability of the method.

Further steps will need to be performed prior to employing the model-augmented monitoring in routine practice. First, combining our biophysical modelling framework with models based on time-varying elastance [39] is currently being investigated [23] to achieve the real-time monitoring, as oppose to around 10-second-simulation-run for one cardiac cycle on a laptop (in the presented work). Secondly, not having access to the ventricular or atrial pressure, we used a validated semi-quantitative method to classify LV

filling pressure as a high or normal preload [27]. Moreover, the filling pressure was kept at the same level during NOR administration, even though NOR is known to increase the LV filling pressure [11]. This approximation is likely to have led to an overestimation of contractility in response to NOR. In the future work we will investigate a possibility of including a venous return model, while keeping the protocol still clinically acceptable.

Finally, the setting of our proof-of-concept study involves aortic pressure measurement. Although it can be easily obtained during radiological interventions, it is not routinely available during GA as only a peripheral artery cannula is typically requested for medical concerns. A transfer between peripheral arterial pressures and aortic pressures will be included in our future work [13; 26].

10.6 Conclusions

This study aimed at evaluating the feasibility of haemodynamic monitoring augmented by employing a patient-specific biomechanical model of heart and circulation set up using routine haemodynamic measurements during neuroradiological procedure. Our framework allowed to create biomechanical models specific for individual patients. Such models then allowed the interpretation of patient data comparatively between normotensive and hypotensive state by plotting simulated PV loops and by quantitative estimation of pharmacologically-induced alterations of the cardiovascular system. Even though further methodological improvements are needed to transfer the technology to the bedside, the presented work represents a significant step towards augmenting cardiovascular monitoring by using biophysical modelling. The availability of such ready-to-use numerical patient-specific models has the potential to cause a paradigm shift in physiological monitoring throughout the medical specialisations.

acknowledgements

We would like to thank Dr Philippe Moireau, the main author of the CardiacLab library, for his support concerning the software environment. We would like to thank Mr José Serrano for his involvement in collecting the data.

Ethics approval and consent to participate

The present observational study was conducted in accordance with French bioethics law (Art. L. 1121-1 of the law no. 2004-806, August 9th, 2004) and with the ethical standards set forth in the Helsinki Declaration of 1975. It has been approved by the Institutional Review Board (IRB) of the French Society of Intensive Care Medicine (Société de Réanimation de Langue Française, CE SRLF 14-34, 17th February 2015). According to the French bioethics law, the IRB waive the need for written informed consent. However, an information letter was given, and oral agreement was obtained from each patient before anaesthesia.

The data collections in the validation subjects with Fontan circulation were performed at Evelina London Children's Hospital, King's College London, under the ethical approval of institutional ethics committee, London UK (Ethics Number 09H0804062). The parents of the included patients gave written consent for participation in the study. The data collection in tetralogy of Fallot patients were performed at Children's hospital, UT Southwestern Medical Center Dallas, under the ethical approval UT Southwestern IRB (STU 032016-009).

Authors' contribution

Conception or design of the work: A.L.G., F.V., A.M., K.P., T.H., D.C., E.G., R.C. Acquisition or analysis or interpretation of data for the work: A.L.G., F.V., K.P., T.H., E.G. Drafting the work or revising it critically for important intellectual content: A.L.G., F.V., A.M., K.P., T.H., D.C., E.G., R.C. Final approval of the version to be published: A.L.G., F.V., A.M., K.P., T.H., D.C., E.G., R.C. Agreement to be accountable for all aspects of the work: A.L.G., F.V., A.M., K.P., T.H., D.C., E.G., R.C.

Competing interests

A.L.G., F.V, D.C. and R.C. are co-owners of the patent entitled "Dispositif cardiaque" (number 1758006, 2017). A research license agreement is currently ongoing between the Anaesthesiology and intensive care department of Lariboisière hospital, Paris, France and Deltex Medical, Chichester, UK.

Bibliography

[1] Arts, T., Delhaas, T., Bovendeerd, P., Verbeek, X., and Prinzen, F. W. (2005). Adaptation to mechanical load determines shape and properties of heart and circulation: the CircAdapt model. *American Journal of Physiology-Heart and Circulatory Physiology*, 288(4):H1943–H1954.

[2] Burkhoff, D. (1994). Explaining Load Dependence of Ventricular Contractile Properties with a Model of Excitation-Contraction Coupling. *Journal of Molecular and Cellular Cardiology*, 26(8):959–978.

[3] Burkhoff, D. (2005). Assessment of systolic and diastolic ventricular properties via pressure-volume analysis: a guide for clinical, translational, and basic researchers. *AJP: Heart and Circulatory Physiology*, 289(2):H501–H512.

[4] Caremani, M., Pinzauti, F., Reconditi, M., Piazzesi, G., Stienen, G. J. M., Lombardi, V., and Linari, M. (2016). Size and speed of the working stroke of cardiac myosin in situ. *Proceedings of the National Academy of Sciences*, 113(13):3675–3680.

[5] Caruel, M., Chabiniok, R., Moireau, P., Lecarpentier, Y., and Chapelle, D. (2014). Dimensional reductions of a cardiac model for effective validation and calibration. *Biomechanics and Modeling in Mechanobiology*, 13(4):897–914.

[6] Casas, B., Lantz, J., Viola, F., Cedersund, G., Bolger, A. F., Carlhäll, C.-J., Karlsson, M., and Ebbers, T. (2017). Bridging the gap between measurements and modelling: a cardiovascular functional avatar. *Scientific Reports*, 7(1).

[7] Chabiniok, R., Moireau, P., Lesault, P.-F., Rahmouni, A., Deux, J.-F., and Chapelle, D. (2012). Estimation of tissue contractility from cardiac cine-MRI using a biomechanical heart model. *Biomechanics and modeling in mechanobiology*, 11(5):609–630.

[8] Chabiniok, R., Wang, V. Y., Hadjicharalambous, M., Asner, L., Lee, J., Sermesant, M., Kuhl, E., Young, A. A., Moireau, P., Nash, M. P., Chapelle, D., and Nordsletten, D. A. (2016). Multiphysics and multiscale modelling, data–model fusion and integration of organ physiology in the clinic: ventricular cardiac mechanics. *Interface Focus*, 6(2):20150083.

[9] Chapelle, D., Le Tallec, P., Moireau, P., and Sorine, M. (2012). Energy-preserving muscle tissue model: formulation and compatible discretizations. *International Journal for Multiscale Computational Engineering*, 10(2).

[10] Critchley, L. A., Lee, A., and Ho, A. M. (2010). A Critical Review of the Ability of Continuous Cardiac Output Monitors to Measure Trends in Cardiac Output:. *Anesthesia & Analgesia*, 111(5):1180–1192.

[11] Cudkowicz, L. (1968). Effect of l–norepinephrine on left ventricular diastolic pressures in man. *Thorax*, 23(1):63–68.

[12] Dellinger, R. P., Levy, M. M., Rhodes, A., Annane, D., Gerlach, H., Opal, S. M., Sevransky, J. E., Sprung, C. L., Douglas, I. S., Jaeschke, R., Osborn, T. M., Nunnally, M. E., Townsend, S. R., Reinhart, K., Kleinpell, R. M., Angus, D. C., Deutschman, C. S., Machado, F. R., Rubenfeld, G. D., Webb, S. A., Beale, R. J., Vincent, J.-L., and Moreno, R. (2013). Surviving Sepsis Campaign: International Guidelines for Management of Severe Sepsis and Septic Shock. *Critical Care Medicine*, 41(2):580–637.

[13] Gaddum, N., Alastruey, J., Chowienczyk, P., Rutten, M. C., Segers, P., and Schaeffter, T. (2017). Relative contributions from the ventricle and arterial tree to arterial pressure and its amplification: an experimental study. *American Journal of Physiology-Heart and Circulatory Physiology*, 313(3):H558–H567.

[14] Guarracino, F., Baldassarri, R., and Pinsky, M. R. (2013). Ventriculo-arterial decoupling in acutely altered hemodynamic states. *Critical Care*, page 7.

[15] Hadjicharalambous, M., Asner, L., Chabiniok, R., Sammut, E., Wong, J., Peressutti, D., Kerfoot, E., King, A., Lee, J., Razavi, R., Smith, N., Carr-White, G., and Nordsletten, D. (2017). Non-invasive Model-Based Assessment of Passive Left-Ventricular Myocardial Stiffness in Healthy Subjects and in Patients with Non-ischemic Dilated Cardiomyopathy. *Annals of Biomedical Engineering*, 45(3):605–618.

[16] Holzapfel, G. A. and Ogden, R. W. (2009). Constitutive modelling of passive myocardium: a structurally based framework for material characterization. *Phil. Trans. R. Soc. A: Mathematical, Physical and Engineering Sciences*, 367(1902):3445–3475.

[17] Huxley, A. F. (1974). Muscular contraction. *The Journal of Physiology*, 243(1):1–43.

[18] Jacob, R. and Kissling, G. (1989). Ventricular pressure-volume relations as the primary basis for evaluation of cardiac mechanics Return to Frank's diagram. *Basic Research in Cardiology*, 84(3):227–246.

[19] Joachim, J., Vallée, F., Le Gall, A., Matéo, J., Lenck, S., Millasseau, S., Houdart, E., Mebazaa, A., and Gayat, É. (2017). Velocity–pressure loops for continuous assessment of ventricular afterload: influence of pressure measurement site. *Journal of Clinical Monitoring and Computing*.

[20] Kimmig, F., Chapelle, D., and Moireau, P. (2019). Thermodynamic properties of muscle contraction models and associated discrete-time principles. *Advanced Modeling and Simulation in Engineering Sciences*, 6(1):6.

[21] King, J. M., Bergeron, C. A., and Taylor, C. E. (2019). Finite state machine implementation for left ventricle modeling and control. *BioMedical Engineering OnLine*, 18(1):10.

[22] Klotz, S., Hay, I., Dickstein, M. L., Yi, G.-H., Wang, J., Maurer, M. S., Kass, D. A., and Burkhoff, D. (2006). Single-beat estimation of end-diastolic pressure-volume relationship: a novel method with potential for noninvasive application. *AJP: Heart and Circulatory Physiology*, 291(1):H403–H412.

[23] Le Gall, A., Vallée, F., Pushparajah, K., Hussain, T., Mebazaa, A., Chapelle, D., Gayat, E., and Chabiniok, R. (2020). Monitoring of cardiovascular physiology augmented by a patient-specific biomechanical model during general anesthesia. A proof of concept study. *PLOS ONE*, 15(5):e0232830.

[24] Lienhart, A., Auroy, Y., Péquignot, F., Benhamou, D., Warszawski, J., Bovet, M., and Jougla, E. (2006). Survey of anesthesia-related mortality in France. *Anesthesiology*, 105(6):1087–1097.

[25] Mayr, V. D., Dünser, M. W., Greil, V., Jochberger, S., Luckner, G., Ulmer, H., Friesenecker, B. E., Takala, J., and Hasibeder, W. R. (2006). Causes of death and determinants of outcome in critically ill patients. *Critical Care*, 10(6):R154.

[26] Muller, L. O., Caiazzo, A., and Blanco, P. J. (2019). Reduced-Order Unscented Kalman Filter With Observations in the Frequency Domain: Application to Computational Hemodynamics. *IEEE Transactions on Biomedical Engineering*, 66(5):1269–1276.

[27] Nagueh, S. F., Appleton, C. P., Gillebert, T. C., Marino, P. N., Oh, J. K., Smiseth, O. A., Waggoner, A. D., Flachskampf, F. A., Pellikka, P. A., and Evangelisa, A. (2008). Recommendations for the Evaluation of Left Ventricular Diastolic Function by Echocardiography. *European Journal of Echocardiography*, 10(2):165–193.

[28] Nash, M. P. and Hunter, P. J. (2000). Computational mechanics of the heart. *Journal of elasticity and the physical science of solids*, 61(1-3):113–141.

[29] Niederer, S. A., Plank, G., Chinchapatnam, P., Ginks, M., Lamata, P., Rhode, K. S., Rinaldi, C. A., Razavi, R., and Smith, N. P. (2011). Length-dependent tension in the failing heart and the efficacy of cardiac resynchronization therapy. *Cardiovascular Research*, 89(2):336–343.

[30] Nordsletten, D., Niederer, S., Nash, M., Hunter, P., and Smith, N. (2011). Coupling multi-physics models to cardiac mechanics. *Progress in biophysics and molecular biology*, 104(1-3):77–88.

[31] Pfaller, M. R., Hörmann, J. M., Weigl, M., Nagler, A., Chabiniok, R., Bertoglio, C., and Wall, W. A. (2018). The importance of the pericardium for cardiac biomechanics: From physiology to computational modeling. *arXiv:1810.05451 [physics]*. arXiv: 1810.05451.

[32] Piaggio, G., Elbourne, D. R., Altman, D. G., Pocock, S. J., Evans, S. J. W., and CONSORT Group, f. t. (2006). Reporting of Noninferiority and Equivalence Randomized Trials: An Extension of the CONSORT Statement. *JAMA*, 295(10):1152.

[33] Popović, Z. B., Khot, U. N., Novaro, G. M., Casas, F., Greenberg, N. L., Garcia, M. J., Francis, G. S., and Thomas, J. D. (2005). Effects of sodium nitroprusside in aortic stenosis associated with severe heart failure: pressure-volume loop analysis using a numerical model. *American Journal of Physiology-Heart and Circulatory Physiology*, 288(1):H416–H423.

[34] Powell-Tuck, J., Allison, S. P., Carlson, G. L., Lewington, A. J., and Pearse, R. M. (2011). British Consensus Guidelines on Intravenous Fluid Therapy for Adult Surgical Patients. British Guidelines on IV fluids.

[35] Ruijsink, B., Moireau, P., Pushparajah, K., Wong, J., Hussain, T., Razavi, R., Chapelle, D., and Chabiniok, R. (2020). Dobutamine stress testing in patients with Fontan circulation augmented by biomechanical modelling. *PLOS ONE*, Under review.

[36] Schäfer, A., Burkhoff, D., and Bauersachs, J. (2019). Haemodynamic simulation and the effect of early left ventricular unloading in pre-shock acute coronary syndrome. *ESC Heart Failure*, 6(3):457–463.

[37] Seemann, F., Arvidsson, P., Nordlund, D., Kopic, S., Carlsson, M., Arheden, H., and Heiberg, E. (2019). Noninvasive Quantification of Pressure-Volume Loops From Brachial Pressure and Cardiovascular Magnetic Resonance. *Circulation: Cardiovascular Imaging*, 12(1).

[38] Sermesant, M., Chabiniok, R., Chinchapatnam, P., Mansi, T., Billet, F., Moireau, P., Peyrat, J., Wong, K., Relan, J., Rhode, K., Ginks, M., Lambiase, P., Delingette, H., Sorine, M., Rinaldi, C., Chapelle, D., Razavi, R., and Ayache, N. (2012). Patient-specific electromechanical models of the heart for the prediction of pacing acute effects in CRT: A preliminary clinical validation. *Medical Image Analysis*, 16(1):201–215.

[39] Suga, H., Sagawa, K., and Shoukas, A. A. (1973). Load Independence of the Instantaneous Pressure-Volume Ratio of the Canine Left Ventricle and Effects of Epinephrine and Heart Rate on the Ratio. *Circulation Research*, 32(3):314–322.

[40] Sun, L. Y., Wijeysundera, D. N., Tait, G. A., and Beattie, W. S. (2015). Association of intraoperative hypotension with acute kidney injury after elective noncardiac surgery. *The Journal of the American Society of Anesthesiologists*, 123(3):515–523.

[41] Vallée, F., Le Gall, A., Joachim, J., Passouant, O., Matéo, J., Mari, A., Millasseau, S., Mebazaa, A., and Gayat, E. (2017a). Beat-by-beat assessment of cardiac afterload using descending aortic velocity–pressure loop during general anesthesia: a pilot study. *Journal of Clinical Monitoring and Computing*.

[42] Vallée, F., Passouant, O., Le Gall, A., Joachim, J., Mateo, J., Mebazaa, A., and Gayat, E. (2017b). Norepinephrine reduces arterial compliance less than phenylephrine when treating general anesthesia-induced arterial hypotension. *Acta Anaesthesiologica Scandinavica*, 61(6):590–600.

[43] van Waes, J. A., van Klei, W. A., Wijeysundera, D. N., van Wolfswinkel, L., Lindsay, T. F., and Beattie, W. S. (2016). Association between intraoperative hypotension and myocardial injury after vascular surgery. *The Journal of the American Society of Anesthesiologists*, 124(1):35–44.

[44] Walker, E. and Nowacki, A. S. (2011). Understanding Equivalence and Noninferiority Testing. *Journal of General Internal Medicine*, 26(2):192–196.

[45] Wang, V., Nielsen, P., and Nash, M. (2015). Image-Based Predictive Modeling of Heart Mechanics. *Annual Review of Biomedical Engineering*, 17(1):351–383.

[46] Wang, V. Y., Lam, H., Ennis, D. B., Cowan, B. R., Young, A. A., and Nash, M. P. (2009). Modelling passive diastolic mechanics with quantitative MRI of cardiac structure and function. *Medical Image Analysis*, 13(5):773–784.

[47] Weiser, T. G., Regenbogen, S. E., Thompson, K. D., Haynes, A. B., Lipsitz, S. R., Berry, W. R., and Gawande, A. A. (2008). An estimation of the global volume of surgery: a modelling strategy based on available data. *The Lancet*, 372(9633):139–144.

[48] Westerhof, N., Lankhaar, J.-W., and Westerhof, B. E. (2009). The arterial Windkessel. *Medical & Biological Engineering & Computing*, 47(2):131–141.

[49] White, W. B., Berson, A. S., Robbins, C., Jamieson, M. J., Prisant, L. M., Roccella, E., and Sheps, S. G. (1993). National standard for measurement of resting and ambulatory blood pressures with automated sphygmomanometers. *Hypertension*, 21(4):504–509.

Conclusions and perspectives

The aim of this conclusion Chapter is to provide final comments regarding the work that has been performed within the PhD thesis, regarding the novelties associated with our results and regarding the perspectives of our approach. We also discuss the future works that can be imagined based on the work performed in this thesis. The discussion related to specific aspects of the thesis are discussed in the dedicated chapters and will not be treated herein.

10.7 Work performed and novelties

This PhD thesis was performed in a multidisciplinary environment, at the intersection between cardiovascular physiology, cardiovascular modelling and clinical specialties such as anaesthesia and intensive care. Many issues have been raised, in line with the aforementioned disciplines, for which we had to develop methods to overcome the associated problems.

Modelling and physiological issues

The biomechanical model used in this PhD thesis was described in details by Chapelle et al. [2] and simplified in Caruel et al. [1]. This cardiovascular model, especially the reduced version, allows to perform simulations with standard computing resources in a time frame compatible with clinical situations occurring in anaesthesia and intensive care (*i.e* one heart beat being simulated in 3 to 6 seconds).

However, for modelling optimisation purposes, and for a larger perspective of proposing a clinical tool that may help physicians in their clinical decision-making, the reduction of the computational time close to the real time (*i.e.* one heart beat being simulated in less than one second) is an emergent issue. Indeed, to take advantage of all the potentialities of such well-defined models (*e.g.* real-time continuous parameter or state estimation, *a priori* prediction of the effects of candidate cardiovascular drugs), mathematical methods would be applied (*e.g* data assimilation using Kalman filtering tools), which would slow down the augmented monitoring framework if the modelling environment is not optimised.

To this end, the simplification of the cardiac mechanics that is part of our biomechanical framework, presented in Part III, in the form of the time-varying elastance model have been proposed. Time-varying elastance modelling is common in cardiac modelling communities but the novelty of our approach stands in the biomechanically-defined patient-specific time-varying elastance function (E(t)) which can be used afterward as a surrogate for cardiac mechanics. Physiological issues related to the very essence of the time-varying elastance concept and related to the estimation of the parameters of the E(t) function ensued. Indeed, the E(t) estimation necessitates the measurement of a virtual volume which is the intersection at zero pressure of a linear approximation of the non-linear end-systolic pressure-volume relationship – V_0. This volume can not be measured neither in vivo nor in vitro. It is only a virtual quantity that characterises a linear approximation of a non-linear phenomenon. However, its estimation is crucial for E(t) definition and the question of proper evaluation of this quantity have raised. We overcame this issue by choosing the method that offers us the most stable estimation, as compared with all the other estimation methods available.

Also, estimation of the end-diastolic pressure-volume relationship constitutive law parameters was associated with similar issues. For example, we had to identify the reference volume V_{ref} without having access to ground truth measurements. Direct validation of our method for this specific issue cannot be achieved and we had to choose indirect validation methods, based on consistency of the results.

Key characteristics of the ESPVR and the EDPVR estimation methods based on phenomenological models [7; 5] used a unique "master" curve constructed using normalisation

processes. These normalised curves are supposed to be reproducible or constant within and across subjects. However, using our biomechanical model we observed that small deviations from this master curve may be observed, and may have an impact on the outputs on the EDPVR or parameters of ESPVR estimations. The inter-individual variability of this master curve, although small in the normalised space, become wide when de-normalised. Our biomechanical approach allows to withdraw the use of such master curves by proposing a complete definition of the parameters of the constitutive laws.

Finally prediction of the response to a therapeutic drug is an interesting modelling perspective. Indeed, coupling pharmacological models with our framework may allow to simulate inotropic, vasoactive or sedative drugs effects on the cardiovascular system. Pharmacokinetics and pharmacodynamics models should be designed. A three-ccompartment pharmacological model is currently studied in our anaesthesiology department to estimate the blood concentration of noradrenaline after unique injection or dosage modification in case of continuous infusion. Moreover the interaction between the blood concentration and the therapeutic effect is studied by setting a dose-response pharmacological model in which the output would be the parameters of the biomechanical framework presented in this PhD thesis, especially those modified by the administration of noradrenaline in Chapter 10.

Operational calibration issues

This PhD thesis was also associated with issues related to the calibration of the models performed with data recorded in routine clinical condition. One of our objectives was to propose a framework in which a heart and vessel model could be turned into patient-specific regime without adding any specific device for data measurements. Therefore, all the measured data required for the model calibration were obtained using routine procedures in neuroradiological interventions settings. To this end, we needed to design a measurement method. Trans-thoracic echocardiography was performed at the beginning of the neuroradiological procedure in order to obtain key geometrical information. The tuning of the Windkessel model parameters was performed sequentially using the continuous flow measurement obtained by trans-oesophageal Doppler recording as an input, and the aortic pressure recorded by the neuroradiologist during the endovascular procedure as output. Even if the non-invasiveness of the framework is a key aspect for translational purposes, in this proof-of concept work we recorded the pressure in the aorta. Future research using peripheral arterial pressure measurements is necessary for validation and translation of our framework into a totally minimally invasive setting.

The passive law parameters estimation was probably the most challenging part of the operational calibration issue. Indeed, invasive measurements of intraventricular pressure and volume during changes in loading conditions are very invasive in patients, and we did not have access to such measurements in patients. In Part II, we developed a method to estimate the passive law parameters from a single measurement of end-diastolic volume (V_{ed}) and pressure (P_{ed}). The V_{ed} can be obtained non-invasively using trans-thoracic echocardiography (TTE) measurements. The P_{ed} is more difficult to assess and necessitates either semi-quantitative assessment using TTE or invasive estimation using pulmonary arterial catheter. We compared our single-beat estimation method against the single-beat estimation developed by Klotz et al. [5] and observed good performances of our biomechanical method with the potential to perform comparisons between and within patients, and to use the patient-specific biomechanical model for inverse problems. A clinical validation study could be performed by comparing the estimation with the measured P_{ed}, either by direct measurement using left heart catheter or by indirect measurement of of pulmonary capillary wedged pressure (P_{cwp}) using pulmonary artery catheter.

One significant issue with our approach lies in our inability to estimate the preload of

the LV (assumed as the atrial pressure P_{at} in our simplified model). In our operational calibration procedure proposed in Chapter 1, we prescribed P_{at} using a trans-thoracic echocardiographic method which allowed to obtained a semi-quantitative assessment of P_{at} (high or low). Future research is necessary to overcome this issue. Continuous right atrial pressure measurement using central venous catheter could be used as a surrogate of LV filling pressure, in case of absence of pulmonary arterial hypertension or right heart failure. Another approach would be to use a venous return model such as described in Hall [3]. In brief the venous return can be defined as the relationship between the mean pressure of the venous system, the atrial pressure, and the resistive phenomena opposing the venous flow. We may propose the following model [6], coupled with the Windkessel model

$$Q_{ao} = \frac{V_{eff}}{R_d C_d} - \left(1 + \frac{C_{vs}}{C_d}\right) \frac{P_{vs}}{Rd}, \tag{10.4}$$

which may allow to estimate the venous pressure (P_{vs}) entering the heart from continuous measurement of cardiac output (Q_{ao}), from calibrated parameters of the Windkessel model (R_d and C_d the distal resistance and capacitance, respectively), and from the calibration of the parameters of the venous system, namely the effective volume (V_{eff}) which is the blood volume able to flow from the arterial to the venous system, and the venous capacitance (C_{vs}). It yields

$$P_{vs} = \frac{V_{eff}}{C_{vs} + C_d} - Q_{ao} \frac{R_d C_d}{C_{vs} + C_d}. \tag{10.5}$$

In our model, the link between P_{vs} and P_{at} is simply set as $P_{at} = P_{vs} + 2.5$mmHg, as in Ruijsink et al. [6]. However, the identification of the parameters V_{eff} and C_{vs} which characterise the venous return model is not easy in routine clinical situation. An approach would be to calibrate the venous return model using an initial calibration procedure in which P_{vs} would be available. Then, the estimation of the mean systemic filling pressure (MSFP) may help to estimate C_{vs}. Assuming the MSFP as the venous pressure at which no blood flows:

$$MSFP = \frac{V_{eff}}{C_{vs} + C_d}, \tag{10.6}$$

and substracting Equation (10.5) and Equation (10.6), and rearranging, it yields:

$$C_{vs} = \frac{Q_c}{MSFP - P_{vs}} C_d \left(R_d - 1\right). \tag{10.7}$$

P_{vs}, Q_c, R_d and C_d can be obtained by the operational calibration procedure described in Chapter 1

Therefore, it would be necessary to estimate MSFP that is not trivial as it corresponds to the pressure in the vascular system measured when the patients has just deceased. An approach would be to set the MSFP to a reasonable average value as was performed in Ruijsink et al. [6]. Another approach would be to use the available clinical methods that estimate MSFP [9], which can be used in a study to calibrate the venous return model. All these methods requires additional measurements such as central venous catheter in order to obtain the right atrial pressure, or specific device (tourniquet). Furthermore, Venous return model parameters C_{vs} and V_{eff} are susceptible to be affected by haemodynamic changes induced by therapeutic drugs, bleeding, or sympathetic tone. Consequently, the calibrated parameters are susceptible to be modified during any haemodynamic modification. The use of respiratory variations in ventilated patients might represent a lead to venous return model parameters estimation. Indeed, cyclic ventilator insufflation modifies the vascular capacitance of the pulmonary circulation. The blood pours into the

systemic circulation and in turn increases V_{eff}. The cyclic intra-thoracic pressure changes are measured by the ventilator. Estimation of atrial pressure variation from intra-thoracic pressure variation can be performed using an adequate model.

By defining a patient-specific biomechanical framework, a key perspective of this PhD thesis is to prepare the basis for implementation of state or parameter estimation methods. Indeed, the operational calibration process, by which we turned the heart and vessels model into patient-specific regime, also allows to identify the parameters that are susceptible to be modified according to the natural evolution of the disease, to the ongoing surgical procedure, or to the medical treatments that can be administered to a specific patient. Using data assimilation methods, if the modelling environment, and if the parametric space are sufficiently well-defined, then solving inverse problems becomes doable. Thereafter, automatisation of the calibration procedure proposed in this PhD thesis document can be considered. We can also imagine the perspective to interpret the pathophysiological information revealed by the automatic adaptation of the parameters of the model according to the evolving clinical situation. We would be able to consider providing recommendations based on this information. To address this issue, we are currently working on the parametrisation of a Kalman filter, using the results of the calibration procedure presented in this PhD thesis.

Clinical issues

This PhD thesis is a proof-of-concept of using a biomechanical model of heart and vessels with routinely acquired patients data to augment haemodynamic monitoring of patient in general anaesthesia. Our framework allows to access advanced physiological information that is hidden in the data and revealed by the patient-specific model. In Part IV, we demonstrated an example of the use of such a framework to analyse the haemodynamic profile of anaesthetised patients, in terms of cardiac bioenergetics, of heart-vessel coupling and of cardiovascular performances. By analysing the calibrated parameters and the simulated pressure-volume loops, we were able to compare the hypotensive with the normotensive patients. Moreover, we were able to analyse the effect of the administration of noradrenaline given to restore blood pressure. The observed results were expected from the knowledge of the pathophysiological conditions occurring while on general anaesthesia (drop of peripheral resistances by the loss of sympathetic tone induced by the anaesthetic drugs). The effect of noradrenaline observed by modelling results analyses were also expected given the pharmacological effects of noradrenaline. However, even though these are positive results from a modelling point of view, from a clinical standpoint, these results were predictable, and could be viewed as of a limited use for a direct patient care. It should be noted that our patients did not express complex cardiovascular diseases. Also the neuroradiological interventions performed is not associated with complex haemodynamic perturbations. However, this proof-of-concept work has paved way to populations with more complex cardiovascular issues, for whom the proposed model-augmented monitoring would be of a significant help. We are currently recording invasive left ventricular pressure and volume data in cardiac cathlab, in patients with specific cardiovascular diseases. Characterisation of their haemodynamic profile using our biomechanical framework will allow us to validate our approach in patients for whom the clinical challenges are more significant.

The augmentation of the current haemodynamic monitoring is not the only advantage of using a patient-specific modelling framework. Indeed, prediction of the effect of the treatment may become an interesting endpoint of future research. From a calibrated configuration of our framework, we could imagine to simulate the effect of the administration of therapeutic drugs prior to its administration to patients. It could help clinicians to adjust the nature and the dosage of the candidates therapeutic drugs. We may also

imagine, as an example, a pragmatic clinical study in which we would compare the results of the calibrated simulations obtained after noradrenaline administration, with the results of the simulations performed using model parameters that would be modified by a relative increase or decrease of baseline value, with a magnitude of change that would have been defined in other set of calibrated patients. Another approach would be to couple a pharmacological model (pharmacokinetic and pharmacodynamic models), with our biomechanical model to simulate the effect of therapeutical drugs.

Also another clinical perspective may come from numerical methods to estimate model state or parameters. Indeed, by using, for example, data assimilation techniques, we would imagine that recommendations may be proposed to the treating physician facing complex haemodynamic situation.

If our framework has the potential to be translated into clinical bedside, it is currently limited by the need to obtain invasive measurements of pressure in the ascending aorta. We focused our population on neuroradiological procedure as it allowed us to record such invasive data. However, generalisability of our approach will need reproducibility of our results when using a peripheral arterial pressure (*i.e.* femoral or radial arterial cannulas or cuffed pressure). We are considering three approaches to overcome this issue. First, we can imagine that the measurement site of arterial pressure has little impact on the observed results provided in Chapter 10. In the 45 patients included in our clinical studies, all of them were monitored using a radial or femoral arterial catheter. A comparative analysis of the results obtained with aortic or with peripheral arterial pressure would be interesting to perform. Second, we can imagine to apply a pressure transfer function from peripheral pressure to estimate the central pressure waveform, such as in Joachim et al. [4]. Again comparative analysis of the results obtained with measured versus estimated central pressure would be interesting. Third, our team is currently working on a one-dimensional model of arterial circulation, such as presented in Chapter 1 Section 1.5.1.2. Also some existing approaches can be considered [8]. Comparative analysis of the results obtained with measured versus simulated central pressure will be interesting.

To our knowledge, such a biomechanical framework, coupled with routinely acquired data on patients under general anaesthesia offers an advantageous compromise between the level of complexity of the modelling framework and the invasiveness of the data necessary for calibration purposes, with great perspectives to use the full biomechanical model potentialities at patients' bedside. Currently efforts are performed to solve the aforementionned issues in order to propose in a close future a prototype of a device that would be used in patients.

10.8 Final conclusion

Haemodynamic monitoring of patients during general anaesthesia in operating theatres or in intensive care wards can be augmented by a patient-specific modelling heart and vessel framework. This PhD thesis describes methods to couple a biomechanical heart and vessels model with routinely acquired data on patients during neuroradiological procedures. These methods and procedures could be implemented within a time and computing resources constraints compatible with clinical issues. Furthermore, the possibilities of using such a patient-specific biomechanical model of heart and vessels at patient bedside are great and may represent a shift toward preemptive therapeutic strategies rather than reactive behaviour. This PhD thesis is the proof-of-concept of the haemodynamic monitoring augmented with a biomechanical model of heart and vessels. After further evaluations of our approach at patients' bedside, the methods could become a part of haemodynamic monitoring systems advancing healthcare

Bibliography

[1] Caruel, M., Chabiniok, R., Moireau, P., Lecarpentier, Y., and Chapelle, D. (2014). Dimensional reductions of a cardiac model for effective validation and calibration. *Biomechanics and Modeling in Mechanobiology*, 13(4):897–914.

[2] Chapelle, D., Le Tallec, P., Moireau, P., and Sorine, M. (2012). Energy-preserving muscle tissue model: formulation and compatible discretizations. *International Journal for Multiscale Computational Engineering*, 10(2).

[3] Hall, J. E. (2011). *Guyton and Hall textbook of medical physiology*. Saunders/Elsevier, Philadelphia, Pa, 12th ed edition.

[4] Joachim, J., Vallée, F., Le Gall, A., Matéo, J., Lenck, S., Millasseau, S., Houdart, E., Mebazaa, A., and Gayat, É. (2017). Velocity–pressure loops for continuous assessment of ventricular afterload: influence of pressure measurement site. *Journal of Clinical Monitoring and Computing*.

[5] Klotz, S., Hay, I., Dickstein, M. L., Yi, G.-H., Wang, J., Maurer, M. S., Kass, D. A., and Burkhoff, D. (2006). Single-beat estimation of end-diastolic pressure-volume relationship: a novel method with potential for noninvasive application. *AJP: Heart and Circulatory Physiology*, 291(1):H403–H412.

[6] Ruijsink, B., Moireau, P., Pushparajah, K., Wong, J., Hussain, T., Razavi, R., Chapelle, D., and Chabiniok, R. (2020). Dobutamine stress testing in patients with Fontan circulation augmented by biomechanical modelling. *PLOS ONE*, Under review.

[7] Senzaki, H., Chen, C.-H., and Kass, D. A. (1996). Single-Beat Estimation of End-Systolic Pressure-Volume Relation in Humans: A New Method With the Potential for Noninvasive Application. *Circulation*, 94(10):2497–2506.

[8] Steele, B. N., Valdez-Jasso, D., Haider, M. A., and Olufsen, M. S. (2011). Predicting Arterial Flow and Pressure Dynamics Using a 1D Fluid Dynamics Model with a Viscoelastic Wall. *SIAM Journal on Applied Mathematics*, 71(4):1123–1143.

[9] Wijnberge, M., Sindhunata, D. P., Pinsky, M. R., Vlaar, A. P., Ouweneel, E., Jansen, J. R., Veelo, D. P., and Geerts, B. F. (2018). Estimating mean circulatory filling pressure in clinical practice: a systematic review comparing three bedside methods in the critically ill. *Annals of Intensive Care*, 8(1):73.

DOCTORAL SCHOOL

Titre : Exploitation conjointe d'un modèle biomécanique patient-spécifique de coeur et vaisseaux et de données mesurées au bloc opératoire pour augmenter le monitorage hémodynamique des patients sous anesthésie générale

Mots clés : Modélisation biomécanique cardiaque ; Calibration patient-spécifique ; Élastance variable ; Relation pression-volume en diastole (EDPVR) ; Effets hémodynamique de la Noradrénaline ; Monitorage cardiovasculaire.

Résumé : L'évaluation hémodynamique des patients sous anesthésie générale est une tache complexe pour les médecins anesthésistes et/ou réanimateurs. Puisque les techniques de monitorage sont imprécises et/ou invasives, il est nécessaire de prendre en compte la balance entre leur utilité, et leur invasivité et/ou leur imprécision. Les méthodes numériques peuvent représenter une alternative en améliorant ce rapport bénéfice/risque pour le patient.
En particulier, la modélisation biomécanique de coeur et vaisseaux présentée dans cette thèse, une fois calibrée sur les données mesurées au bloc opératoire, peuvent permettre de simuler, entre-autres, un cathétérisme cardiaque gauche. Nous avons pu analyser le profil hémodynamique de 45 patients sous anesthésie générale, et interpréter les effets de la Noradrénaline administrée pour corriger une hypotension artérielle chez 16 patients, en termes de bioénergétique cardiaque, et de couplage ventriculo-aortique, à partir de boucles pression-volume ventriculaires simulées.
Notre approche est originale car elle s'intègre dans une démarche rigoureuse basée sur la physiologie cardiovasculaire et la mécanique des milieux continus permettant ainsi de conserver une signification physique et physiologique aux résultats de la modélisation.
Cette thèse présente également des méthodes originales, permettant de calibrer le modèle à partir d'une quantité limitée de donnée patient. Nous avons mis au point des méthodes d'estimation des paramètres de la loi passive de comportement du coeur en diastole, réunissant l'approche biomécanique, difficile à mettre en oeuvre en clinique, et l'approche phénoménologique, plus efficace mais moins rigoureuse.
Nous avons également exploré les potentialités d'un modèle d'élastance variable, dérivé du modèle biomécanique. Nous avons pu montrer que dans une gamme de variation raisonnable, le modèle d'élastance variable pouvait être utilisé en lieu et place du modèle biomécanique, permettant d'envisager l'utilisation de notre approche dans des conditions de monitorage pour lesquelles l'estimation en temps réel est un enjeu important.
Cette thèse représente une preuve de concept de l'exploitation conjointe des données mesurées couramment au bloc opératoire et d'un modèle biomécanique de coeur et vaisseaux pour augmenter le monitorage hémodynamique des patients sous anesthésie générale. Elle représente également la première étape du transfert de la méthode vers la pratique clinique.

Title : Coupling data measured in operating theatre with patient-specific biomechanical model of heart and vessels to augment haemodynamic monitoring of patients undergoing general anaesthesia.

Keywords : Cardiac biomechanical modelling ; Patient-specific calibration ; Time-varying elastance ; End-diastolic pressure-volume relationship (EDPVR) ; Noradrenaline haemodynamic effects ; Cardiovascular monitoring

Abstract : Haemodynamic evaluation of anaesthetised patients in operating theatre or in intensive care units can be challenging. Monitoring devices can be inaccurate and/or invasive. Physicians have to evaluate the usefulness of the information given by the monitor, and its potential harms linked to its invasiveness before implementing the technique. Modelling methods may be an interesting alternative to improve the risk/benefit balance for the patients.
Biomechanical modelling of heart and vessels, when turned into patient-specific regime using patients' data measured in operating theatre, can allow simulation of cardiovascular physiology, including pressure-volume relationships through the cardiac cycle. In 45 patients undergoing general anaesthesia, we analysed the haemodynamic profile in terms of cardiac bioenergetics or ventricular arterial coupling, and we were able to evaluate the effects of Noradrenaline administered for 16 hypotensive patients, on cardiac efficiency, using pressure-volume loops estimated from a patient-specific biomechanical model.
Our approach is original as it is based on a rigorous cardiovascular physiological description and on continuum mechanics theory allowing physical and physiological interpretation of the modelling results.
This PhD thesis presents also original methods for model calibration, from limited data availability. We developed a passive constitutive law estimation method which reunites the biomechanical approach, usually difficult to implement in clinical settings, and the phenomenological approach, more efficient but less rigorous.
We also explored the potentials of a time-varying elastance model, derived from the full biomechanical model. We demonstrated that for reasonable variation ranges, the time-varying elastance model could be used as a surrogate for the biomechanical model. This approach improves the computational time and resources, allowing to consider the transfer of our approach in real-time monitoring conditions.
This PhD thesis is a proof of concept of the coupling between biomechanical modelling of heart and vessels and data measured in operating theatre to augment cardiovascular monitoring in anaesthetised patients. This is also the first step toward transfer of the method from bench to bedside.

Institut Polytechnique de Paris
91120 Palaiseau, France